

Seismo-stratigraphy and numerical basin modeling
of the southern Brazilian continental margin
(Campos, Santos, and Pelotas basins)

INAUGURAL - DISSERTATION

Zur Erlangung der Doktorwürde
der Naturwissenschaften-Mathematischen Gesamtfakultät
der Ruprecht-Karls-Universität
Heidelberg

vorgelegt von
Ingenieur Geologe
Jorham Contreras
aus Caracas, Venezuela

Heidelberg, im Juni 2011

Gutachter:
Prof. Dr. Thilo Bechstädt
PD Dr. Stefan Götz

Tag der mündlichen Prüfung: 29.07.2011

Abstract	v
Kurzfassung	vii
Chapter 1	1
General introduction	
1.1 Southern Atlantic extensional sedimentary basins	1
1.2 Project description and scope of the thesis	3
1.3 Database	3
1.4 Thesis outline and objectives	4
1.5 Geological setting	6
1.5.1 Geodynamic evolution and structural framework	6
1.5.2 Basin fill and hydrocarbon prospectivity	8
Chapter 2	11
Methods and applicability in the southern Brazilian margin	
2.1 Sequence stratigraphy	11
2.2 Inverse-basin modeling	14
2.3 Forward stratigraphic modeling	16
Chapter 3	19
3. Seismic stratigraphy of key segments of the southern Brazilian continental margin: Campos, Santos and Pelotas basins	
3.1 Introduction	19
3.2 Database and methods	
3.2.1 Seismic transects and time-depth conversion	19
3.2.2 Well data and correlation	20
3.2.3 Seismic stratigraphy	20
3.3 Structural framework	25
3.4 Basin fill	26
3.4.1 Barremian to middle Aptian	32
3.4.2 Aptian-Albian transition	33
3.4.3 Albian to Maastrichtian	36
3.4.4 Paleogene	38
3.4.5 Neogene	41

3.5. Discussion	44
3.5.1 Structural development	44
3.5.2 Aptian salt deposition	45
3.5.3 Seismo-stratigraphy and model resolution	46
Chapter 4	49
Inverse-basin modeling	
4.1 Introduction	49
4.2 Methodology	50
4.3 Input parameters	50
4.3.1 Temporal and spatial resolution	51
4.3.2 Lithologies and compaction parameters	52
4.3.3 Crustal flexural parameters	53
4.3.4 Paleobathymetry and sea-level	54
4.4 Subsidence modeling	
4.4.1 Subsidence/uplift trends	58
4.4.2 Genetic components of total subsidence	62
4.4.3 Sediment flux and paleobathymetry	66
4.4.4 Controlling factors on the subsidence development	67
4.4.4.1 Syn-rift continental thinning and transition to oceanic crust	68
4.4.4.2 Continental divergence	71
4.5 Evolution of accommodation space	
4.5.1 Barremian syn-rift to Albian post-rift stage	72
4.5.2 Late Cretaceous early drift stage	75
4.5.3 Paleogene-Neogene mature drift stage	77
4.6 First conclusions: seismo-stratigraphy and inverse-basin modeling	80
Chapter 5	83
Forward stratigraphic modeling	
5.1 Introduction	83
5.2 Geological framework	85
5.3 Method and input parameters	
5.3.1 General outline and workflow	
5.3.2 Model dimensions and essential modeling parameters	85
5.3.2.1 Temporal and spatial resolution	87
5.3.2.2 Initial bathymetric profile	88
5.3.2.3 Eustatic sea-level	89
5.3.2.4 Subsidence and flexural variables	89

5.5.3 Sedimentary parameters	
5.3.3.1 Lithologies, textural variables and compaction	90
5.3.3.1 Sedimentation rates, erosion and transport	90
5.4 Modeling restrictions	92
5.5 Forward modeling results	92
5.5.1 Barremian-Aptian syn-rift stage	93
5.5.2 Middle Aptian-Albian post-rift stage	101
5.5.3 Late Cretaceous early drift stage	103
5.5.4 Paleogene mature drift stage	105
5.5.5 Neogene mature drift stage	106
5.6 Discussion	
5.6.1 Syn-rift crust deformation (Barremian-Middle Aptian, 130-115 Ma)	110
5.6.2 Salt deposition in the Campos and Santos basins (Late Aptian, 115-112 Ma)	112
5.6.3 Post-rift to drift sedimentary evolution (Albian to recent times, 112-0 Ma)	114
5.6.4 Deep-water depositional systems and implications for hydrocarbon prospectivity	116
Chapter 6	
Final conclusions	123
References	129
Appendix A	
A1: Algorithms and sedimentation profiles within 2D stratigraphic forward modeling with PHIL™	
Appendix B	
B1: Input text file variables and workflow for forward modeling in the Pelotas Basin	
B2: Input text file variables and workflow for forward modeling in the Santos Basin	
B3: Input text file variables and workflow for forward modeling in the Campos Basin	
Author's publications and abstracts related to the thesis	
Acknowledges	

Abstract

During the evolution of southern Brazil from rift to “passive” margin, the offshore Campos (CB), Santos (SB), and Pelotas (PB) basins developed highly differing architectures regardless of their associated syn-rift origin. Based on 2D seismic reflection profiles and wells, the three basins have been investigated in terms of seismo-stratigraphy and numerical basin analysis. Within the Barremian-Holocene basin infill (130-0 Ma), twelve to fourteen regional seismic horizons have been mapped and calibrated with bio-/chronostratigraphic ages from the available wells. They define seismo-stratigraphic depositional sequences, which have been classified in terms of accommodation/sedimentation and bounding stratigraphic surfaces. Qualitative interpretations of the evolution of accommodation space and the controlling factors (eustasy, subsidence, sediment supply) have been subsequently quantified by applying inverse-basin modeling. This procedure allowed the restoration of the basin geometry and paleowater depths during each of the chronostratigraphic layers. Furthermore, a comprehensive analysis of the genetic components of total subsidence – thermo-tectonic, flexural, and compaction-induced subsidence – provided the temporal interactions and individual contribution of each subsidence component to basin formation. The obtained subsidence data and sediment supply history, combined with seismo-stratigraphy, represent the input information for forward stratigraphic modeling. This method aims to simulate the stratigraphic evolution in terms of a wide range of modeling variables that simulate interdependent tectonic and sedimentary processes. Sensitivity analysis of modeling parameters revealed the most important controls on the basin development, and provided the best-fit values to construct plausible tectono-stratigraphic models to the present-day basin configuration. This integrated approach allows us to assess the inherent model uncertainties from the sequence-stratigraphic interpretation and evaluate the reliability of various possible geological scenarios.

The results show that six subsidence/uplift trends (ST1-ST6), each of 7 to 51 m.y. duration, controlled the Barremian to Holocene basin development. These trends and their distribution along the shelf-to-basin transition are directly linked to the syn-rift-to-drift geodynamic evolution of the southeastern Brazilian margin. Syn-rift extension triggered high thermo-tectonic subsidence (trend ST1) and controlled the creation of accommodation space in the three basins during the Barremian. However, the results show a distinctive crustal evolution of the single basins; Barremian syn-rift continental extension across the Pelotas Basin involved extensive magmatism and a thick volcanic crust affected by post-rift thermal contraction since Early Aptian times (trend ST2).

As continental break-up propagated northward from the PB to the CB, the mechanisms of lithospheric deformation and subsidence patterns changed between the basins. In the SB and CB, minor magmatism and brittle deformation during the Early-Middle Barremian (trend ST1) evolved to depth-dependent continental stretching during the Late Barremian (trend ST2). The thinned continental

crust featured laterally constant subsidence rates, generating wide sag-salt depocenters across the Santos-Campos margin segment. During the Albian post-rift and Cenomanian-Holocene drift evolution (ST3-ST6) changes in the sediment supply and the flexural loading were due to onshore tectono-magmatic events. These key factors were responsible for the differences in architecture and hydrocarbon prospectivity between the three basins analyzed. Based on the process/response relationship established during modeling, the most important stratigraphic-structural processes on the shelf-to-basin sedimentary systems include: (i) tectonic uplift of the source areas triggering increased sediment supply with progradation and deep-water turbidite flows; (ii) flexurally-induced rebound of the shelf realm facilitates sediment bypass and catastrophic shelf-slope failure; (iii) formation of salt basins and salt remobilization, enhancing the instability of the shelf-edge and modifying the flexural loading distribution; (iv) bottom-currents redistributing the deep-marine sediment infill.

This study on the Brazilian continental margin shows that: (i) changes in subsidence and sediment supply on the continental margin varied over 3rd to 2nd order time intervals, and were not subordinate to eustatic sea-level changes; (ii) flexural and compaction-induced subsidence represent the most important controls on accommodation space during the mature drift stage; (iii) structural and plate-tectonic reconfigurations cannot be directly inferred from qualitative sequence stratigraphic frameworks of continental margins; (iv) depositional systems are controlled by a wide range of interconnected tectonic and sedimentary parameters that go beyond qualitative observations from sequence stratigraphy.

Quantitative modeling of the evolution of continental margins must consider a wide range of variables. Crustal deformation and the geomorphological evolution of the continental margin, as well as local-scale sea-level fluctuations are as important as accommodation space and lithologies. This approach provides more accurate interpretation of the ancient tectono-sedimentary systems, which represent key contributions to a better understanding of the complex geodynamic and tectono-stratigraphic evolution of continental margin sedimentary basins.

Kurzfassung

Die Entwicklung des südlichen Kontinentalrandes von Brasilien von einem Riftgraben zu einem passiven Kontinentalrand zeigt unterschiedliche Verläufe im Campos- (CB), Santos- (SB) und Pelotasbecken (PB). Ausnahme ist die anfänglich analog verlaufende Synrift-Phase. In allen drei Becken wurden Bohrlochinformationen und reflexionsseismische 2D Transekte unter seismostratigraphischen bzw. sequenzstratigraphischen Gesichtspunkten ausgewertet, ferner wurde eine numerische Beckenmodellierung durchgeführt. Für die Beckenfüllung vom Barreme ins Holozän (130-0 Ma) konnten (je nach Becken) zwölf bis vierzehn regional bedeutsame seismische Horizonte auskartiert werden, welche mit Hilfe von bio- und chronostratigraphischen Angaben angrenzender Bohrungen kalibriert werden konnten. Sie entsprechen seismostratigraphischen Ablagerungseinheiten, welche im Hinblick auf Akkommodation, Sedimentation und begrenzende stratigraphische Horizonte klassifiziert wurden. Diese qualitative Interpretation der Beckenentwicklung im Hinblick auf die Entwicklung des Akkommodationsraum und der kontrollierenden Faktoren wie Eustasie, Subsidenz und Sedimenteintrag wurde in der Folge mit Hilfe von Rückwärtsmodellierung quantifiziert. Diese Methode des „backstrippings“ erlaubt die Bestimmung der Beckengeometrie und der Paläowassertiefen für jede chronostratigraphische Einheit. Darüber hinaus wurden die Einzelkomponenten der Subsidenz (Thermotektonik, flexurelle Verbiegung und kompaktionsbedingte Versenkung) analysiert. Hieraus konnten die zeitlichen Interaktionen dieser Komponenten erkannt werden und deren Beitrag zum Beckenaufbau. Diese Quantifizierung von Subsidenz und Sedimenteintrag liefert in Kombination mit der seismostratigraphischen Interpretation die Eingangsdaten für die anschließende stratigraphische Vorwärtsmodellierung. Dieser zweite Modellerschritt dient dazu, die stratigraphische Entwicklung unter Berücksichtigung des großen Spektrums an Modellvariablen darzustellen und dabei die Dynamik der tektonischen und sedimentären Prozesse zu erkennen. Eine Sensitivitätsanalyse der Modellparameter ermöglichte die Identifizierung und Wichtung der Kontrollfaktoren der Sedimentbeckenentwicklung. Hieraus ergeben sich die bestmöglichen Eingabeparameter für ein plausibles tektonostratigraphisches Modell, vom Rifting bis zur heutigen Sedimentbeckenkonfiguration. Dieser integrative Ansatz ermöglicht eine Abschätzung der inhärenten Unsicherheiten des Modells, die in einer „klassischen“ sequenzstratigraphischen Interpretation nicht möglich sind sowie eine Einschätzung über den Wahrscheinlichkeitsgrad verschiedener geologischer Szenarien.

Eine Auswertung der Subsidenzdaten zeigt, dass sich die Barreme- bis Holozän-Entwicklung in allen drei Becken aus sechs Subsidenz- und Anhebungstrends (ST1-ST6) zusammensetzt. Jeder Trend umfasst eine Zeitspanne von 7 bis 51 Mio. Jahren. Diese Trends sowie deren Verbreitung entlang des Schelf-Becken Transektes stehen in direktem Zusammenhang mit der geodynamischen Entwicklung während der Synrift- und Driftphase des südöstlichen Kontinentalrandes von Brasilien. Die Synrift-Extension im Barreme verursachte eine hohe thermo-tektonische Subsidenz

(ST1) und damit einen vergrößerten Akkommodationsraum, in dem Sedimente abgelagert wurden. Allerdings weist die Entwicklung der einzelnen Becken Unterschiede auf. Im Pelotas-Becken war die Extension während des Barreme mit ausgedehntem Vulkanismus verbunden. Diese im PB dicke vulkanische Kruste beeinflusste im frühen Apt die thermische Kontraktion im Postrift-Stadium (ST2).

Während der nordwärts voranschreitenden Öffnung des Südatlantiks vom PB ins CB änderten sich die Mechanismen der Deformation der Lithosphäre und die Subsidenzmuster, damit auch die zeitliche Zuordnung. Die beginnende Riftphase im frühen bis mittleren Barreme ist im Santos- und Campos-Becken durch ein sprödes Deformationsverhalten ausgezeichnet, Magmatismus ist nur untergeordnet (ST1). Die syn-Riftphase fällt ins späte Barreme und ist durch eine tiefenabhängige kontinentale Dehnung charakterisiert (ST2). Die ausgedünnte kontinentale Kruste zeigt im Santos- und Campos-Becken lateral einheitliche Subsidenzraten; die entstehenden Salzbecken werden einem „Sag-Basin“ zugeordnet. Während der Postrift-Entwicklung im Alb und der Driftphase vom Cenoman bis heute (ST3-ST6) beeinflussten tektono-magmatische Ereignisse im brasilianischen Hinterland das Ausmaß des Sedimenteintrags und damit der flexurellen Krustenbeanspruchung. Diese Steuerfaktoren sind für die architekturellen Unterschiede zwischen den Becken verantwortlich, aber auch deren unterschiedliche Prospektivität für Kohlenwasserstoffe. Die wichtigsten, durch die Modellierung aufgezeigten Process/Response-Beziehungen sind: (i) Heraushebung des Liefergebietes erzeugt erhöhten Sedimenteintrag und Progradation im Flachwasser, Turbidite im Tiefwasser; (ii) „flexureller Rebound“ des Schelfes begünstigt Sediment-Bypass und katastrophale Massenverlagerungen am Schelfabhang; (iii) die Entstehung von Salzbecken und die Remobilisation des Salzes erhöht die Instabilität des Schelfrandes und modifiziert die Verbreitung der flexurellen Auflast; (iv) Bodenströmungen bewirken eine Umverteilung tiefmariner Sedimentablagerungen.

Weitere wesentliche Ergebnisse dieser Arbeit über den brasilianischen Kontinentalrand sind: i) Änderungen der Subsidenzrate und Sedimentzufuhr traten am brasilianischen Kontinentalrand in Zyklen von dritter bis zweiter Ordnung auf, die unabhängig von eustatischen Meeresspiegelschwankungen sind; ii) flexurelle und durch Kompaktion induzierte Subsidenz sind die wichtigsten Kontrollfaktoren der Entwicklung des Ablagerungsraumes während der fortgeschrittenen Driftphase (mature drift); iii) strukturelle und plattentektonische Rekonfigurationen lassen sich nicht direkt aus qualitativen sequenzstratigraphischen Interpretationen passiver Kontinentalränder ableiten; iv) die Entwicklung von Ablagerungssystemen werden durch eine Vielzahl von miteinander verbundenen tektonischen und sedimentären Parametern gesteuert, welche sich nicht allein durch qualitativ-sequenzstratigraphische Untersuchungen erkennen lassen.

Quantitative Modelle der Entstehungsgeschichte von Kontinentalrändern müssen ein breites Spektrum unterschiedlicher Variablen berücksichtigen. Die Betrachtung von Krustendeforma-

tion und geomorphologischer Entwicklung eines passiven Kontinentalrandes über die Zeit sowie lokaler Meeresspiegelschwankungen sind ebenso wichtig wie Veränderungen des Akkommodationsraumes oder der darin abgelagerten Lithologien. Der hier vorgelegte Ansatz bietet die Möglichkeit einer akkurateren Interpretation tektono-sedimentärer Systeme und liefert einen wichtigen Beitrag für ein besseres Verstehen der komplexen geodynamischen und tektonostratigraphischen Entwicklung von Sedimentbecken an passiven Kontinentalrändern.

1. Introduction

1.1 Southern Atlantic extensional sedimentary basins

The evolution of rifted continental margins and extensional sedimentary basins represents a key issue in recent academic and industry investigations. The main objectives aim to the prediction of the deformation mechanisms leading to continental break-up and the thermal history of the lithosphere during the phase of continental divergence. These processes represent key controls on the source-to-basin sedimentary systems and the occurrence of hydrocarbon accumulations in several extensional margins worldwide, including the South Atlantic, Norwegian, Iberian-Newfoundland and northwest Australian continental margins.

The southern Brazilian and West African conjugate margins encompass several of the most prolific oil-bearing basins worldwide (Coward et al., 1999). They were originated during the continental break-up of Gondwana in the Jurassic to Early Cretaceous (200-130 m.y. ago) and the subsequent opening of the South Atlantic Ocean. During the initial phase of continental thinning, brittle extension, fault-block tilting and marine water incursions created accommodation space for accumulation of continental and transitional sedimentary deposits. Although several hypothesis and mechanisms have been proposed to explain the process of continental rupture and the formation of rifted Atlantic-type continental margins (Kendall et al., 2005; Cochran and Karner, 2007; Kusznir and Karner, 2007), many questions about the thermal flow and modes of deformation during continental break-up, the nature of the continent-ocean transition, and the dynamic sedimentary systems controlling the margin architecture, remain uncertain.

The Campos, Santos and Pelotas basins constitute the rift-basin system in the southern Brazilian continental margin. These marginal sediment depocenters have accumulated a stratigraphic succession up to 9 km of thickness, including basaltic flows and continental to deep-marine sediments, which record the entire syn-rift to mature drift development of the margin. The Campos Basin occupies an area of 115,000 km², limited to the north by the Vitória-Trindade Chain and to the south by the Cabo Frio High separating it from the Santos Basin (Mohriak et al., 1990). The larger Santos Basin (350,000 km²) is limited to the south by the Florianópolis High and Florianópolis Fracture Zone (FFZ), which separate it from the Pelotas Basin. Southward, the Pelotas Basin (210,000 km²) extends to the Chuí Lineament and the Polonio High, separating it from the Punta del Este Basin on the shelf of northern Uruguay (Bassetto et al., 2000).

The Campos and Santos basins, two of the most prolific sedimentary basins in the Southern Atlantic domain, have been subject of intense exploration campaigns and scientific investigations since the 1970's. Existing onshore and offshore wells, field mapping and sampling, geotechni-

cal laboratory experiments, reservoir characterization and remote sensing surveys, all coupled with the major advances in 2-D, 3-D and 4-D geophysical models provide immense geological databases for oil industry investigations. In cooperation with research institutions and universities, a large number of scientific publications have revealed valuable information on structural and magmatic processes leading to continental break-up and the tectono-stratigraphic evolution of extensional sedimentary basins (e.g. Kumar et al., 1977; Ojeda, 1982; Guardado et al., 1989, 2000; Mohriak et al., 1990, 2002, 2008; Chang et al., 1992; Cainelli and Mohriak, 1999; Karner, 2000; Bassetto et al., 2000; Cobbold et al., 2001; Meisling et al., 2001; Modica and Brush, 2004). The Pelotas Basin, located in the southernmost portion of the Brazilian margin, has been less investigated due to the unsatisfactory drilling activities and uncertainties on the hydrocarbon systems (Coward et al., 1999; Talwani and Abreu, 2000; Gladczenko et al., 1997; Deckelman et al., 2006; Rosa, et al., 2006). However, only few published investigations include a genetic analysis of the syn-rift to mature drift development integrating qualitative and quantitative data (e.g. Guardado et al., 1989; Chang et al., 1992; Karner and Driscoll, 1999; Karner et al., 2003 and Karner and Gambôa, 2007, Mohriak et al., 2008). Based on the existing published information, 2D seismic and well data supplied by ANP Brazil and TGS-NOPEC, this research aims to the analysis of the Barremian-Holocene stratigraphic succession of the Campos, Santos and Pelotas basins and compare the evolution of the three basins.

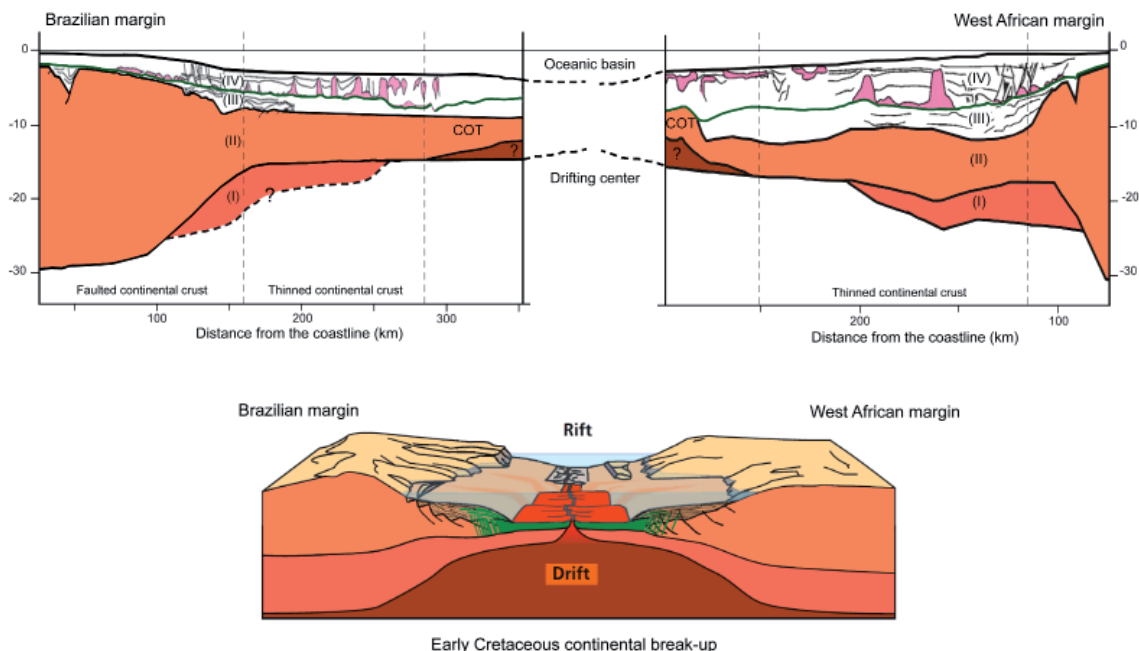


Fig. 1.1 Model of crustal deformation across the conjugate Brazilian and West African rifted margins; modified from Aslanian et al. (2009). Four main crustal layers are identified: (I) an anomalous velocity layer only confirmed on the West African realm; (II) stretched continental crust; (III) syn-rift sub-salt continental clastic deposits intercalated with volcanic series; (IV) salt, post-rift and drift basin fill.

1.2 Project description and scope of the thesis

The research project is linked to the SAMPLE (South Atlantic Margin Processes and Links with onshore Evolution) Priority Program 1375, funded by the German Research Foundation (DFG). This multidisciplinary research plan aims to analyze the origin and evolution of the South Atlantic continental margins and clarify a series of open questions related to continental breakup and post-breakup continental divergence. The main scientific areas of interests involve mantle dynamics and magmatism, lithospheric deformation and thermal evolution during continental rupture (Iaffaldano and Bunge, 2009; Hirsch et al., 2010; Scheck-Wenderoth et al., 2010), post-rift topographic evolution and links to climate and tectonics (Eitel et al., 2006; Franco-Magalhaes, et al., 2010), and sedimentary processes and fluid systems into the basin infill (Stollhofen et al., 2008; Anka et al., 2009; Contreras et al., 2010). These studies and other recent investigations (e.g. Huisman and Beamont, 2008; Aslanian et al., 2009) have revealed complex mechanisms of lithospheric extension (i.e. depth-dependent stretching, mantle exhumation) and magmatic events affecting the composition of the continental crust, the long-term subsidence development and thermal history of passive margin sedimentary basins.

This doctoral thesis focuses on the southeastern Brazilian continental margin. 2D seismic reflection profiles and twenty-one calibration wells provide the stratigraphic configuration and sedimentologic data on the Barremian-Holocene (130-0 Ma) succession deposited along the continental shelf to the deep-marine Pelotas, Santos and Campos basins (Fig. 1). Sequence stratigraphy and the integrated approach of inverse-basin and forward stratigraphic modeling allowed to quantitatively analyze and simulate the Barremian syn-rift to Holocene drift margin development, and estimate the strong influence of the geomorphological evolution of the continental margin, and paleoclimate conditions, on the evolution of sediment depocenters and depositional systems offshore Brazil. This research includes a coherent tectono-stratigraphic model for the specific syn-rift deformation styles of the Pelotas and the Santos-Campos margin segments and provide insights into the key processes controlling the formation of sag basins and deposition of evaporites along the Brazilian and West African conjugate margins in the South Atlantic domain.

1.3 Database

Seismic reflection profiles

The analyzed regional seismic transects are between 300 and 340 km long each. They extend NW-SE perpendicular to continental margin, covering from the continental shelf (150 m of water depth) to the oceanic basin (3,500-4,500 m of water depth). The seismic lines from the Santos and Pelotas basins were supplied in depth domain, while the line from the Campos Basin was time-depth converted based on seismic stacking velocities.

Well data

Twenty-one calibration wells penetrated along the continental shelf to upper slope (up to 220 km offshore) show offsets between 100 and 30 km from the seismic lines. Nine wells are located in the Campos Basin and six in each the Santos and Pelotas basins. The majority of wells reaches the Aptian basin fill; only five of them penetrates the Hauterivian-Barremian volcanic rift deposits. Well information includes checkshot surveys, formation tops, lithofacies data and standard log suites (i.e. gamma ray, sonic, density and resistivity). In addition, biostratigraphic data from one well in each basin is available.

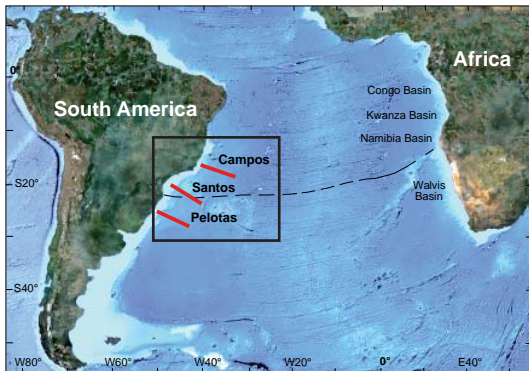
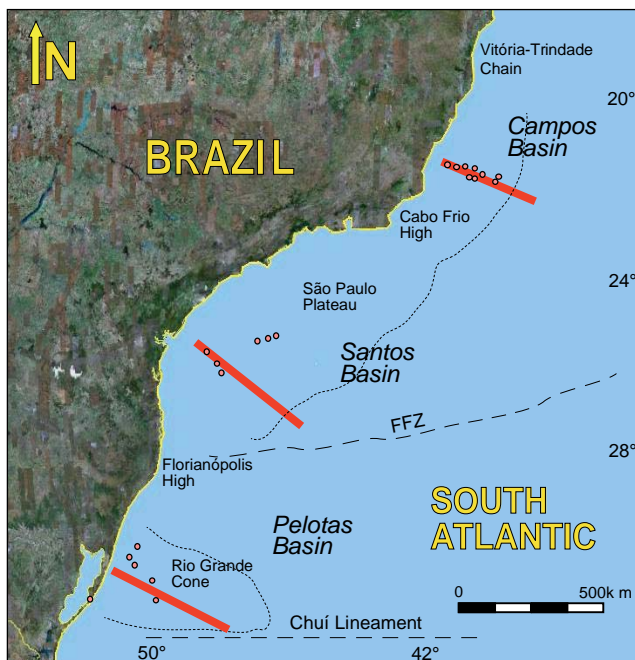


Fig. 1.2 Study area on the Southeastern Brazilian margin, including the Campos, Santos and Pelotas basins. Red lines indicate the 2D seismic reflection profiles and red points indicate the location of the correlation wells.



1.4 Thesis outline and objectives

This thesis consists of five chapters, starting with the general introduction and description of the analytical and modeling methods, followed by three other chapters which correspond to individual papers published or submitted to peer-review scientific journals (see Appendix).

Chapter 3 includes the sequence stratigraphic interpretation and subsidence analysis of twelve to fourteen second-order depositional units (3-50 m.y. duration) established within the Barremian-Holocene basin fill (130-0 Ma). A description of the modeling procedure, key parameters and software is included; further information is available in Appendix A. Key objectives of this section include: (i) seismic interpretation, mapping of key regional seismic reflectors and their tie with the bio-/chronostratigraphic ages and formation tops from the calibration wells; (ii) classification of the the seismo-stratigraphic units in terms of the internal stratal patterns, boundary stratigraphic surfaces, lithologies and depositional environments.

Chapter 4 presents a comprehensive quantitative analysis of the subsidence evolution and the restoration of the basin architecture and paleowater depths during the Barremian-Holocene basin development. Main objectives of this contribution are: (i) quantified rates of total subsidence, its genetic components (thermo-tectonic, flexural and compaction-induced subsidence) and sediment supply; (ii) structural analysis and interpretation of the seismic geometries as a function of accommodation space and sedimentation; (iii) location of the continental-oceanic crust transition and its implications for the subsidence distribution and development; (iv) determine the individual impact of subsidence, eustasy and sediment supply on the depositional patterns; (v) the implications of plate-tectonic forces for the configuration of the margin, including lithospheric deformation, changes in sea-floor spreading rates and far-field intra-plate deformation.

Based on the seismo-stratigraphic framework, subsidence and sediment supply data derived from inverse-basin modeling, Chapter 5 includes the forward stratigraphic modeling of the Barremian-Holocene sedimentary basin infill. This method allows to reproduce the basin development at a temporal scale of 2 m.y. duration, and predict the ancient basin conditions. Sensitivity analysis of the input data and a set of user-defined variables provided best-fit values of several sedimentary and deformation processes on the basin development and distribution of lithofacies. Key objectives include: (i) quantify physical controls on the precipitation of evaporites and sediment dispersal systems, with particular emphasis on rates of subsidence, sediment supply, erosion and transport methods; (ii) determine the main tectonic controls on the basin configuration, including syn-rift crust deformation, evolution of sediment source areas and salt deformation; (iii) construct a plausible tectono-stratigraphic model with the best-fit to the present-day tectono-stratigraphic configuration, showing the distribution of lithofacies and porosity; (iv) appraise the most relevant controls on the deep-water basin architecture and hydrocarbon potential, including causal mechanisms and occurrence of turbidites, mass transport complexes and bottom-currents.

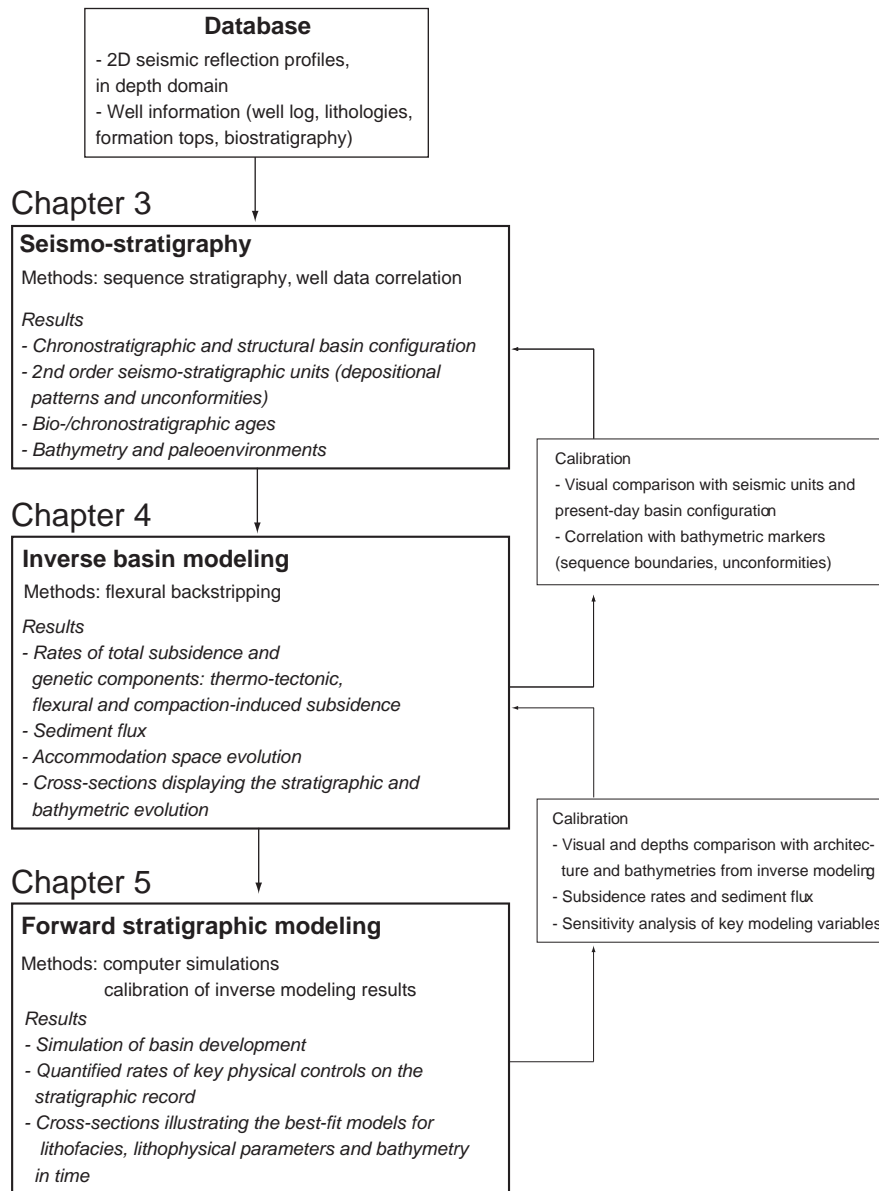


Fig. 1.3 Basin analysis workflow

1.5 Geological setting

1.5.1 Geodynamic evolution and structural framework

During the Triassic distension phase and rupture of the Pangea mega-continent (250-200 Ma), the Gondwana and Laurasia blocks evolved separately (Moulin et al., 2010). Intra-continental extension of Gondwana was initiated in the Jurassic with a period of major flood basalts (Karoo volcanism; Eagles and König, 2008). As a result, Africa and South America formed two separate plates, which split apart since the Early Cretaceous (approx. 145-140 Ma). Although kinematics of the South Atlantic opening still involve numerous uncertainties, it is widely accepted that rifting initiated in the south of the Argentinean-African margins, and propagated northward to the Brazilian

and West African margins (Rabinowitz and LaBrecque, 1979; Stollhofen et al., 1998; Mohriak et al., 2002; Torsvik et al., 2009; Moulin et al., 2010). Existing reconfigurations of the continental divergence history indicate that seafloor spreading along the Pelotas-Namibia margin started during the Hauterivian (133-130 Ma). From the Barremian to Aptian (130-112 Ma) magmatism and accretion of oceanic crust continued across the Santos Basin (Meisling et al., 2001; Mohriak et al., 2002), and reached the Campos Basin by Early Albian times (112-110 Ma; Moulin et al., 2010). Based on these margin reconfigurations and structural analysis, five tectonic stages controlled the evolution of the Pelotas, Santos and Campos basins: (1) pre-rift, Jurassic to Valanginian; (2) syn-rift, Hauterivian to late Barremian; (3) syn-rift sag, late Barremian to Late Aptian; (4) post-rift, early-middle Albian; (5) drift, late Albian to Holocene (Chang et al., 1992; Karner et al., 1997, 2003; Bassetto et al., 2000).

During the Barremian-Aptian continental break-up (stages 2 and 3), distinct mechanisms of lithosphere deformation along the length of the Pelotas-Campos margin segment took place. In the southernmost Brazilian continental margin, the Pelotas Basin is floored by Hauterivian-Barremian volcanic deposits (seaward dipping reflectors, SDRs) affected by high-angle extensional faults. The nature of the lower crust remains uncertain, but by analogy with the Namibian conjugate margin (Gladchenko, et al., 1998; Bauer et al., 2000; Talwani and Abreu, 2000), it may correspond to a high-density igneous crust-mantle interface intruded by the Tristan da Cunha plume. North of the Florianópolis Fracture Zone (FFZ), the configuration of the crust changes. The structural configuration of the lithosphere below the Campos and Santos basins displays two crust domains with different deformation styles: the upper crust layer is affected by brittle extension below the shelf and gradually thins in direction to the modern continental slope, where extensional faulting appears to be absent; the lower crust layer (5-10 km thick) displays major stretching and seem to be affected by magmatic intrusions toward the transition to oceanic crust (Aslanian et al., 2009). These interpretations are consistent with another investigations on syn-rift continental deformation (Kusznir and Karner, 2007; Huisman and Beamont, 2008), which indicate that depth-dependent stretching and exhumation of the lower crust/mantle domain represent the dominant processes leading to continental break-up along the Santos-Campos margin segment.

During the Aptian syn-rift sag phase in the Santos and Campos basins, thermal subsidence widely distributed along the shelf-slope transition, and generated restricted sediment depocenters with smooth topography and relative uniform paleobathymetries (from 600 m to 950 m of water depth). Approximately in the Late Aptian, arid climate conditions and high evaporation rates (Skelton, 2003) triggered hypersaline conditions in these marginal sag basins. As a result, widespread evaporite precipitation occurred along Southern Atlantic conjugate margins, which eventually prolonged toward the Equatorial Atlantic domain (Davison, 2007). With the continental break-up along the Santos-Campos margin segment in the Late Aptian-Albian, fully oceanic circulation in

the Brazilian continental margin occurred. During the Cenomanian-Holocene drift development, differential thermal contraction and increasing flexural sediment loading controlled the creation of accommodation space and development of the continental slope, accompanied by intense salt remobilization in the Santos and Campos basins. Halokinesis-related structures include salt diapirs, listric, inverse and thrust faults, turtle and rollovers structures, which represent potential stratigraphic-structural traps for hydrocarbon accumulations.

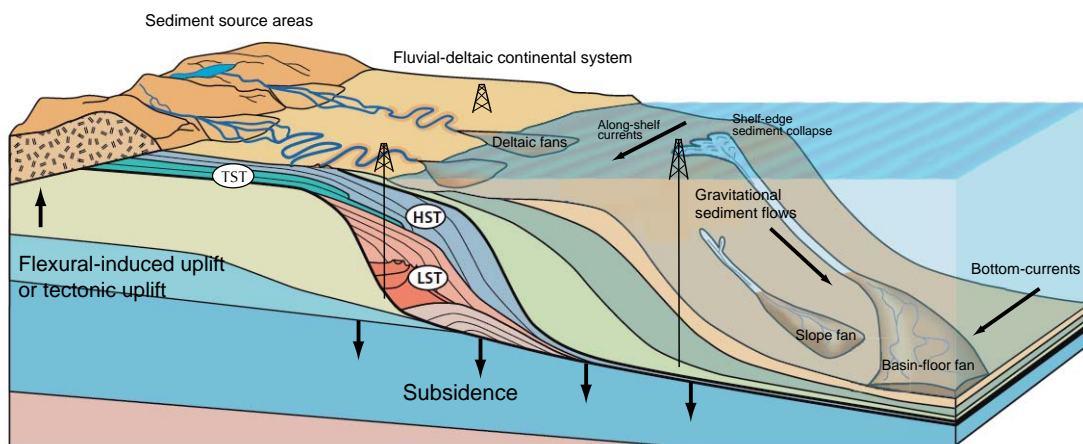


Fig. 1.4 Source to basin dynamic depositional systems, indicating key sedimentary and deformation processes affecting the stacking patterns and deep-marine deposition.

1.5.2 Basin infill and hydrocarbon prospectivity

The tectono-stratigraphic evolution and sedimentary infill of the Pelotas, Santos and Campos basins was initially analyzed based on exploratory 2D seismic reflection profiles and wells along the continental shelf areas to the upper slope (Pereira et al., 1986; Guardado et al., 1989; Mohriak et al., 1990; Rangel et al., 1994; Pereira and Feijó, 1994; Fontana, 1996). Due to the large hydrocarbon reservoirs present in the Barremian-Miocene sedimentary basin infill, exploration activities migrated toward the deep-marine setting. During this development, economic risk assessments demanded technological advances in drilling techniques, acquisition and processing of geophysical data. It has made available high-resolution deep seismic, gravity and magnetic profiles, which allow to interpret the deep structure of the crust and improve the existing models on lithosphere deformation and chronostratigraphy of the sedimentary basins offshore Brazil (Bassetto et al., 2000; Karner, 2000; Karner and Gambôa, 2007; Winter et al., 2007; Moreira et al., 2007; Bueno et al., 2007).

In this study, the analyzed stratigraphic succession comprises the Barremian to Holocene interval (130-0 Ma), which includes from the last part of the syn-rift stage to the present-day mature drifting (tectonic stages 2 to 5). The Barremian succession in the Pelotas Basin consists of volcanic series (SDRs) and intercalated continental siliciclastic deposits toward the top. The time-equivalent succession in the Santos and Campos comprises continental-transitional sedimentary deposits with sporadic volcanic intervals toward the base. Late Barremian-Early Aptian global anoxic conditions (Skelton, 2003) allowed the deposition of lacustrine organic-rich shales and mud-rich carbonates in deep fault-bounded syn-rift depocenters. Up-section, Middle to Late Aptian carbonate and fluvial-deltaic deposits and evaporites distributed across the Santos and Campos sag depocenters. The salt succession shows thicknesses of up to 2-2.5 km and represents a regional seal for sub-salt hydrocarbon systems. At the same time, open-marine conditions during the initial stage of seafloor spreading characterized the Pelotas Basin.

After continental break-up in the Middle Aptian (Pelotas Basin) to Albian (Campos, Santos basins), the post-rift development was characterized by major carbonate progradation to aggradation. During the Cenomanian to Coniacian early drift stage (99.6-89.3 Ma), carbonate platforms were drowned during coastal transgression and deposition of marine shales. A period of deep-water anoxia in the late Cenomanian-Turonian allowed regional deposition of organic-rich shales and marls (Mello and Maxwell, 1990). This succession represents proven hydrocarbon source rocks in the Santos Basin (Coward et al., 1999). From the Santonian to the Maastrichtian (85.8-65.5 Ma), different depositional patterns characterized each of the basins investigated. In the Santos Basin, thick sediment wedges prograded basinward. In the Campos and Pelotas basins, overall coastal retrogradation prevailed to the Maastrichtian. The Paleogene and Neogene (65.5-0 Ma) basin fill reflects the complex interactions of accommodation space, sediment supply and salt-induced deformation. In general, the Campos and Pelotas basins were controlled by overall Paleocene-Holocene coastal progradation, which was interrupted by short-term periods of retrogradation to aggradation. In the Santos Basin, a predominant Paleocene-Oligocene retrogradational pattern changed to progradation-aggradation since the Early Miocene. With the continental margin development, differential subsidence (basin tilting) and increasing sediment load triggered intense salt remobilization. Salt-related structures (e.g. diapirs, rollover structures) form potential structural-stratigraphic hydrocarbon traps in the Late Cretaceous-Neogene succession. At the same time, salt welds and extensional faults formed migration pathways from the sub-salt source rocks (i.e. Late Barremian-Aptian lacustrine shales) to post-salt reservoirs, including Albian mixed carbonate-clastic successions and Late Cretaceous-Neogene turbidites.

Hydrocarbon prospectivity in the Santos and Campos basins extend from the shallow to the ultra-deep water region and involve a variety of reservoirs above and below the salt, including Neocomian-Barremian fractured basalts near the top of the continental basement, Barremian to Aptian

carbonates and fluvial-deltaic successions, Early Albian carbonates, and Late Albian-Miocene turbidites. These intervals have been charged principally from Barremian-Aptian source rocks deposited in graben basins with restricted saline lacustrine environments (Mello and Maxwell, 1990). Thermal modeling and vitrinite reflectance analyses indicate that these organic-rich intervals reached adequate depths and temperature conditions for oil generation during the Eocene (Guardado et al., 2000). In the Pelotas Basin, comparable hydrocarbon systems have not been found so far. The main uncertainties refer to the presence of good-quality and mature source rocks, which appear to be absent in the Barremian-Aptian syn-rift succession. Alternative organic-rich intervals include Permian lacustrine shales, but they seem overmature. In addition, Cenomanian-Turonian and Tertiary marine shales show adequate overburden thicknesses for oil generation, but their quality and organic content have not been determined. Nonetheless, exploration activities have recently increased due to the occurrence of gas hydrates confirming the presence of hydrocarbons in the Paleogene-Neogene deep-marine succession (Costa and Silva, 2010).

2. Methods and applicability in the southern Brazilian margin

The initial phase of the project addresses the 2D seismo-stratigraphic interpretation of the three seismic sections and the correlation with sedimentologic and stratigraphic data from the calibration wells. SMT Kingdom 7.5 software package was used to carry out the seismic interpretation, well correlation and seismic-well tie. The second phase includes the numerical basin analysis, integrating inverse-basin and forward stratigraphic modeling. The models were constructed using PHIL™ software (Process- and History- Integrated Layers; Bowman and Vail, 1999), which provide synthetic chronostratigraphic plots than can be compared with the seismic and well data.

2.1 Sequence stratigraphy

The term 'sequence' defines a conformable succession of genetically related strata bounded by unconformities (Sloss, 1963; Mitchum, 1977). It represents the primary unit of a sequence stratigraphic model (Payton, 1977). Based on this concept and the interpretation of stratal geometries in seismic reflection profiles, the term 'seismic stratigraphy' was introduced by Vail et al. (1977), and was directly related with the construction of the global eustatic sea-level chart. The original approach of 'sequence stratigraphy' considered eustasy as the main controlling factor on the stacking patterns into a depositional sequence and the type of its bounding unconformities.

Since the 1980s, different authors have adopted distinctive approaches to define a depositional sequence and the bounding stratigraphic surfaces (Posamentier, et al., 1988; van Wagoner et al., 1990; Hunt and Tucker, 1992). These investigations considered the effects of the tectonic subsidence on the signature of eustatic sea-level events, and incorporated outcrop and well data. As a result, the term 'relative sea-level' (or 'base level') was introduced to describe the dynamic surface of balance between erosion and deposition controlled by the interaction of eustasy and subsidence. The space between the base level and the depositional substratum defines the amount of accommodation available for sedimentation. Therefore, the interaction between sediment supply and accommodation space exert the main control on the direction of the shoreline: either transgression if the shoreline migrates in the basinward direction, or regression if it migrates landward (Posamentier and Vail, 1988).

Sequence stratigraphy aims to analyze the stratigraphic record and unconformities in terms of the rates of sedimentation and accommodation space (Catuneanu, 2006). This method allows to classify a succession of strata based on the stacking patterns and their bounding stratigraphic surfaces. Catuneanu et al. (2009) present a synopsis of the most important sequence stratigraphic models and summarize their scopes, limitations and reliability. The large applicability of sequence stratigraphy lies on the variety of disciplines involved (sedimentology, geomorphology, structural geology, basin analysis, oceanography) and the different datasets that can be analyzed.

Sequence stratigraphy represents one of the most used geophysical-geological tools in basin analysis, which can be employed in a variety of sedimentary environments, from continental to deep marine settings, and including siliciclastic and carbonate lithologies. The integration with well data (lithologies, biostratigraphy, geophysical logs) allows the evaluation of the main controls on the sedimentary history and determine the individual influence of subsidence/uplift trends, eustasy and sediment supply on the stratigraphic record.

Based on interplay of sediment supply and accommodation space available, three main types of sediment stacking patterns can occur: (i) retrogradation (transgression), when accommodation outpaces sedimentation and the coastline migrates in the landward direction; (ii) aggradation, when sedimentation and accommodation are in balance, generating vertical sedimentation and a steady position of the coastline, (iii) progradation (regression), when sedimentation outpaces the accommodation space and the coastline migrates in the basinward direction (Fig. 2.1). Furthermore, according to the driving factor on a regressive trend (either base level or sediment supply), it can be classified in: ‘forced regression’ when the base level falls and the coastline is forced to regress irrespective of sediment supply, generating wide exposure and strong erosion of the shelf top (sequence boundary type 1; Vail et al., 1984); ‘normal regression’ when the sediment supply

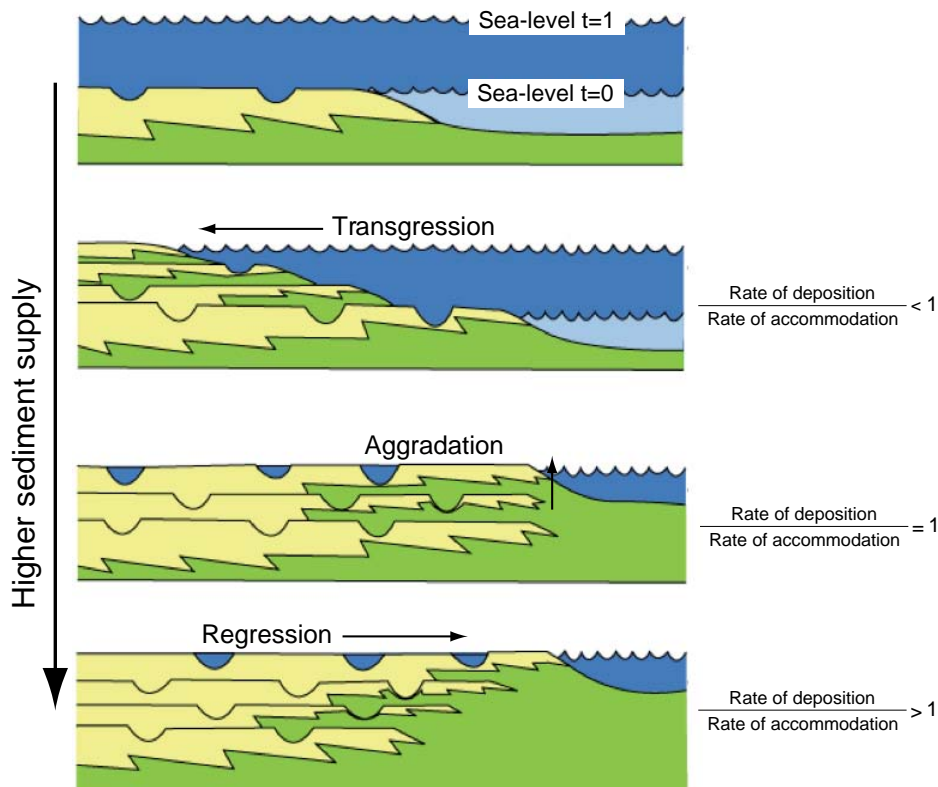


Fig. 2.1 Sediment stacking patterns and migration of the coastline according to the relationship accommodation-sedimentation rates.

surpasses the accommodation available and the coastline regresses, generating only minor exposure and erosion of the shelf top (sequence boundary type 2).

The succession of sediment deposited during any of these particular stages of shoreline shift form a 'system tract', which represents the basic stratigraphic unit within a depositional sequence. Systems tracts are interpreted based on stratal stacking patterns, position within the sequence and types of bounding surfaces, and are assigned particular positions along an inferred curve of base-level changes at the shoreline (Fig. 2.2).

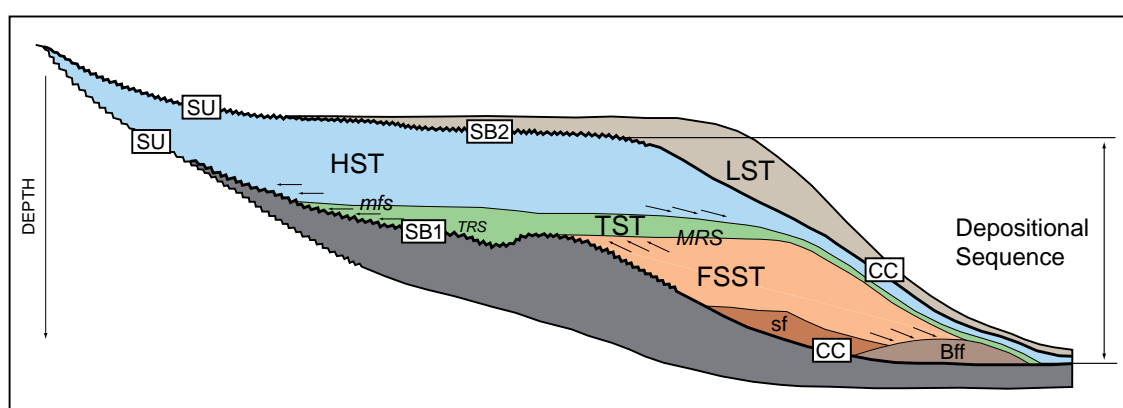


Fig. 2.2 Systems tracts and bounding stratigraphic surfaces. The sequence boundaries at the base and top are marked by subaerial unconformities (SU) along the shelf top and their correlative conformities (CC) basinward. According to the causal factor on the unconformity and rate of erosion of the shelf, sequence boundaries can be classified in type 1 (SB1, widespread erosion) and type 2 (SB2, minimal erosion). The lower part of the succession in the deep marine setting comprises the slope (sf) and basin-floor fans (bff) deposited during a major sea-level fall triggering a falling-stage system tract (FSST; forced regression). The maximum regressive surface (MRS) forms when progradation shifts to retrogradation, which marks the base of the transgressive system tract (TST). The maximum flooding surface (mfs) defines the base of the highstand system tract (HST), characterized by normal regression to aggradation. A subaerial unconformity type 2 (SB2) marks the base of the lowstand system tract (LST) of the next depositional sequence. Small arrows indicate the dominant internal stratal terminations (Modified from Catuneanu, 2006).

Sequence stratigraphic framework of the Campos, Santos and Pelotas basins

The basal boundary of the sedimentary succession in the Campos, Santos and Pelotas basins is defined by a high-amplitude reflector of Barremian age (130 Ma), which represents the top of the rheological basement. Beneath this reflector, seismic geometries indicate a different configuration of the crust between the Pelotas and the Santos-Campos basins: i) in the Pelotas basins seaward dipping reflectors (SDRs) affected by high-angle extensional faults evidence the volcanic nature of this margin segment; ii) in the Campos and Santos basins, although great salt thicknesses obscure the pre-Barremian reflector arrangements, it was certainly determined that SDRs are limited and the extensional faults show lower angles than in the Pelotas basins.

Above the Barremian reflector, the sedimentary basin fill show major differences between the three basins analyzed: i) in the Campos Basin, Barremian-Holocene thicknesses range between 1,600 m on the inner shelf and 9,400 m on the lower slope-basin margin; ii) in the Santos Basin, thicknesses range between 800 m and 5,300 m; iii) in the Pelotas Basin, the Barremian to Holocene thicknesses range between 1,700 m and 7,500 m. The twelve to fourteen seismic reflectors mapped were tied with biostratigraphic data and formation tops from the calibration wells, and integrated with existing paleo-environmental reconstructions (e.g. Koutsoukos, 1987; Dias-Brito, 1987; Pereira and Feijó, 1994; Rangel et al., 1994) and the formal chronostratigraphic units defined in previous studies (Winter et al., 2007; Moreira et al., 2007; Bueno et al., 2007). This result in a consistent sequence stratigraphic model for the Barremian-Holocene sedimentary basin infill, including ages, lithologies and depositional environments for each the Pelotas, Santos and Campos basins, which represent the input information for subsequent inverse-basin modeling.

2.2 Inverse-basin modeling

Numerical basin modeling is one of the most efficient computer-aided tools to reconstruct and genetically analyze the sedimentation patterns and unconformities in the stratigraphic record. Furthermore, basin modeling allows to predict the stratal geometries and characteristics of the basin infill beyond the temporal resolution of the input data or between control points. It is widely used in the academic and industry community to better understand the evolution of sedimen-

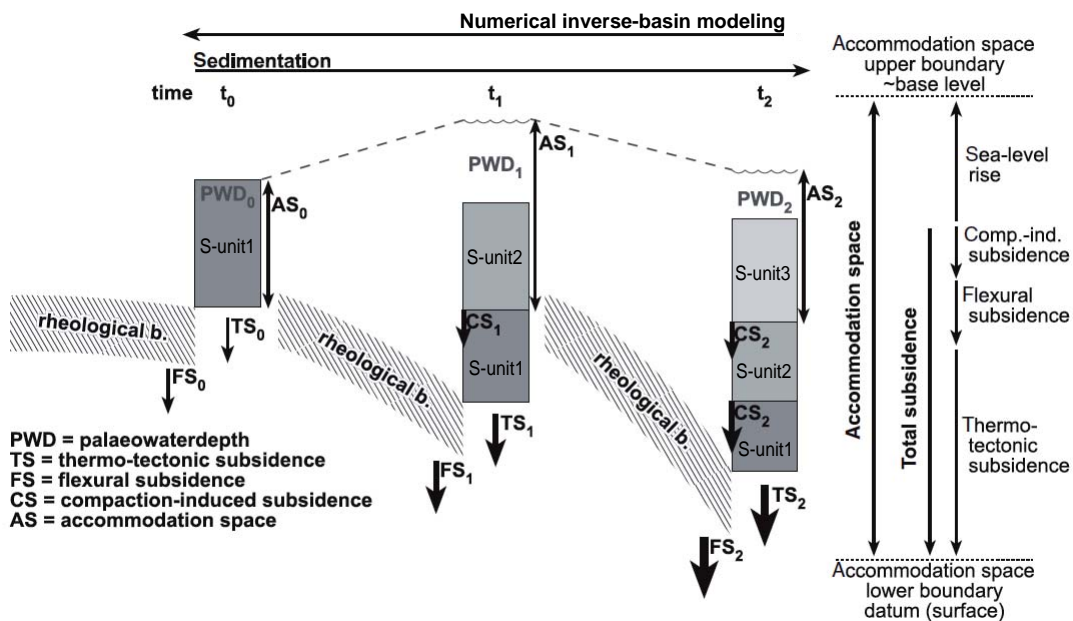


Fig. 2.3 Sketch illustrating the flexural inverse-basin modeling process ('backstripping'). x-axis, time; y-axis, burial depth; stratigraphic units (S-units 1 to 3) show different greyscales; arrows below the stratigraphic columns illustrate vectors of tectonic and flexural subsidence (thick arrow, high subsidence; thin arrow, low subsidence). The principle of development of accommodation space is illustrated on the right. Modified from Emmerich et al. (2008).

tary basins and test the impact of specific geological variables on the stratigraphic record and hydrocarbon systems. Although this method can be applied to different tectonic regimes, it has been mostly used in extensional settings in order to determine lithosphere stretching rates, analyze the subsidence history and evaluate the physical factors determining deposition (Nadin and Kuszniir, 1995, 1996; Roberts et al., 1995, 1997, 1998; Bowman and Vail, 1999; Zühlke et al., 2004; Kuszniir and Karner, 2007; Veselovsky et al., 2008).

The stratigraphic simulator PHIL™ (Bowman and Vail, 1999) fully considers the flexural response of the lithosphere to the sediment and water loads (Fig. 3). The model is constrained by the chronostratigraphic framework of the Campos, Santos and Pelotas basins derived from seismostratigraphy and calibration wells. The modeling procedure starts with the present basin configuration and infill; then, chronostratigraphic time layers are incrementally removed and the key processes controlling accommodation space are quantified in each chronostratigraphic layer, until the top of the rheological basement (in our example the top Barremian) is reached.

Subsidence analysis and evolution of accommodation space

Numerical results from inverse-basin modeling provide quantified rates of total subsidence, its genetic components (thermo-tectonic, flexural and compaction-induced subsidence) as well as sediment flux. The obtained subsidence values depict several trends, reflecting the temporal and lateral variations in the depth of the top basement. Graphic results include cross-sections showing the restored basin architecture and paleobathymetry in each chronostratigraphic layer. In order to constrain the local-scale subsidence changes and their association with a specific basin location, four basin segments have been established and separately analyzed: shelf, upper-middle slope, lower slope, and deep basin. Sensitivity analyses of the effective elastic thickness (T_e) allow a preliminary evaluation on the implications of the flexural rigidity of the crust for the syn-rift to drift basin development.

Thermo-tectonic subsidence was the dominant control on total subsidence and creation of accommodation space from the Barremian syn-rift to the Maastrichtian early drift stage (ST1 to ST3). In the Paleogene-Neogene mature drift stage (ST4 to ST6), total subsidence is controlled by the flexural response of the crust as driven by changes in sediment flux. The compaction-induced subsidence component generally represents 10-15% of total subsidence. The lateral and temporal subsidence patterns during the Barremian and Aptian (ST1 and ST2) allowed to approximate the location of the transition from continental to oceanic crust (COT), which coincides with a fault zone and a bathymetric scarp identified in the seismic profiles of the Campos and Santos basins. During the initial post-breakup margin evolution, decreasing subsidence rates characterized all three basins (ST3). Thermal readjustment resulted from changes in sea-floor spreading rates in the

Southern Atlantic. On the other hand, flexural readjustments resulted from changes in sediment loading, which are linked to the geomorphological evolution of the mountain ranges in the hinterland (sediment source areas) and syn-sedimentary salt deformation. Based on the depositional patterns offshore, the source-basin sedimentary systems have been analyzed and integrated with thermochronology data (e.g. Gallagher et al., 1994; Strugale et al., 2007; Franco-Magalhaes, 2010). Results show the close relationship between periods of exhumation of the continental highlands and progradation of the shelf margin. The mature drift stage is marked by an increase in flexural subsidence and gradual reduction of accommodation space. Eustatic sea-level fluctuations became an important factor on the sediment stacking patterns and sand volumes delivered to the deep-marine setting. The interplay between eustasy and sediment supply controlled the occurrence of turbidites, the main producing hydrocarbon reservoirs in both the Campos and Santos basins.

2.3 Forward stratigraphic modeling

Different from inverse basin modeling, forward stratigraphic modeling starts with the initial basin conditions in the Barremian (130 Ma). In this study, forward stratigraphic modeling has been applied to simulate the tectono-stratigraphic evolution and quantify physical factors controlling the distribution of lithofacies and paleowater depths (e.g. subsidence, sediment flux, erosion, transport methods, salt tectonics). It incorporates thermo-tectonic subsidence rates and sediment flux derived from inverse modeling.

During the simulation procedure, sensitivity tests of essential input variables (effective elastic thickness, subsidence rates, sediment supply) provided the most suitable values to achieve the stratal geometries and lithologies from the seismic and well datasets. The parameters are repeatedly calibrated within a geologically reasonable range, according to the chronostratigraphic framework and inverse modeling results. Therefore, the best-fit model can be achieved by different combinations of input parameters, leading to a limited range of possible geological scenarios. Nonetheless, the combination of inverse-basin and forward modeling in this study allows to progressively adjust the results and recognize the main factors introducing inaccuracies in the final model.

Stratigraphic simulation and main controls on the basin development

Forward stratigraphic modeling allows to quantify the key structural and sedimentary controls on the basin development and construct a consistent model for the tectono-stratigraphic evolution and distribution of lithofacies in each the Campos, Santos and Pelotas basins. Using sensitivity analysis of crust-related parameters (e.g. effective elastic thickness and flexural wavelength), it is possible to simulate the implications of syn-rift volcanism and depth-dependent stretching for

the configuration of the crust as well as erect a conceptual model for the different crust deformation styles between the Pelotas and the Campos-Santos margin segments. According to this hypothesis, these processes appear to have been crucial for the formation of deep lacustrine depocenters with deposition of hydrocarbon source rocks and the precipitation of evaporites in the Campos and Santos basins. As observed in the seismic and well data, each of the studied basins developed highly distinct architectures during the post-rift to drift development. The main controlling factors on these particular developments include: (i) the different mechanical behaviour of the crust between the Pelotas volcanic-margin segment and the Santos and Campos non-volcanic segments; (ii) the evolution of the sediment source areas and drainage systems in the onshore domain, triggering major variations in the sediment supply between basins; (iii) the interplay of flexural sediment loading and salt deformation; (iv) sand volumes delivered to deep-marine setting and the influence of bottom-currents.

3. Seismic stratigraphy of key segments of the southern Brazilian continental margin: Campos, Santos and Pelotas basins

3.1 Introduction

Although the Pelotas, Santos and Campos basins shared a comparable rift origin during the Early Cretaceous break-up of Gondwana, the stratigraphic signature of syn-rift lithosphere deformation and the post-rift geodynamic evolution is highly variable between the three basins. A number of studies on the southern Brazilian rifted margin have focused on the tectono-stratigraphic evolution of these marginal depocenters and its implications for the hydrocarbon potential (Ojeda, 1982; Guardado et al., 1989; Mohriak et al., 1990, 2008; Karner and Driscoll, 1999a; Davison, 1999, 2007; Bassetto et al., 2000; Karner, 2000; Cobbold et al., 2001; Meisling et al., 2001; Modica and Brush, 2004; Bueno et al., 2007; Karner and Gambôa, 2007; Moreira et al., 2007; Winter et al., 2007). However, most of these investigations are focused on a single basin and its most prolific sedimentary units, providing precise and high-resolution tectono-stratigraphic analysis, but with different temporal and spatial scales between the basins. Besides, the variety of geophysical and geological datasets (seismic, gravity and magnetic profiles, stratigraphy and sedimentology from wells) are not always homogeneous between the basins, and therefore they neither allow direct comparisons nor consistent regional-scale interpretations. The seismo-stratigraphic model in this study has been constructed on comparable seismic and well datasets in each basin, which facilitate the identification of correlation markers and tie the basin-specific stratigraphic record into the regional geodynamic framework. Key objectives of the seismo-stratigraphic interpretation include: (i) a rigid sequence stratigraphic framework for the continental shelf top to deep basin margin; (ii) the relationship between seismic sequences and the basin development; (iii) qualitative analysis of controlling factors on the stratigraphic geometries and unconformities, and their subsequent validation by quantitative basin modeling (Chapters 4 and 5).

3.2 Database and methods

3.2.1 Seismic transects and time-depth conversion

Fig. 3.1 shows the 2D seismic and well data supplied by ANP Brazil and TGS-NOPEC for this study. Lines from the Santos (320 km long) and Pelotas (340 km) basins were available in depth domain. The line from the Campos Basin (300 km) had to be time-depth converted, based on seismic stacking velocities.

3.2.2 Well data and correlation

Calibration wells were employed to tie the interpreted seismo-stratigraphic units and sequence boundaries with the formation tops and bio-/chronostratigraphic ages. Table 3.1 includes the

Barremian-Holocene stages of basin evolution, seismo-stratigraphic units, sedimentary thicknesses and lithologies from the available wells, and integrated with the formal chronostratigraphic units defined in previous studies (Fontana, 1996; Winter, et al., 2007; Moreira et al., 2007; Bueno et al., 2007). In addition, an outline of paleoenvironments based on facies and biostratigraphic data from three wells was available (Figs. 3.2, 3.3 and 3.4).



Fig. 3.1 Location of 2D seismic reflection profiles (red lines) and correlation wells (red points). Dashed lines represent the main structural-bathymetric provinces. FFZ: Florianópolis Fracture Zone.

3.2.3 Seismic stratigraphy

Twelve to fourteen seismic reflectors were traced for each basin, which define depositional units of second order (3-50 m.y. duration; Catuneanu, 2006) with specific stratal geometries. From their stacking patterns, four types of depositional units were recognized: forced regressive (FR), normal regressive (NR), retrogradational (RT) and aggradational-progradational (AP) (nomenclature after Catuneanu et al., 2009; Neal and Abreu, 2009). Based on the stratigraphic configuration and data resolution, subaerial unconformities and their correlative conformities define sequence boundaries type 1 or type 2 (see Section 2.1; Vail et al., 1984; Catuneanu, 2006). Intervals of high salt thicknesses and intense halokinesis cause a reduction in the seismic resolution below the Late Aptian salt succession. Therefore, the top Barremian-Aptian reflectors have been interpreted based on seismic facies outside salt domains. Uncertain formation tops were interpolated based on check-shots and synthetic seismograms. The integration of all seismic and well data resulted in a coherent chronostratigraphic framework, which represents the input information for inverse-basin and forward stratigraphic modeling.

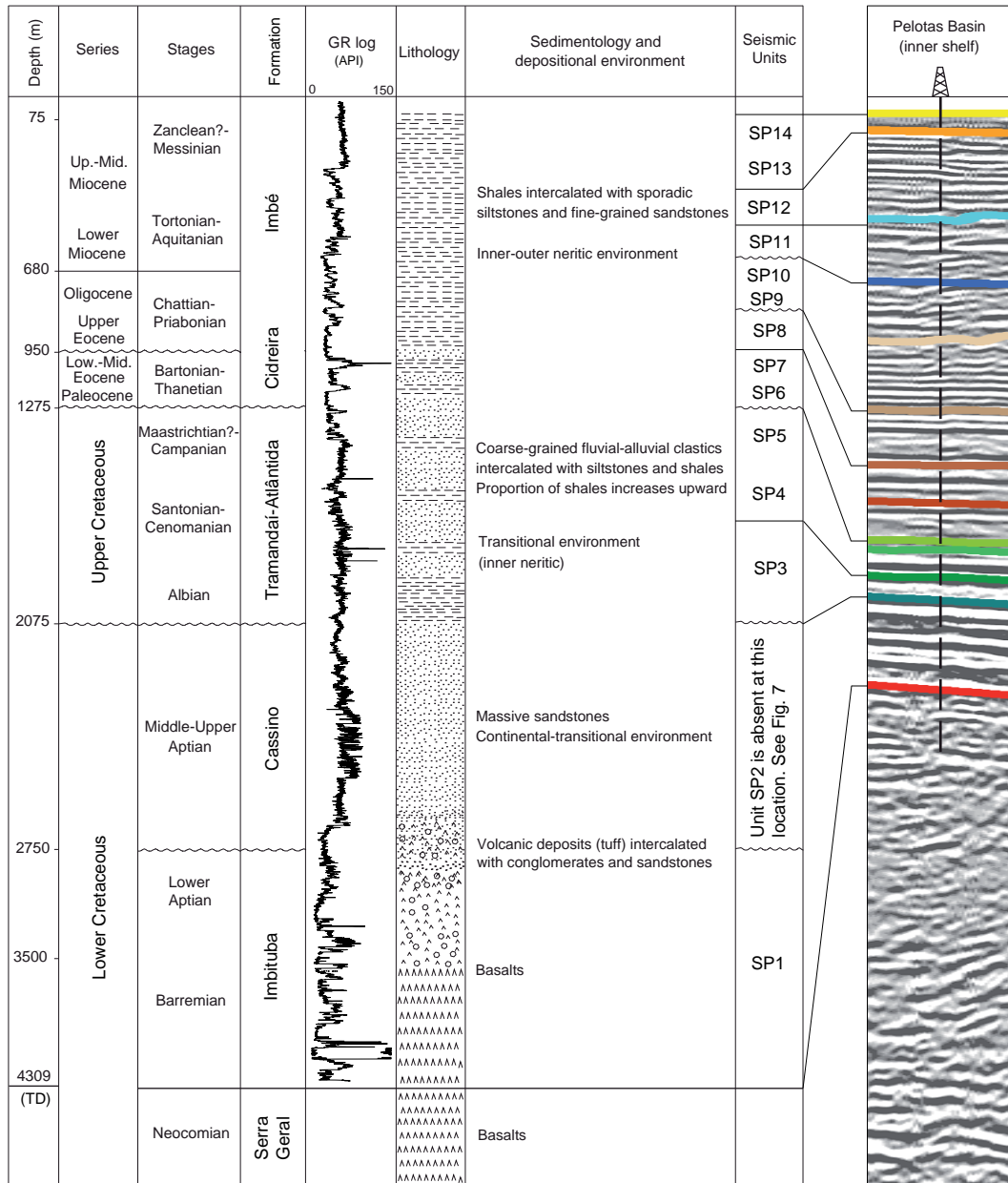


Fig. 3.2 Well-seismic tie in the Pelotas Basin. Location of the well is shown in Fig. 3.5. Total depth (TD) of the well: 4,309 m, in the Barremian unit. Information used for well-seismic tie includes: unconformities, biostratigraphic ages, lithologies, GR log and stacking patterns. Seismic units SP1-SP14 are described in Tables 3.1 and 3.2.

3.3 Structural framework

The Atlantic Hinge Zone extends sub-parallel to the continental margin between 30-50 km offshore in the Pelotas to Campos basins and continues northward to the Brazilian equatorial margin (Matos, 2000). This hinge zone was originated during the Hauterivian and late Barremian phase of extension (Karner et al., 1997, 2003). To the west of the hinge zone, the continental basement is shallow, approximately horizontal and unconformably overlain by up to 2,000 m of Aptian-Albian to Holocene sediments. To the east, the continental basement and the overlying Barremian-

3. Seismic stratigraphy

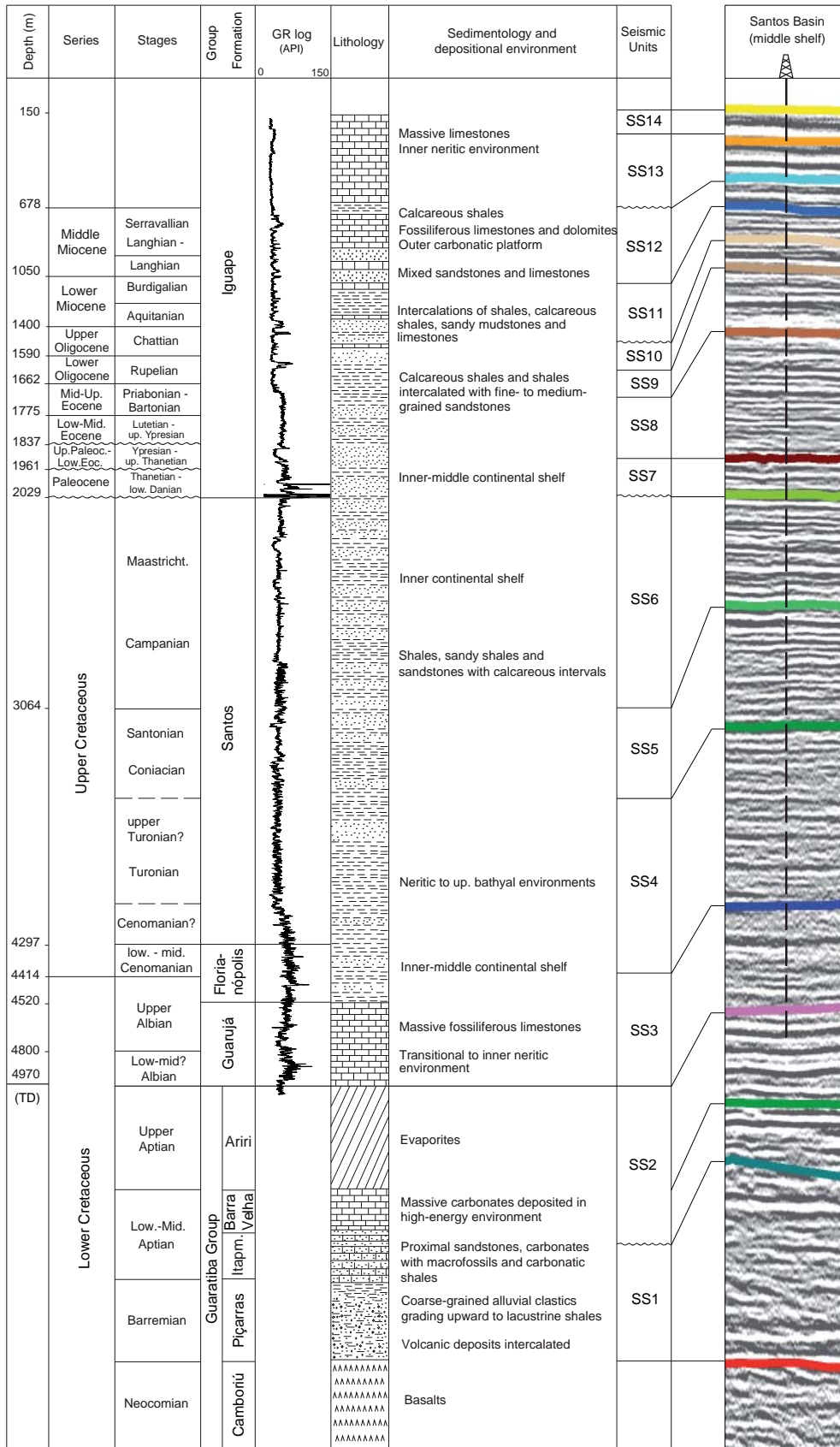


Fig. 3.3 Well-seismic tie in the Santos Basin. Location of the well is shown in Fig. 3.6. Total depth (TD) of the well: 4,970 m, Upper Aptian. Information used for well-seismic tie includes: unconformities, biostratigraphic ages, lithologies, GR log and stacking patterns. The Lower Aptian-Neocomian basin fill includes lithologic data from adjacent wells and previous studies (Moreira et al., 2007). Seismic units SC1-SC12 are described in Tables 3.1 and 3.2.

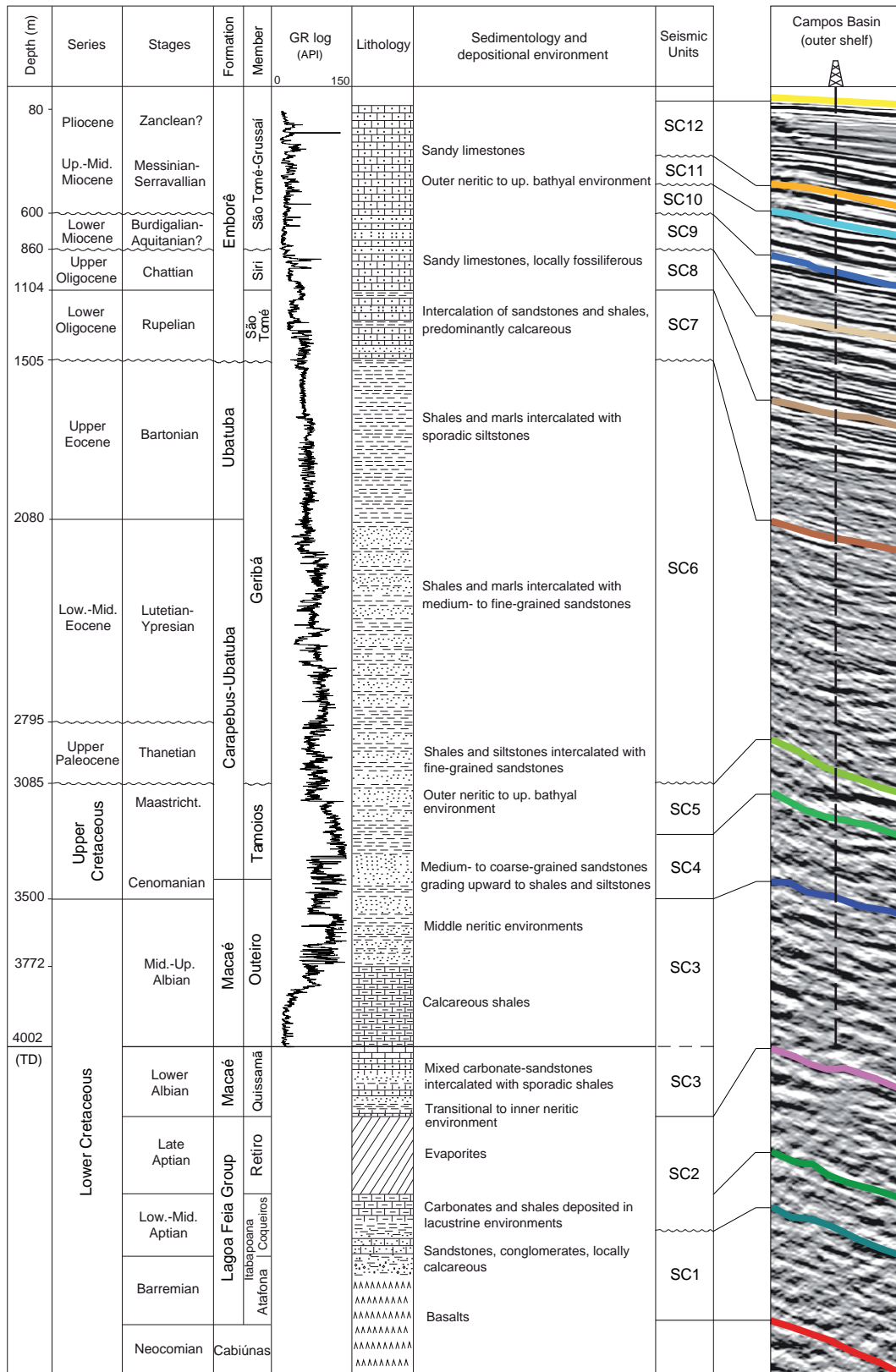


Fig. 3.4 Well-seismic tie in the Campos Basin. Location of the well is shown in Fig. 3.7. Total depth (TD) of the well: 4,002 m, middle Albian. Information used for well-seismic tie includes: unconformities, biostratigraphic ages, lithologies, GR log and stacking patterns. The lower Albian-Neocomian basin fill includes lithologic data from adjacent wells and previous studies (Winter et al., 2007). Seismic units SC1-SC12 are described in Tables 3.1 and 3.2.

Table 3.1 Integrated chronostratigraphy (well data) and sequence stratigraphy (seismic) of the Barremian-Holocene basin fill. Between twelve and fourteen seismic units have been recognized in each of the Campos (SC1-SC12), Santos (SS1-SS14) and Pelotas (SP1-SP14) basins. Formation names (in italic type) are based on existing stratigraphic studies (Winter, et al., 2007; Moreira et al., 2007; Bueno et al., 2007). Sequence stratigraphic surfaces include: SB1: type 1 sequence boundary, SB2: type 2 sequence boundary, SB2: type 2 sequence boundary, MRS: maximum flooding surface; MRS: maximum regressive surface; TRS: transgressive ravinement surface; D: disconformity, ES: local-scale erosional surface.

Period	Epoch	Age (Ma)	CAMPÓS BASIN		SANTOS BASIN		PELOTAS BASIN															
			Seismic units	Well information	Seismic units	Well information	Seismic units	Well information														
Cretaceous	Upper	Paleoc.	DRIFT	SC 12	São Tomé Mb.: sandst., calcareous sandst. and shales. Up to 1,200 m Grussal Mb.: calcareous sandstones and limestones. 200 m	DRIFT	SS 14	SP 14	Imbé Fm. Widespread deposition of shales and siltstones. Up to 3,500 m													
				SC 11	Siri Mb.: calcareous sandstones with microfossils. 250 m			SS 13	Ponta Aguda Fm. Sandstones with sporadic siltstones and shales. Up to 1,200 m													
				SC 10	Mid-low. slope: <i>Carapebus and Ubatauba fms.</i> (Geribá Mb.)			SS 12	Iguape Fm. Shales, marls and calcareous sandstones. 425 m													
				SC 9				SS 11														
				SC 8	São Tomé Mb.: sandstones, calcareous sandstones and shales. Up to 800 m			SS 10	Marambaia Fm. Outer shelf to slope, shales, marls siltstones and sporadic coquinas. Up to 1,490 m													
				SC 7	Grussal Mb.: calcareous sandstones and limestones. 300 m			SS 9														
			DRIFT	SC 6	<i>Carapebus Fm. and Ubatauba Fm.</i> (Geribá Mb.). Up to 1,000 m	SS 8		SS 7	<i>Ponta Aguda and Marambaia fms.</i> Approx. 60 m	SP 6												
				SC 5	<i>Carapebus Fm.</i> : sandstones, siltstones with sporadic conglomerates and shales. 530 m	SC 4	<i>Ubatuba Fm.</i> (Tamoios Mb.): shales, marls and sporadic diamictite. 460 m	SS 6	Santos Fm.: sandstone (turbidite intervals) intercalated with siltstones and shales. 2,500 m	SS 5	Juréia Fm.: not reached by available wells											
					Goitacás Fm.: fluvial-deltaic sandstones and conglomerates. 200 m		<i>Itajaí-Açu Fm.</i> : hemipelagic fine-grained sediments; sporadic turbidite sandstones. Intercalated basalts. 1,120 m															
				Lower	Albian	112	SC 3	Outeiro Fm.: calc. shales, limestones, dolomites, sporadic sandstones. 500 m	POST RIFT	SS 4	Florianópolis Fm.: alluvial-deltaic sandstones and shales. 115 m	SP 5	Cidreira and Imbé fms. Sandstones and siltstones with sporadic shales. Maximum thickness 800-1,000 m									
							SC 2	Retiro Fm.: halite, anhydrite. Up to 350 m						SS 3	Guarijá Fm.: carbonates and sands. 830 m							
							SC 1	Lagoa Feia Gp.								SAG	Macaré Gp.	Atriri Fm.: halite, anhydrite, dolomites. 180 m	SS 2	Tramandaí Fm.: sandst., siltstones, shales Atlântida Fm.: calcareous shales and marls. Total thickness 1,900 m		
		Lagoa Feia Gp.	Macaré Gp.					Cassino Fm.: sandstones, conglomerates and siltstones. Approx. 330 m														
																					Coqueiros Fm.: fine sandstones, shales, limestones. 250 m	Cassino Fm.: sandstones, conglomerates and siltstones. Approx. 220 m

Holocene sediment wedge dip oceanwards. Sediment thicknesses increase to more than 7,500 m toward the oceanic domain with strong differential basin subsidence and tilting of the basement. The Barremian-early Aptian succession onlaps the basement topography at the hinge zone in the landward direction. In a seaward direction, it dips with angles of 30°-35° in the Santos and Pelotas basins and 15° in the Campos Basin. The Albian to Holocene basin fill shows lower dips, between 10° and 15°, in the three analyzed reflection profiles.

The Barremian-Holocene succession in the Santos and Campos basins show comparable tectono-stratigraphic features, whereas the Pelotas Basin differs considerably (Figs. 3.5, 3.6 and 3.7). In the latter basin, the Barremian-Aptian basin fill extends from the continental shelf to the deep marine basin, and consists of reflectors with long lateral continuity only disrupted by high-angle extensional faults below the continental shelf. Syn-rift deep half-grabens were not recognized (Fig. 3.8). Aptian salt and consequently salt deformation is absent. Within the Paleogene-Neogene succession, local tectonic and flexural readjustments generated high-angle faults. In addition, mud diapirs affect the deep-marine succession along the lower slope.

In the Santos and Campos basins, the following structural features are recognized: (i) listric and high-angle extensional faults, which affected the continental crust and Barremian-early Aptian volcanic series and clastic deposits; (ii) salt domes on the continental slope; (iii) salt-induced listric, inverse and thrust faults in the Late Cretaceous and Tertiary supra-salt sediments; (iv) a fault zone between the lower slope and abyssal plain. Fault-bounded half-grabens recognized on the shelf to upper slope (Fig. 3.8a, b) record the Hauterivian-late Barremian extensional phase leading to continental break-up. Unfaulted sub-parallel reflectors of early-middle Aptian age cap these extensional depocenters and continue toward the central-distal parts of the basin. The salt province of the Santos and Campos basins spans approximately 230 km in NW-SE direction and reaches from the middle shelf to the lower slope-abyssal plain transition. Salt deformation includes upslope extensional and downslope compressional structures. On the middle-outer shelf of the Santos Basin, salt deposits are between 600-700 m thick and internal reflectors are barely disturbed (Fig. 3.9b). However, on the continental slope, salt deformation triggered highly variable thicknesses and chaotic, contorted reflector packages. In the Campos Basin, salt is approximately 300-400 m thick and internally composed of contorted reflectors. Thickness increases to approximately 2,800 m on the lower continental slope, where only few reflectors can be traced between salt domes. (Fig. 3.9a).

Toward the lower continental slope of the Santos and Campos basins, the distal edge of the salt province is marked by a bathymetric scarp, which coincides with a fault zone and an abrupt change in the basin topography (Figs. 3.6 and 3.7). This scarp has been tentatively interpreted as the signature of the transition from continental to oceanic crust (COT), although subsequent quantitative basin analysis will clarify the significance of this feature.

3.4 Basin fill

Based on stacking patterns and well information, the Barremian-Holocene basin fill in the Santos, Campos and Pelotas basins has been divided in 12-14 stratigraphic units (Table 3.1). They form coherent seismo-stratigraphic frameworks, which facilitate the reconstruction of basin architecture and comparison between the basins. Based on the available biostratigraphic data, depositional environments have been interpreted (Figs. 3.2, 3.3 and 3.4). Recent studies (Bueno et al., 2007; Moreira et al., 2007; Winter, et al., 2007) provided litho-/chronostratigraphic information used to calibrate the stratigraphic units. Ages and regional distribution of the seismo-stratigraphic units are shown in Figs. 3.5, 3.6 and 3.7. Additionally, the insets of Figs. 3.8, 3.9 and 3.10 illustrate smaller-scale reflector patterns and specific architectural features. Table 3.2 summarizes reflector

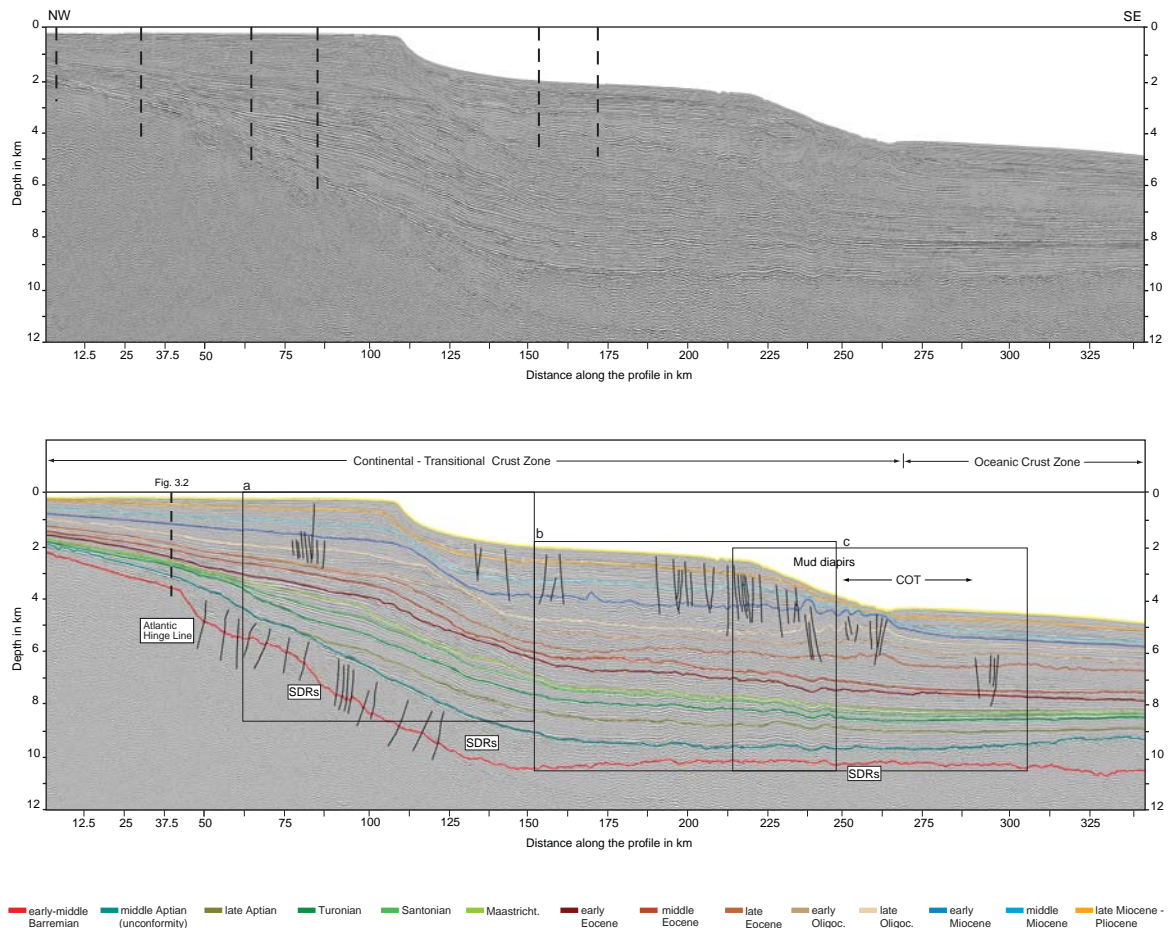


Fig. 3.5 Uninterpreted and interpreted seismic reflection profile of the Pelotas Basin (depth domain). Location in Fig. 1. Vertical exaggeration 8:1. Dashed lines indicate the location of the available wells. Inset (a) shows high-angle extensional faults crossing SDRs (Neocomian) and igneous-clastic (Barremian) series (Fig. 3.8a). SDRs are imaged from the continental shelf to the lower slope; they represent transitional crust (also named proto-oceanic crust) accreted during the initial continental rupture in the southern Atlantic margin. The basin geometry is characterized by flexural prograding wedges; salt deposits are absent. Inset (b) shows reflector truncations near the shelf break, which resulted from recurrent Tertiary transgressive/regressive depositional trends (Fig. 3.9a). In the lower slope-abyssal plain transition, mud diapirs and listric faults disrupt the Paleogene succession. Inset (c) shows the eastern edge of Neocomian-Barremian SDRs near the transition from continental/transitional to entirely oceanic crust (Fig. 3.10a).

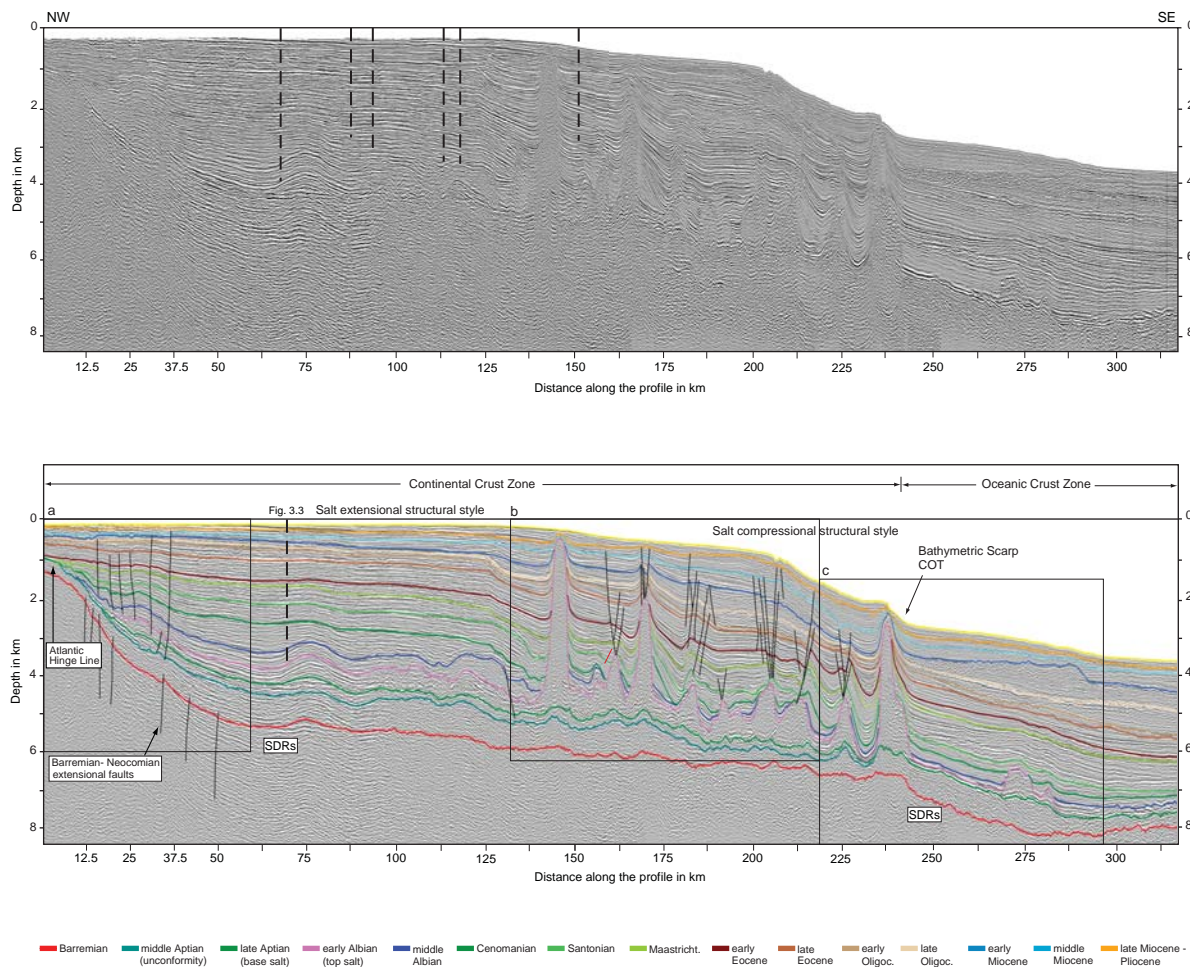


Fig. 3.6 Uninterpreted and interpreted seismic reflection profile of the Santos Basin (depth domain). Location in Fig. 1. Vertical exaggeration 8:1. Dashed lines indicate the location of the available wells. Inset (a) shows high-angle extensional faults crossing the continental basement (Neocomian) and overlying igneous-volcaniclastic series of Barremian age (Fig. 3.8b). High-angle faults in the Late Cretaceous-Tertiary successions suggest reactivation of syn-rift extensional structures. On the continental shelf, salt deposits are nearly horizontal and undeformed (salt extensional structural style). Inset (b) shows compressional salt deformation along the continental slope, which generated narrow and prominent salt anticlines, which propagate vertically almost to the sea-bottom (Fig. 3.9b). They separate sedimentary depocenters and turtle structures (salt compressional structural style); conjugate listric and growth faults are observed in the crest of the salt diapirs. Inset (c) shows the eastern limit of SDRs, which coincides with the transition from continental to oceanic crust (COT). Further to the east (between 270-285 km), an interval of mobile salt deposited on oceanic crust (Fig. 3.10b).

geometries, depositional trends and sequence stratigraphic surfaces, i.e., sequence boundaries (SB), maximum regressive surfaces (MRS), transgressive ravinement surfaces (TRS) and maximum flooding surfaces (mfs).

Major differences between the three basins include: (i) In the Pelotas Basin, the Barremian to Holocene thicknesses range between 1,700 m and 7,500 m. Available well control reaches the Barremian basin fill at a maximum depth of 6,100 m on the continental shelf. Three wells close to the seismic line reach only the Lower Tertiary (Imbé/Cidreira Fms.). Information from further two wells reaching the Barremian had to be projected into the seismic lines for distances of 1-30 km

3. Seismic stratigraphy

introducing limited uncertainties in the bio-/lithostratigraphic subdivision of the basin fill. (ii) In the Santos Basin, the Barremian to Holocene thicknesses range between 800 m on the inner shelf and 5,300 m on the lower slope. Available well control reaches the Aptian at a maximum depth of 4,970 m (Ariri Fm.) on the upper slope. (iii) In the Campos Basin, Barremian to Holocene thicknesses range between 1,600 m on the inner shelf and 9,400 m on the lower slope-basin margin. Available well control reaches the basement on the shelf, but only the Aptian at a maximum depth of 4,630 m (Lagoa Feia Fm.) on the slope.

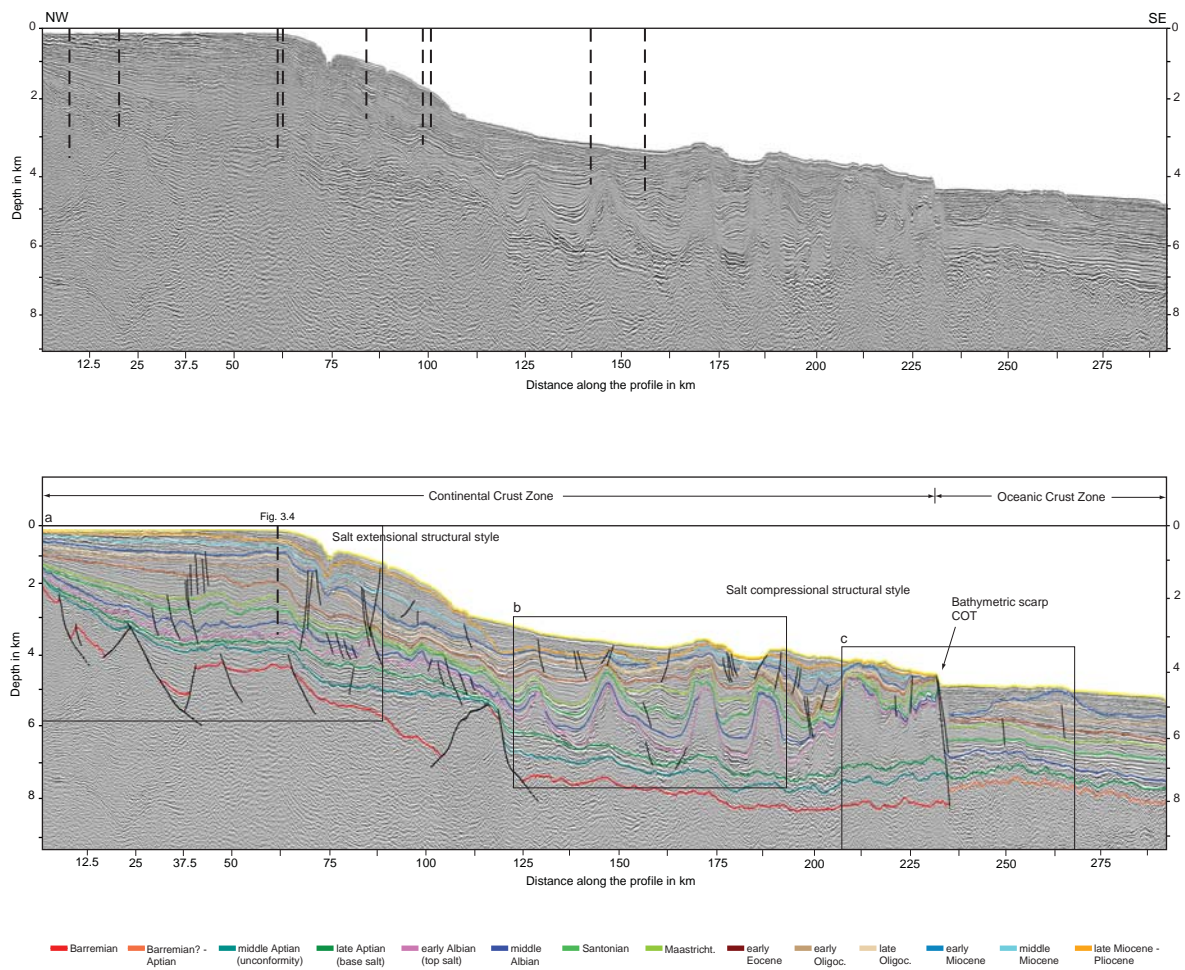


Fig. 3.7 Uninterpreted and interpreted seismic reflection profile of the Campos Basin (depth domain). Location in Fig. 1. Vertical exaggeration 8:1. Dashed lines indicate the location of the available wells. Inset (a) shows syn-rift asymmetric half-grabens of Barremian-Early Aptian age from the continental shelf to the middle slope (Fig. 3.8c). The middle Aptian unconformity (117 Ma) truncates underlying syn-rift reflectors. Middle Aptian-early Albian unfaulted and extended reflectors represent fluvial-deltaic and lacustrine deposits (sag basin fill) grading upward to evaporites. Salt anticlines intrude the Late Cretaceous-Tertiary successions. Salt-related structures along the shelf-middle slope (extensional salt structural style) include basinward dipping rafts, rollover structures and listric faults. Inset (b) shows reverse faults and salt thickening on the middle-lower slope (salt compressional structural style; Fig. 3.9c). Inset (c) shows the transition from continental to oceanic crust (COT), which marks the distal edge of the sag and salt successions at the foot of the continental slope (Fig. 3.10c).

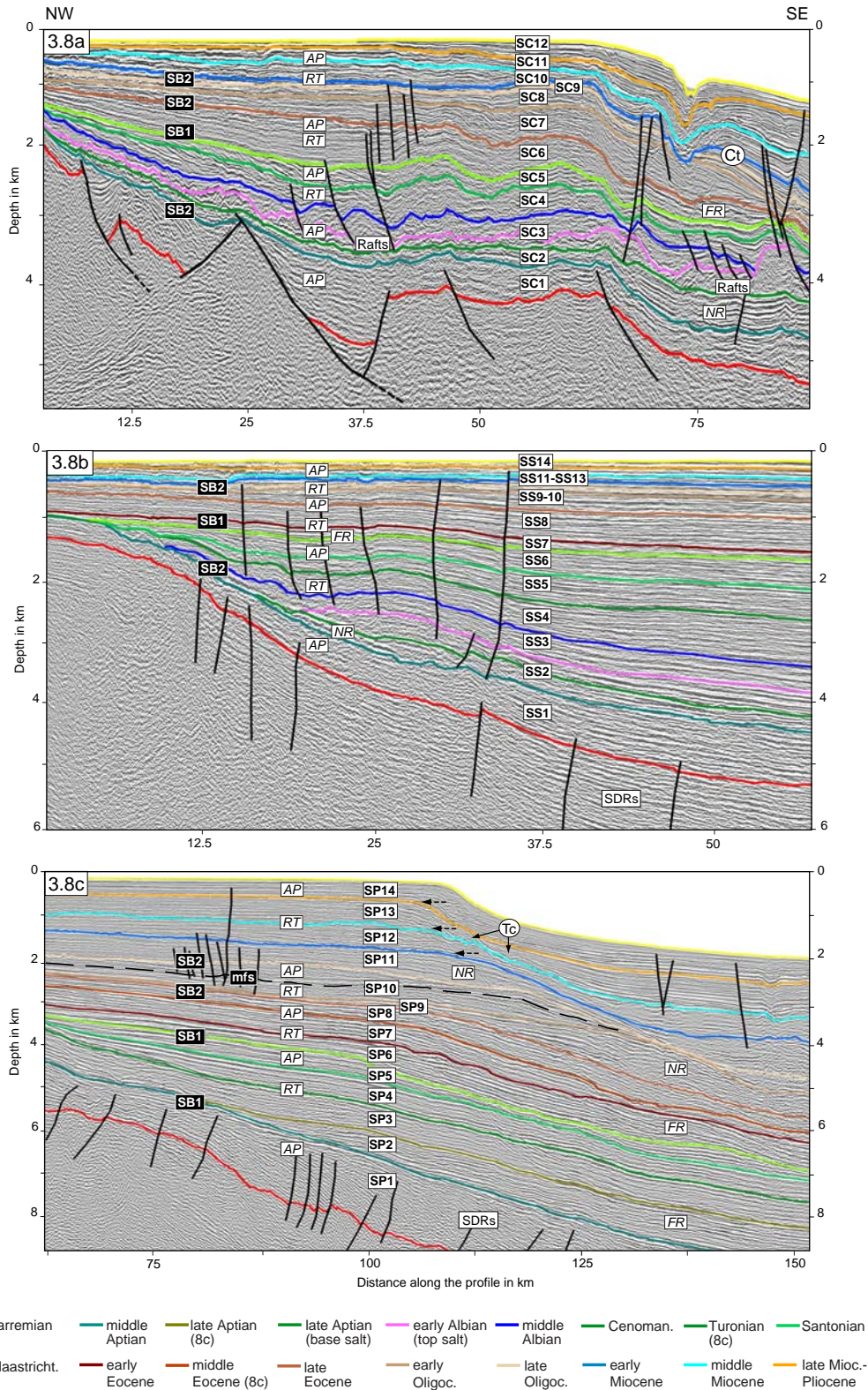


Fig. 3.8 Insets of the interpreted seismic reflection profiles on the inner-middle continental shelf of the Pelotas (3.8a), Santos (3.8b) and Campos (3.8c) basins. For locations see Figs. 3.5, 3.6 and 3.7 respectively. Seismo-stratigraphic units (bold type) are described in Tables 3.1 and 3.2. Depositional patterns (italic type) and sequence stratigraphic surfaces (white letters, black background) include: FR forced regression; NR normal regression; AP aggradation-progradation; T transgression; SB1, SB2 sequence boundary type 1 or 2 respectively; mfs maximum flooding surface. Each basin shows a specific syn-rift basin architecture. In the Pelotas Basin, high-angle extensional faults die out in the middle Barremian succession. In the Santos Basin, high-angle extensional faults affect the upper Barremian basin fill, and in the Campos Basin the early Aptian. In the Pelotas Basin, the middle-late Aptian succession (SP2) represents the transition to the post-rift stage; in the Campos and Santos basins, this succession constitutes the sag basin fill (SC2 and SS2). Highly deformed salt and post-salt successions on the Campos shelf include listric faults and rafts; in the Santos shelf, the salt succession is barely disturbed and shows nearly horizontal reflectors. In the Pelotas Basin, salt is absent; sub-parallel reflectors are only affected by stratigraphic surfaces and crustal flexure. Bottom current channels and contourites (Ct) cut into the Upper Oligocene-Holocene basin fill (SC8-SC12) of the Campos Basin. In the Pelotas Basin, turbidite channels (Tc) affect the Lower-Middle Miocene basin fill (SP12-SP13). Offset and landward migration of the shelf-break is marked with dashed arrows.

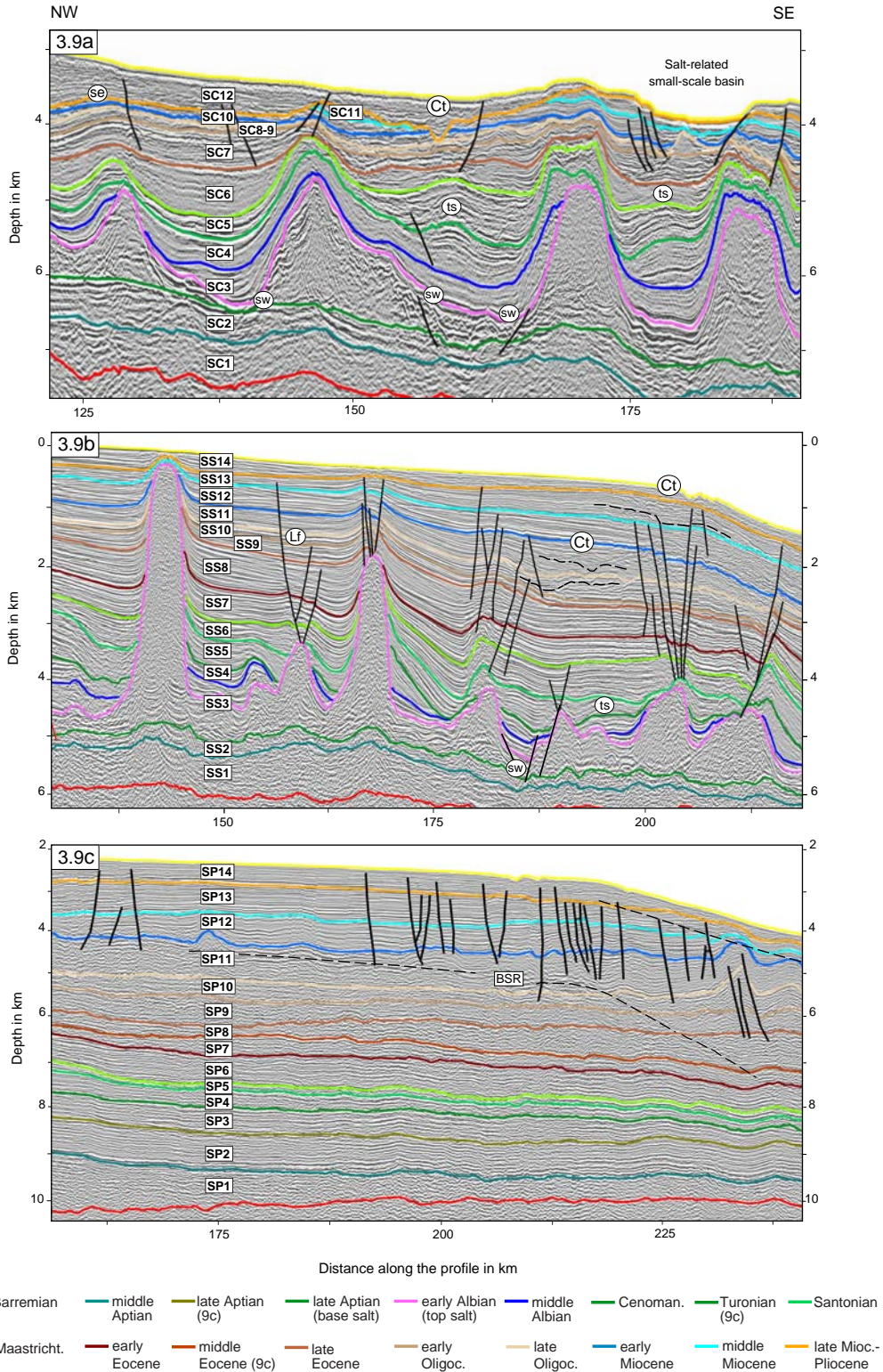


Fig. 3.9 Insets of the interpreted seismic reflection profiles on the continental slope showing the flexural basin fill in the Pelotas Basin (3.9a), and the salt diapiric province in the Santos (3.9b) and Campos (3.9c) basins. For locations see Figs. 3.5, 3.6 and 3.7 respectively. Seismo-stratigraphic units (bold type) are described in Tables 1 and 2. The middle Aptian unconformity (and its correlative conformity) is identified in all three seismic profiles (base of units SC2, SS2, SP2). The base of evaporites in the Campos Basin is marked by a high-amplitude reflector (late Aptian, 115 Ma). In the Santos Basin, this surface either was not possible to recognize due to intense salt doming or is absent. Salt anticlines show internal chaotic facies. Onlap against salt diapirs and turtle structures (ts) characterizes the post-rift to drift succession in the Campos and Santos basins. Salt-related listric faults (Lf) affect the entire Late Cretaceous-Tertiary basin fill. Salt remobilization and faulting generate salt welds (sw). In the Campos Basin, Late Miocene-Pliocene gravity-mass flows, bounded at the base by an erosion surface (se), affect the Oligocene-Miocene succession (units SC10-SC11); on the middle-lower slope, turbidite-contourite systems (Ct) are recognized. In the Pelotas Basin, salt deformation is absent and only high-angle faults disrupt the seismic reflectors; bottom simulating reflectors (BSR) suggest the accumulation of gas hydrates.

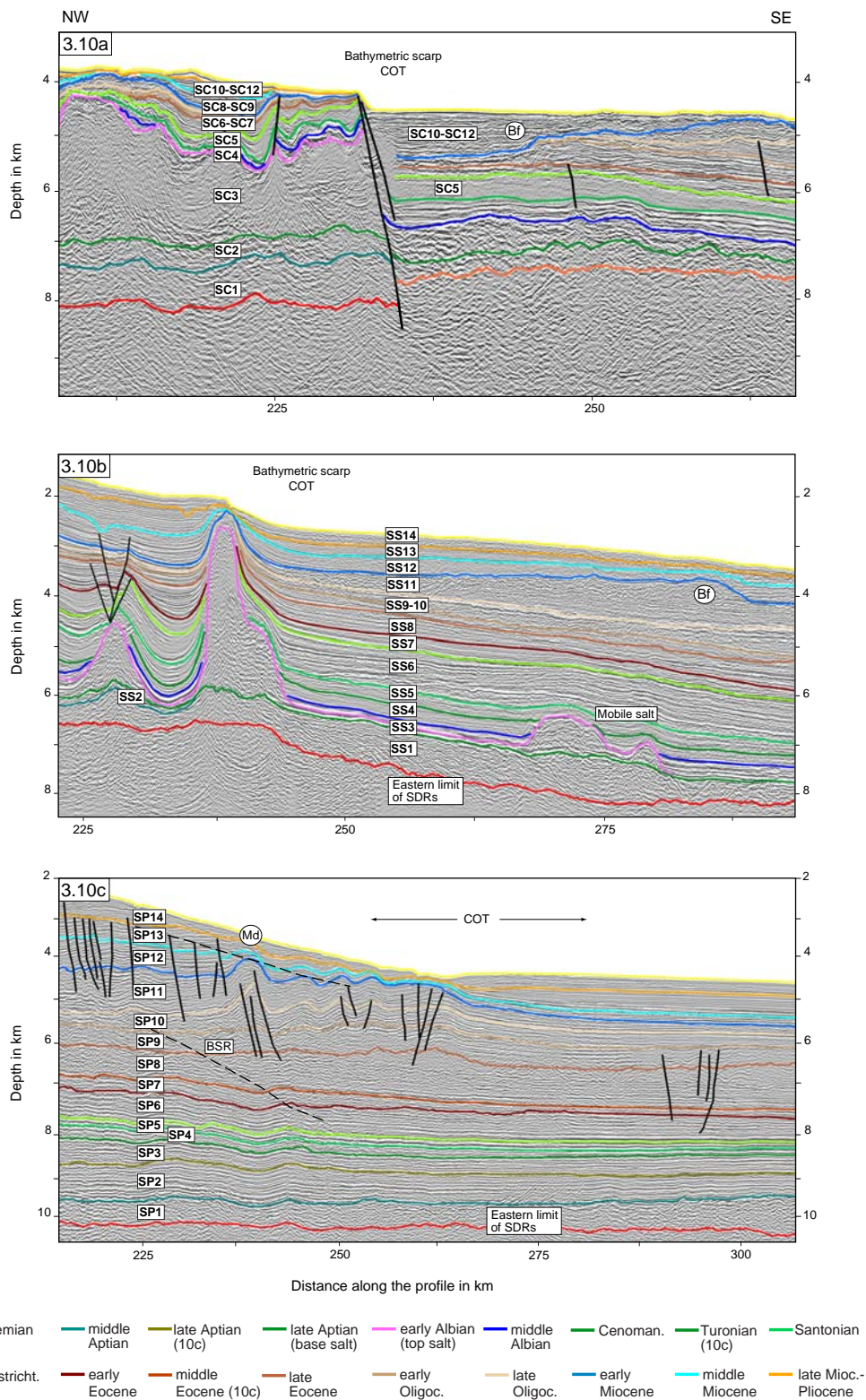


Fig. 3.10 Insets of the interpreted seismic reflection profiles across the distal basin margin of the Pelotas (10a), Santos (10b) and Campos (10c) basins. For locations see Figs. 3.5, 3.6 and 3.7 respectively. Seismo-stratigraphic units (e.g. SC1-SC12) are described in Tables 1 and 2. The transition from continental to oceanic crust (COT) is marked by a bathymetric scarp (10b, 10c). In the Santos Basin (10b) an interval of mobile salt overlies SDRs and oceanic crust; in the Campos Basin (10c), this feature defines the eastern salt edge. In both the Santos and Campos basins, Miocene gravity mass flows cut into the Oligocene succession and form basin floor fans (Bf). In the Pelotas Basin, the transition from continental/proto-oceanic crust to oceanic crust covers a wide distance (approx. 30 km). In the lower continental slope, mud diapirs (Md) and listric faults affect the Oligocene-Miocene basin fill. Bottom simulating reflectors (BSR) suggest the occurrence of gas hydrates.

3.4.1 Barremian to middle Aptian

The Barremian-middle Aptian syn-rift interval has been defined by Karner et al. (1997) and Bate et al. (1999) based on ostracod zonations from the Gabon-Angolan margin. Derived from integrated quantitative kinematic-isostatic modeling, Karner and Driscoll (1999b) established a correlation between the West African and southeastern Brazilian margins.

Pelotas Basin

The base of unit SP1 is defined by a seismic reflector at depths of 2,000 m to 9,000 m between the continental shelf and basin margin. On the shelf, wedges of seaward-dipping reflectors (SDRs) are truncated by high-angle extensional faults (Fig. 3.8c), which cut into the lower Barremian basin fill above (~130-128 Ma) and the basement below. Up-section, prograding sigmoidal reflectors represent mixed volcanic series and clastic deposits, which extend over the whole Pelotas continental margin and reach thicknesses between 250 m and 900 m. On the middle slope, reflectors become sub-horizontal and continuous toward the deep basin margin (Fig. 3.9c). The top of the seismic unit SP1 is marked by an early Aptian unconformity (~122 Ma), interpreted as a type 1 sequence boundary (SB1), with large subaerial exposure of the shelf to the modern upper slope. According to the available well information and to published results (Dias et al., 1994; Bueno et al., 2007), this succession is composed of Barremian basalt flows (Imbituba Fm.) and late Barremian-Aptian continental alluvial deposits (Cassino Fm.), passing basinward to marine shales. In contrast to the Santos and Campos basins, there is no evidence available for organic-rich shales in syn-rift depocenters of the Pelotas Basin.

Santos Basin

The basal reflector of unit SS1 extends from a depth of 1,000 m underneath the continental shelf to 7,800 m below the basin margin (Fig. 3.6). No wells reaching the pre-Aptian succession were available for the study. The lower part of the basin fill has been interpreted based on reflector terminations and geometries. On the continental shelf, extensional faulting dies out into middle-upper Barremian reflectors; this interval shows a maximum thickness of 500 m on the continental shelf and 1,000 m on the continental slope. Toward the lower slope, unit SS1 thins and amalgamates with seaward-dipping reflectors (SDRs) (Fig. 3.10b). Above, unfaulted prograding sub-parallel reflectors of early Aptian age dip basinward. Internal reflectors are not well developed, but show indications for salt-related deformation. Average thicknesses vary between 300 and 400 m. A middle Aptian unconformity (117 Ma) and its correlative conformity marks the contact with the middle Aptian basin fill (unit SS2). This surface has been interpreted as a type 2 sequence boundary (SB2). Lithologic data and interpretations from Moreira et al. (2007) indicate that the Barremian-lower Aptian succession is composed of alluvial siliciclastics and distal organic-rich shales (Piçarras and Itapema Fms.). They pass upward to fine-grained lacustrine carbonates

(Barra Velha Fm.), which represent favorable source rocks. Intercalated stromatolitic carbonates have reservoir quality.

Campos Basin

On the shelf, the early basin fill (unit SC1) shows high-amplitude reflectors dipping basinward, truncated by synthetic listric faults (Fig. 3.8a). Half-grabens contain Barremian clastics with maximum thicknesses of 2,500 m, which correspond to the Itapabona and Atafona Fms. (Table 3.1). The lower-middle Barremian succession consists of progradational coarse-grained fluvial-deltaic and alluvial clastics. On the middle-lower continental slope, seismic resolution is often limited because of the high-impedance of the overlying evaporites; discontinuous reflectors define several depocenters probably bounded by extensional faults. Although sub-salt resolution is limited, there is evidence (e.g. erosional truncations) that on the upper-middle slope gravity mass flows eroded into the syn-rift basin fill. On the lower slope, a bathymetric scarp associated with a fault zone marks the distal boundary of Barremian reflectors (Fig. 3.10a). Eastward, seismic geometries are chaotic and unclear.

A thin package of sub-parallel reflectors, up to 150 m thick, caps previous extensional depocenters and forms the upper part of unit SC1. This interval represents the upper Barremian-lower Aptian succession, which is mainly composed of marls and shales, locally carbonates and intercalated fine-grained sandstones (Atafona Fm.). Similar to the Santos Basin, the contact between SC1 and SC2 is marked by a type 2 sequence boundary of middle Aptian age (117 Ma). Lithologic well data show conglomerate sandstones below this boundary and fine-grained sandstones above, which may indicate subaerial exposure of the inner-middle shelf. They pass upward into organic-rich shales and marls deposited in lacustrine environments, which include the most important source rocks offshore Brazil (Katz and Mello, 2000). Productive pre-salt reservoirs are intercalated carbonates rich in macro-fossils (Coqueiros Fm.; Pereira et al., 1984; Guardado et al., 1989; Davison, 1999).

3.4.2 Aptian-Albian transition

The Aptian/Albian basin fill of the Santos and Campos basins is similar despite the marked influence of salt diapirs. The Pelotas basin fill, however, is distinctly different.

Pelotas Basin

In the Pelotas Basin, well information shows a larger supply of siliciclastics and higher paleowater depths than in the basins to the north; these conditions inhibited carbonate deposition during the Early-Middle Aptian. Unit SP2 represents a forced regressive wedge capping the early Aptian

unconformity and has an average thickness of 800 m (Figs. 3.5 and 3.8c). Internal sub-parallel reflectors dip basinwards and downlap the upper slope. From the middle slope, reflectors become sub-horizontal and show low amplitudes toward the deep basin margin. This interval is time-equivalent to the salt succession in the Santos and Campos basins. Although the available wells do not reach this unit, located in the depth range of 6-8 km, by correlation with the shelf-interior basin (upper Cassino Fm.), fluvial-alluvial conglomerates, sandstones and intercalated shales have been interpreted. Basinward, low-amplitude reflectors suggest pelagic deposition. The volcanic Curumim Fm. (Dias et al., 1994) was not reached by the available wells and could not be recognized based on seismic facies. It is assumed to exist only in the northern part of the Pelotas Basin, near the Florianópolis High (Bueno et al., 2007).

Santos Basin

On the inner-middle shelf, unit SS2 is characterized by a package of sub-horizontal and parallel prograding reflectors with a total thickness of 300 m. They represent normal regressive fluvial-deltaic sandstones grading upward to retrogradational lacustrine calcareous shales. Basinward, reflectors are discontinuous, oblique and contorted showing average thickness of 500-600 m, which represent fine-grained siliciclastics deposited in deep lacustrine environments. The upper part of unit SS2 corresponds to widespread thick evaporites. Along the shelf, seismic reflectors remain almost horizontal, display only minor salt deformation and thicknesses vary between 600-700 m (Fig. 3.8b). The transition from the underlying clastic basin fill to the evaporites (i.e. halite with some intervals of anhydrites and dolomite) seems seismically gradational (Fig. 3.9b). On the slope, salt domes are internally characterized by chaotic seismic facies and thicknesses are highly variable; only few discontinuous reflectors can be traced at the base of the salt structures. In the deep basin margin, an interval of mobile salt is intercalated with low-amplitude reflectors and overlies seaward-dipping reflectors (SDRs) and oceanic crust (Fig. 3.10b). The facies change to the post-salt carbonates is transitional and semi-horizontal along the continental shelf. On the slope it is very irregular and defined by salt intrusions into the Upper Cretaceous-Tertiary basin fill. The age of the upper salt succession was inferred from the overlying lower Albian carbonates to be pre-110 Ma (Section 3.5.2).

Unit SS3 is characterized by sub-parallel, sigmoidal reflectors with a total thickness of up to 600 m. In its lower part, up to 200 m thick, onlap against the middle-inner shelf indicate Albian retrogradation after salt deposition. In the upper part, up to 400 m thick, reflectors downlap the inner shelf and become parallel toward the top, indicating platform aggradation to progradation. The basin fill consists of coarse-grained sandstones on the inner shelf and thick carbonates on the middle-outer shelf, which represent one of the most productive reservoirs intervals in the Santos Basin (Guarujá Fm.). On the slope, unit SS3 shows salt-related deformation. Thicknesses decrease across the

middle-lower slope. Only few sub-parallel and sigmoidal reflectors can be distinguished, which onlap against salt diapirs and form turtle structures. In the deep basin margin, discontinuous low-resolution reflectors correspond to the deep-water shales and marls of the Itanhaém Fm.

Campos Basin

On the inner-middle shelf, seismic unit SC2 consists of prograding reflectors partially contorted by salt-induced deformation. Toward the outer shelf to upper slope, high-amplitude sub-parallel and sigmoidal reflectors are observed. Directly above the middle Aptian (117 Ma) unconformity, the basin fill includes fluvial-deltaic sandstones on the inner shelf, passing laterally and vertically to retrogradational lacustrine calcareous shales. Thicknesses range from 200 m on the shelf to 500-600 m on the slope. Although salt remobilization has obscured the eastern limit of the early-middle Aptian basin fill, abrupt thinning toward the lower slope is evident in the Campos (as well as the Santos) Basin. Up-section, evaporites characterize the upper part of unit SC2.

The lower boundary of the salt basin fill dips in a basinward direction and is defined by a high-amplitude reflector identified from the inner shelf to lower slope (Figs. 3.8a and 3.9a, late Aptian horizon). Sub-parallel to contorted reflectors represent the lower salt succession (i.e. halite and anhydrite), which passes upward to chaotic seismic facies of mixed evaporite-carbonate deposits. Toward the middle slope, reflector geometries are entirely chaotic due to compressional salt deformation. Thicknesses vary between 300-400 m on the shelf to 2,800 m on the slope. In the deep basin margin, pelagic deposits of Aptian age directly overlie interpreted oceanic crust. The contact with the post-salt carbonates is transitional and semi-horizontal on the continental shelf, but very irregular on the slope where it is defined by salt intrusions into the Albian-Miocene basin fill.

Unit SC3 is strongly affected by salt-induced deformation. Sub-parallel reflectors with few onlaps against the inner-middle shelf (Early Albian retrogradation) pass laterally and vertically to sigmoidal and contorted layers, which suggest platform aggradation. On the middle-outer shelf, basin tilting and increased burial depths of the salt succession created contorted-chaotic reflection patterns and extensional listric faults, which reach upward into the Maastrichtian basin fill (Fig. 3.8a). On the slope, salt deformation caused thickness variations from 100 m to 700 m. A few downlaps of lenticular-shaped bodies in salt-related mini-basins and basal erosional contacts suggest turbidite deposition coeval with halokinesis. Toward the oceanic crust, reflectors show very low amplitudes, semi-parallel facies and erosional truncations. Four wells, located between the platform and the middle slope, penetrated up to 500 m shallow-marine carbonates of the Outeiro Fm. (Macaé Group). This formation contains porosities of approx. 15-20% and includes proven hydrocarbon reservoirs (Coward et al., 1999). Basinward, mud-rich carbonates are intercalated with carbonate-clastic gravity mass flows, a succession with apparent reservoir potential and good-quality seals.

3.4.3 Albian to Maastrichtian

After extensive carbonate platform development during the Albian, the entire southern Brazilian margin experienced long-term drowning. Depositional environments deepened continuously and each of the studied basins features a distinctive depositional pattern.

Pelotas Basin

Unit SP3 includes the interval between the Late Aptian and the Coniacian (~115-89 Ma). It is bounded at the base by a late Aptian-early Albian unconformity, interpreted as a maximum regressive surface (MRS). This succession extends from the inner shelf to the oceanic basin. On the shelf-upper slope realm, sub-parallel and sigmoidal reflectors show onlapping. On the middle slope, reflectors are sub-horizontal, conformable and continuous to the deep basin margin. This retrogradational wedge features reduced faunal diversities and average thicknesses of 500 m. The sedimentary successions penetrated by the available wells and lateral change facies suggest that clastic input continued but either decreased or became more widely distributed, allowing carbonate precipitation in the Albian. On the shelf top, fluvial-deltaic clastics (Tramandaí Fm.) intercalated with high-energy carbonates (Portobelo Fm.) pass to shales and mud-rich carbonates toward the basin (Atlântida Fm.).

The contact with the Coniacian-Santonian seismic unit SP4 is marked by an early Coniacian (90 Ma) erosional unconformity, interpreted as a transgressive ravinement surface (TRS). Above, seismic reflectors onlap the inner-middle shelf. Basinward, the reflectors become parallel, conformable and extend continuously to the lower slope and deep basin margin. Thicknesses range from 100-200 m on the continental shelf and in the oceanic basin to 700-800 m on the slope. The conformable Santonian-Maastrichtian basin fill above (unit SP5) shows aggradational parallel reflectors with long lateral continuity to the deep basin margin. Thicknesses vary between 300 m on the shelf top to 150 m on the slope to basin margin. Sigmoidal and occasional contorted reflectors with downlap terminations suggest bypass and turbidite transport toward the slope. Available well data show widespread Turonian-Maastrichtian shales and siltstones of the Imbé Fm., intercalated on the inner-middle shelf with sandstones (up to 200 m of thickness) of the Cidreira Fm.

Santos Basin

The upper Albian-Maastrichtian basin fill has been subdivided in three seismic units: (i) SS4, upper Albian-Turonian, (ii) SS5, Coniacian-Santonian, and (iii) SS6, Campanian-Maastrichtian. Unit SS4 reaches up to 650 m of thickness on the outer shelf and decreases to 120 m on the basin margin. Horizontal, high-amplitude reflectors extend over the continental platform for about 125 km, suggesting a shift to coastal retrogradation. On the slope, reflectors dip with very low

angles and are truncated by salt diapirs. An interval of late Cenomanian-Turonian organic-rich shales and marls with thicknesses of up to 250 m (Itajaí-Açu Fm.) correlates with similar lithologies in the Campos Basin. These organic shales seal both underlying Albian carbonates of the Guarujá Fm. and represent proven source rocks for the shallow-water reservoirs of the Tubarão and Merluza fields (Davison, 1999; Modica and Brush, 2004).

A Turonian-Coniacian (~90-92 Ma) disconformity marks the contact with unit SS5. This level, interpreted as a maximum transgressive surface (mfs), documents an important basinwide deepening trend. Nonetheless, paleontological data indicates that paleobathymetry remained shallower than in the Campos and Pelotas basins. From Coniacian to Maastrichtian (units SS5 and SS6), reflector geometries are very homogeneous and indicate a long-term period of coastal aggradation to progradation. Horizontal sub-parallel reflectors on the inner-middle shelf pass to sigmoidal clinofolds with basal downlap toward the outer shelf. Average thicknesses are 1,200 m, although in the diapiric province up to 2,500 m occur. These high anomalous thicknesses are related to tectonic uplift and erosion of the Serra do Mar and Serra da Mantiqueira in the hinterland (Cobbold et al., 2001). As a result, large sediment volumes were transported to the continental slope and rise and filled depocenters between salt diapirs. Sand-rich turbidite fans represent important reservoirs in salt-related stratigraphic-structural traps (Cainelli and Mohriak, 1999). The increased sedimentary loads contributed to further salt withdrawal.

Campos Basin

The upper Albian to Maastrichtian basin fill includes two seismo-stratigraphic units: (i) upper Albian-Santonian (unit SC4), and (ii) Santonian-Maastrichtian (unit SC5). In general, the Albian and Late Cretaceous successions show major variations in thickness from 200 m on the shelf to 3,000 m in salt-related depocenters (Fig. 3.7). Unit SC4 consists of sigmoidal and contorted reflectors with few onlap terminations on the inner-middle platform, which evidence the Late Albian transition from aggradation to retrogradation. These deposits are truncated by listric faults on the outer shelf to the upper slope. Basinward, reflector geometries are difficult to define; the succession becomes transparent, major thickness variations and few onlaps against the salt domes are recognized. In the deep basin margin, parallel to sub-parallel reflectors show high amplitudes. During the late Cenomanian and Turonian, deep-water anoxia caused the deposition of organic-rich shales and marls (Dias-Brito and Azevedo, 1986; Pereira, 1992). A Turonian-Coniacian (90 Ma) disconformity, which could be identified in one well, marks the upper boundary of the anoxic shales of the lower Ubatuba Fm. This surface represents a depositional hiatus during continued basin deepening as indicated by biostratigraphic data (Table 3.1). Well data shows an increase in the proportion of sandstones during the Santonian (Tamoios Mb.), and the seismic reflectors on the inner shelf show downlap terminations (upper unit SC4). These features suggest a short-term period of aggradation-

progradation, which is expected to be confirmed by subsequent basin modeling.

The Campanian-Maastrichtian unit SC5 is characterized on the shelf margin by sigmoidal and oblique reflectors with few onlap terminations on the inner shelf (retrogradation) grading laterally and vertically to downlap on the middle-outer parts (progradation). At the top, reflectors are truncated by a type 1 subaerial unconformity (SB1) of Maastrichtian-late Paleocene age. This surface was also recognized in the Santos and Pelotas basins (Table 3.1). On the upper slope, discontinuous oblique-contorted reflectors suggest significant marine erosion and turbidite deposition. In the Santonian to Tertiary basin fill, potential stratigraphic-structural hydrocarbon traps have been encountered on the continental slope. Traps frequently form lenses and turtle structures with up-dip pinch-out against salt walls, which can also be found in the Santos Basin (Figs. 3.9a, 3.9b). Pelitic sediments and basin-floor fans are characterized by discontinuous reflectors truncated by frequent erosional surfaces probably triggered by submarine currents. Well data confirm the occurrence of well-sorted sandstones with intercalated impermeable shales and marls, which fill the depocenters between salt diapirs. The sandstones show lithological and textural characteristics comparable with major turbidite reservoirs (Carapebus Fm.) described by Davison (1999) and Guardado et al. (2000).

3.4.4 Paleogene

The Cretaceous-Paleogene contact is marked by a shelf-wide erosional unconformity. This unconformity correlates with a 2nd order eustatic sea-level fall in the Late Paleocene (approx. 58 Ma, Selandian) and serves as an inter-basin marker horizon. It was clearly identified in the available wells by a Maastrichtian-late Paleocene erosional hiatus, and by truncation of the Maastrichtian reflectors in seismic. In the three studied basins, three to five stratigraphic units with variable durations constitute the Paleogene basin fill (Table 3.2).

Pelotas Basin

The Paleogene succession is composed of five seismo-stratigraphic units: SP6 to SP10. These are bounded by four regional chronostratigraphic horizons: late Paleocene-early Eocene, middle Eocene, late Eocene and Oligocene (Table 3.2). The current database does not allow to sufficiently resolve the lower Paleocene basin fill in detail (Fig. 3.2). The entire upper Paleocene-Oligocene succession (SP6-SP10) is mainly composed of fluvial-deltaic sandstones and widespread fine-grained terrigenous rocks (siltstones and shales) with low porosities and major lateral variations in thickness, from 700 m on the shelf to 2,350 m on the slope.

The upper Paleocene-lower Eocene forced regressive succession (unit SP6) is characterized by sub-parallel reflectors dipping in the basinward direction and downlapping the upper slope; this

interval is absent on the shelf (Fig. 3.8c). The upper interval consists of onlapping sub-parallel and nearly horizontal reflectors, which cover the slope fans and extend from the shelf to the deep basin margin (Figs. 3.9c and 3.10c). The overlying retrogradational unit SP7 consists of parallel reflectors, onlapping against the previously eroded inner-middle shelf parts. A maximum flooding surface (mfs) marks the transition to aggradational horizontal reflectors, which characterize the upper part of unit SP7, and unit SP8 in the upper Eocene. On the slope sub-parallel reflectors are generally continuous to the deep basin margin. Average thicknesses range from 700 m on the shelf to 1,000 m on the slope. An erosional unconformity (~30-33.9 Ma) on the shelf, interpreted as a type 2 sequence boundary (SB2), and its correlative conformity basinward mark the contact with the Oligocene basin fill.

The normal regressive unit SP9 consists of oblique reflectors, downlapping the erosional unconformity on the upper slope (Fig. 3.8c). Toward the lower slope, reflectors become sub-parallel and dip-angles are reduced. A second erosional unconformity on the shelf top, interpreted as maximum regressive surface (MRS) of Early Oligocene age (30 Ma), and its correlative conformity basinward marks the contact with the overlying unit SP10. This unit is sub-divided into two intervals by another unconformity of Early-Late Oligocene age (28.45 Ma), which is indicated by a high-amplitude sub-horizontal reflector that represents a maximum flooding surface (mfs; Fig. 3.8c). The lower interval of SP10 consists of sub-parallel reflectors onlapping the shelf top, which indicate coastal retrogradation. The upper interval is characterized by parallel aggrading clinoforms, truncated at the top by an erosional unconformity of early Miocene (17-20 Ma) age. Beyond the shelf break, contorted reflectors of unit SP10 downlap the upper-middle slope. Extensional faults and mud diapirs disrupt low-amplitude horizontal reflectors on the lower slope, which extend to the deep basin margin. In these areas, few reflectors appear to cross-cut sedimentary strata or mimic the sea-bottom. They correspond to bottom simulating reflectors (BSR), which have been associated with gas hydrates in the Tertiary basin fill (Fontana, 1989; Castillo et al., 2009). Well log analysis suggests the occurrence of Oligocene fining-upward sandstones on the upper slope.

Santos Basin

Meisling et al. (2001) and Modica and Brush (2004) described marked differences in the Paleogene stratigraphic and structural framework between the northern, central and southern parts of the Santos Basin. For our study, a single seismic line from the southern Santos Basin was available. Thicknesses of the Paleogene basin fill range between 500 to 1,600 m; this interval is, therefore, thinner than in the Campos and Pelotas basins. The lower Paleocene basin fill (lowest SS7 unit, 60 m thick) was only identified in a single well on the outer shelf (Fig. 3.3). It includes a forced regressive wedge bounded both at the base and top by erosional unconformities, and composed of reworked sandstones and siltstones of the Ponta Aguda and Marambaia Fms.

(Table 3.1). Above, four additional units have been identified: lower Eocene (SS7), upper Eocene (SS8), lower Oligocene (SS9) and upper Oligocene (SS10).

The upper Paleocene-lower Eocene unit SS7 comprises a retrogradational package between 200 m and 600 m thick, which is composed of parallel and horizontal reflectors with great lateral continuity and downlap terminations on the outer shelf-upper slope. Fluvial-deltaic sedimentation (Ponta Aguda Fm.) passes laterally to shales and marls intercalated with few turbidite sandstones on the slope (Marambaia Fm. and Meresias Mb.; see Moreira et al., 2007). In the basin margin, parallel, continuous reflectors with low amplitudes have been interpreted as pelagic deposits (Fig. 3.10b). Persistent erosion of the hinterland and high terrigenous input to shelf areas caused thickening of the middle-upper Eocene basin fill. Unit SS8 consists of parallel, horizontal reflectors with coastal onlap in the lower part and aggrading-prograding clinofolds in the upper part. Thicknesses range between 800 m on the shelf margin and 1,200 m on the slope. In the deep basin margin, low-amplitude reflectors are discontinuous and truncated by erosional surfaces.

The contact with the Oligocene unit SS9 appears to be conformable. This unit consists of horizontal, parallel reflectors onlapping against the middle-outer shelf. Up-section, they extend to the inner shelf and comprise a thin aggradational package. The aggradational-progradational upper Oligocene unit SS10 consists of sub-parallel reflectors downlapping the middle-outer shelf and truncated at the top by an early Miocene unconformity. On the shelf top, the Oligocene unit shows an average thickness of 300 m, which increases up to 600 m on the slope. In this region, reflectors either onlap against salt domes or cap them and extend continuously to the distal edge of the diapiric province. Well data indicate intercalations of shallow-water carbonates, sandstones and shales passing laterally to shales and siltstones, which are widely deposited from the upper slope to the basin margin. Basinward, turbidite sandstones decrease in thickness, whereas shales and siltstones increase and envelope sandstone wedges with favorable reservoir potential. Sigmoidal, oblique reflectors with downlap terminations along the slope (and within the entire Paleogene-Neogene succession) suggest a complex interaction between contourite drifts and turbidite systems (Stow et al., 2002). The contourites are characterized by low-amplitude reflectors downlapping an erosion surface, with mounds of sub-parallel reflectors in basinward direction (Fig. 3.9b). They amalgamate with contorted reflectors from turbidite flows. Gravity mass-flows spread into the oceanic basin and overstep the distal edge of the diapiric province. They form thin wedges with chaotic reflector arrangement in the easternmost part of the line, which may correspond to basin-floor low-density turbidites (Fig. 3.10b).

Campos Basin

Biostratigraphic data show that lower Paleocene deposits are absent on the shelf margin; it is

unclear if they exist downslope. Total thickness of the Paleogene basin fill ranges between 500 m and 1,900 m. An Eocene-Oligocene unconformity (33.9 Ma) documents a second order eustatic sea-level fall, which generated a type 2 sequence boundary (SB2) separating two stratigraphic intervals: (i) upper Paleocene-Eocene (unit SC6), and (ii) Oligocene (units SC7 and SC8). On the shelf, unit SC6 is approx. 400 m thick, whereas on the slope to basin margin it ranges between 100 m and 1,400 m. Internal semi-horizontal, sub-parallel reflectors on the shelf laterally pass to contorted reflectors and downlap terminations on the upper slope. Up-section, onlapping reflectors indicate a retrogradational trend in the middle Eocene, overlain by aggradational-progradational deposits (upper part of unit SC6). Well data reveal early and middle Eocene disconformities on the continental shelf (Fig. 3.4 and Table 3.1), which represent second order sea-level rises (Hardenbol et al., 1998). These events triggered landward migration of depocenters and sediment starvation basinward of the shelf break, evidenced by reduced thicknesses in the slope to deep basin. Well data show sandstones with intercalations of carbonates on the inner shelf. On the slope, sandstones with shales form internally chaotic wedges between salt structures. Sub-parallel and discontinuous reflectors are interpreted as gravity-transported sediments.

Above the 33.9 Ma unconformity (SB2), the lower Oligocene regressive unit (SC7) consists of sub-parallel to sigmoidal reflectors downlapping the outer shelf to upper slope. The upper Oligocene unit SC8 is characterized by a thin package of onlapping reflectors on the inner-middle shelf (retrogradation) capped by aggrading-prograding clinoforms, which extend continuously to the shelf break. This pattern is related to a rapid consumption of accommodation space, probably due to the continued exhumation of the Serra do Mar and Serra da Mantiqueira in the hinterland, and the subsequent deviation of sediment pathways from the Santos to the Campos Basin (Modica and Brush, 2004). Thicknesses of the Oligocene vary from 200-500 m on the shelf top to 100-1,000 m in inter-diapir depocenters. Only few parts of the upper unit SC8 were recognized due to intense subaerial shelf exposure and downslope submarine erosion in the Early Miocene. On the deep basin margin, this succession is 300-400 m thick, composed of contorted and sub-parallel reflectors, which are disrupted by Miocene mass flows (Fig. 3.10a). Well data indicate that Oligocene turbidite sandstones are better sorted and cleaner compared to their Eocene counterparts. However, both units incorporate important hydrocarbon reservoirs (Coward et al., 1999).

3.4.5 Neogene

The base of the Neogene succession is marked by eustatic-driven erosional unconformity of Early Miocene age (17-20 Ma) in the three basins. This surface has been interpreted as a type 2 sequence boundary (SB2). Up-section, four seismo-stratigraphic units have been identified within the Neogene-Holocene basin fill: (i) lower Miocene, (ii) middle Miocene, (iii) upper Miocene, and (iv) Pliocene-Holocene.

Pelotas Basin

Horizontal, parallel reflectors truncated by amalgamated erosional unconformities near the shelf break characterize the Neogene-Holocene basin fill. Units SP11-SP13 show offlap and reflect an overall trend of retrogradation of the shelf break (Fig. 3.8c). Average total thicknesses of the Neogene succession vary between 700 m and 2,850 m, and main lithologies include proximal deltaic sandstones passing basinward to intercalated shales, siltstones and sandstones. On the middle to outer shelf, the lower Miocene unit SP11 consists of downlapping sub-parallel reflectors capping an early Miocene unconformity. This succession, between 100 m (shelf) and 900 m (lower slope) thick, fills erosional channels cutting into the underlying unit SP10. In the upper part, reflectors become parallel and onlap against the shelf, bounded at the top by a maximum regressive surface of erosion (MRS). It was clearly identified near the shelf break, but passes to a correlative conformity in shelf- and basinward directions. Toward the slope, sub-parallel to contorted reflectors represent a package of sediments approximately 800 m thick. Erosional scours and reflector truncations suggest recurrent periods of turbidite deposition during the whole Miocene. High-angle faults identified on the shelf and middle-lower slope disrupt this unit and propagate upward to the Plio-Pleistocene deposits. In the transition to the deep basin margin, mud diapirs and associated extensional faults are recognized (Fig. 3.10c) and the thicknesses decrease to 100 m. Unit SP12 of Middle Miocene age is characterized by horizontal reflectors onlapping against the middle to outer shelf. Along the slope, reflectors are sub-parallel and show long lateral continuity. This pattern extends to the conformable unit SP13, which record a retrogradational trend in the upper Miocene succession bounded at the top by an intra-late Miocene maximum flooding surface (approx. 9 Ma, Tortonian). The uppermost Pliocene-Holocene unit SP14 consists of horizontal layers with downlap terminations on the outer shelf to upper slope. In a basinward direction, units SP13 and SP14 thicken and internal horizontal to sigmoidal reflectors show again downlap terminations. In the deep basin margin, low-amplitude horizontal layers represent pelagic sediments.

On the Pelotas middle-lower continental slope (2,000-4,000 m of water depth), two high-amplitude reflectors extend almost parallel to the sea-bottom surface and cut through the stratified Eocene-Miocene succession (Figs. 3.9a and 3.10a). These have been interpreted as BSR; nearby mud diapirs probably represent escape features related to gas migrating toward the sea floor. The upper reflector (500-700 m below the sea-bottom) seems to define the gas hydrate stability zone (GHSZ), and the lower reflector (2,000-3,500 m below the sea-bottom) the boundary of the zone where gas occurs in pore space (see Clennell, 2000). However, the available well data do not validate this interpretation.

Santos Basin

Horizontal, parallel reflectors with occasional oblique arrangement form the wide continental shelf

of Neogene to Holocene age. Total thicknesses increase from 300-400 m on the shelf to more than 1,300 m in the central basin part. Due to the very small thickness of the lower Miocene unit SS11 (up to 150 m), seismic geometries are difficult to observe. Only few downlaps are recognized; well data show mixed clastic-carbonate deposits. The middle Miocene unit SS12 consists of extended horizontal and parallel reflectors with thickness between 100 and 300 m. On the outer shelf, carbonate shelf ramps (Iguape Fm.) reach thicknesses of up to 500 m and define an array of retrogradational to aggradational horizontal reflectors. Basinward, the lower-middle Miocene basin fill shows increasing thicknesses. They accelerated flexural subsidence, increased slope gradients and drove persistent salt-withdrawal as evidenced by up-dip stratal terminations against diapirs. Gravity flows overstepped the diapiric province and distorted the deep-water Oligocene succession (Fig. 3.10b). The top of unit SS12 is marked by an erosional unconformity (9-11 Ma), which remains uncertain between a type 2 sequence boundary and a regressive ravinement surface in a wave-dominated shelf setting (Galloway, 2004). Above, the upper Miocene unit SS13 is characterized by horizontal reflectors, up to 200 m thick on the slope and 800 m on the slope. Frequent downlap terminations from the outer shelf to the lower slope indicate turbidite deposition, which seems to prevail until recent times (unit SS14). In the deep basin margin, reflectors show low amplitudes and truncation by erosional surfaces. Well data indicate upper Miocene-Pleistocene carbonates on the shelf top passing basinward to shales with occasional sandstones intercalated.

Campos Basin

On the Campos shelf margin, internal sub-parallel prograding clinoforms comprise four amalgamated depositional units (SC9 to SC12), which are separated by erosional unconformities or depositional hiatuses (Table 3.1). Total thicknesses range between 500 m on the shelf and 1,000 m in salt flow-induced depocenters. The most proximal wells reach the fluvial-deltaic Barreiras Fm. and São Tomé Mb. (Emboré Fm.). They show lateral transitions to the mixed carbonate-clastic Grussaí Mb. (Emboré Fm.) on the outer shelf to upper slope. Depocenters between salt domes preserve disconnected wedges of basinward dipping divergent and sigmoidal layers. They represent turbidite deposits, which either downlap onto the underlying Oligocene basin fill (unit SC8), or are truncated by salt domes, synthetic and antithetic growth faults. The normal regressive unit SC9 seems to become retrogradational in the upper part. This premise is based on a thin interval of fining-upward sandstones (up to 10 m thick) identified in two of the available wells. However, an erosional unconformity at the top (middle Miocene surface of regressive wave ravinement) hampers an accurate interpretation. Basinward, prominent erosional truncation resulted from submarine channels near the shelf break (Fig. 3.8a) and deep marine currents in the diapiric province to the abyssal plain (Figs. 3.9a, 3.10a). Therefore, its original geometry and thickness remain unclear.

Well data reveal two middle Miocene and late Miocene disconformities, which separate the

overlying seismic units SC10 and SC11 (Table 3.1). Sub-parallel and few oblique seismic reflectors indicate overall shelf progradation to recent times. Near the shelf break, erosional channels truncate the whole Miocene-Holocene succession and indicate long lasting turbidite deposition, which seems to prevail until recent times. Across the middle to lower slope, sigmoidal and contorted reflectors downlap on an erosional surface of Late Miocene-Pliocene age (Fig. 3.9a, unit SC12). This interval represents reworked shales, siltstones and sandstones covering most of the salt domes. They provide a potential top-seal for the underlying turbiditic high-quality reservoir sandstones of Oligocene and early Miocene age. Toward the deep basin margin, sub-parallel, sigmoidal and locally contorted reflectors form basin floor fans bounded by erosional surfaces (Fig. 3.10a). This succession represents large volumes of turbiditic fines, probably redistributed by bottom currents, which overstepped the salt province and cut into the deep-water Paleogene-Neogene basin fill (stratigraphic units SC7-SC9).

3.5 Discussion

3.5.1 Structural development

The half-grabens on the shelf to upper slope of the Santos and Campos basins were controlled by Hauterivian-late Barremian syn-rift extensional faulting (see Fig. 3.8, and Karner et al., 1997). Unfaulted sub-parallel reflectors of early-middle Aptian age, capping these depocenters indicate the transition from fault-controlled brittle deformation to depth-dependent lithospheric thinning, which was triggered by ductile stretching of the lower crust leading to continental break-up (Kusznir and Karner, 2007). Therefore, this succession is interpreted as sag basin fill, which involved continued syn-rift extension without major extensional faulting of the upper crust (Karner, 2000; Karner and Gambôa, 2007).

High-angle faults, which extend into the continental basement, affect the lower-middle Barremian basin fill of the Pelotas Basin; asymmetric half-grabens are absent (Fig. 3.8c). This succession extends from the continental shelf to the deep basin margin. Seaward-dipping reflectors (SDRs) indicate a volcanic-margin segment, which experienced crustal thickening during the Barremian syn-rift stage (see also Talwani and Abreu, 2000 and Blaich et al., 2009). This is in contrast to minor volcanism in the Santos and Campos basins. The overlying upper Barremian-Aptian succession consists of unfaulted reflectors dipping basinward. This interval seems to represent the onset of post-rift thermal subsidence and flexural response of the crust because of increasing sediment and water loads (Section 4.4.1). No Aptian salt is present in the Pelotas Basin.

The Atlantic Hinge Zone is present in all three basins and also continues northwards (Matos, 2000). It is due to Hauterivian and late Barremian rift extension (Karner et al., 1997, 2003) and

represents the western limit of maximum extension and basin tilting since the Barremian, which considerably affected the location of rift-to-drift sediment depocenters. At the hinge zone characteristic geometries occur: in landward direction the Barremian-lower Aptian succession onlaps the basement, in seaward direction the reflectors dip with 30°-35° in the Santos and Pelotas basins, and 15° in the Campos Basin. This flexure of the syn-rift package indicates differential subsidence between faulted blocks of continental basement west of the hinge zone and stretched continental crust (Campos/Santos basins) or transitional crust (Pelotas Basin) east of the hinge zone.

In the three studied basins, the overlying Albian to Holocene basin fill shows dips of 10° to 15°. This change in dip resulted from the onset of seafloor spreading between the early Aptian to early Albian. Continental divergence and lithospheric cooling generated basinwide thermal subsidence, typical of 'passive' continental margins. During the Late Cretaceous, long-term accommodation space increased and resulted in shelf margin retrogradation and aggradation. In the Tertiary, falling eustatic sea-level and crustal cooling combined to generate lower accommodation rates. As a result, the shelf margin switched to long-term overall progradation.

In the Santos and Campos basins, Aptian evaporites occur between the inner-middle shelf and the deep-water continental rise. Compressional and extensional structures are linked to the basal detachment surface. Previous studies (Demercian et al., 1993; Cobbold et al., 1995; Mohriak et al., 1995, 2008) described several mechanisms of salt deformation in the offshore Brazilian basins. This study shows that diapirs, listric faults, inverse faults, rollover structures, pinch-out truncations and turtle structures affect the post-salt succession. However, the Santos and Campos basins feature significant differences in the salt-related structural styles. They resulted from the basin-specific extension of the salt layer (slightly wider in the Santos Basin) and the asynchronous onset of salt remobilization due to the interplay of sediment loading and basin tilting, which will be analyzed by forward modeling (Section 5.5.2)

3.5.2 Aptian salt deposition

Biostratigraphic data indicate that the evaporite basin fill is pre-110-105 Ma in the Campos Basin and pre-110 Ma in the Santos Basin: the top of the evaporites has been constrained by a seismic reflector at the base of the overlying Early Albian carbonates. The age of sub-salt fluvial-deltaic to lacustrine deposits could be biostratigraphically dated as late Aptian only in the Campos Basin. The salt succession was apparently deposited in a short time span in the latest Aptian (112-115 Ma). This estimate is compatible with the ages of post-113.2 Ma and post-116 Ma suggested for the Santos Basin evaporites by Davison (2007) and Karner and Gambôa (2007). Mohriak et al. (2008) proposed similar ages of approx. 112-115 Ma, while Torsvik et al. (2009) assumed late Aptian (pre-112 Ma) ages.

The salt province in the Santos and Campos basins spans approximately 230 km in NW-SE direction (Figs. 3.6 and 3.7). In a shelfward direction, the proximal (western) limit is clearly defined by onlap against syn-rift sag deposits near the hinge zone. The distal (eastern) boundary of the salt province and the geodynamic setting of the underlying succession has been interpreted controversially: (i) syn-rift in origin, overlies continental crust, and the distal edge of the salt province is marked by the transition from continental to oceanic crust (COT) (Demercian et al., 1993; Bassetto et al., 2000; Karner, 2000; Torsvik et al., 2009); (ii) post-breakup in origin and overlies mainly proto-oceanic and oceanic crust (Jackson et al., 2000; Marton et al., 2000; Davison, 2007).

The seismic data of this study show that (i) the sag basin fill extends from the hinge line to the interpreted COT; (ii) in the Campos Basin the salt succession invariably overlies sag deposits; (iii) in the Santos Basin a similar sag-salt arrangement is observed, but an interval of mobile salt overstepped the COT and overlies SDRs and entirely oceanic crust (Fig. 3.10b). These features indicate that middle-late Aptian sag depocenters evolved to salt basins during the last syn-rift stage. Hypersaline conditions in deep lakes of the sag margin resulted from either seepage of seawater through the Walvis Ridge-Rio Grande Rise (Nunn and Harris, 2007), intermittent marine incursions over this structural barrier (Karner and Gambôa, 2007), or a combination of both processes. Based on the available seismic and well data it is not possible to determine the processes controlling salt precipitation. Nevertheless, reflector geometries in the sag and salt basin fills do not show any signature of marine incursions (e.g. marine coastal onlap or marine flooding surface). Furthermore, the first recorded marine fauna appears in the post-rift Early Albian succession.

3.5.3 Seismo-stratigraphy and model resolution

The seismo-stratigraphic interpretation of the Barremian-Holocene succession reflects specific depositional patterns during each of the syn-rift, post-rift and drift stages of basin development. The stratigraphic signature and timing of continental extension and break-up is highly variable between the three basins analyzed. The effects of syn-rift lithospheric deformation represent a crucial factor to better understand the long-term flexural evolution of the single basins and the individual impact of the sediment loading on depositional patterns, subsidence distribution and salt deformation. Therefore, although qualitative sequence-stratigraphic models involve key control factors on accommodation space, there is a range of processes that may have strong influence on the stratal patterns and the basin architecture that require a quantitative approach (e.g. flexural rigidity of the crust and flexural-induced rebound of the shelf). In order to correctly analyze the individual impact of eustasy, subsidence and sediment supply on the evolution of accommodation space and shelf-to-basin depositional systems, is necessary the integration of seismo-stratigraphic interpretations with numerical basin analysis (Chapter 4). This method allows to assess inherent model uncertainties from sequence stratigraphy and develop best-fit plausible quantified models to the present-day tectono-stratigraphic basin configuration.

Table 3.2 Seismo-stratigraphic units, depositional patterns and main reflector geometries established in the Barremian-Holocene sediment fill. Between twelve and fourteen seismic units have been recognized in each of the Campos (SC1-SC12), Santos (SS1-SS14) and Pelotas (SP1-SP14) basins. Depositional patterns (italic type): AP: normal regression; RT: forced regression; NR: normal regression; AP: aggradation-progradation. Sequence stratigraphic surfaces (in bold type) include: SB1: type 1 sequence boundary, SB2: type 2 sequence boundary (Vail et al., 1984); mfs: maximum flooding surface; MRS: maximum regressive surface; TRS: transgressive ravinement surface.

Period	Epoch	Age (Ma)	TECHNICAL			CAMPOS BASIN				SANTOS BASIN				PELOTAS BASIN				
			Dep. Patt.	Seismic Units	Reflector geometries	Dep. Patt.	Seismic Units	Reflector geometries	Dep. Patt.	Seismic Units	Reflector geometries	Dep. Patt.	Seismic Units	Reflector geometries				
Cretaceous	Upper	Maastricht.	70.6	AP	Top: from 950 m to 4,800 m	REGRESSION	SS 6	Shelf: horizontal and extended reflectors; sporadic downlap on outer shelf	AP	SS 6	Shelf: horizontal and extended reflectors; sporadic downlap on outer shelf	TRANSGRESSION	SP 5	Shelf: onlap, extended and parallel reflectors	TRANSGRESSION	SP 5	Shelf: onlap, extended and parallel reflectors	
				RT	Onlap at the base. Up-section downlap		RT	Slope: sub-parallel reflectors truncated by salt diapirs. Up-dip pinch-out, turtle structures, growth faults		RT	Slope: parallel to sub-parallel reflectors; occasional turbidites channels							
		Paleocene	Up.	61.7	SB1	Top: from 640 m to 4,500 m	DRIFT	SB1	Unclear and discontinuous semi-horizontal reflectors	FR	SS 7	Top: 490 m to 5,850 m	FR	SP 6	Deep basin: low-amplitude, horizontal	FR	SP 6	Deep basin: low-amplitude, horizontal
					FR	Deep basin: contorted, lenticular reflect.		FR	Unclear and discontinuous semi-horizontal reflectors		FR	Deep basin: low-amplitude horizontal						
	FR				Slope: up-dip pinch-out, chaotic arrangement (turbidite wedges)	FR		Unclear and discontinuous semi-horizontal reflectors	FR		Deep basin: low-amplitude horizontal							
	Lower	Albian	112	RT	Base: from 1,150 to 6,000 m	AGGRADAT.	RT	Shelf: horizontal, extended onlapping reflect.	AP	SS 4	Shelf: horizontal, extended onlapping reflect.	TRANSGRESSION	SP 3	Shelf: onlap, extended parallel reflectors	TRANSGRESSION	SP 3	Shelf: onlap, extended parallel reflectors	
				NR	Sub-parallel, contorted reflectors; downlap, high-amplitude base of salt		NR	Slope: prograding sub-parallel; up-dip pinch-out, turtle structures, growth faults		NR	Slope: sub-parallel reflectors, up-dip pinch-out, turtle structures, growth faults		NR	Mid. slope-deep basin: parallel to sub-parallel reflectors; low-amplitude in the deepest basin domain				
		Barremian	130	125	SB2	Top: 1,330 m (shelf) to 8,500 m (basin)	VOLCAN.	SB2	Shelf: truncation by high-angle faults	FR	SS 1	Unclear and discontinuous reflectors in the slope-basin margin; SDRs	POST RIFT	SP 2	Downlap the upper slope. Onlap up-section. Sub-parallel, horizontal basinward	VOLCANISM PROGRADATION	SP 2	Downlap the upper slope. Onlap up-section. Sub-parallel, horizontal basinward
					FR	Asymmetric half-grabens		FR	Shelf: truncation by high-angle faults		FR	Unclear and discontinuous reflectors in the slope-basin margin; SDRs		FR	Base: 1,700 m to 8,800 m		FR	Base: 1,700 m to 8,800 m
	Neogene	Miocene	Up.	28.45	NR	Top: from 100 m to 3,400 m	REGRESSION	NR	Downlap, submarine canyons, gravitational flows and erosion surfaces	AP	SS 13	Deep basin: oblique and sigmoid reflectors; basin-floor fans	TRANSGRESSION	SP 14	Onlapping parallel and horizontal; downlap on the outer shelf. Slope: sub-parallel; occasional erosion channels	REGRESSION	SP 14	Onlapping parallel and horizontal; downlap on the outer shelf. Slope: sub-parallel; occasional erosion channels
	RT				Shelf: sub-parallel and extensive	RT		High-amplitude horizontal reflectors (carbonate build-up)	RT		Slope: downlap, truncation ext. faults	RT		Slope: downlap, truncation ext. faults				
NR	Downlap. Truncation with listric faults				NR	Downlap. Truncation with listric faults		NR	Slope: divergent-sigmoid		NR	Slope: divergent-sigmoid		NR	Slope: divergent-sigmoid			
SB2	Top: from 430 m to 3,800 m				SB2	Top: from 430 m to 3,800 m		SB2	Top: from 430 m to 3,800 m		SB2	Top: from 430 m to 3,800 m		SB2	Top: from 430 m to 3,800 m		SB2	Top: from 430 m to 3,800 m
Paleogene	Eocene	Up.	37.2	AP	Top: from 640 m to 4,500 m	DRIFT	AP	Shelf: sub-parallel, semi-horizontal reflectors. Base and top are erosional	RT	SS 8	Deep basin: sigmoid and oblique reflectors; erosion surfaces (bottom currents)	TRANSGRESSION	SP 8	turbidite-contourites	TRANSGRESSION	SP 8	turbidite-contourites	
RT				Downlap at the base; onlap at the top	RT		Shelf: horizontal, extended reflectors	RT		Shelf: horizontal, extended reflectors	RT		Shelf: horizontal, extended reflectors	RT		Shelf: horizontal, extended reflectors		
NR				Erosion channels (turbidites)	NR		Downlap at the base; onlap at the top	NR		Slope: up-dip pinch-out against salt diapirs;	NR		Slope: up-dip pinch-out against salt diapirs;	NR		Slope: up-dip pinch-out against salt diapirs;	NR	Slope: up-dip pinch-out against salt diapirs;
SB2				Top: from 430 m to 3,800 m	SB2		Top: from 430 m to 3,800 m	SB2		Top: from 430 m to 3,800 m	SB2		Top: from 430 m to 3,800 m	SB2		Top: from 430 m to 3,800 m	SB2	Top: from 430 m to 3,800 m
FR				Slope: up-dip pinch-out, chaotic arrangement (turbidite wedges)	FR		Deep basin: contorted, lenticular reflect.	FR		Deep basin: contorted, lenticular reflect.	FR		Deep basin: contorted, lenticular reflect.	FR		Deep basin: contorted, lenticular reflect.	FR	Deep basin: contorted, lenticular reflect.

4. Inverse-basin modeling

4.1 Introduction

Although the geodynamic evolution of the southern Brazilian margin have been extensively documented (Bassetto et al., 2000; Cobbold et al., 2001; Modica and Brush, 2004; Mohriak et al., 2002, 2008; Torsvik et al., 2009), only few published studies attempt to determine the patterns and temporal changes in subsidence and sediment supply controlling the present-day basin architectures (e.g. Guardado et al., 1989; Chang et al., 1992; Karner and Driscoll, 1999b; Karner et al., 2003 and Karner and Gambôa, 2007). Based on the existing seismo-stratigraphic framework, numerical basin modeling has been employed in order to quantitatively analyze the evolution of accommodation space in each the Campos, Santos and Pelotas basins, and to constrain the stratal geometries previously interpreted.

A number of studies on other continental margins have utilized basin modeling to model lithosphere extension and calculate physical controls (tectonism, thermal flow, flexure) on the basin geometry, subsidence and depositional settings (Nadin and Kuszniir, 1995, 1996; Roberts et al., 1995, 1997, 1998; Bowman and Vail, 1999; Zühlke et al., 2004; Kuszniir and Karner, 2007; Veselovsky et al., 2008). Inverse-basin modeling as derived from flexural backstripping is a method used to restore the sedimentary basin fill, layer by layer, in order to isolate subsidence of the margin due to the flexural sediment loading and tectonism. This method was developed and initially applied for calculating subsidence history curves using well data by Steckler and Watts (1978), and for estimating total tectonic subsidence/uplift along seismic sections by Watts (1988). Thermal contraction of the lithosphere is the dominant mechanism affecting the tectonic subsidence following initial rifting and lithosphere thinning. Then, Watts et al. (1982) confirmed that during the post-rift to drift development of continental margin basins, the sediment and water loads gradually increase and caused lithosphere flexure (Watts et al., 1982). These conceptual advances resulted from the integration of high-resolution seismic and well data and the inclusion of a wider range of input parameters in the model, leading to the development of the last generation of two- and three-dimensional numerical basin modeling techniques (Fig. 4.1).

Inverse-basin modeling follows a sequence stratigraphic approach that considers changes in accommodation space and sedimentation as the two principal controls on sedimentary systems (Bowman and Vail, 1999). Total subsidence is the result of three genetic components – thermo-tectonic, flexural and compaction-induced subsidence. Accommodation space as a function of eustatic sea-level fluctuations and total subsidence is limited by: (i) sea-level (approximately base-level), and (ii) a lower reference horizon in the subsurface, which limits the rheological uncompactable basement from the overlying basin fill where compaction processes are still active. Numerical

modeling in this study fully considers a 2D model of flexural response of the lithosphere, which gives data of much higher resolution than 1D isostatic backstripping of individual wells. In addition, the integrated approach with sequence stratigraphy provides an improved model for subsidence/uplift and sediment supply with reduced error margins. Key objectives of inverse-basin modeling include: i) quantified subsidence/uplift rates in time and space with their genetic components: thermo-tectonic, flexural and compaction-induced subsidence; ii) genetic model of major physical controls on the basin fill: subsidence, eustatic sea-level and changes in sediment flux; iii) comparative analysis of the basin development in the Campos, Santos and Pelotas basins; iv) inferred plate-tectonic development, e.g., syn-rift lithospheric deformation, changes in sea-floor spreading rates and far-field intra-plate deformation affecting the southern Brazilian margin.

4.2 Methodology

Inverse-basin modeling in this study aims to restore the basin architecture and quantitatively analyze the evolution of accommodation space. The model has been performed with the simulation program package PHIL™ (Process- and History- Integrated Layers; Bowman and Vail, 1999), which allows flexural backstripping of 2D transects through time. The program attempts to break each process down into discrete events. Then, the modeled cross-sections are divided into evenly spaced locations or cells (see Appendix A). The events that determine the physical state at a location are controlled by the conditions existing within the surrounding locations, as well as the available sediment supply. The cell spacing is defined by the user, and must be an adequate value that allows to constrain the lateral variations in stratigraphic and structural events observed in the data.

Inverse-basin modeling starts with the recent basin configuration and infill; the chronostratigraphic time layers are incrementally removed, taking full consideration of the flexural rigidity of the crust. Upon the removal of each unit, the underlying layers are decompacted in response to the extracted sediment load, and the water-level is adjusted. Then, total subsidence, its genetic components as well as the sediment flux are calculated for each time layer until the top of the rheological basement is reached (in our example the top lower Barremian). The comparison of the obtained basin configuration with the lithofacies and bathymetric data from the wells allows the calibration of the paleowater depths, and when necessary the readjustment of the input bathymetries until obtain a reasonable restoration. In addition, sensitivity test of the effective elastic thickness (T_e) and taper limits (extension of the flexural wavelength affected by the imposed loads) allowed to determine the best-fit values providing the most plausible models and quantitative results.

4.3 Input parameters

The model requires the following input parameters: (i) present-day sedimentary thicknesses as derived from the seismo-stratigraphic framework (see Tables 3.1 and 4.1); (ii) lithologies,

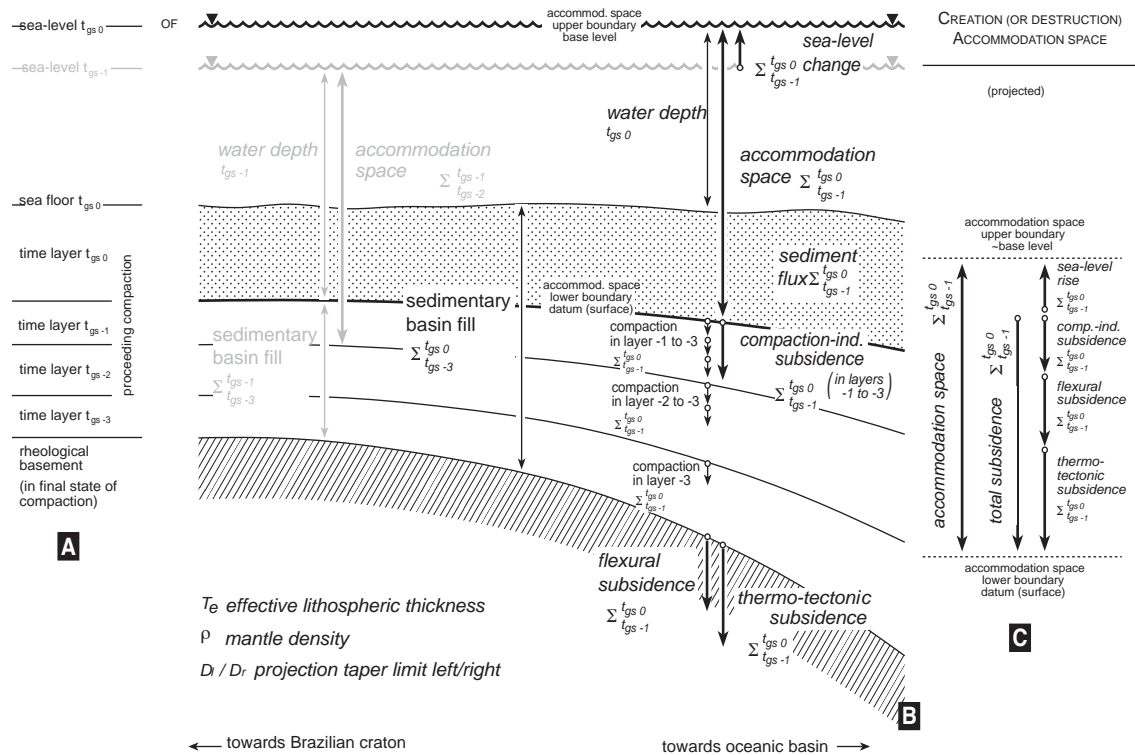


Fig. 4.1 Genetic components and principal parameters of accommodation space development considered in 2D inverse basin modeling. Modified from Zühlke et al. (2004). (A, left corner) indicates that the current basin state is marked by the time layer 0 ($t_{gs 0}$; gs – geological stage). Abbreviations t_{gs-1} to t_{gs-3} indicate consecutively older time layers. Main factors (in italics) comprise: accommodation, sea-level changes, subsidence components and sediment flux. (B, right side) shows that in the accommodation-oriented basin flexural analysis, total subsidence is leveled to the datum (lower boundary) of accommodation space, and includes the sum of thermo-tectonic, flexural and compaction-induced subsidence. In contrast, basement-related subsidence refers exclusively to thermo-tectonic and flexural subsidence. (C, right corner) point out the norm-vectors marking the final total subsidence and accommodation space. This example depicts a configuration where all rates are positive, i.e. subsidence and a eustatic sea-level rise occur. Sediment flux during time layer 0 is significantly increased compared to during time layers t_{gs-3} to t_{gs-1} . As a result of high sediment flux, water depth has decreased although eustatic sea-level has risen and thermo-tectonic subsidence has remained constant from time layer t_{gs-1} to t_{gs-0} . Flexural and compaction-induced subsidence have increased from time layer t_{gs-1} to t_{gs-0} .

densities and porosities for each lithotype considered in the modeling and calibrated by the wells (Table 4.2); (iii) flexural basin variables, including the effective elastic thickness, taper limit and mantle density (Table 4.3); (iv) eustatic sea-level; (v) paleobathymetry for each time layer based on biostratigraphic and facies data from the calibration well (Table 4.4).

4.3.1 Temporal and spatial resolution

Twelve to fourteen second order depositional units (3-50 m.y. duration, cf. Catuneanu, 2006) define the temporal resolution of the model, which includes time steps between 4.4 and 31.6 m.y. (series level in the timescale of Gradstein et al., 2004). Each of the seismic profiles (in depth domain) is between 300 km and 340 km long, and cover from the continental shelf to the deep-water continental rise (Section 3.2). For modeling purposes, each seismic line has been divided into 400-450 cells, with a lateral spacing of 650 m in the Santos Basin, and 750 m in the Campos and Pelotas basins (Table 4.3).

Time layers	Average thickness [m]								
	Campos			Santos			Pelotas		
	Shelf	Slope	Basin	Shelf	Slope	Basin	Shelf	Slope	Basin
Pliocene-Holocene	150	400	500	150	2,000	150	300	600	350
Late Miocene	450	100*	100*	200	500	250	450	700	500
Middle Miocene	400*	100*	100	200*	500*	400	400*	800*	250
Early Miocene	150*	250	100	100	350	550	500	1,000	200
Late Oligocene	200	300	200	100	300	400	600	400	250
Early Oligocene				300	200	150	100	600	400
Late Eocene	500	500	300	900	800	500	150	650	1,000
Middle Eocene							400	600	350
Early Eocene	500*	700*	400	350*	350*	300	400*	800*	500
Paleocene									
Maastrichtian	450	800	500	500	300	400	150	100	100
Campanian									
Santonian							100	500	200
Coniacian	500	600	600	600	300	200			
Turonian									
Cenomanian				800	500	200	400	900	600
Albian	400	500	300	500	300	200			
Aptian	400*	2,000	400	900*	2,000	400	300*	1,300	600
Barremian	1,500	1,000	200 (?)	800	1,000	300 (?)	250	600	600

Table 4.1 Average thicknesses of the Early Cretaceous to Holocene sedimentary succession obtained from the previous seismo-stratigraphic analysis. * Intervals affected by strong erosion.

4.3.2 Lithologies and compaction parameters

The sedimentary facies penetrated by the wells have been attributed to eleven siliciclastic lithologies, nine carbonate lithologies and evaporites (undifferentiated). Average initial textural porosities, bulk rock densities and compaction rates are listed in Table 4.2. The algorithm for compaction considers the decrease in the rock volume as a function of the burial depth, and based on existing empirical and experimental approaches (Goldhammer, 1997; Welte et al., 1997; Bowman and Vail, 1999). In basin modeling, compaction of carbonates has often been neglected. However, Goldhammer (1997) indicate that carbonate muds with a high amount of microporosity experience significant compaction of approx. 50% of the original volume during the initial burial history (150 to 200 m of overburden). In carbonate sands, initial porosities of approx. 40-45% exist, but little compaction is assumed to occur up to 200-300 m of burial depths. During deep burial, processes like pressure-solution may cause compaction rates of up to 30% (Anderson and Fressen, 1991; Scholle and Halley, 1985).

Lithology	Density [kg/m ³]	Initial porosity [φ_0]	Compact. rate [r_0]
Coarse sand to cobbles	2650	0.40	0.0001
Quartz silt size	2650	0.30	0.0010
Quartz silt/clay	2650	0.45	0.0030
Quartz sand/clay	2650	0.40	0.0020
Interbedded quartz/silt	2650	0.50	0.0005
Interbedded silt/clay	2750	0.50	0.0020
Marine mud	2750	0.50	0.0030
Clay	2750	0.50	0.0030
Silt/coal	2450	0.60	0.0080
Clay/coal	2300	0.85	0.0090
Coal	2000	0.92	0.0100
Cemented carbonate	2800	0.45	0.0001
Carbonate fine grainstone	2800	0.60	0.0010
Carbonate coarse grainstone	2800	0.70	0.0005
Carbonate boundstone	2800	0.60	0.0020
Micrite	2800	0.70	0.0040
Algal laminates	2800	0.60	0.0005
Dolomite	2900	0.40	0.0001
Gypsum	2330	0.10	0.00001
Evaporites	2150	(?) 0.05	0.00001

Table 4.2 Lithologies, initial porosity and compaction rates considered for inverse basin modeling.

4.3.3 Crustal flexural parameters

The flexural response of the crust is governed by three main parameters: (i) the effective elastic thickness (T_e); (ii) the plate-end-boundary distance (rheological taper limit); and (iii) the mantle density (see Table 4.3). The plate-end-boundary distance defines the landward boundary of the flexural wavelength that respond to the imposed sediment and water loads in the basin. This parameter is highly dependent on the flexural rigidity of the crust, which in this study has been analyzed as a function of the effective elastic thickness T_e (Watts, 2001). According to existing investigations on the flexural rigidity and thermal evolution of the crust (e.g. Ziegler and Cloetingh, 2004; Lavier and Manatschal, 2006; Leroy et al., 2008), it is expected that variations in the degree of volcanism and lithospheric thickness along the Pelotas-to-Campos margin segment (Section 1.5) have produced temporal and spatial changes in the flexural rigidity of the crust. These variations have been determined by sensitivity tests of the effective elastic thickness (T_e), providing the best-fit values to reconstruct the basin configuration and paleobathymetries.

For each of the basins analyzed, the effective elastic thickness has been tested between 5 km and 30 km. After iterative modeling runs and calibrations, a T_e value of 12 km has produced the

best-fit model to the present-day basin configuration in the Campos and Santos basins. In the Pelotas Basin, the best match has been achieved with a T_e value of 20 km, which is comparable to 25 km on the conjugate Namibian continental margin by Stewart et al. (2000). However, forward stratigraphic modeling in Chapter 5 will allow to evaluate the evolution of T_e and calibrate inverse-basin modeling results.

Modeling Parameters	Values
Cell width [m]	650 - 750
Effective elastic thickness Lithosphere (T_e) [km]	12 - 20
Plate-end-boundary distance [km]	0 - 100
Mantle density [g/km^3]	3350

Table 4.3 Crustal flexural parameters considered for inverse-basin modeling.

Time layers	Maximum paleobathymetry [m]		
	Campos	Santos	Pelotas
Late Miocene	3,500	3,700	3,900
Middle Miocene	3,100	3,400	4,000
Early Miocene	2,900	3,150	4,100
Late Oligocene	2,600	3,000	
Early Oligocene	2,500	3,100	3,800
Late Eocene	2,400	3,000	
Middle Eocene	2,200		3,600
Early Eocene		2,600	2,900
Paleocene			
Maastrichtian	2,300	2,100	2,600
Campanian			
Santonian	1,500	1,550	1,730
Turonian		1,400	1,500
Cenomanian	1,050	1,000	1,200
Albian	800	800	950
Aptian	470	700	800
Barremian	300	300	200

Table 4.4 Maximum values of paleobathymetry considered for the inverse-basin modelling. They mark the evolution of paleowater depths in the deep basin margin, at distances of 300-340 km from the coastline.

4.3.4 Paleobathymetry and sea-level

The model requires bathymetries at the time of deposition of each chronostratigraphic layer. They have been estimated during the sequence stratigraphic analysis according to lithofacies and faunal associations from the calibration wells. The most reliable paleobathymetric markers are subaerial erosion surfaces identified in both wells logs and seismic lines (erosional reflector truncations), e.g., Early Aptian, Middle Aptian and Late Paleocene (see Table 3.2). In addition to our own database, results from other biostratigraphic and paleo-environmental studies have been used to reduce the model uncertainties (Koutsoukos, 1984, 1987; Dias-Brito, 1987; Dias-Brito and Azevedo, 1986; Pereira and Feijó, 1994; Rangel et al., 1994).

The impact of eustatic sea-level fluctuations on the accommodation space and deep-water sand volumes has been analyzed according to the eustatic sea-level curve shown in Figure 4.2. This curve incorporates second order changes from the sea-level curve of Hardenbol et al. (1998) re-calibrated with the time scale of Gradstein et al. (2004) based on equivalent biozones. Third-order sea-level changes have not been included because of the lower resolution of the seismostratigraphic data (2nd order depositional units, 3-50 m.y. duration), their less defined amplitudes and partly disputed eustatic origin.

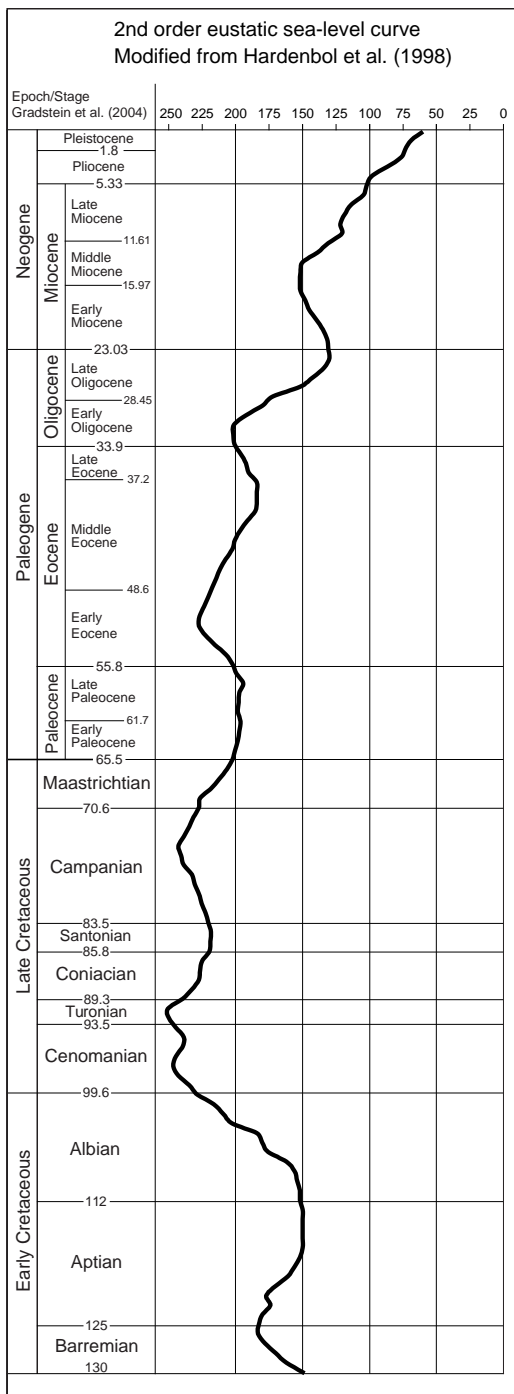


Fig. 4.2 Second order eustatic sea-level curve from Hardenbol et al. (1998), used as input parameter to forward stratigraphic modeling. The sea-level curve has been re-calibrated to the geological time scale of Gradstein et al. (2004) based on comparable biozones.

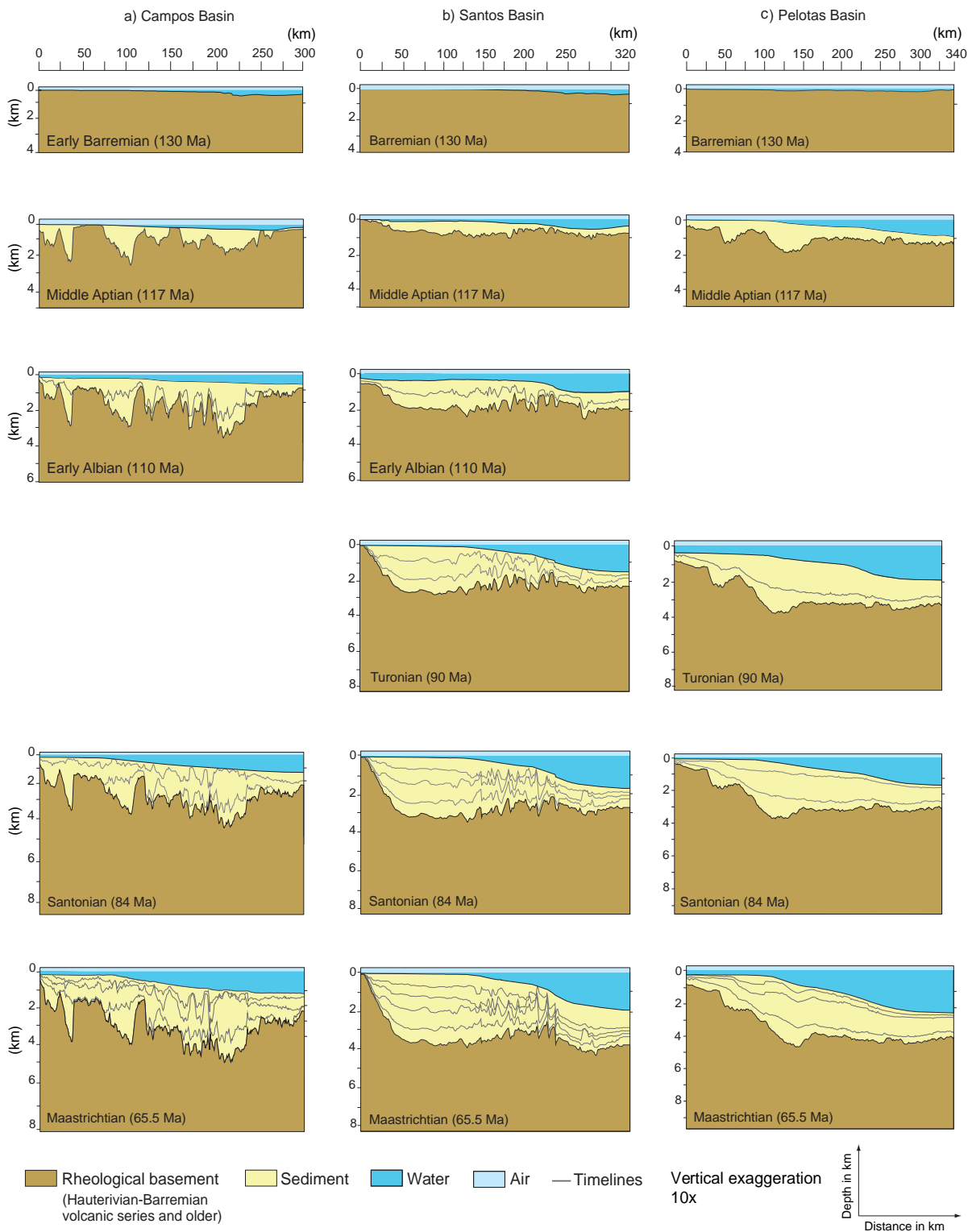


Fig. 4.3 Two-dimensional chronostratigraphic plots illustrating the basin architecture and paleowater depths for twelve time layers in the Campos, Santos and Pelotas basins. Vertical and horizontal scales are in km. Basin architectures were fairly similar during the Barremian syn-rift stage. By the early Albian, shallow water marine environments (900 m of maximum paleowater depths) and salt deformation in the Campos and Santos basins contrast with a flexural monocline basin architecture and deep-water marine environments (up to of 1,800 m of paleowater depth) in the Pelotas Basin. During the Late Cretaceous and Tertiary each of these basins evolved separately; they display specific architectures, paleobathymetry, and sediment fill distribution.

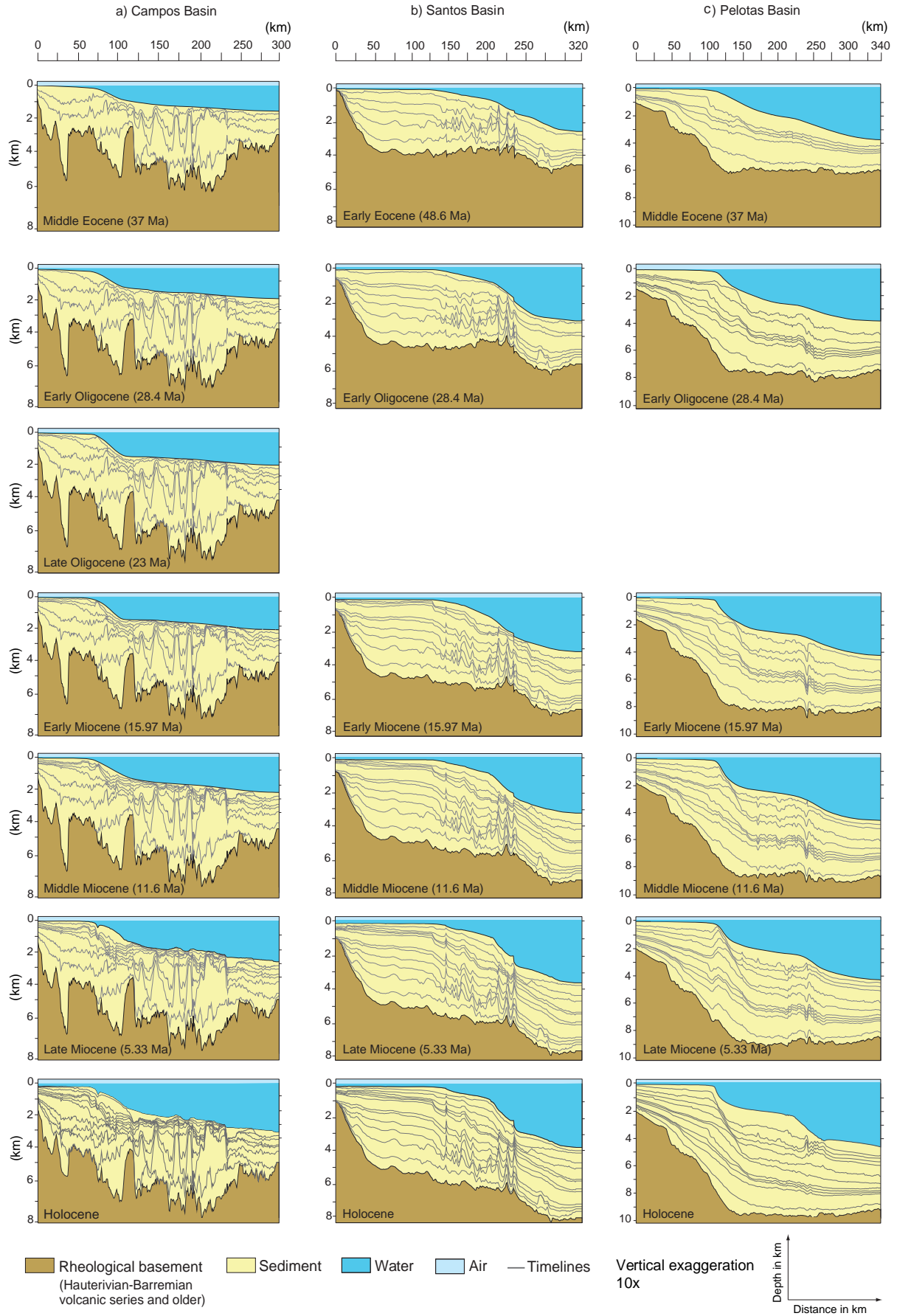


Fig. 4.3 (continuation) Two-dimensional chronostratigraphic plots illustrating the basin architecture and paleowater depths.

4.4 Subsidence modeling

Two-dimensional inverse-basin modeling provides the following numerical results at each cell along the cross-section and for each chronostratigraphic layer: i) rates of total subsidence and its three genetic components: thermo-tectonic, flexural and compaction-induced subsidence; ii) decompacted rates of sediment supply; iii) accommodation space in combination with 2nd order eustatic sea-level fluctuations, which can be visualized in the restored cross-sections showing the evolution of basin architecture and paleobathymetry (Fig. 4.3).

4.4.1 Subsidence/uplift trends

The Barremian to Holocene subsidence development shows significant temporal and lateral differences between the Campos, Santos and Pelotas basins. These differences are not only related to the structural framework during the syn-rift and drift stages, but also to the distance to continental source areas and the sediment volumes supplied. Figs. 4.4, 4.5 and 4.6 illustrate the subsidence evolution in time. Fig. 4.4 highlights in detail the syn-rift to post-rift subsidence (ST1 to ST3 trends) and major lateral changes along the transition from continental to oceanic crust. Fig. 4.5 illustrates the entire syn-rift to drift subsidence evolution, which comprises six major subsidence trends, each of about 7 to 50 m.y. duration (ST1 to ST6). For better comparison, the Campos, Santos and Pelotas continental margin segments have been subdivided into the following stratigraphic-structural realms: (i) continental shelf, (ii) upper-middle continental slope, (iii) lower continental slope, and (iv) oceanic basin margin to abyssal plain. Fig. 4.6 shows the basinwide subsidence evolution, incorporating subsidence/uplift values representative of the entire shelf-basin transition. These are compared with the sediment flux in order to visualize the relation of total subsidence to flexural-induced component.

In the three studied basins, there is an initial rapid decrease in subsidence from the Barremian (ST1 trend) to middle Aptian (ST2 trend). Along the shelf-slope segments of the Campos Basin, subsidence rates diminish from 300-350 m/m.y. to 110-180 m/m.y., whereas in the Santos and Pelotas basins this decrease is less abrupt from approximately 100-190 m/m.y. to 60-90 m/m.y. (Figs. 4.4 and 4.5). However, lateral subsidence patterns in the Campos and Santos basins are fairly similar. Subsidence peaks and lows along the continental shelf (Fig. 4.4, 0-80 km from the NW boundary of the profile) reflect the extension of rift half-grabens and shoulders (hanging wall, foot wall). On the slope, subsidence was distributed more uniformly. Near the transition from the lower slope to abyssal plain (Fig. 4.4, 230-240 km from the NW boundary of the profile), a maximum in subsidence rates is recognized. In contrast, the Pelotas Basin shows a relatively uniform distribution of low subsidence, which suggests that syn-rift faulting culminated earlier, around the Hauterivian-early Barremian. Furthermore, coexisting rift volcanism probably compensated the vertical fault-displacement and subsidence of hanging-wall blocks.

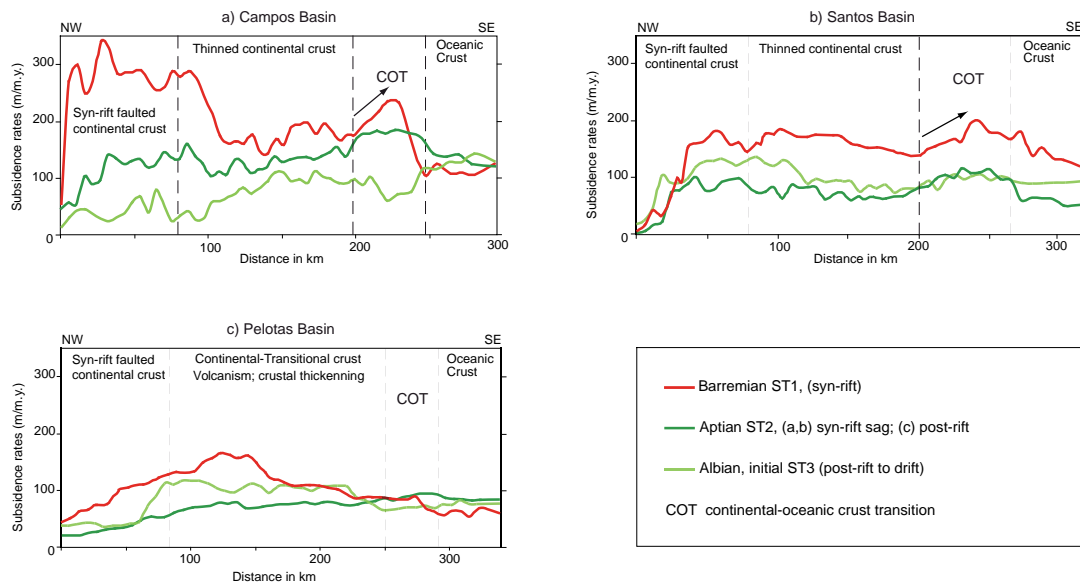


Fig. 4.4 Syn-rift to post-rift subsidence evolution along the shelf-basin transition. Three selected time layers include: Barremian (red), Aptian (dark green), Albian (light green). On the continental shelf, peaks and lows in Barremian subsidence rates represent fault-bounded subsiding depocenters (hanging walls) separated by uplifted blocks (foot walls). In the Santos and Campos basins, Barremian and Aptian relatively constant subsidence (100-180 m/m.y.) dominated the upper-middle slope (thinned continental crust). Near the lower slope-abyssal plain transition (COT), increased crustal thinning controlled maximum Barremian-Aptian subsidence rates (150-245 m/m.y.). During the Albian post-rift stage, thermal cooling triggered more uniform subsidence rates. In the Pelotas Basin, lateral changes in Barremian subsidence rates during extensional faulting (uplifted and subsiding blocks) are masked by the thermal effect of abundant volcanism (SDRs). Along the continental slope, Barremian subsidence rates gradually decrease in eastward direction, toward the volcanic center. Although Barremian subaerial rifting evolved to Aptian-Albian underwater oceanic drifting, subsidence patterns remain similar.

Significant depositional gradients did not exist and differential tectonic and flexural-induced subsidence was largely absent. In both the Campos and Santos sag basins, subsiding depocenters bordering the shelf margin expanded in basinward direction during the Aptian. Deposition regionally expanded and capped fault-bounded depressions. In the Pelotas Basin, ST2 extends to the late Aptian. This trend is characterized by a subsidence increase along the shelf-upper slope realm, which attenuated in the direction of the oceanic volcanic center (Figs. 4.4 and 4.5).

The subsidence development, as well as stratal geometries and depositional environments from seismic and well data, indicate that ST2 covers the final syn-rift stage (117-112 Ma) in the Campos and Santos basins. In contrast, ST2 in the Pelotas Basin marks the transition from the syn-rift to the post-rift stage (approx. 125-115 Ma). This temporal offset in basin development is related to the diachronous south-to-north opening of the South Atlantic (Moulin et al., 2010).

From the early Albian (Campos and Santos basins) or late Aptian (Pelotas Basin) to the Maastrichtian, the ST3 trend indicates a long-term subsidence decrease in all three basins. Margin development was now controlled by lithospheric thermal contraction, which represents the early drift stage (110-65.5 Ma). In the Maastrichtian, subsidence rates were at their minimum (15-20 m/m.y.) in all the three basins (Figs. 4.6). Only in areas of high sediment loading or salt

outflow, slightly higher rates occur (e.g., Santos slope, Fig. 4.5b-c). Despite these sediment flux variations, each basin shows comparable subsidence patterns. This indicates that flexural-isostatic sediment loading was not a major control on the subsidence development.

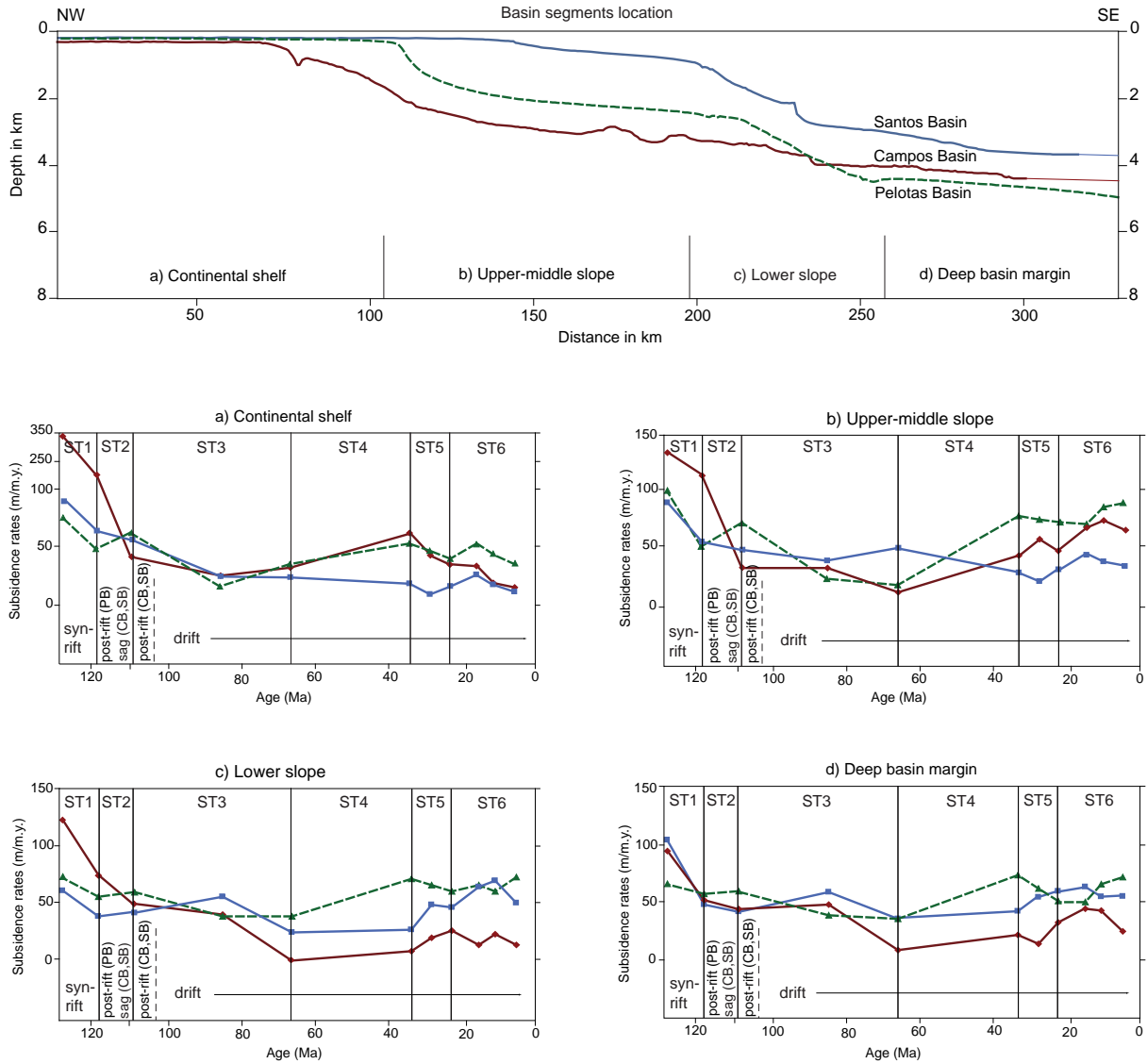


Fig. 4.5 Diagrams of quantitative subsidence development in the Campos (red line), Santos (blue line) and Pelotas basins (green line). The seismic transects have been divided into four segments: continental shelf (a), upper-middle slope (b), lower slope (c) and deep basin margin (d). Six main trends (ST1-ST6) controlled the Barremian-Holocene subsidence development. They last from 7 to 51.5 my each and are closely related to the syn-rift to drift basin tectonic stages. The first subsidence trend (ST1) is indicated by rapid decrease in subsidence rates; it represents the final phase of syn-rift extensional faulting during the Barremian. The early Aptian-early Albian trend (ST2) represents the transition to the syn-rift sag stage in the Campos and Santos basins and to the post-rift basin development in the Pelotas Basin. The Albian-Maastrichtian trend (ST3) records the stage of sea-floor spreading and lithospheric cooling with increasing age of the crust (phase of regional thermal subsidence). During the Tertiary (ST4-ST6), alternating periods of decreasing and increasing subsidence are variable along the shelf-basin transition in each basin. These patterns resulted from changes in sediment flux (see Fig. 4.6) and distribution of the flexural-isostatic sediment loading.

During the Paleogene and Neogene, subsidence/uplift trends were highly variable along the shelf-basin transition and between basins (Fig. 4.5). Other than in the Cretaceous, subsidence patterns are closely related to variations in sediment flux and resulting accommodation changes (Fig. 4.6), which lagged up to one time step behind their triggering changes. In the Campos and Pelotas basins, after minimum subsidence in the Maastrichtian, ST4 is marked by a major increase in sub-

sidence (up to 55-80 m/m.y.) during the Paleocene and Eocene. This pattern correlates with high sediment input and therefore increased flexural loading. In the Santos Basin, constant subsidence rates prevailed as sediment pathways from continental source areas were deviated to the Campos Basin (Modica and Brush, 2004) and thus sediment loading decreased.

During the Oligocene (ST5), the Campos continental shelf and slope areas underwent rapid subsidence due to a peak in sediment supply and flexural loading. Basinward, sedimentation and subsidence rates diminish (Fig. 4.5). In the Santos Basin, moderate subsidence extended along the shelf to upper slope. However, on the middle-lower slope and deep basin margin, turbidite depocenters developed and triggered differential subsidence. In the Pelotas Basin, the Oligocene subsidence rates slightly decreased along the entire section. This pattern is interpreted as the result of crustal rebound, with a considerable lag time to the strong Eocene subsidence trend, partially counterbalanced by Oligocene sediment supply and flexural loading.

The sixth subsidence trend (ST6) lasts from the early Miocene until today. In the early Miocene, all three margin segments experienced a renewed increase in subsidence. However, from middle Miocene to recent times, subsidence of the shelf considerably decreased (10-40 m/m.y.). This low subsidence in addition to the Tertiary eustatic sea-level fall caused significant reduction of the accommodation space. Second order eustatic sea-level fluctuations and submarine erosional channels (e.g. in the Campos basin) caused intermittent erosion and sediment transport to the slope-basin margin and so differential subsidence prevails until recent times. In all three basins, this trend is interpreted to represent the mature drift stage.

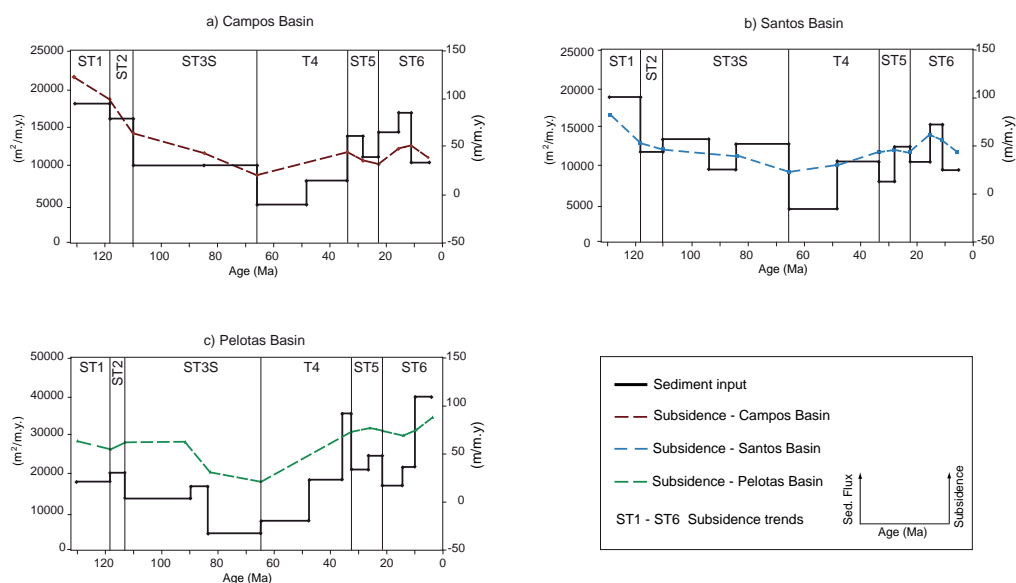


Fig. 4.6 Barremian-Holocene subsidence development (color line) and sediment flux history (black line). Subsidence values are representative of entire shelf-basin transition. From Barremian to Maastrichtian (trends ST1 to ST3) decreasing subsidence rates evolved separately from changes in sediment flux. From Paleogene to recent times (ST4 to ST6), increasing and decreasing subsidence rates are associated to variations in sediment supply, e.g. Late Eocene-Early Oligocene high sediment flux is concomitant with increased subsidence values.

Basinwide subsidence rates have been compiled in Table 4.5. Rates listed represent mean values of total subsidence and its genetic components: thermo-tectonic, flexural and compaction-induced subsidence representative of the entire shelf-to-basin transition. They allow to constrain regional subsidence patterns and to analyze the interactions between individual subsidence components (flexural subsidence) and sediment flux (Section 4.4.3).

Subsidence Trends [m.y.]	[m/m.y.] Series	Campos Basin				Santos Basin				Pelotas Basin			
		Total	Th-Tect	Flex	Comp	Total	Th-Tect	Flex	Comp	Total	Th-Tect	Flex	Comp
ST6 23-0	L. Miocene	38	6	27	6	35	10	22	4	78	18	46	17
	E. Miocene	42	7	26	8	45	12	24	9	71	21	37	15
ST5 33.9-23	L. Oligoc.	34	9	19	6	30	12	12	5	62	23	28	12
	E. Oligoc.	35	15	15	7	43	16	21	8	66	26	32	11
ST4 65.5-33.9	L. Eocene	47	18	23	7	48	23	16	10	70	26	33	15
	E. Eocene	34	14	15	6	36	17	16	5	41	23	14	6
ST3 110-65.5	Maastricht.	18	12	5	2	25	17	6	3	29	22	6	3
	Albian	52	33	12	7	45	30	12	3	84	50	25	11
ST2 117-110	Aptian	98	64	32	7	52	36	15	3	77	48	21	8
ST1 130-117	Barremian	131	96	36	0	77	55	24	0	89	67	24	0

Table 4.5 Rates of total subsidence and genetic subsidence components: thermo-tectonic (Th-tect), flexural (Flex), and compaction-induced subsidence (Comp) for the Barremian-Holocene basin evolution (130-0 Ma). Subsidence rates are representative of the entire shelf-basin transition (basinwide). Lateral variations of total subsidence rates can be observed in Fig. 4.5.

4.4.2 Genetic components of total subsidence

The individual contribution of thermo-tectonic, flexural and compaction-induced subsidence to generate total subsidence is shown in Fig. 4.7. Although thermo-tectonic subsidence values progressively decreased after continental break-up, during the Paleogene and Neogene total subsidence increased and features alternating maximum and minimum peaks. It indicates that with continental margin development, total subsidence was progressively controlled by the flexural response of the crust as driven by changes in sediment loading, whereas the thermo-tectonic component became secondary.

During the Barremian syn-rift fault-controlled extension (ST1), thermo-tectonic subsidence accounted for 60% to 75% of total subsidence. At the same time, the flexural loading slightly increased, driving about 20% of total subsidence. The burial of coarse-grained sandstones and volcanoclastic series (Itapabona, Piçarras and Imituba formations of Barremian age) generated only minor compaction-induced subsidence (up to 5% of total subsidence). During the Early Aptian (ST2), the Santos Basin experienced a decrease in thermo-tectonic subsidence, and the

proportion of flexural subsidence in total subsidence increased to 25%. In contrast, in the Pelotas and Campos basin the proportions of thermo-tectonic and flexural subsidence remained constant during the Aptian. The compaction-induced subsidence reached about 10% of total subsidence in the three basins.

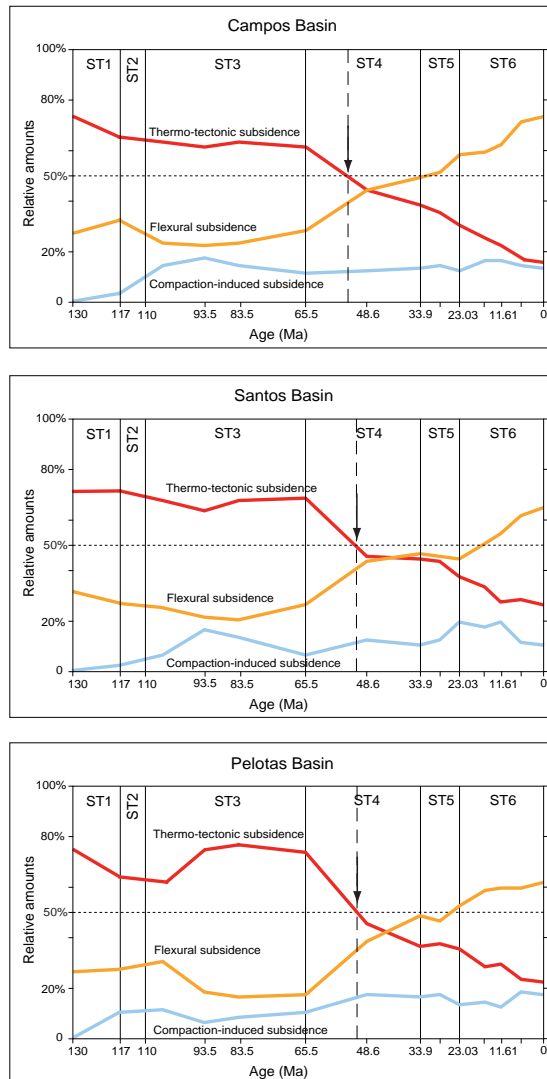


Fig. 4.7 Evolution of genetic components of total subsidence: thermo-tectonic subsidence (red), flexural subsidence (yellow) and compaction-induced subsidence (blue). The relative amounts of each component are representative of the entire shelf-to-basin transition (basinwide). During the Barremian syn-rift to Aptian post-rift stages (ST1-ST2), thermo-tectonic subsidence represents 60-75% of total subsidence. In the Late Cretaceous (ST3), the relative amount of thermo-tectonic subsidence remained nearly constant until the Turonian (93.5 Ma). In the upper ST3, thermo-tectonic subsidence increased to 80% of total subsidence. During the Paleogene (ST4-ST5), the relative amount of thermo-tectonic subsidence decreased until it became secondary. Since the Early Eocene (arrow) the combined flexural and compaction-induced subsidence controlled total subsidence. In the Neogene mature drift stage (ST6), thermo-tectonic subsidence reached its minimum (17-25% of total subsidence), whereas the flexural component of total subsidence increased to its maximum (60-65% of total subsidence). Compaction-induced subsidence generally represents about 10-15% of total subsidence; higher relative amounts of 20-25% in the Cenomanian (93.5 Ma) and in the Middle Miocene (11.61 Ma) are associated to overburden of highly compactible marine shales or high sediment supply respectively (see Fig. 4.6).

The long-term decrease in total subsidence rates during the Late Cretaceous (ST3) resulted from post-rift to early drift cooling of the lithosphere. During this stage, the flexural component remained subordinate, especially from the Santonian to the Campanian (upper ST3) when the relative amount of thermo-tectonic subsidence renewed to 70-80% of total subsidence. At the end of the Cretaceous, flexural-induced subsidence constituted 20-25% of total subsidence, and compaction-induced subsidence 12-15%. This pattern has been associated to the deposition of low-density marine shales and relative small overburden thicknesses.

During the Paleogene and Neogene (ST4-ST6), the thermo-tectonic subsidence rates decreased by 30-40%, from 14-23 m/m.y. in the Paleocene to 6-18 m/m.y. in the Late Miocene (Table 4.6). On

the other hand, the rates of flexural subsidence increased between 1.4-3 times during the Paleogene and Neogene, generating an increase of 40-60% in total subsidence, from 18-29 m/m.y. to 38-78 m/m.y. These patterns reflect that since the Paleocene total subsidence rates gradually became up to 4 times higher than thermo-tectonic subsidence. These changes are crucial for the correct analysis of accommodation space and quantification of the flexural sediment loading.

Table 4.6 Development of total and thermo-tectonic subsidence/uplift trends. Positive values represent subsidence; negative values represent uplift (subsidence decrease). From ST1 to ST3, thermo-tectonic subsidence was the dominant component in total subsidence, and thus they followed comparable patterns. The only exception occurred in the Turonian-Santonian: thermo-tectonic subsidence increased, but total subsidence continued to decrease. Trend ST4 includes total subsidence rates 2-2.5 times higher than thermo-tectonic subsidence rates (absolute values are listed in Table 4.5). During ST5 and ST6, these factors increased to 2.5-4 times. Oligocene-Holocene total subsidence/uplift trends contrasts with overall thermo-tectonic uplift.

Subs. Trend	Time layers	Campos				Santos				Pelotas					
		Total Subsidence [m/m.y.]	Th-tect. subs. Rates [m/m.y.]	Change [%]	%	Total Subsidence [m/m.y.]	Th-tect. subs. Rates [m/m.y.]	Change [%]	%	Total Subsidence [m/m.y.]	Th-tect. subs. Rates [m/m.y.]	Change [%]	%		
ST6	Mid. Mioc. - Holoc.	38	-9	+35	-14	35	-22	+57	-23	10	-23	+78	+10	18	-14
	Early Miocene	42	+20	45	-22	45	+55	0	12	0	71	+15	21	-9	
ST5	Mid. - Late Oligoc.	34	+3	30	-40	30	-33	-25	12	-25	62	-6	23	-12	
	Early Oligocene	35	-22	43	-17	43	-10	-31	16	-31	66	-6	26	0	
ST4	Mid. - Late Eocene	45	+32	48	+22	48	+33	+35	23	+35	70	+71	26	+13	
	Paleoc. - E. Eocene	34	+89	36	+14	36	+44	0	17	0	41	+105	23	-4	
ST3	Camp. - Maastrich.	18	-59	25	-69	25	-40	-37	17	-37	29	-7	22	-8	
	Turon. - Santonian	44	-8	37	+3	37	-12	+22	33	+22	30	-42	24	-40	
ST2	Mid. Alb. - Turonian	48	-7	42	+3	42	-7	-10	27	-10	52	-38	40	-20	
	Early Albian	52	-47	45	-44	45	-13	-21	30	-21	84	+9	50	+4	
ST1	Early Aptian	98	-29	64	-33	64	-32	-34	36	-34	77	-13	48	-33	
	Barremian	131	-	96	-	77	-	-	55	-	89	-	72	-	

Geohistory plots illustrate burial depths of top basement in time (Fig. 4.8). The diagrams include the evolution of total subsidence, thermo-tectonic subsidence and bathymetry in two different locations (i.e. shelf and middle slope). They allow to visualize lateral variations in subsidence and basement depths, key factors on the thermal evolution of the potential hydrocarbon source rocks intervals (i.e. Barreman-Aptian and Cenomanian-Turonian). As thermo-tectonic subsidence was the dominant component during the Barreman syn-rift to Maastrichtian early drift basin stages, both subsidence curves describe a comparable pattern during this time interval. On the conti-

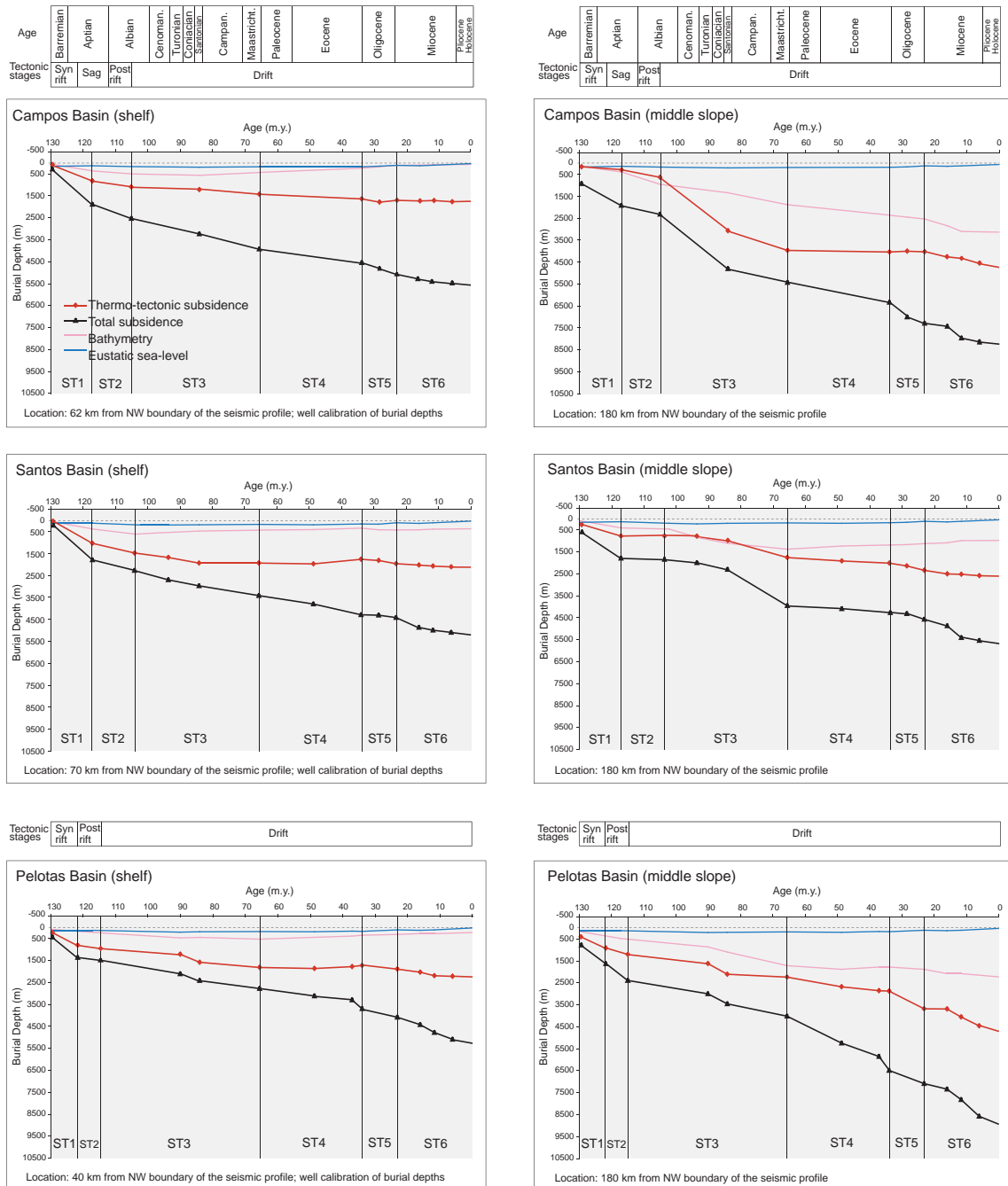


Fig. 4.8 Geohistory plots indicating burial depths of the top basement in time (130-0 Ma). They fully account for flexural loading. The diagrams include the evolution of total subsidence, thermo-tectonic subsidence and bathymetry in two different locations: continental shelf and middle slope for each the Campos, Santos and Pelotas basins. Changes in eustatic sea-level are also indicated. Burial depths on the shelf (diagrams on the left side) are calibrated with available wells.

mental shelf, burial depths of the basement increased from 0-100 m in the Hauterivian-Barremian to around 2,000-2,500 m in the Middle Aptian. In the Campos and Santos basins, this period of rapid overburden is followed by a smoother trend of thermo-tectonic subsidence (sag phase), which triggered a gradual increase in Middle-Late Aptian burial depths of the top basement. In the Pelotas Basin, the Barremian-Aptian development comprises the smallest increase in burial depths during the whole rifted to passive margin development, which indicates that post-rift thermal contraction and increasing sediment loading largely controlled the basin development.

During the Paleocene and Eocene, a flexural-driven trend of rapid burial occurred, especially in the Pelotas Basin during the Late Eocene. Although the top basement significantly subsided to approx. 3,500-4,500 m on the shelf and 4,500-6,500 m on the slope, accommodation space was progressively consumed and paleowater depths remained nearly constant. Since the Oligocene, marked differences in the burial rates exist between the three basins. In the Santos and Pelotas basins basement subsidence decelerated, but in the Campos Basin the top basement continued to rapidly subside. The Middle Miocene was particularly important for basement subsidence in both the Campos and Santos basins; in the Pelotas Basin, the greatest increase in burial depths occurred from the Middle Miocene to recent times.

4.4.3 Sediment flux and paleobathymetry

Sediment flux was obtained by calculating the two-dimensional area of accumulated sediment within each time layer. It is expressed in $\text{m}^2/\text{m.y.}$ and involves total clastic input and carbonate production. In the Campos and Santos basins, changes in sediment flux occurred with ratios of 1:2 between successive time intervals of $\varnothing 10$ m.y. duration. In the Pelotas Basin, sediment flux was about 2.5 times higher, and temporal changes occurred with ratios of 1:3 in successive time intervals. These variations depend on the evolution of continental source areas and submarine sediment redistribution. During syn-rift extension, half-grabens were the main sink, and adjacent fault-bounded uplifted blocks have been interpreted as the main source terrains. High sediment input rates (20,000-25,000 $\text{m}^2/\text{m.y.}$) triggered progradation and aggradation of coarse-grained siliclastic wedges. In the Aptian, the Pelotas Basin was characterized by a slight increase in the sediment flux and rising paleowater depths during the post-rift basin development. Conversely, the syn-rift sag stage in the Santos and Campos basins was characterized by a decrease in sediment supply and relative constant paleowater depths (150-500 m) during the Early and Middle Aptian. However, precipitation of evaporites in the Late Aptian triggered a maximum peak in the sedimentation rates and very low paleobathymetric conditions (less than 100 m).

From the Albian post-rift to the Maastrichtian drift stage, sediment supply was highly variable between basins. In the Campos Basin, sediment flux was roughly constant from Albian to Maastrichtian times. In the Santos Basin, two periods of high sediment input are recognized: Ceno-

manian, and Santonian-Maastrichtian. In the Pelotas Basin, sediment flux peaked during the Turonian-Coniacian, but declined abruptly between the Santonian and Maastrichtian. Regardless of these basin-specific changes in sediment supply, all three basins feature a long-term increase in paleowater depths during the Late Cretaceous. By the Maastrichtian water depths of shelf margin areas reached 400-500 m, and about 1,700-2,100 m toward the lower slope.

From the Paleocene to Early Eocene, sediment flux in the Santos and Campos Basin considerably decreased, but increased in the Pelotas Basin. From Middle to Late Eocene, sediment flux recovered and reached up to 8,000 m²/m.y. in the Campos, 12,000 m²/m.y. in the Santos Basin, and maximum values of 30,000 m²/m.y. in the Pelotas Basin. In the Oligocene, increasing sediment input rates in the Campos Basin contrasts with low values in the Santos and Pelotas basins. Neogene sediment flux in the Campos and Santos basins fluctuated between 10,000 m²/m.y. and 17,000 m²/m.y., with maximum values in the Middle Miocene. In the Pelotas Basin, sediment input rates increased from 20,000 m²/m.y. in the Early Miocene to 32,000 m²/m.y. in the Late Miocene. These basin-specific temporal changes in sediment flux triggered significant differences between basins in Paleogene and Neogene bathymetry (Fig. 4.3).

4.4.4 Controlling factors on the subsidence development

Lithosphere deformation and continental break-up triggered the most important changes in thermo-tectonic subsidence during the syn-rift, post-rift and early drift stages of basin development (ST1 to ST3). Conversely, during the mature drift stage (ST4 to ST6) total subsidence was primarily generated by the flexural sediment loading (Fig. 4.7). Therefore, total subsidence trends and qualitative interpretations of the Paleogene-Neogene basin fill and stratal patterns do no longer reflect changes in thermo-tectonic subsidence. The flexural-driven increase in accommodation space must be considered for basin analysis; otherwise, thermo-tectonic subsidence rates will be overestimated, leading to misinterpretations of the rifted margin development and of plate-tectonic reconfigurations in the Atlantic realm. In order to determine the importance of each tectonic evolution stage (syn-rift, post-rift, drift) in the total amount of Barremian-Holocene subsidence, the individual contribution of each subsidence trend and the cumulative proportions are plotted in Fig. 4.9.

In addition, subsidence/uplift trends during the post-rift to drift subsidence evolution have been compared with existing models on the South Atlantic opening and evolution of sea-floor spreading rates (Cande et al., 1988; Nürnberg and Müller, 1991). It allows to appraise the effects of changes in sea-floor spreading rates on the subsidence patterns. These models represent the most complete published reconstructions of the Early Cretaceous to Miocene sea-floor spreading history, incorporating on- and offshore geological and gravity data, marine magnetic anomalies and also SeaSat and GeoSat altimeter information.

4.4.4.1 Syn-rift continental thinning and transition to oceanic crust

Widespread unfaulted sub-parallel reflectors and paleobathymetries indicate that syn-rift brittle deformation of the upper crust finished before the Middle Aptian in the three basins. These observations on the seismic data are largely consistent with the lateral and temporal subsidence patterns from Barremian to Albian times (Fig. 4.4). On the continental shelf, maximum and minimum peak subsidence values (from 0 to 80 km along the transects) represent syn-rift half-grabens (hanging walls) and shoulders (foot walls) with specific subsidence/uplift rates. The rift topography and subsidence was more prominent in the Campos and Santos basins where syn-rift extensional faulting prevailed until the Late Barremian-Early Aptian. Basinward, laterally uniform subsidence values reflect the transition from fault-controlled extension on the shelf to depth-dependent lithosphere stretching in the central basin part. These interpretations are consistent with existing structural-kinematic models on the southern Brazilian and West African conjugate margins (e.g. Karner and Driscoll, 1999b and Karner et al., 2003), and also with observations from the Exmouth Plateau in the northwest Australia (Karner and Driscoll, 1999b) and the Newfoundland-Iberia margin (Crosby et al., 2008), which indicate that after brittle extension, creation of accommodation space continued by stretching of the lower crust.

Based on wide-angle seismic and gravity data, Contrucci et al. (2004), Moulin et al. (2005), and Aslanian et al. (2009) confirmed that the continental crust along the Congo-Angolan margin also thins abruptly below the continental slope. These authors presented clear evidence of a lateral decrease in crustal thickness from 30-35 km in the proximal continental margin to 5-10 km below the continental slope. It is suggested that two crustal layers with different rheological properties form the lithosphere below the pre-salt sag basins; the upper layer affected by brittle extension and the lower layer affected by ductile deformation. Karner and Driscoll (1999b) suggest that an intra-crustal decoupling zone separates these two crust domains. This surface has a ramp-flat-ramp geometry, which extends from below the continental shelf (at Moho depth) across the stretched continental crust and encounters the upper crust near the ocean/continent boundary. Then, syn-rift sag lithosphere deformation focus on the lower layer, which may represent atypical oceanic crust, lower continental crust, intruded continental crust or serpentized mantle (Moulin et al., 2005). This layer is partly exhumed near the transition from continental to oceanic crust (Boillot et al., 1987; Lavier & Manatschal, 2006). Based on kinematic constraints of the depth-dependent extensional model and the interpreted crustal configuration of the Brazilian and West African margins, Moulin et al. (2005) confirmed that an intra-crustal decoupling surface may explains the similar structuration of both margins.

Lithospheric thinning and the occurrence of an intracrustal detachment are key aspects for an improved understanding of the subsidence development during continental break-up. This relates especially to the transitional area between continental and oceanic crust (COT) where the detach-

ment cuts the upper crust and serpentinization of the mantle may occur (Reston, 2007). Based on the lateral variations of syn-rift subsidence in Fig. 4.4, three main structural settings appear to control the syn-rift to post-rift Campos and Santos basin architecture: (i) fault-related extension, (ii) depth-dependent extension, and (iii) oceanic crustal accretion. On the middle-lower continental slope where crustal stretching primarily occurred, Barremian-Aptian subsidence values are regularly distributed. Subsidence rates increase towards the abyssal plain, with a maximum of 125-240 m/m.y., at 230-240 km from the NW boundary of the seismic profile. This subsidence peak coincides with a bathymetric scarp located at the base of the lower slope, where the COT probably occurs. In the Santos Basin a 400 m vertical displacement is recognized along a fault system in this area (compare with Fig. 3.6). In the Campos Basin the vertical displacement reaches 280 m (Fig. 3.7). The uneven distribution of Barremian-Aptian subsidence along the distal portion of the stretched crust may indicate that this bathymetric scarp represents the westward dipping ramp of the intra-crustal detachment. As the depth of detachment decreases toward the east, subsidence rates increase. This decoupling zone smoothes the rheological contrast between continental and oceanic crust at about 340 km offshore (Fig. 4.4a-b, 230-240 km on the seismic profiles). As the bathymetric scarp represents the eastern limit of significant continental extension, this zone must have been effective prior to continental break-up. This structural barrier seems to also form the eastern limit of the late Aptian salt basins. Eastward of the bathymetric scarp, subsidence rates diminish, triggered by thermal uplift of the lithosphere near the rifting center and subsequent emplacement of heated and less dense oceanic crust.

Southward of the Florianopolis Fracture Zone (FFZ), creation of transitional crust (proto-oceanic crust; see Meyers et al., 1996) was initiated in the Neocomian (anomaly M11-M4; Gladchenko et al., 1997). At the foot of the Pelotas slope (approx. 340 km offshore; equivalent to 260 km from the NW boundary of the seismic profile), concave seaward-dipping reflectors (SDRs) of Barremian age disappear and indicate the change from transitional to oceanic crust. Widespread thermal subsidence of volcanic series (SDRs) during the Barremian attenuated vertical motions of hanging- and foot-wall blocks toward the shelf, generating more laterally uniform subsidence values than in the Santos and Campos basins (Fig. 4.4). The transition from Barremian subaerial volcanism (SDRs) to Aptian sea-floor spreading did not generate significant changes in the lateral subsidence distribution. Consequently, the transition from continental to oceanic crust could not be constrained by subsidence analysis, seismic or bathymetric features. The COT has been interpreted at the distal boundary of seaward dipping reflectors (SDRs), which occurs below the transition from lower slope to oceanic basin (250-290 km).

The relative proportion of syn-rift subsidence (Barremian to Early Aptian, ST1) in overall Barremian to Holocene basin subsidence varies considerably between the three basins: approximately 10-15% in the Pelotas Basin, 15-20% in the Santos Basin, and 25-30% in the Campos Basin. In

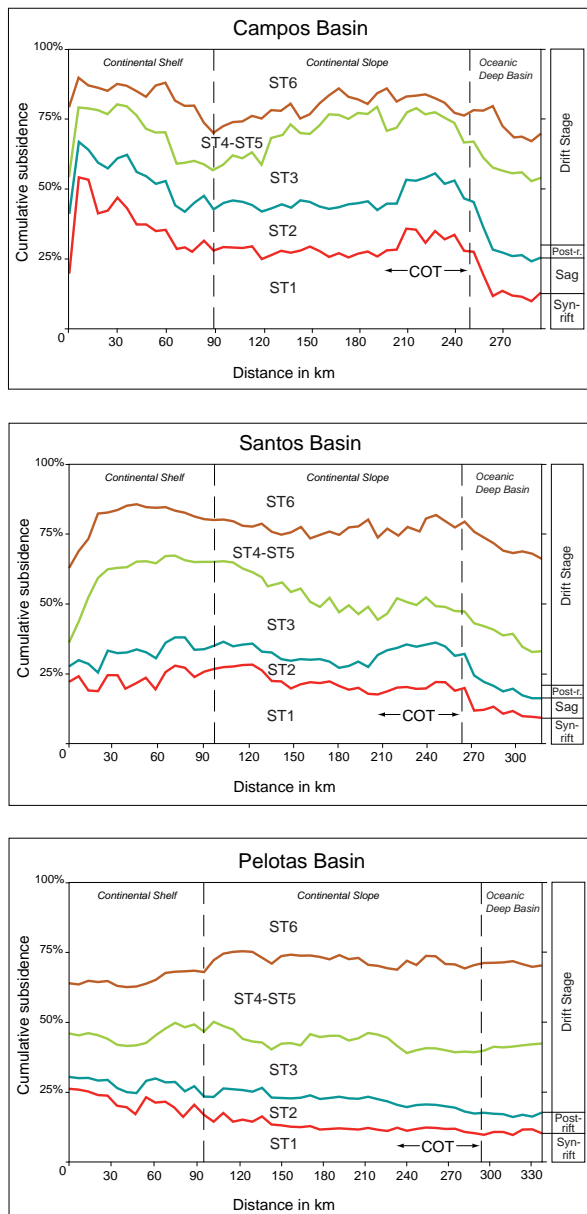


Fig. 4.9 Barremian to Holocene cumulative total subsidence along the Campos, Santos and Pelotas basins. Each line marks separately the relative proportion of each subsidence trend in Barremian-Holocene total subsidence. In the Campos Basin, Barremian-Aptian syn-rift subsidence (ST1+ST2; red+green line) represents approx. 50% of Barremian-Holocene total subsidence. In the Santos and Pelotas basins, syn-rift subsidence was slower, and accounts for 30% and 25% of Barremian-Holocene subsidence respectively. Most subsidence, and thus accommodation space, was achieved during the Albian-Holocene post-rift to drift stages (ST3-ST6), between 50% and 70% of Barremian-Holocene total subsidence. It is necessary to take into consideration that the shelf-to-basin subsidence distribution through time was governed by the interactions of thermo-tectonic and flexural subsidence.

general, the relative proportion of syn-rift subsidence increase northward, concomitant with the propagation of continental break-up. During ST2, the relative proportion of Aptian post-rift subsidence reached 10-12% in the Pelotas Basin; this low impact has been associated to the crustal thickening during extensive volcanism producing a considerably increase in the flexural strength of the crust and delayed the thermal contraction (see also Ziegler and Cloetingh, 2004; Leroy et al., 2008). With the northward transition to thinned continental crust, the relative proportion of Aptian sag subsidence in total Barremian-Holocene subsidence reached 12-15% in the Santos Basin and 18-20% in the Campos Basin.

4.4.4.2 Continental divergence

In the Late Cretaceous early drift stage, decreasing thermo-tectonic subsidence due to lithospheric cooling generated a relatively uniform subsidence signature in the three basins (ST3). However, the individual analysis of the genetic components of total subsidence reveals significant variations in the proportions of thermo-tectonic and flexural subsidence between the Pelotas and the Santos-Campos basins. The implications of the volcanic (Pelotas) and non-volcanic (Campos, Santos) crustal configuration have been evaluated by sensitivity analyses of T_e , and the resultant subsidence patterns. Previous investigations of Burov and Diament (1995) and Kusznir et al. (1995) indicate that the flexural bending of the upper elastic crust increases as the flexural rigidity diminishes. Based on this premise, it is expected that the Campos and Santos basins, floored by thinned continental crust (T_e values of 12 km), are considerably more sensitive to loading than the Pelotas Basin floored by thick volcanic crust (T_e of 20 km). These changes in flexural rigidity were manifested in the proportion of flexural subsidence during the Late Cretaceous: in both the Santos and Campos basins the flexural subsidence component reached 20-25%, but in the Pelotas Basin did not exceed 18% (Fig. 4.7). This distinct impact of the flexural rigidity of the crust between basins prevailed until the Early Eocene, approximately 82 m.y. after the continental break-up. Since this time, the contribution of the flexural sediment loading to basin formation was comparable in both the volcanic and non-volcanic segments of the southern Brazilian margin. This model of post-breakup subsidence is compatible with the thermal model of Leroy et al. (2008), which confirms the effects of continental stretching and the flexural strength of the crust on the long-term flexural response of passive margins.

Despite the differences in the proportions of thermo-tectonic and flexural subsidence, the three basins display a peak in the thermo-tectonic component during the Santonian (70-80% of total subsidence). By comparison with models for the opening of the South Atlantic, it was possible to recognize that changes in mid-oceanic seafloor spreading rates coincide with distinctive thermo-tectonic subsidence patterns. Although seafloor spreading rates are not well constrained during the Quiet Cretaceous Magnetic Zone (125-83 Ma), estimates indicate that spreading rates reached considerably high values of 75 mm/yr during the initial opening of the South Atlantic, between Chron M4 (~130 Ma) and Chron C34 (83.5 Ma) (Rabinowitz and LaBrecque, 1979; Cande et al., 1988; Nürnberg and Müller, 1991). Between Chron C34 (83.5 Ma) and Chron C27 (~64 Ma) spreading rates decreased from 75 mm/yr to 30 mm/yr. This interval is concomitant with a Santonian-Maastrichtian trend of high thermo-tectonic subsidence across the conjugate Brazilian margin (Fig. 4.7). Furthermore, low rates of sea-floor spreading appear to have diminished ridge-push plate forces toward the continental margin, enabling slightly increasing subsidence values toward the continental shelf (Fig. 4.5a).

During the Paleogene and Neogene (ST4 to ST6), subsidence changes were primarily controlled by the evolution of continental source areas and the sediment supply rates. Thermo-tectonic subsidence was secondary in total subsidence. For this reason, and because of the thermal stabilization of the lithosphere around 65 m.y. after continental break-up, it is unlikely that changes in spreading rates affected the subsidence development during the Paleogene and Neogene. In this stage, the most significant variations in the subsidence patterns occur along the continental slope and deep basin margin of the Santos and Campos basins. These temporal and lateral changes were associated to salt deformation and remobilization of the sediment infill as well as submarine volcanic events (Oreiro, 2006). In the Pelotas Basin, where salt deformation is absent, the basin architecture was largely controlled by differential thermal subsidence due to lithospheric cooling and a more regular distribution of the flexural sediment loading. Consequently, subsidence variations along the slope-to-basin transition are less prominent than in the Campos and Santos basins. In the three basins, higher rates of compaction-induced subsidence are associated to periods of rapid sediment loading, including the Late Eocene and the Middle Miocene, when sediment compaction represented 16-20% of total subsidence (Fig. 4.7).

As shown in Fig. 4.9, the Albian-Holocene margin development (ST3-ST6) in the Pelotas Basin accounts for approximately 70-80% of the total amount of basin subsidence that occurred since the Barremian. In the Campos and Santos basins, continental stretching and syn-rift subsidence were more significant (up to 45%); thus, the proportion of subsidence during the drift stage represents only 55-60% of Barremian-Holocene subsidence. These variations in the amount of subsidence occurring during each tectonic stage have strong implications for the thermal evolution of potential source rocks intervals. Our results suggest that syn-rift (Aptian) and early drift (Cenomanian) organic-rich successions in the Santos and Campos basins may have reached appropriate temperature conditions for hydrocarbon generation earlier than in the Pelotas Basin, where most subsidence occurred in the mature drift stage.

4.5 Evolution of accommodation space

In the following sections, the evolution of accommodation space has been restored and analyzed in terms of quantitative results from inverse-basin modeling and their correspondence with seismo-stratigraphic features and stratal patterns. The genetic analysis of sequence stratigraphic surfaces and relative sea-level incorporates 2nd order eustatic changes and subsidence/uplift values (Fig. 4.10).

4.5.1 Barremian syn-rift to Albian post-rift stage

Reconstruction of the tectono-stratigraphic framework and timing of syn-rift faulting in sub-salt basins is limited by the resolution of the seismic and biostratigraphic data available. The reconstruction of the Barremian to Aptian stratigraphic boundaries is based on the correlation of changes in subsidence, paleobathymetry, eustatic sea-level, stratal geometries and thicknesses. They were cross-checked with the results of previous studies (e.g. Karner et al., 1997; Karner and Gambôa, 2007; Mohriak et al., 2008).

In the Pelotas, Santos and Campos basins, seismic units SP1, SS1 and SC1 record the Barremian stage of syn-rift extension (subsidence trend ST1). The volumes of basaltic flows and faulting show temporal and regional variations from south to north. Extensional faulting prevailed until the lower-middle Barremian (~130-128 Ma), coeval with widespread subaerial volcanism (SDRs) in the Pelotas Basin. During this stage, fault displacement and thermal contraction of the volcanic crust were the main controls on accommodation space. Due to the large volumes of basaltic flows, all accommodation available progressively filled during the Early-Middle Barremian (depositional unit SP1). At least 1,000-1,200 m of Barremian volcanic series and clastic deposits were regionally accumulated. By the Late Barremian, subaerial volcanism diminished and paleowater depths gradually increased to 200-250 m along the continental shelf and up to 700 m in the central basin part. Lacustrine environments with deposition of organic-rich shales are not recorded from the syn-rift depocenters in the Pelotas Basin. Up-section, the early Aptian unconformity (~122 Ma) records a eustatic sea-level fall with subaerial exposure of the shelf to upper slope, interpreted as a sequence boundary type 1 (SB1; Vail et al., 1984).

In the Santos Basin, most syn-rift faults terminate in the upper Barremian (~128-125 Ma) and only minor traces of volcanism have been identified. The lower part of unit SS1 thins and amalgamates with seaward-dipping reflectors on the lower slope. Up-section, a 150 m-thick package of prograding sub-parallel reflectors, unfaulted and with long lateral continuity to the lower slope, represents the lower part of the sag succession. In the Campos Basin, syn-rift faults extend to the early Aptian basin fill (~122-120 Ma). Unit SC1 shows highly variable thickness and strong facies changes due to the rift topography. Volcanic series were only recognized as part of the Hauterivian continental basement. In both the Santos and Campos basins, the Early-Middle Barremian basin fill consists of coarse-grained alluvial and fluvial-deltaic regressive deposits. This trend was controlled by high sediment supply despite a gradual base level rise during syn-rift subsidence. The Late Barremian-Early Aptian succession is composed of fluvial-deltaic sandstones intercalated with stromatolitic carbonates, organic-rich shales and marls deposited in restricted lacustrine environments and during intercalated periods of progradation and retrogradation. This interval contains the most important source rocks offshore Brazil (Katz and Mello, 2000), intercalated with carbonate and clastic reservoirs.

The Middle-Late Aptian succession in the Pelotas Basin records a trend of rapid creation of accommodation space and base level rise due to post-rift thermal contraction of the crust (trend ST2). Northward, syn-rift lithospheric stretching persisted, and so basin sagging controlled the development of the Santos and Campos basins. During the Aptian, sag depocenters gradually expanded to approximately 230 km wide, from the middle continental shelf to the transition to oceanic crust (Figs. 4.3). Total or partially restricted water circulation, a smooth topography with average paleowater depths of 150-500 m characterized these basins in the Early Aptian. The transition from fault-controlled deformation of the upper crust to ductile stretching in the lower crust layer was marked by decrease in subsidence values and a gradual reduction in accommodation space from the continental shelf to the lower slope (Fig. 4.5a-c). Sediment input exceeded the accommodation rates and prograding fluvial-deltaic sediments capped previous fault-bounded syn-rift depocenters. In the deep basin margin subsidence rates are nearly constant (Fig. 4.5d); this pattern characterizes the area where major lithospheric stretching occurred.

A middle Aptian unconformity (117 Ma) on the inner to middle shelf and its marine conformity basinward truncates the reflectors and seals prospective clastic-carbonate syn-rift deposits in both the Campos and Santos basins. It has been interpreted as a type 2 sequence boundary (SB2) (Vail et al., 1984) caused by a second order eustatic sea-level fall (Hardenbol et al., 1998). It correlates with the pre-Chela unconformity on the conjugate West African margin (Karner et al., 2003). The discrepancy in age of the Aptian regressive trend between the Pelotas (~122 Ma) and the Campos/Santos basins (117 Ma) is linked to basin-specific transition from syn-rift to post-rift subsidence rather than to temporal eustatic changes. During the Middle Aptian, sediment dispersion widths increased and paleowater depths gradually rose to approximately 700 m in the central part of both the Santos and Campos basins. As a result, fluvial-deltaic deposits evolved laterally and vertically to fine-grained deep lacustrine deposits. In the Late Aptian, arid climate conditions facilitated the development of hypersaline environments (Skelton, 2003; Lentini et al., 2010) and widespread deposition of evaporites. Inverse-basin modeling does not provide conclusive results on the origin and water-level conditions of the salt depocenters. The salt depositional setting remains undecided between a shallow water-shallow basin, shallow water-deep basin, or a deep water-deep basin; these uncertainties are expected to be clarified by forward modeling in Chapter 5. Nonetheless, the restored basin geometry and bathymetric conditions suggest that salt deposition started in deep sag basins with a shallow-to-deep water setting between 150 m on the shelf and 900 m in the central part.

The post-rift stage comprises the Middle-Late Aptian (122-115 Ma) in the Pelotas Basin and the Albian (112-99.6 Ma) in the Campos and Santos basins. In the Pelotas Basin, the lower to middle Aptian basin fill is represented by a regressive wedge (unit SP2) deposited during a period of high sediment supply and low eustatic sea-level. In absence of calibration wells penetrating this

unit, by correlation with the shallow-water succession it was interpreted to consist of fluvial-alluvial conglomerates, sandstones and intercalated shales. This unit is bound at the top by a middle Albian (~115 Ma) maximum regressive surface (MRS), which marks the onset of retrogradation (unit SP3) during the post-rift basin development. Along the shelf, retrogradational to aggradational mixed carbonate-siliciclastic systems were deposited in water depths of 100-300 m. They graded basinward to marine shales with some hemipelagic carbonate intercalations with water depths of approx. 1,200-1,400 m (Fig. 4.3). In the Campos and Santos basins, uniform subsidence rates and reduced clastic input after salt deposition resulted in a gradual increase of paleobathymetry during the Albian. In both basins, the early Albian post-rift stage is recorded by carbonate retrogradation, followed by middle-late Albian aggradation-progradation (units SC3, SS3). This period was particularly important for the Santos basin development, where a 120-130 km-wide carbonate platform was developed. Productive hydrocarbon reservoirs include shallow-marine carbonates of the Outeiro Fm. in the Campos Basin and carbonates of the Guarujá Fm. on the middle to outer shelf of the Santos Basin (Coward et al., 1999).

4.5.2 Late Cretaceous early drift stage

During the Late Cretaceous, lithospheric thermal contraction and a eustatic sea-level rise caused an increase in accommodation space and bathymetry. Although the rates of accommodation generally exceeded sediment supply, the sediment volumes delivered for each of the Pelotas, Santos and Campos basins were highly variable in time and triggered basin-specific depositional and subsidence patterns.

From the Cenomanian to the Coniacian, thermal subsidence and rising eustatic sea-level controlled the retrogradational pattern in the three basins (units SC4, SS4 and SP3), which in the Pelotas Basin persisted until the Maastrichtian. This trend of rapid basin deepening generated Turonian to Coniacian (92-90 Ma) disconformities (see Table 3.1). Biostratigraphic analyses and subsidence modeling indicate that the paleobathymetry on the Campos and Santos shelf margins increased from approx. 200 m in the Albian to 350 m in the Santonian. Toward the distal domain, paleowater depths varied from 800 m to 1,800 m in the Campos Basin and up to 1,400 m in the Santos Basin. The Pelotas shelf margin was characterized by comparable bathymetry (300-400 m), although toward the central-distal basin domain water depths reached approx. 2,000 m in the Santonian.

Following this overall trend of basin deepening and retrogradation, onshore tectonic uplift severely affected the sedimentary systems offshore. The exhumation histories of the topographic highlands have been constrained by apatite fission track analysis (e.g. Zanotto, 1993; Gallagher et al., 1994; Borba et al., 2002; Tello Saenz et al., 2003, 2005; Ribeiro et al., 2005). Results indicate that the

main sediment source areas (including from south to north the Dom Feliciano Belt, Torres Arch, Río Grande Arch, Serra do Mar and Serra da Mantiqueira) show specific timing and rates of exhumation. Therefore, the sediment volumes delivered offshore were highly variable in time and between basins. Although the combination of sequence-stratigraphy and inverse-basin modeling allows to establish the relationship between onshore uplift and offshore sedimentation, the chronostratigraphic framework (depositional units with between 4.4 m.y. and 31.6 m.y. duration) does not allow to certainly define the effects of shorter-duration tectonic and eustatic events, which will be later analyzed by forward stratigraphic modeling.

Almeida and Carneiro (1998), Cobbold et al. (2001), and Ribeiro et al. (2005) indicate that the exhumation of the Serra do Mar mountain range started around the Turonian-Coniacian, peaked during the Santonian to Maastrichtian, and finished in the Paleocene. This event particularly affected the Santos Basin, where regardless of the eustatic sea-level highstand in the Late Cretaceous, high rates of sediment supply triggered wide progradation (units SS5-SS6). Significant sediment bypass to the continental slope and rise occurred. By the Maastrichtian, thick deep-water clastic wedges had increased sediment loading and subsidence along the upper-middle slope, while the shelf top experienced erosion and unloading because of flexural rebound of the crust (Fig. 4.5).

In contrast, sediment supply to the Pelotas and Campos basins was nearly constant during the Late Cretaceous. This pattern of sediment distribution may be attributed to the inherited topography of the Paraíba do Sul drainage system, which by the Santonian-Paleocene diverted most sediment pathways towards the Santos Basin (Cobbold et al., 2001; Modica and Brush, 2004). Despite the long-term decrease in subsidence (trend ST3), the rise in eustatic sea-level created enough accommodation space to surpass the sediment supply in both the Pelotas and Campos basins, and consequently an overall retrogradational pattern dominated (units SC4-SC5 and SP4-SP5). Two short-term periods of aggradation to progradation have been associated to eustatic sea-level falls, one in the Santonian and another in Middle-Late Maastrichtian (see Table 3.2). Although structural reconfigurations in the hinterland of the Pelotas Basin are little constrained, fine-grained clastic sedimentation offshore reflect long transport distances and tectonic quiescence in the onshore domain. A Turonian-Santonian magmatic event (Caldas igneous intrusion; Gallagher et al., 1994; Cobbold et al., 2001; Meisling et al., 2001) coincided with a slight increase in the sediment supply (Fig. 4.6), which accentuated the short-term progradational trend.

Toward the deep-marine setting, the three basins experienced an increase in the flexural subsidence component and slope gradients. This trend, as well as deep-marine sand volumes reached by the calibration wells, channels with basal erosional scours identified in seismics (Fig. 3.9), suggest that intermittent turbidite deposition persisted throughout the Late Cretaceous (until recent times) in the three basins. The combined effect of the increasing sediment loading and

basin tilting due to differential thermal contraction generated intense dipward salt remobilization in the Campos and Santos basins since the Albian. Sand-rich gravity mass-flows filled small inter-diapir depocenters, while intercalated mud-rich debris flows occasionally overstepped the eastern salt edge and were deposited on the oceanic abyssal plain (see Fig. 3.10). Turbidite deposits represent highly productive hydrocarbon intervals in both the Campos (Carapebus and Emboré Fms.) and the Santos basins (Juréia and Ponta Aguda Fms.; Table 3.1). Intercalated evaporites and shales act as the main stratigraphic seals (Campos Basin: Retiro and Ubatuba Fms.; Santos Basin: Ariri, Itajaí-Açu and Marambaia Fms.). In the Pelotas Basin, mass-flow deposition resulted in thick sediment wedges on the continental slope. However, seismic and well log data indicate that the mud/sand ratio is considerably higher than in the Campos and Santos basins, and therefore the low porosities reduce reservoir quality of these sediments.

4.5.3 Paleogene-Neogene mature drift stage

The lower part of the Paleogene basin fill was affected by a rapid decrease in accommodation space and strong shelfal erosion. This event is evidenced by a eustatic-driven erosional unconformity of Late Paleocene age recognized in the three basins (Table 3.2). The removed fluvial-deltaic to shallow-marine deposits were transported as gravity-mass flows downslope, which aggravated flexural and compaction-induced subsidence in the deeper basin.

After the Late Paleocene forced regressive trend, increasing subsidence rates (lower ST4) and rising eustatic sea-level controlled the basin development during until the Early Eocene. Accommodation rates exceeded sediment flux, and retrogradation occurred in the three basins. From the Middle Eocene to Oligocene, sediment supply increased in all three basins. This trend has been associated to intra-plate compression and uplift during the Incaic phase of Andean orogeny (40-50 Ma; Cobbold et al., 2001), particularly important in the Santos hinterland (Serra do Mar and Serra do Mantiqueira). Although in different degrees, the flexural sediment loading and total subsidence amplified in the three basins (upper ST4). Because of the progressive consumption of shelfal accommodation space during the Eocene and Oligocene, sediment stacking patterns became highly sensitive to eustatic sea-level fluctuations. A late Eocene eustatic sea-level fall generated a type 2 sequence boundary in both the Campos and Pelotas basins, which marks the Eocene-Oligocene contact (between units SC6-SC7, and units SP8-SP9). As for the Santos Basin, coastal retrogradation shifted to aggradation-progradation in the Late Eocene (unit SS8) in spite of reduced sediment input, but In contrast to the former basins, shelfal erosion did not occurred.

In the Campos and Pelotas basins, the Oligocene succession comprises two stratigraphic units (SC7-SC8 and SP9-SP10 respectively), which define a complete base-level cycle:

early Oligocene normal regression (NR), middle Oligocene retrogradation (RT), and middle-late Oligocene aggradation-progradation (AP) (Table 3.2). This composite succession is bound at the top by an early Miocene sequence boundary (SB2). In the Pelotas Basin, decreasing subsidence values along the shelf contrast with the high subsidence rates in the slope to deep basin margin. These lateral changes reflect shelf sediment unloading and redeposition basinward. Further evidence are the dip-oriented channels and erosive scours cutting into the Miocene-Oligocene

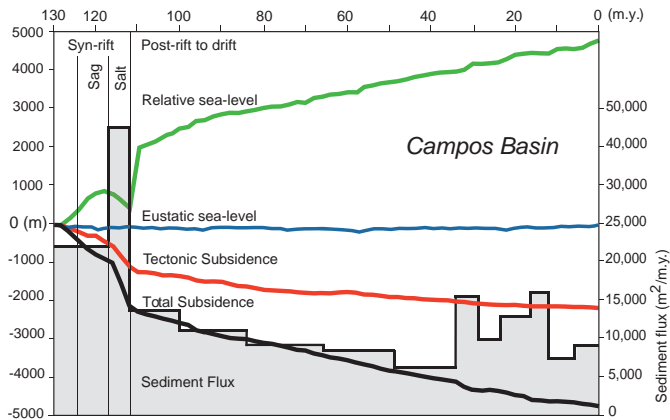
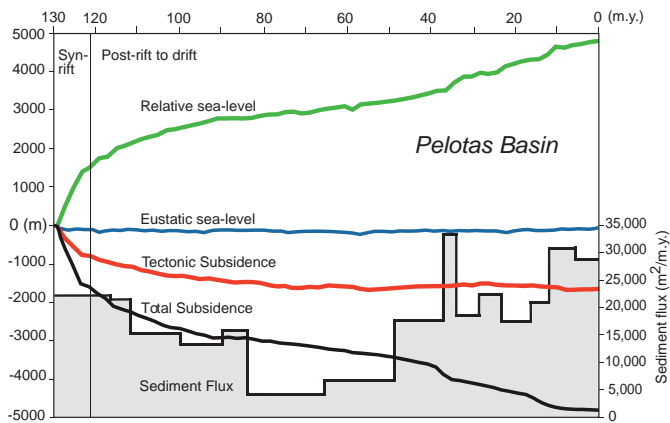
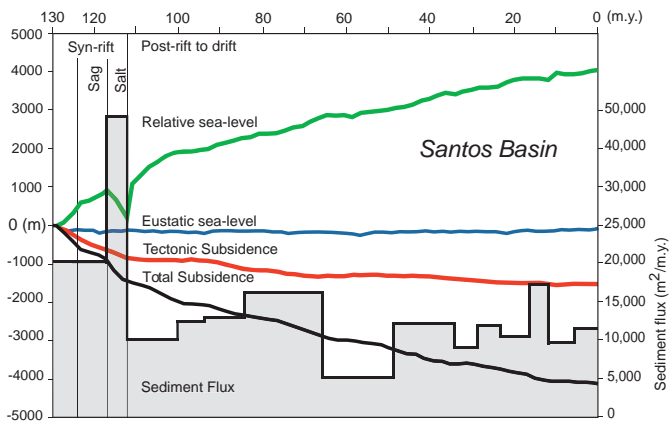


Fig. 4.10 Relative sea-level evolution as a function of eustatic sea-level, thermo-tectonic subsidence, total subsidence and sediment flux. These values were calculated in the deepest basin part, between 360-380 km from the coastline.



basin fill near the shelf break (Fig. 3.8a) and deep-marine erosive surfaces at the base of turbidite sandstones penetrated by the available wells along the continental slope (see Fig. 5.2). Northward, uplift of the Serra do Mar mountain range persisted throughout the Oligocene and drainage pathways eventually shifted from the Santos to the Campos Basin (Modica and Brush, 2004). As a result, sediment supply to the Campos increased in the Early Oligocene, and large volumes of sediment were transported to the continental slope-deep basin margin. High flexural subsidence in the basinward direction was concurrent with crustal rebound and exposure of the shelf area (similar to the Pelotas Basin). Marine shale and intercalated turbidites filled salt-bound depocenters and buried most of the salt diapirs in the Campos Basin. This trend of increased sediment loading coincided with a period of minor salt remobilization, which will be later constrained by forward stratigraphic modeling. Toward the deep basin margin, shingled-oblique reflectors indicate that turbidite and/or debris flows traveled beyond the continental rise and formed basin-floor fans. In the Santos Basin, reduced sediment supply and a rise in eustatic sea-level caused retrogradation during the Early Oligocene (unit SS8). This pattern shifted to aggradation-progradation in the Late Oligocene (unit SS9), when a eustatic sea-level fall caused a decrease in accommodation space, and so the sediment supply dominated. In contrast to the Campos Basin, the Oligocene in the Santos Basin represents a period of decreased sediment loading and gradual basin tilting, which appear to have induced downslope salt compression and diapirism. In the both the Campos and Santos basins, slope-parallel bottom currents cross-cut turbidite and pelagic deposits, causing deep-marine sediment remobilization and redistribution of the sediment loading, processes later analyzed by forward stratigraphic simulations.

During the Neogene, the accommodation space gradually decreased due to the long-term eustatic sea-level fall. Sediment stacking patterns were controlled by changes in the sediment input rates overprinted by eustatic sea-level fluctuations. Intercalated shelfal erosional truncations within the Miocene succession reflect periods of shelf-edge collapse or downslope sediment transport, causing further flexural loading basinward, and rebound in the landward direction. As a result, subsidence values were highly variable along the shelf-to-basin transition. Deep-marine erosional surfaces mark the base of turbidite and debris flows, more frequent within the Plio-Pleistocene basin fill (Figs. 3.8 and 3.9).

The base of the Miocene basin fill is marked by a sequence boundary (SB2), used as a stratigraphic marker horizon between the three basins. It resulted from a second order eustatic sea-level fall of Burdigalian age (17-20 Ma). On the Santos inner shelf, this surface amalgamates with an earlier, eustatic-driven unconformity of late Oligocene age (21-23 Ma). Lower Miocene normal regressive (NR) successions change to retrogradational (RT) middle Miocene deposits (units SC9, SS11, SP11; Table 3.2). Up-section, three stacked progradational-aggradational units (SC10-SC12) comprise the middle Miocene-Holocene succession in the Campos Basin. This interval was controlled

by continued high sediment supply and a reduction in accommodation space due to a long-term eustatic sea-level fall. A strike-oriented submarine channel close to the shelf break cut into the Miocene-Holocene deposits (Fig. 3.8c), generating abundant bypass and redeposition toward the continental slope. Miocene sandstones capped remaining depocenters between salt diapirs. This resulted in stacked potential reservoirs of Miocene age with underlying Eocene-Oligocene sand-rich turbidite fans trapped in salt-related depocenters.

In the Santos Basin, sediment input rates slightly increased during the Miocene, although they still remain lower than in the Campos and Pelotas basins. Early-middle Miocene retrogradation (upper part of unit SS11) shifted to aggradation-progradation (unit SS12) because sediment flux surpassed the accommodation rates. A eustatic sea-level fall (9-11 Ma) triggered shelfal erosion and a renewed normal regression (unit SS13), which shifted to aggradation-progradation since the latest Miocene (6 Ma; unit SS14). This aggradational pattern is associated to recurrent collapse of the shelf front, with deposition of turbidites and debris flows along the slope. Toward the deep basin margin, fine-grained debris flows overstepped the diapiric province and form basin-floor fans with chaotic patterns, which distorted the Oligocene to Miocene basin fill (Fig. 3.10b).

In the Pelotas Basin, lower Miocene normal regressive deposits (unit SP11) are covered by a maximum regressive surface (MRS) of middle Miocene age (14-15 Ma, Langhian). Lithologies and stratigraphic thicknesses offshore suggest that drainage systems in the vicinity of the Rio Grande do Sul state (e.g. Rio de la Plata and Lagoa dos Patos) delivered great volumes of sediment to the southeastern Brazilian margin, creating the Rio Grande Fan. The retrogradational units SP12 and SP13 resulted from a trend of flexurally-induced subsidence and a second order eustatic sea-level rise in the Middle Miocene. Up-section, an intra-late Miocene (9 Ma, Tortonian) maximum flooding surface (mfs) marks a shift to aggradation-progradation (upper part of SP13 and SP14). This depositional trend persists until today.

4.6 First conclusions: seismo-stratigraphy and inverse-basin modeling

The integration of sequence stratigraphy and inverse-basin modeling provides a consistent model of controlling factors of accommodation space (subsidence, eustacy and sediment supply) and their individual influence on shelf development and depositional systems in each the Campos, Santos and Pelotas basins.

On the southern Brazilian margin, subsidence/uplift changes exerted the primary control on the evolution of accommodation space and second order depositional sequences. From rifting to drifting, the development of the margin can be subdivided into six subsidence trends (ST1-ST6) of 7-50 m.y. duration. They main controlling factors on the subsidence development and

distribution include: i) syn-rift lithosphere deformation; ii) intra-plate balance forces during continental divergence (e.g. ridge-push stress, continental transpression during the Andean orogeny); iii) changes in sediment supply; iv) salt remobilization. The flexural rigidity of the crust represents a key factor on the crustal response to the sediment and water loads, and therefore must be considered during basin modeling and reconstruction of paleowater depths. Equating total subsidence with thermo-tectonic subsidence and neglecting flexural (and compactional) response leads to strongly erroneous tectonic models.

South to north propagation of continental break-up and lithospheric deformation determined lateral changes and temporal offsets in basin development along the Brazilian margin. In the three continental shelf basins, the syn-rift basin stage is characterized by decreasing subsidence during the Barremian (ST1). Thermo-tectonic subsidence was at this time the main component of total subsidence, and consequently controlled the creation of accommodation space. Eustatic sea-level changes exerted only a minor control on syn-rift accommodation space. The Pelotas volcanic-margin segment features a thickened and a more rigid crust, which controlled the rapid change from syn-rift continental-transitional to post-rift marine environments and subsidence (ST2). The Santos and Campos non-volcanic segments feature a thinned continental crust, which generated widespread relatively constant subsidence values (ST2) and the formation of restricted marine syn-rift sag and salt basins.

Based on the lateral and temporal distribution of Barremian-Aptian subsidence in the Santos and Campos basins, the bathymetric scarp at the lower slope-abyssal plain is interpreted to be the continental-oceanic crust transition (COT) and the eastern boundary of major syn-rift continental thinning. Eastward of the bathymetric scarp, thermal uplift near the rift center caused noticeable decrease in subsidence rates (260-320 km). In the Pelotas Basin, the transition from proto-oceanic to oceanic crust is less obvious in the regional subsidence patterns and basin geometry. The boundary between both crustal types was constrained by the termination of Barremian seaward-dipping reflectors near the lower continental slope.

During the Late Cretaceous early drift stage, uniform basinwide subsidence characterized the Brazilian margin (ST3). Decreasing thermo-tectonic (and total) subsidence resulted from thermal relaxation of the lithosphere, typical of 'passive' continental margin development. Thermal readjustment of the crust resulted from changes in sea-floor spreading rates in the South Atlantic: Santonian-Maastrichtian lower sea-floor spreading rates and reduced ridge-push forces coincided with a period of increased thermo-tectonic subsidence in all three basins. The tectonic evolution of the mountain ranges in the margin hinterland (Serra do Mar, Serra da Mantiqueira, Don Feliciano Belt) considerably influenced the sedimentation rates offshore. Therefore, source areas development needs to be considered in passive margin studies.

After the Florianópolis High was submerged in the Albian, major eustatic sea-level fluctuations and regional structural events can be traced from the Pelotas to the Campos Basin. Important stratigraphic markers are: (i) Cenomanian to Turonian eustasy-driven unconformities at the top of the Albian carbonate units; (ii) Cenomanian to Coniacian transgression, causing widespread deposition of pelitic sediments during a period of global anoxia; (iii) late Paleocene eustasy-controlled shelf-wide unconformity, overlain by Maastrichtian to Eocene reworked sediments during a forced regression.

While thermo-tectonic subsidence rates diminished during the mature drift stage, flexural and compaction-induced subsidence increased and progressively became the dominant control on total subsidence (trends ST4-ST6). Periods of maximum and minimum sediment flux during the Paleogene and Neogene show a good correlation with total subsidence trends. Periods of shelf retrogradation and progradation depend primarily on changes in sediment flux, flexural and compaction-induced subsidence rather than on changes in thermo-tectonic subsidence and eustatic sea-level fluctuations.

Subsidence, eustatic sea-level fluctuations and sediment supply are important controlling factors of the sedimentary architecture of the Campos, Santos and Pelotas basins. Furthermore, these processes and their interactions strongly influenced the development of hydrocarbon systems: (i) Barremian to middle Aptian and Cenomanian to Turonian rapid basin subsidence in combination with oceanic anoxic conditions resulted in deposition of organic-rich shales; (ii) Late Cretaceous high accommodation gain overbalanced by sediment supply caused prograding delta sandstones and turbidite reservoirs (units SS5 and SS6) in the Santos Basin; (iii) Eocene to Miocene creation of accommodation space (eustasy and flexural response of the crust) allowed the deposition of sand-rich reservoirs in the Campos Basin (units SC6 to SC11); (iv) a Neogene peak of clastic input to the southern Santos Basin coincided with abundant unfilled accommodation space, left over from the Paleogene; as a result, thick Miocene successions (units SC11 to SS13) with seal characteristics formed; concomitantly, Late Cretaceous source rocks came into the oil-window; these source rocks are overlain by Eocene-Oligocene potential reservoirs; (v) after the Late Cretaceous, abundant accommodation space was available in the Pelotas Basin: this enabled the sedimentation of thick clastic prograding wedges, which contain sandstones within basin floor fans, encased in impermeable shales. The thick Tertiary succession played an important role in the maturity development of gas- and oil-generating Upper Cretaceous marine source rocks.

5. Forward stratigraphic modeling

5.1 Introduction

Forward stratigraphic modeling aims to predict and quantify the physical processes controlling the infill of sedimentary basins (e.g. subsidence, sediment distribution, transport mechanisms). The method allows to visualize the predicted depositional history (forwards in time) and carry out sensitivity tests of selected modeling parameters. The combination of inverse-basin and forward modeling has been applied in a number of academic and industry investigations to quantify mechanisms and timing of lithosphere deformation, estimate the distribution and controlling factors on the thermal and subsidence evolution (e.g. Kusznir et al., 1995; Roberts et al., 1997; Karner et al., 2003) and analyze the tectonic and sedimentary controls on depositional systems (e.g. Bowman and Vail, 1999; Leyrer et al., 1999; Scheibner et al., 2003; Burgess et al., 2006, 2008; Emmerich et al., 2008; Hasler et al., 2008; Veselovsky et al., 2008).

In this study, two-dimensional forward modeling simulates the Barremian syn-rift to Holocene drift development of the Pelotas, Santos and Campos basins (Fig. 5.1). The modeling procedure includes the quantification of inter-dependent sedimentary processes (rates of sedimentation, sea-level, erosion) and deformation processes (subsidence, flexural rigidity of the crust, salt tectonics), which provide a better understanding of the structural-sedimentary interactions that controlled the basin architecture through time. The results are compared with the seismo-stratigraphic framework, depositional geometries and numerical results from inverse-basin modeling (Fig. 5.3). This integrated approach allows to assess inherent model uncertainties from the sequence-stratigraphic interpretation, and develop best-fit plausible quantified models to the tectono-stratigraphic basin evolution.

The simulation software PHIL™ (Bowman and Vail, 1999) includes algorithms for calculation of key deformation and sedimentary processes on rifted margins: thermo-tectonic subsidence, flexural rigidity of the crust, sediment supply, sediment transport, among others. The models presented in this study have multiple links to reservoir and seal facies characterization, with emphasis on gravitational mass flows, sand volumes exported to the deep-marine setting and quantification of lithophysical parameters (porosity and compaction). The main objectives of this Chapter are: (i) modeling of the flexural rigidity of the crust and its effects on the syn-rift deformation style and long-term flexural response (ii) physical controls on the lithofacies arrangement and paleo-water depths, with particular emphasis on subsidence/uplift rates, sediment flux and gravitational sediment flows; (iii) modeling of the sag-salt basin formation and quantification of key controlling parameters; (iv) reproduce the formation of salt structures and their implications for the basin architecture and distribution of lithofacies.

5. Forward stratigraphic modeling

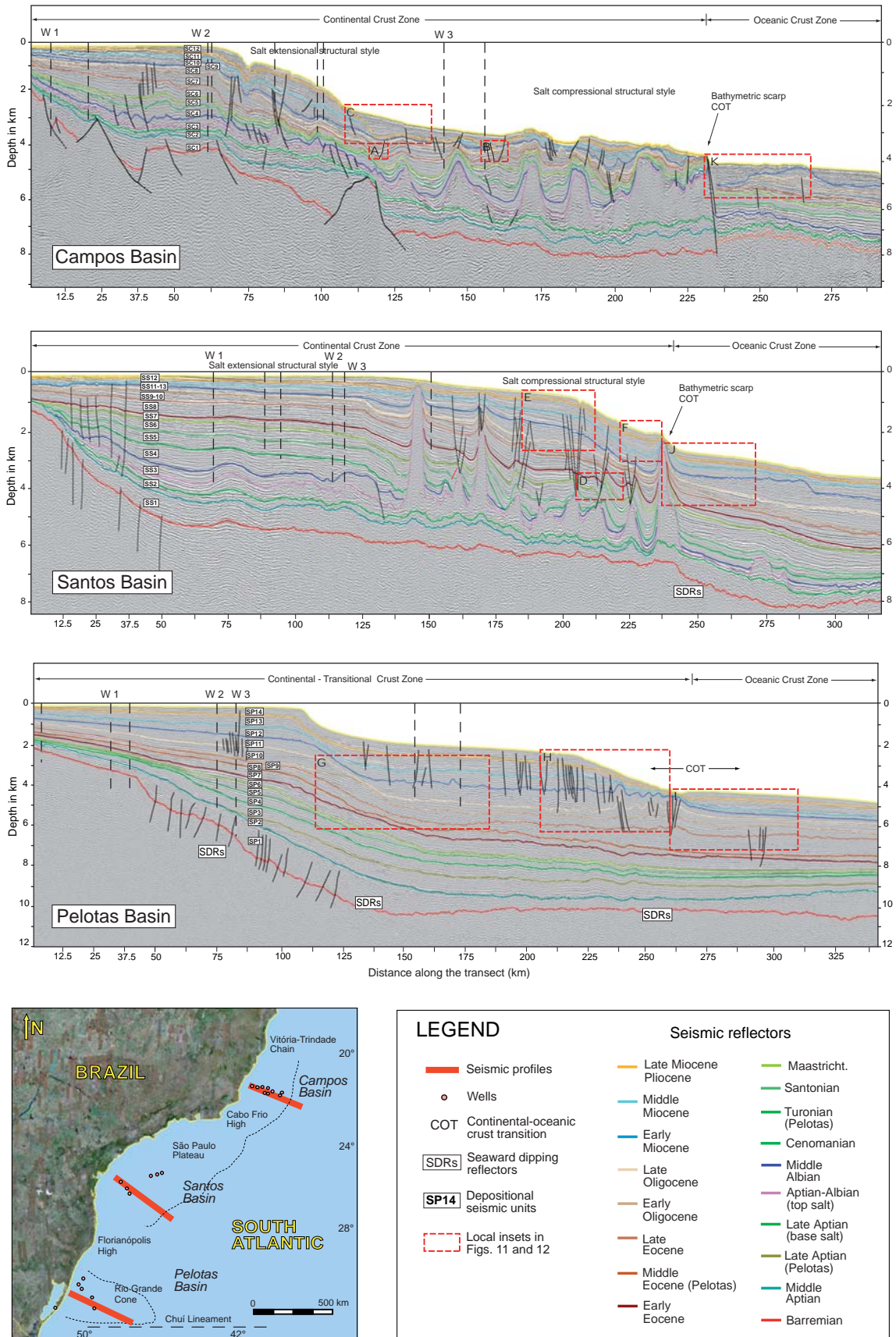


Fig. 5.1 Seismo-stratigraphy of the Campos (a), Santos (b) and Pelotas basins (c) with locations of seismic lines and wells (d). W1-W3 correlations are shown in Fig. 5.2. See Figs. 11-12 for insets (A) to (K). Twelve to fourteen seismo-stratigraphic units (SC1-SC14) are calibrated to well data including biostratigraphic ages (Chapter 3).

5.2 Geological framework

The mechanisms of syn-rift lithosphere deformation along the Brazilian continental margin, and the resultant different types of crust along the Pelotas volcanic and the Santos-Campos non-volcanic margin segments, had strong implications for the style of deformation and sediment dispersal systems during the Barremian and Aptian. Above, the Barremian-Holocene basin infill was divided into twelve to fourteen seismo-stratigraphic units, which have been classified and analyzed in terms of stratal patterns and accommodation changes in Chapters 3 and 4. In this Section, Table 5.1 summarizes the main depositional patterns, unconformities, chronostratigraphy and lithologies.

The northward propagation of continental break-up during the Early Cretaceous resulted in an asynchronous post-rift development, from the Middle Aptian in the Pelotas Basin to the Early Albian in the Campos Basin. This stage was crucial for the formation of Aptian shallow-marine environments in the Pelotas Basin, while restricted marine sag depocenters filled by organic-rich lacustrine sediments and evaporites characterized the Santos and Campos basins. During the Albian, aggradation-progradation of carbonate platforms record the post-rift to early drift margin development. With the continued Southern Atlantic oceanic expansion, paleowater depths rapidly increased and fine-grained clastic marine successions dominated the Cenomanian-Turonian basin fill. Since the Coniacian, the interplay of subsidence, eustasy and sediment supply triggered distinctive depositional patterns and stratigraphic sequences in each basin. Maastrichtian-Neogene tectono-magmatic events in the hinterland and salt deformation in the Santos and Campos basins (Demercian et al., 1993; Cobbold et al., 2001) had a strong influence on the subsidence distribution, shelf-to-basin sediment dispersal systems and the occurrence of turbidites and mass transport complexes (MTCs).

5.3 Method and input parameters

5.3.1 General outline and workflow

Based on the chronostratigraphic information and inverse-basin modeling results (i.e. subsidence and sediment supply rates), forward modeling provides basin architectural models with the best-fit to the tectono-stratigraphic configuration observed in the seismic and well data. The stratigraphic simulator PHIL™ (Bowman and Vail, 1999) incorporates a comprehensive set of parameters, which according to their impact in the final model can be categorized in: (i) essential input parameters, including time and spatial dimensions, initial bathymetry, eustatic sea-level, flexural variables, subsidence/uplift rates, sediment supply and lithologic variables (Sections 5.3.2 and 5.3.3); (ii) sedimentary parameters, including a set of user-defined variables that allow to fine-tune the final model (Table 5.3).

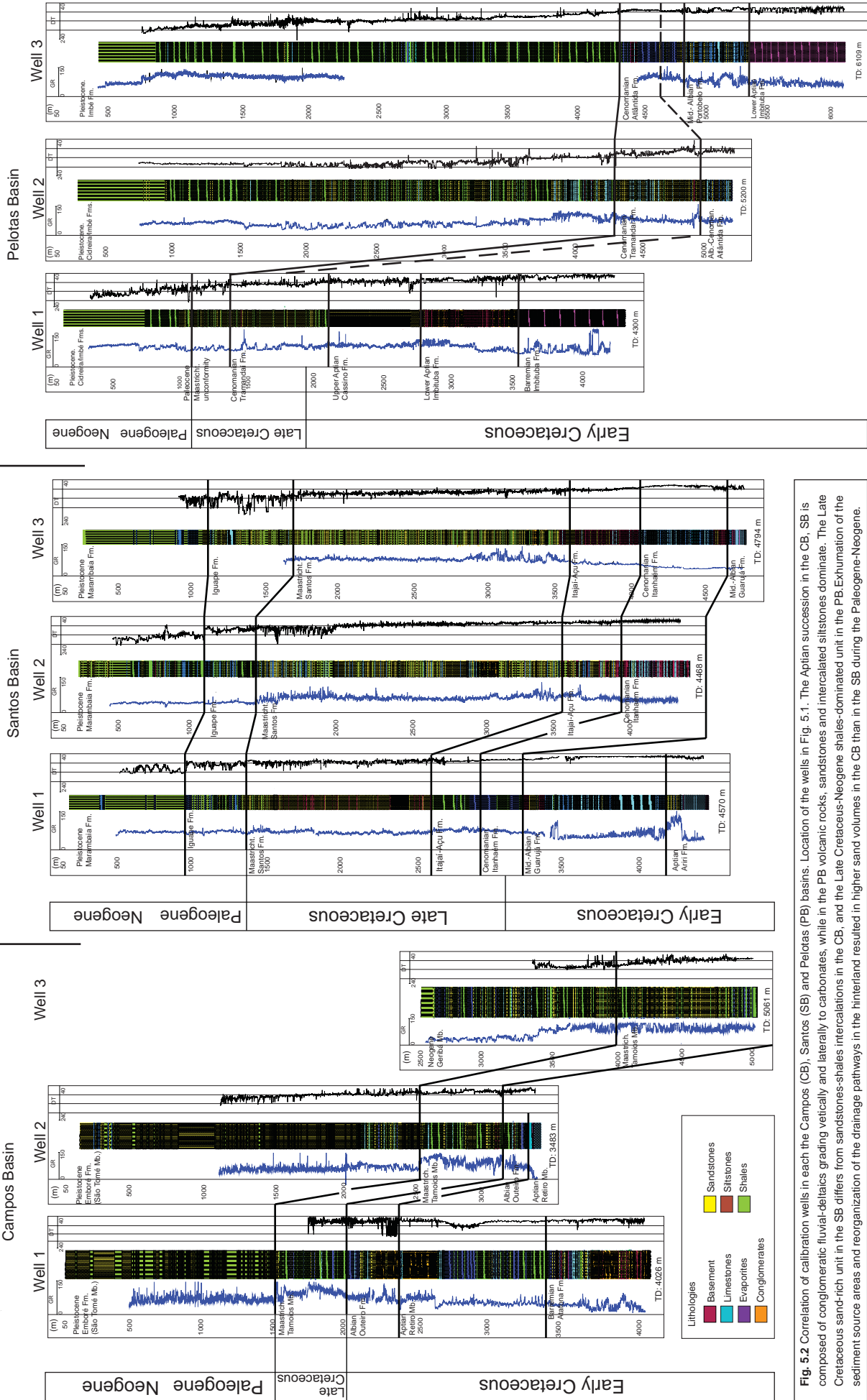


Fig. 5.2 Correlation of calibration wells in each the Campos (CB), Santos (SB) and Pelotas (PB) basins. Location of the wells in Fig. 5.1. The Aptian succession in the CB, SB is composed of conglomeratic fluvial-deltaics grading vertically and laterally to carbonates, while in the PB volcanic rocks, sandstones and intercalated siltstones dominate. The Late Cretaceous sand-rich unit in the SB differs from sandstones-shales intercalations in the CB, and the Late Cretaceous-Neogene shales-dominated unit in the PB. Exhumation of the sediment source areas and reorganization of the drainage pathways in the hinterland resulted in higher sand volumes in the CB than in the SB during the Paleogene-Neogene.

Period	Epoch	Age (Ma)	Tectonic Stages	CAMPOS BASIN				SANTOS BASIN				PELOTAS BASIN																				
				Dep. Patt.	Seismic Units	Reflector geometries	Dep. Patt.	Seismic Units	Reflector geometries	Dep. Patt.	Seismic Units	Reflector geometries																				
Neogene	Quat.	Holocene	DRIFT	REGRESSION	SC 12	NR	Downlap, submarine canyons, gravitational flows and erosion surfaces	TRANSRESS. AGGRADATION	SS 14	AP	Shelf: horizontal reflectors Slope: salt deformation; turbidite-contourites Deep basin: oblique and sigmoid reflectors; basin-floor fans	TRANSRESS. AGGRADATION	SP 14	AP	Onlapping parallel and horizontal; downlap on the outer shelf. Slope: sub-parallel; occasional erosion channels																	
		Pleistocene														1.8	NR	Top: from 100 m to 3,400 m	SS 13	NR	Top: 400 m to 3,700 m High-amplitude horizontal reflectors (carbonate bull-up) Salt deformation. Slope and basin floor fans	SP 13	MFS	Top: 160 m to 5,050 m								
	Miocene	Up.														11.61	SC 11	NR	Shelf: sub-parallel and extensive Slope: divergent-sigmoid Downlap. Truncation with listric faults	SS 12	AP	Top: 480 m to 4,700 m	SP 12	MRS	Shelf: onlapping parallel reflectors Slope: downlap; truncation ext. faults							
		Mid.														15.97	SC 10	AP	Top: from 430 m to 3,800 m Shelf: sub-parallel, oblique Downlap at the base; onlap at the top Erosion channels (turbidites)	SS 11	NR	Top: 490 m to 5,850 m Shelf: horizontal, extended reflectors Slope: up-dip pinch-out against salt diapirs; turbidite-contourites	SP 11	NR	Deep basin: parallel, sub-horizontal							
		Low.														23.03	SC 9	NR		SS 10	AP		SP 10	MFS								
	Paleogene	Oligocene														Up.	28.45	SC 8	AP	Top: from 640 m to 4,500 m Shelf: sub-parallel, semi-horizontal reflectors. Base and top are erosional	SS 9	RT	Top: 960 m to 6,000 m Shelf: horizontal and extended reflectors; sporadic downlap on outer shelf	SP 9	NR	Shelf: parallel and nearly horizontal reflectors, vertical faults Downlap at the base; onlap at the top						
																Low.	33.9	SC 7	NR		SS 8	AP		SP 8	AP							
		Eocene														Up.	37.2	SC 6	RT	Top: from 640 m to 4,500 m Shelf: sub-parallel, semi-horizontal reflectors. Base and top are erosional	SS 7	FR	Top: 490 m to 5,850 m Unclear and discontinuous semi-horizontal reflectors	SP 7	MFS	Slope: downlap, erosional channels, bypass and turbidite deposition Downlap terminations on the Maastricht. Mud diapirs on lower slope						
																Mid.	48.6										FR	FR	FR			
		Paleoc.														Up.	61.7	SC 5	RT	Top: from 950 m to 4,800 m Shelf: parallel, sub-parallel, horizontal reflectors Onlap at the base. Up-section downlap Erosional truncation at the top	SS 6	AP	Top: 960 m to 6,000 m Shelf: horizontal, extended reflectors; sporadic downlap on outer shelf	SP 6	MRS	Slope: parallel to sub-parallel reflectors; occasional turbidites channels Deep basin: low-amplitude horizontal						
Low.			65.5	SB1	SB1	SB1																										
Cretaceous		Upper	Maastricht.	DRIFT	TRANSRESS. AGGRADATION	SC 4	AP	Truncation with growth faults (seaward dipping rafts) Contorted and chaotic facies	TRANSRESS. AGGRADATION	SS 5	MFS	Deep basin: low-amplitude reflectors truncated by erosion surfaces	TRANSRESS. AGGRADATION	SP 5	RT	Shelf: onlap, extended parallel reflectors Mid. slope-deep basin: parallel to sub-parallel reflectors; low-amplitude in the deepest basin domain																
			Campanian														83.5	RT	SS 4	AP	SP 4	TR										
	Santonian		85.8														SC 3	AP	Deep basin: low-amplitude sub-parallel reflectors	SS 3	RT	SS 3	RT	SP 3	RT							
	Coniacian		89.3																							RT	RT	RT				
	Turonian		93.5														SC 2	RT	Sub-parallel, contorted reflectors; downlap; high-amplitude base of salt	SS 2	RT	SS 2	NR	SP 2	MRS	Downlap the upper slope. Onlap up-section. Sub-parallel, horizontal basinward						
	Senoman.	99.6	NR																								NR	NR				
	Lower	Albian	112														DRIFT	TRANSRESS. AGGRADATION	SC 1	SB2	Asymmetric half-grabens Fault truncations and downlap	TRANSRESS. AGGRADATION	SS 1	SB2	Shelf: truncation by high-angle faults Unclear and discontinuous reflectors in the slope-basin margin; SDRs Base: from 1,000 m (shelf) to 7,500 m (basin)	TRANSRESS. AGGRADATION	SP 1	SB1	Base: 1,700 m to 8,800 m Sub-parallel, sigmoid reflectors (SDRs) truncated by high-angle extension fault Base: 2,000 m (shelf) - 9,300 m (basin)			
		Aptian	125																											SB2	SB2	SB2
		Barremian	130																											SYN RIFT	SYN RIFT	SYN RIFT
			130																											SYN RIFT	SYN RIFT	SYN RIFT

Table 5.1 Seismo-stratigraphic units obtained from previous sequence stratigraphic analysis (Contreras et al., 2010). Ages, depositional trends, sequence stratigraphic surfaces and formal lithostratigraphy of the Campos, Santos and Pelotas basins.

The modeling procedure includes sensitivity tests of specific parameters, and calibration of both the final model and the database (Fig. 5.3). The complexity in dealing with salt tectonics was managed by the incorporation of local-scale subsidence/uplift variations and quantifying the lateral and temporal changes in the thickness of the salt layer as the overburden thickness increases. This approach allowed to mimic salt flow and restore the salt basin geometry.

5.3.2 Model dimensions and essential modeling parameters

5.3.2.1 Temporal and spatial resolution

Similar to the inverse-basin modeling, the sections were divided into 400-450 cells with a lateral spacing of 650 m in the Santos Basin, and 750 m in the Campos and Pelotas basins. This practice allows direct comparisons between input and output values from both modeling techniques.

Forward stratigraphic modeling uses equal time increments to analyze the basin conditions and record the corresponding stratal line. The Barremian-Holocene (130-0 Ma) stratigraphic record was modelled with a 2 m.y. time step, providing a model with a higher temporal resolution when compared with previous sequence-stratigraphy and inverse-basin modeling.

5.3.2.2 Initial bathymetric profile

Forward modeling starts with the Barremian basin topography, which represents the top of the rheological basement in the model. The reconstruction of the initial paleobathymetric profile is based on lithologies and inferred depositional environments from seven calibration wells penetrating the Barremian basin fill. In addition, the litho-chronostratigraphic framework from recent publications (Bueno et al., 2007; Moreira et al., 2007; Winter et al., 2007), and the Barremian basin configuration derived from inverse-basin modeling were also considered for calibration purposes.

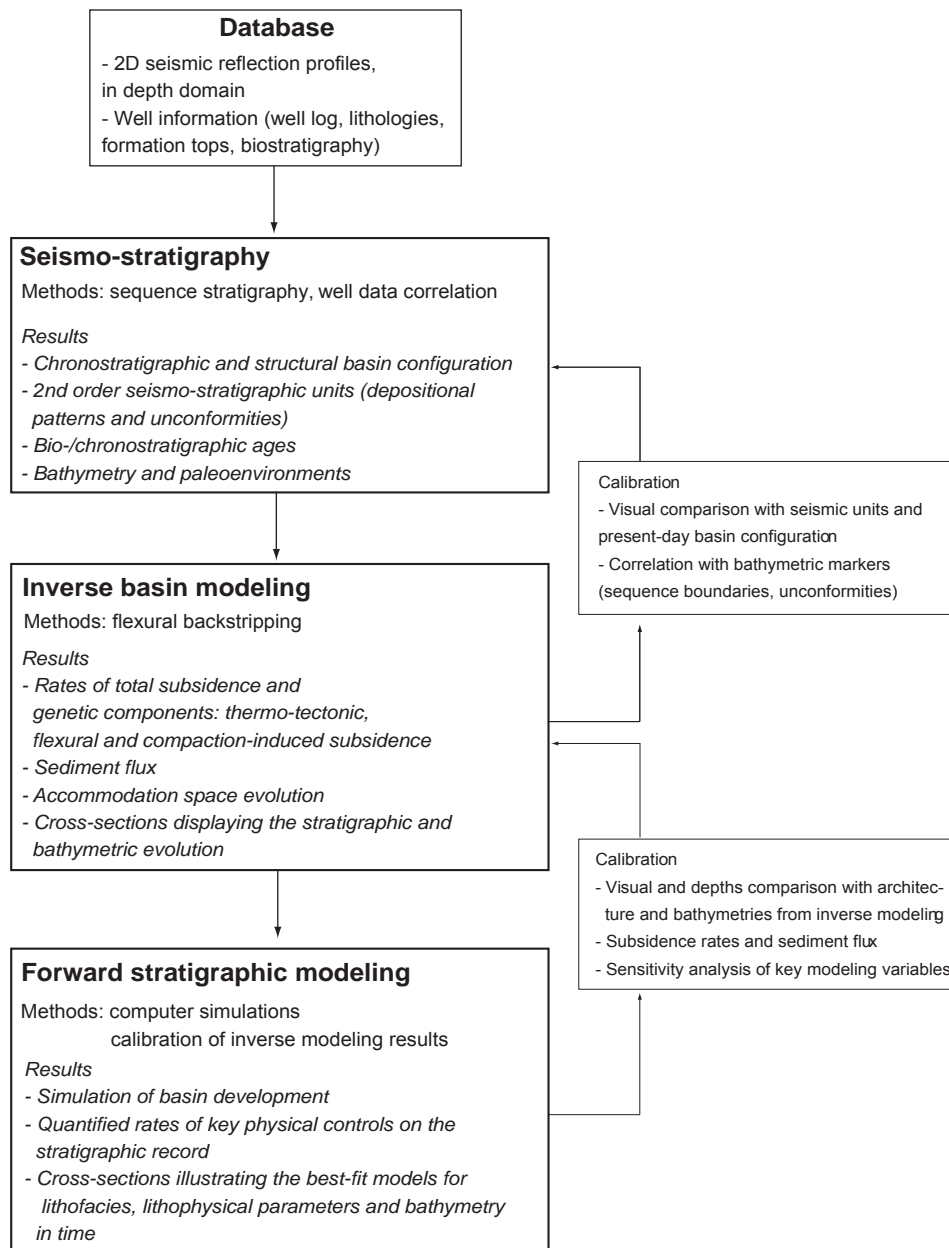


Fig. 5.3 Workflow of the integrated numerical basin analysis. For seismic and well data see Fig. 5.1. The workflow comprises iterative calibration and sensitivity analysis of input parameters in order to achieve the best-fit model to the present-day basin configuration.

The first modeling runs to determine the Barremian bathymetric profile included subsidence and eustatic sea-level. It allowed to simulate the required accommodation space for the lower Barremian basin fill as inferred from seismic and well data. Subsequently, sediment supply rates (see Section 5.3.3.2) were included in order to reproduce the thicknesses and distribution of lithofacies of the lower Barremian succession. The predicted bathymetric conditions along the Santos and Campos segments show water depths of 200-300 m in Early Barremian fault-bounded depocenters located below the modern shelf. Toward the central basin part (80-230 km along the sections) depositional gradients stayed below 1° and water depths gradually reached 350 m. In the easternmost region (modern abyssal plain), paleowater depths decreased to 100-150 m. On the Pelotas shelf segment, Early Barremian fault-bounded depocenters reached maximum water depths of 200 m. Along the central and distal basin parts (modern slope and abyssal plain), paleowater depths gradually increased to 350-400 m at depositional gradients of approximately 1.5°.

5.3.2.3 Eustatic sea-level

Based on the good match between the restored bathymetric conditions and the paleo-environmental conditions inferred from the sedimentological and biostratigraphic data, the eustatic sea-level curve of Hardenbol et al. (1998), re-calibrated with the time scale of Gradstein et al. (2004), was also incorporated in forward modeling. This approach enables a direct comparison of the predicted accommodation changes in forward modeling with the restored basin configuration from inverse-basin modeling and depositional trends from the sequence-stratigraphy.

5.3.2.4 Subsidence and flexural variables

As described in Chapter 4, six main trends of subsidence/uplift (ST1-ST6) controlled the Barremian-Holocene margin development. These trends depict significant lateral and temporal variations in time and between basins, which depend on the interaction of three genetic components of total subsidence: thermo-tectonic, flexural and compaction-induced subsidence (see Section 4.4.2). Forward modeling incorporates the thermo-tectonic subsidence/uplift rates derived from previous subsidence analysis (Table 4.5). Considering the structural complexities of the studied area, especially in the Campos and Santos basins, a realistic model required thermo-tectonic subsidence rates each 5 km. Areas strongly affected by salt flow required subsidence values over 0.5-1 km of lateral spacing.

The flexural model is governed by three main parameters: (i) the effective elastic thickness (T_e); (ii) the plate-end-boundary distance (rheological taper limit); and (iii) the mantle density (Section 4.3.3). The effective elastic thickness is a parameter that reflects the flexural response of the lithosphere to loading (flexural rigidity of the crust). Forward stratigraphic modeling allows to test the T_e values used in inverse-modeling (20 km in the Pelotas Basin; 12 km the Campos and Santos

basins) and determine its changes over time and across the margin. The latter two parameters correspond to fixed values derived from inverse-basin modeling, taper limit (100 km) and mantle density (3350 g/Km³; Table 4.3).

Subsidence Trends [m.y.]	[m/m.y.] Series	Campos Basin				Santos Basin				Pelotas Basin			
		Total	Th-Tect	Flex	Comp	Total	Th-Tect	Flex	Comp	Total	Th-Tect	Flex	Comp
ST6 23-0	L. Miocene	38	6	27	6	35	10	22	4	78	18	46	17
	E. Miocene	42	7	26	8	45	12	24	9	71	21	37	15
ST5 33.9-23	L. Oligoc.	34	9	19	6	30	12	12	5	62	23	28	12
	E. Oligoc.	35	15	15	7	43	16	21	8	66	26	32	11
ST4 65.5-33.9	L. Eocene	47	18	23	7	48	23	16	10	70	26	33	15
	E. Eocene	34	14	15	6	36	17	16	5	41	23	14	6
ST3 110-65.5	Maastricht.	22	15	5	2	25	17	6	3	29	22	6	3
	Albian	60	37	16	7	50	32	13	3	84	50	25	11
ST2 117-110	Aptian	119	81	35	7	65	41	19	4	77	48	21	8
ST1 130-117	Barremian	142	105	37	0	82	60	22	0	94	75	14	0

Table 5.2 Rates of total subsidence and its genetic components (thermo-tectonic, flexural and compaction-induced subsidence) after forward simulations. Six main subsidence trends (ST1-ST6) describe the Barremian-Holocene (130-0 Ma) subsidence development in each of the Campos, Santos and Pelotas basins. Subsidence rates represent average values representative of the entire shelf-to-basin transition; in order to obtain a better approach, they can be complemented with local scale subsidence rates shown in Fig. 5.6. By comparison with Table 4.5 it is possible to recognize the effects of temporal changes in T_e on the Barremian-Albian subsidence values.

5.3.3 Sedimentary parameters

5.3.3.1 Lithologies, textural variables and compaction

Compaction-induced subsidence is calculated for each time layer according to the changes in rock volume during the overburden history. As for the inverse-basin modeling, forward stratigraphic modeling considers eleven siliciclastic lithotypes, nine carbonate types, and evaporites, obtained from the calibration wells. Each of these lithologies features specific empirical parameters (i.e. initial porosities, densities and compaction coefficient), which control the porosity loss and compaction rates (Table 4.2).

5.3.3.2 Sedimentation rates, erosion and transport

Decompacted sediment supply rates derived from inverse-basin modeling represent the sediment input values for forward modeling. Sediment supply rates are expressed in m²/m.y. and reflect the 2D cross-sectional area filled by sediment within each time layer. Based on the input data, forward modeling reproduces the deposition/erosion systems, transport and sedimentation in order to match the stratigraphic basin configuration. The results indicate basinwide changes in the rates of

Sedimentary Parameters	Empirical Range ¹	Campos Basin ²	Santos Basin ²	Pelotas Basin ²
Siliciclastic Deposition				
Supply [m ² /m.y.]	0-10 ⁴	5x10 ³ - 17x10 ³	5x10 ³ - 18x10 ³	4x10 ³ - 33x10 ³
Traction transport [%]	0-100	10-40	30-40	20-50
Sand fraction [%]	0-100	5-40	15-50	10-30
Suspension Width of the mixing layer [m]	1-200	5-10	5-10	5-10
Suspension Dispersion distance [km]	5-100	25	25	30
Siliciclastic Depositional Environments				
Fluvial gradient [°]	0.001-0.00001	-	-	-
Coastal plain gradient [°]	0.0	0.0001	0.0001	0.0001
Shoreface gradient [°]	0.01-0.001	0.001-0.005	0.001-0.005	0.001-0.005
Depositional front gradient [°]	0.1-0.01	0.02-0.07	0.02-0.05	0.01-0.09
Coastal plain width [km]	0-200	80-140	100-180	40-90
Rollover width [km]	1-5	7	8	5
Depth of the offlap break [m]	10-20	50-300	40-270	20-280
Barrier island height [m]	0-10	-	-	-
Barrier island width [m]	0-15	-	-	-
Carbonate Production				
Shelf Lagoon				
Maximum growth rate [m/m.y.]	5 - 100	5 - 70	5 - 60	5 - 40
Depth of maximum growth [m]	2 - 25	10 - 80	10 - 70	25 - 110
Width of the depth function [m]	5 - 40	30	30	30
Shelf Margin				
Maximum growth rate	1 - 100	170 - 200	180 - 225	120 - 140
Depth of the maximum growth	1 - 20	70 - 80	70 - 80	60 - 70
Width of the depth function [m]	5 - 40	20	20	20
Width of the distance function [km]	0.1 - 5	10	10	10
Slope				
Maximum growth rate	10 - 500	250	270	190
Depth of the maximum growth [m]	2 - 25	40	40	40
Suspension distance [km]	1 - 50	50	50	50
Maximum suspension depth [m]	3 - 40	150	150	150
Carbonate Depositional Environments				
Sabkha gradient [°]	0.0 - 0.00001	0.00001	0.00001	-
Tidal flat gradient [°]	0.0001 - 0.0006	0.001	0.001	0.001
Tidal range [m]	0 - 15	10	10	10
Back-reef gradient [°]	0.1 - 0.001	0.007	0.007	0.005
Shelf margin crest [m]	1 - 20	50 - 150	50 - 150	40 - 100
Fore-slope gradient [°]	0.01 - 1.1	0.02	0.02	0.015
Rollover width [km]	0.5 - 3	4	5	3
Pelagic Deposition				
Maximum production rate [m/m.y.]	1 - 40	10 - 45	2 - 40	6 - 40
Calcite Compensation Depth [m]	3 - 4.5	4	4	4
Dissolution width [m]	500 - 2000	500	500	500
Siliciclastic damping limit [m/m.y.]	1 - 150	60	80	40
Production time increment [m/m.y.]	0.001 - 0.025	0.021	0.021	0.021
Gravity-Flow Deposition				
Minimum bathymetric relief [m]	100 - 400	100 - 220	80 - 220	80 - 220
Slope-fan threshold depth [m]	0 - 30	20	20	20
Basin-floor fan gradient [°]	0.001 - 0.0001	0.0015	0.0011	0.002
Slope-fan gradient [°]	0.03 - 0.001	0.001	0.001	0.001
Relative-water-level trigger-factor [m/m.y.]	0 - (-25)	-1	-1	-4
Turbidite volume factor []	0-?	0.8	0.9	0.6
Erosion				
Shoreface erosion rate [m/m.y.]	0 - 150x10 ⁶	50 - 70x10 ⁶	50 - 70x10 ⁶	50 - 80x10 ⁶
Surface erosion rate [m/m.y.]	0 - 500	500 - 1000	500 - 1000	500 - 1500
Channel erosion rate [m/m.y.]	0 - 10000	-	-	-
Channel depth [m]	0 - 1000	-	-	-
Channel margin gradient [°]	0.01 - 1	-	-	-
Channel spacing [km]	1 - 100	-	-	-
Marine currents [m]	-	5,000	5,000	5,000-8,000

Table 5.3 List of sedimentary parameters adjusted during forward stratigraphic simulations. The values used in this study have been determined by sensitivity tests until the best-fit models to the present-day basin configuration were achieved. These are compared with geologically reasonable ranges published in Bowman and Vail (1999).

sedimentation instead of local-scale changes, which can be extremely variable between different basin segments and trough time (e.g. the shelf edge vs. intra-slope salt troughs). Both the input and the resultant best-fit sedimentation rates are plotted in Fig. 5.5. The good match between both models, usually with less than 10% variation except for evaporite deposition (Late Aptian) and periods of basement tectonic reactivations (Maastrichtian), indicates the high degree of plausibility in the sedimentation rates achieved by the combination of inverse and forward modeling.

A significant contribution of forward modeling in this study involves the individual quantification of siliciclastic influx, carbonate sediment as well as in situ carbonate production rates. Siliciclastic deposition primarily depends on the sediment supply rates included in the model and their distribution. Carbonate deposition will depend on the carbonate production rates (controlled by bathymetry and siliciclastic supply) and their subsequent redistribution. The algorithm for erosion considers shoreface erosion, channel incision, surface bevelling and submarine redistribution by marine currents (Appendix A). Each of these interfaces is controlled by a set of variables (Table 5.3) that define the minimum differential relief to activate erosion and the maximum volume of sediment to be added to the clastic supply. The deposition algorithms reproduce both coastal and gravitational sedimentation for both siliciclastic and carbonate sediment, considering four transport methods: traction, suspension, gravity-flow and slumping. Sediment traction and suspension principally depend on the lithologies, bathymetric profile, lateral dimensions and energy conditions. Gravity-flow sedimentation will depend on the stability conditions of the basin floor, sediment compaction, and changes in the relative sea-level (Bowman and Vail, 1999).

5.4 Modeling restrictions

Forward stratigraphic modeling in this study includes the following restrictions: i) the results depend on the original seismostratigraphic interpretation as calibrated by wells; ii) best-fit models are not necessarily unique models, but may be achieved with different combinations of input parameters within geologically reasonable ranges of values; iii) sedimentation rates depend on the resolution of biostratigraphic data and their tie to absolute ages in chronostratigraphic charts; iv) lateral salt remobilization has been simulated as a function of vertical salt flow and changes in salt thickness through time; vi) detailed studies of diagenesis, which may affect porosity/depth curves, and thus compaction rates, have not been available.

5.5 Forward modeling results

Forward stratigraphic simulations of the Barremian-Holocene basin fill demonstrates how the final basin model is sensitive to multiple uncertain sedimentary and deformation variables, such as lithotypes, sediment volumes injected into the basin, transport efficiency and halokinesis-induced redistribution. Sensitivity tests indicate that modeling parameters must be evaluated within a range

of possibilities and by considering maximum, minimum and best-fit values, rather than specific and unique values. Iterative modeling runs and observation of the model response provided the best approximations to the effective elastic thickness (Fig. 5.4), sediment supply (Fig. 5.5) and subsidence/uplift rates (Fig. 5.6, Table 5.2). Additional sensitivity analyses of sedimentary parameters (Table 5.3) allowed to fine-tune the model and determine the most important sediment-related factors between several uncertain parameters controlling the basin development and distribution of lithofacies. Chronostratigraphic cross-sections were generated for each the Pelotas, Santos and Campos basins (Figs. 5.7, 5.8 and 5.9 respectively). Four key time layers (top Aptian, top Maastrichtian, top Eocene, and present-day) have been chosen to visualize and discuss the architectures, distribution of lithofacies and porosity evolution between the three basins.

Spatial and temporal variations in T_e as well as the interactions of thermo-tectonic and flexural subsidence confirmed the strong influence of continental extension on the distinct syn-rift configuration between the Pelotas and the Santos-Campos margin segments (Fig. 5.10; Section 5.6.1). Forward modeling results confirmed that syn-rift crustal thinning and the consequent decrease in the flexural strength of the crust were crucial factors for the formation of sag and salt depocenters (Section 5.6.2). During the post-rift to mature drift stages, continental basement reactivations and salt-induced sediment remobilization affected the long-term flexural response of the crust, triggering significant departures from the theoretical 'thermal curve' of passive margins as predicted in the McKenzie model (1978). Our results, combined with existing investigations on the tectonic evolution of the Brazilian continental margin (e.g. Zalán and Oliveira, 2005) provide a better understanding of the basin-specific sediment supply histories and the source-to-basin depositional systems. Furthermore, since forward modeling simulates the interactions between tectonic subsidence, eustatic sea-level and sedimentation rates, it is possible to test the relationship between these causal mechanisms and the occurrence of either turbidites or mass transport complexes (i.e. debris flows, block slides and slumps; classification of Moscardelli and Wood, 2008), widely recognized in the three basins analyzed (Figs. 5.11 and 5.12).

5.5.1 Barremian to Aptian syn-rift stage

Brazilian Margin (general)

During the Barremian syn-rift stage, thermo-tectonic subsidence exerted the main control on total subsidence and creation of accommodation space (subsidence trend ST1; Fig. 5.6). However, magma-dominated continental extension in the Pelotas Basin evolved northward to fault-dominated and ductile continental extension in the Santos and Campos basins. These mechanisms and the resultant variations in the flexural rigidity of the crust contribute to generate half-graben basins with specific geometries and varying subsidence patterns in each basin.

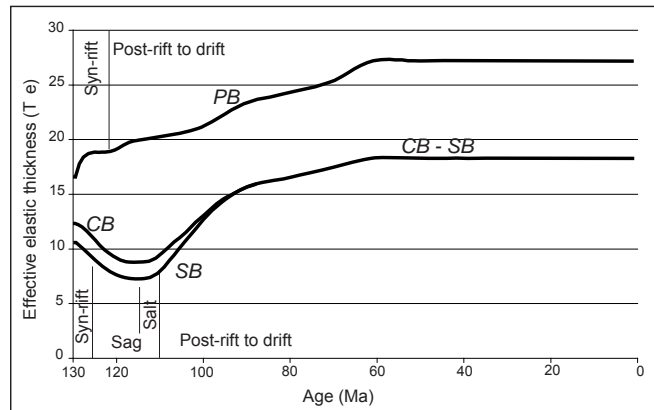


Fig. 5.4 Evolution of the effective elastic thickness (T_e) of the lithosphere from forward stratigraphic modeling for the Brazilian continental margin (Barremian to recent). Changes in T_e result from syn-rift mantle upwelling, accretion of oceanic crust and long-term cooling (Section 5.6.1).

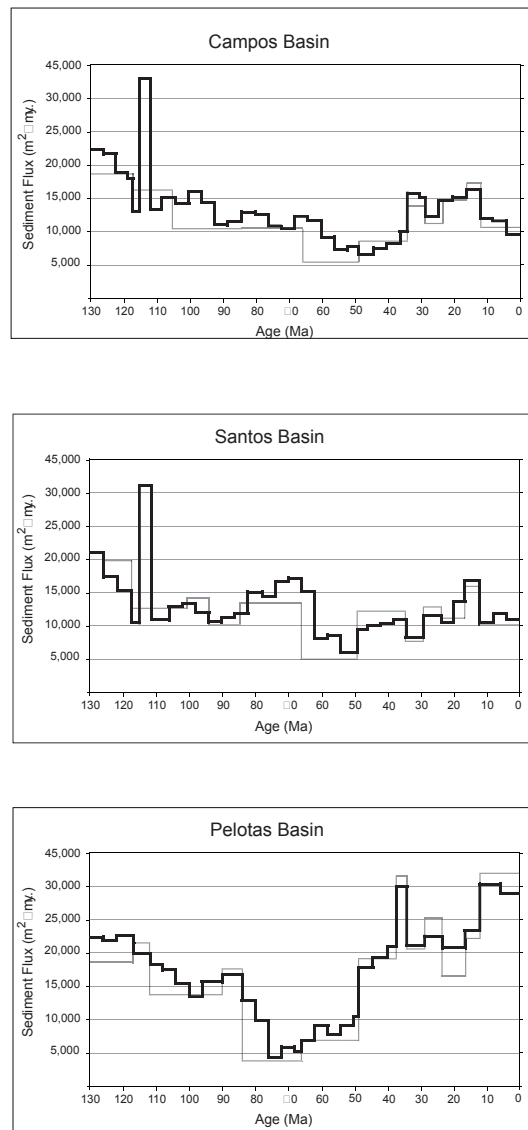


Fig. 5.5 Sediment flux histories during the Barremian to Holocene (130-0 Ma) for the Campos, Santos and Pelotas Basins. The thin gray line represents input sediment rates derived from inverse basin modeling. The thick black line shows re-calibrated sediment supply rates from forward stratigraphic modeling (compare with Fig. 4.6).

Fig. 5.6

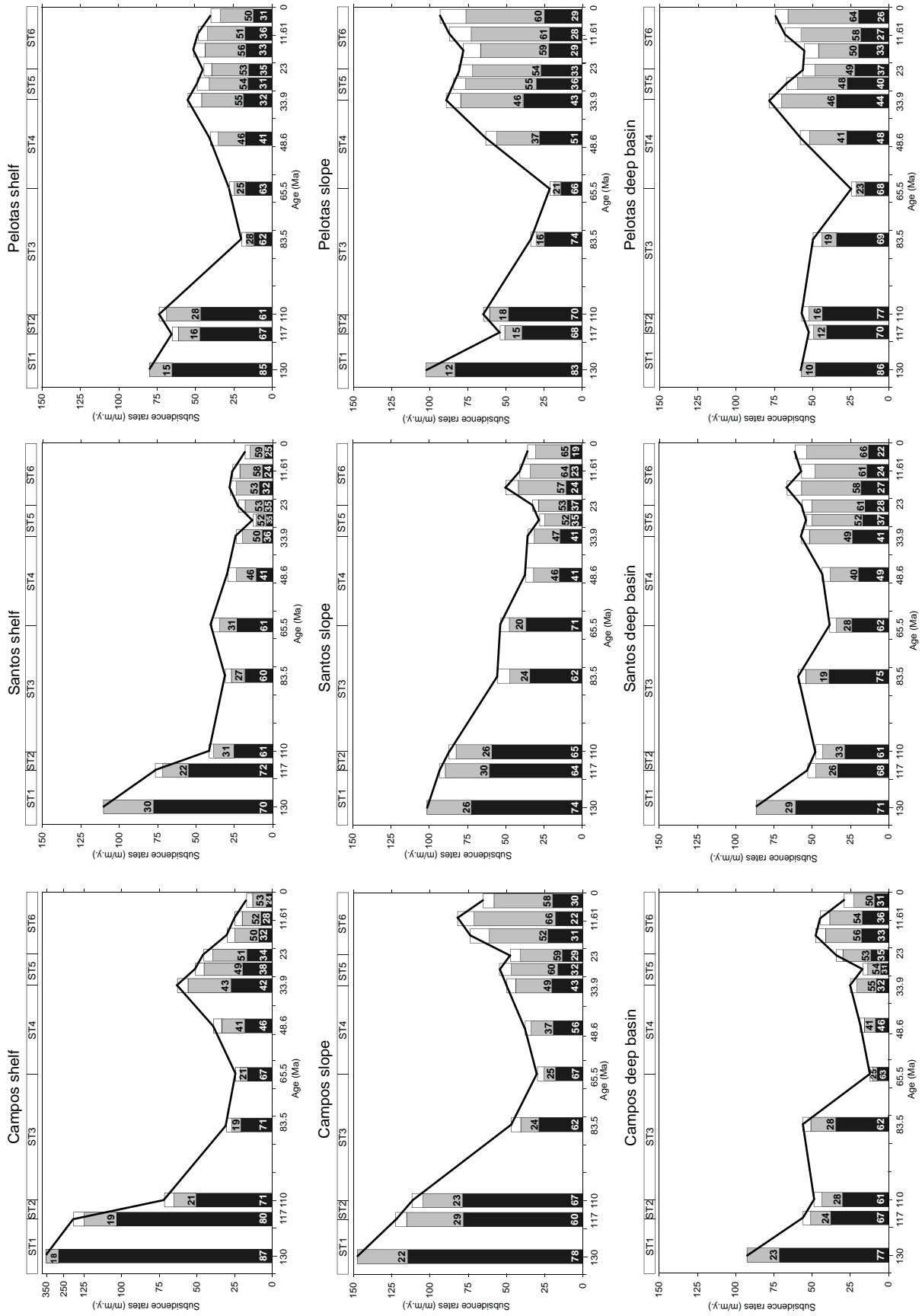


Fig. 5.6 Total subsidence (line) and its genetic components, thermo-tectonic (dark gray), flexural (light gray) and compaction-induced (white) subsidence, separated for shelf, slope and deep basin areas. Six main subsidence trends (ST1-ST6) controlled the Barremian-Holocene basin development in each of the Campos, Santos and Pelotas basins. From ST1 to ST3 (Barremian to Maastrichtian), thermo-tectonic subsidence was the dominant component on total subsidence with comparable trends in the three basins. Since the Early Eocene (48.6 Ma, middle ST4) flexural subsidence from sediment and water loading represented the dominant control on total subsidence. Subsidence trends were highly variable along the Brazilian margin.

Pelotas Basin (specific)

During the Early-Middle Barremian syn-rift stage, the effective elastic thickness of the volcanic-type transitional crust increased by about 12% (from 17 to 19 km). As the crust became more rigid, the flexural loading effect and fault displacement diminished (later discussed in Section 5.6.1.) High-angle extensional faults die out into Barremian volcanic wedges (SDRs) and the flexural component accounted for only 14-17% of total subsidence (Fig. 5.6). The accommodation space available was progressively consumed by widespread volcanic series and high clastic supply in the Late Barremian. As a result, paleowater depths were fairly constant (100-200 m) during the whole Barremian. As the volcanic and tectonic activity diminished, alluvial to fluvial-deltaic deposits dominated the Early-Middle Aptian basin infill (Cassino Fm.). With the onset of sea-floor spreading in the Middle Aptian (~120-118 Ma), thermal lithospheric contraction controlled the subsidence trend ST2. As expected, the subsidence distribution was laterally irregular, with the higher subsidence values in the central basin part (75-80 m/m.y.), between the basement-supported continental shelf and the thermally-uplifted spreading center. During the post-rift stage, the shelf realm experienced recurrent erosion due to relative sea-level fluctuations. One particularly important event was a eustatic fall in the Middle Aptian (122 Ma), which caused retrogradation of the coastline over approximately 50 km and the erosion of 150-200 m of sediment from the shelf top. As the relative sea-level increased in the Late Aptian-Early Albian, coastal retrogradation and sediment bypass with debris flows occurred. Fault-bounded structural highs were drowned, and consequently the rates of erosion and sediment supply diminished by around 15% (Fig. 5.5). By the Early Albian, paleowater depths in the central basin had reached 650-700 m (Fig. 5.7).

Santos and Campos basins (specific)

Along the Santos-Campos margin segments, T_e values gradually decreased during the Barremian-Aptian syn-rift stage (Fig. 5.4). As the crust became less rigid, the response to the sediment loading amplified, and so the flexural component reached 18-30% of total subsidence (Fig. 5.6). It also enhanced fault-displacement and rotation of hanging-wall blocks, resulting in half-graben basins with subsidence rates of 115-350 m/m.y. The Early Barremian unit (lower syn-rift sequence; Carminatti et al., 2008) consists of volcanic series covered by alluvial and fluvial-deltaic coarse-grained prograding wedges deposited in low bathymetries (100-150 m). Up-section, the Middle Barremian-Early Aptian unit (upper syn-rift sequence) involve cycles of fluvial-deltaic

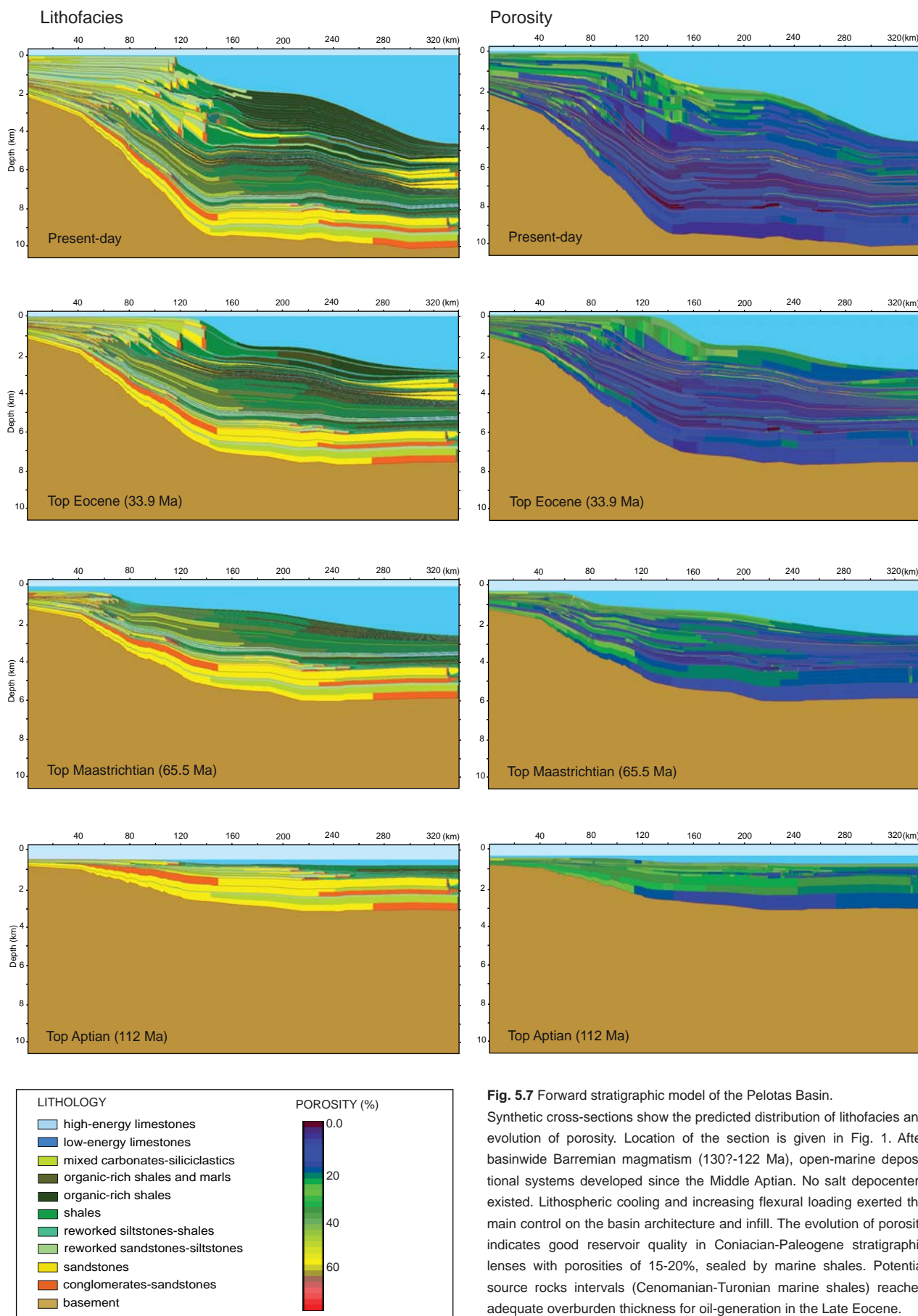


Fig. 5.7 Forward stratigraphic model of the Pelotas Basin. Synthetic cross-sections show the predicted distribution of lithofacies and evolution of porosity. Location of the section is given in Fig. 1. After basinwide Barremian magmatism (130?-122 Ma), open-marine depositional systems developed since the Middle Aptian. No salt depocenters existed. Lithospheric cooling and increasing flexural loading exerted the main control on the basin architecture and infill. The evolution of porosity indicates good reservoir quality in Coniacian-Paleogene stratigraphic lenses with porosities of 15-20%, sealed by marine shales. Potential source rocks intervals (Cenomanian-Turonian marine shales) reached adequate overburden thickness for oil-generation in the Late Eocene.

5. Forward stratigraphic modeling

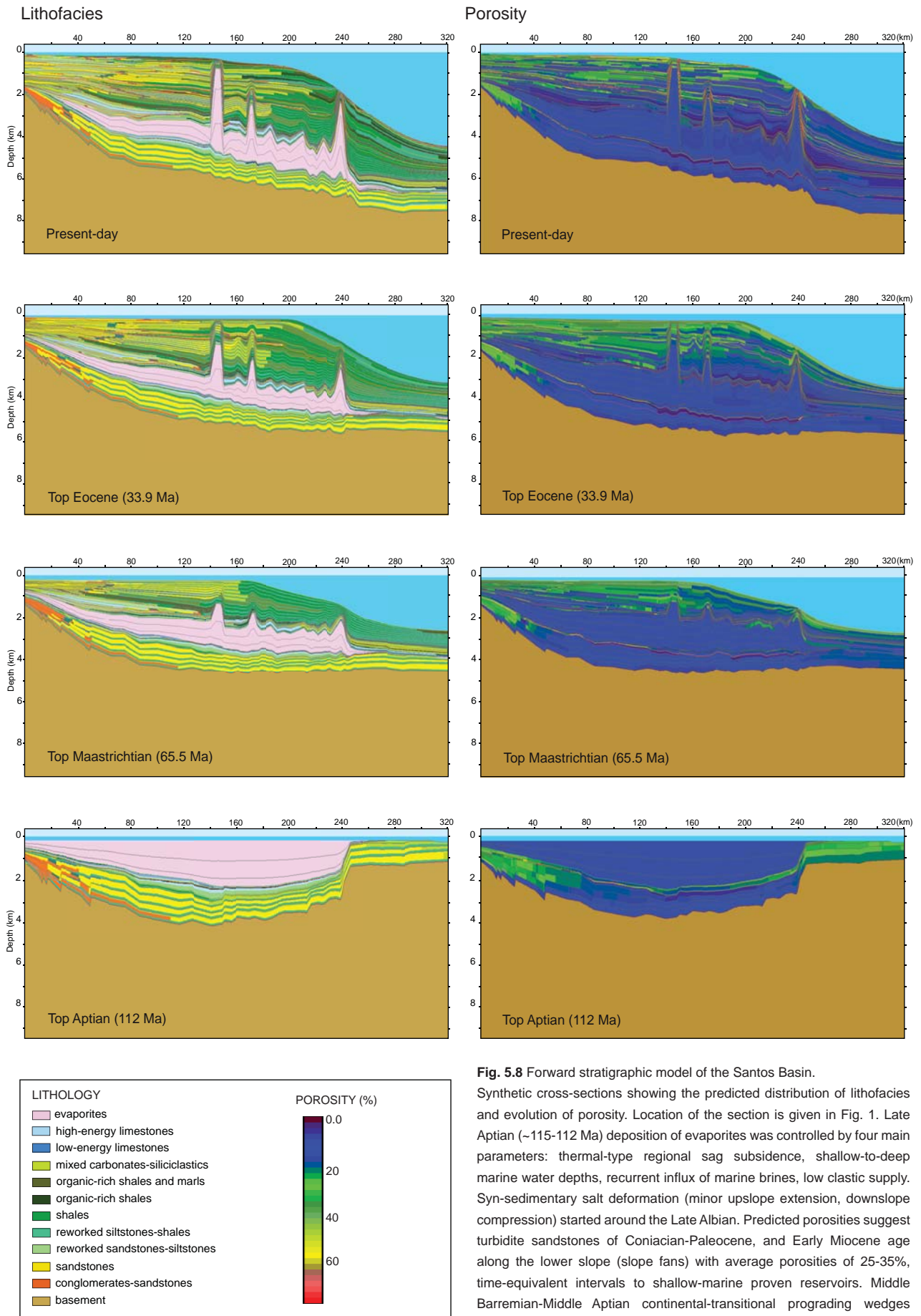


Fig. 5.8 Forward stratigraphic model of the Santos Basin. Synthetic cross-sections showing the predicted distribution of lithofacies and evolution of porosity. Location of the section is given in Fig. 1. Late Aptian (~115-112 Ma) deposition of evaporites was controlled by four main parameters: thermal-type regional sag subsidence, shallow-to-deep marine water depths, recurrent influx of marine brines, low clastic supply. Syn-sedimentary salt deformation (minor upslope extension, downslope compression) started around the Late Albian. Predicted porosities suggest turbidite sandstones of Coniacian-Paleocene, and Early Miocene age along the lower slope (slope fans) with average porosities of 25-35%, time-equivalent intervals to shallow-marine proven reservoirs. Middle Barremian-Middle Aptian continental-transitional prograding wedges below the salt succession preserve porosities between 20-25%.

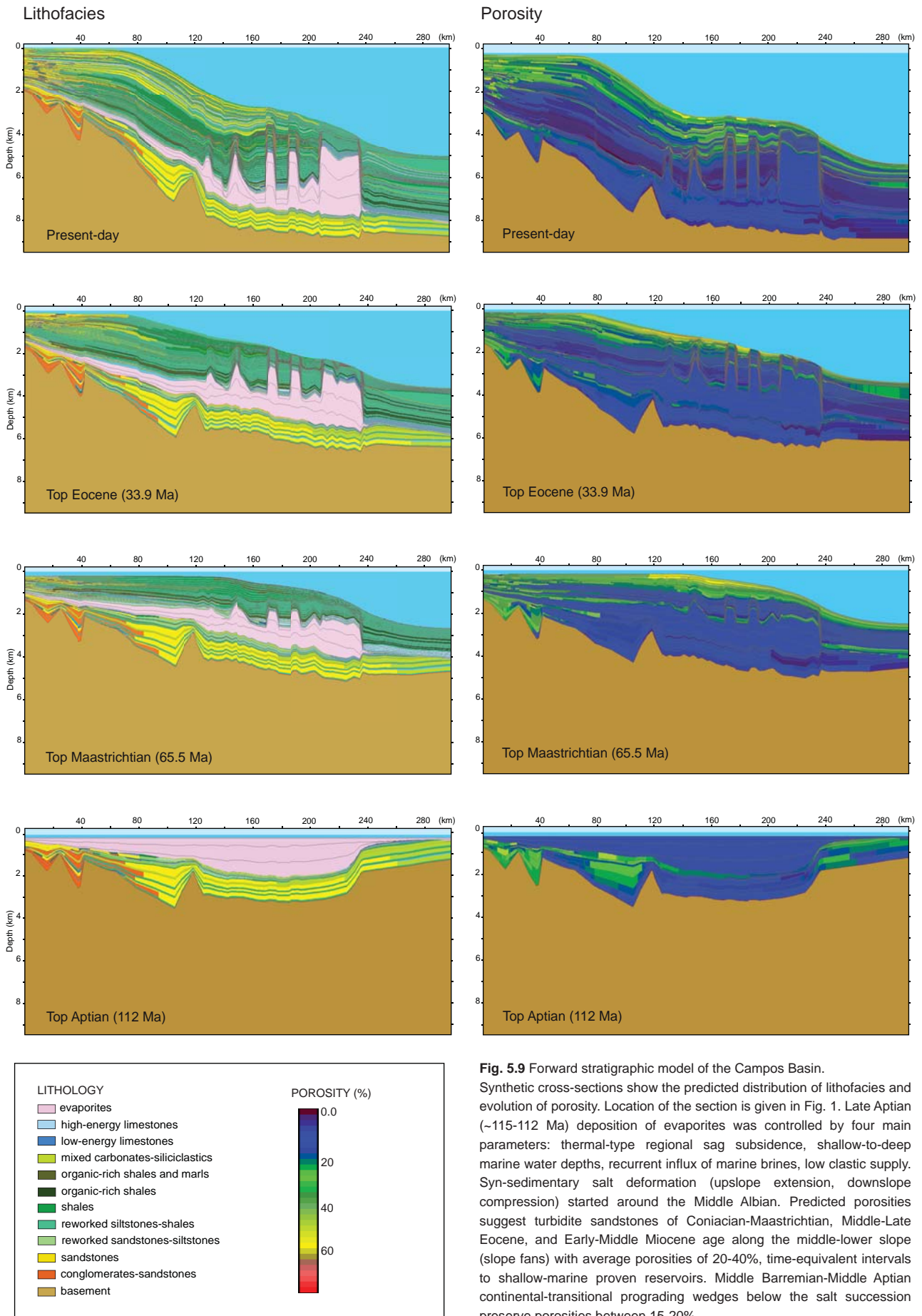


Fig. 5.9 Forward stratigraphic model of the Campos Basin. Synthetic cross-sections show the predicted distribution of lithofacies and evolution of porosity. Location of the section is given in Fig. 1. Late Aptian (~115-112 Ma) deposition of evaporites was controlled by four main parameters: thermal-type regional sag subsidence, shallow-to-deep marine water depths, recurrent influx of marine brines, low clastic supply. Syn-sedimentary salt deformation (upslope extension, downslope compression) started around the Middle Albian. Predicted porosities suggest turbidite sandstones of Coniacian-Maastrichtian, Middle-Late Eocene, and Early-Middle Miocene age along the middle-lower slope (slope fans) with average porosities of 20-40%, time-equivalent intervals to shallow-marine proven reservoirs. Middle Barremian-Middle Aptian continental-transitional prograding wedges below the salt succession preserve porosities between 15-20%.

progradation-aggradation followed by retrogradation of lacustrine mud-rich carbonates and aggradational limestones at the top (Coqueiros and Barra Velha Fms.). The transitional siliciclastic units show thicknesses of around 400-450 m and predicted porosities of 15-20% (Figs. 5.8 and 5.9); intercalated carbonate-dominated intervals show average thicknesses of 100-120 m and porosities between 1-5%. They were deposited in water depths of 350-400 m, which gradually decreased upward to 50-100 m during the next fluvial-deltaic progradational trend. Near the adjacent horst structures, a lower siliciclastic supply and bathymetries between 30-150 m enabled carbonate production rates of 105 m/m.y. in the Campos Basin and 90 m/m.y. in the Santos Basin. These structural highs formed local-scale rimmed platforms composed of high-energy carbonates, mainly coquinas and microbialites with present-day porosities between 10-14%. Toward the central basin part, subsidence rates diminished by approximately 50% (75-120 m/m.y.). This pattern reflects the lateral transition from brittle extension to thermally-controlled basin sagging. During the Early to Middle Aptian, paleowater depths gradually increased to 500-550 m along the modern upper-middle slope, and up to 950 m toward the lower slope-oceanic basin. The basin infill included reworked fluvial and bioclastic deposits intercalated with mud-rich hemipelagic carbonates.

Syn-rift sag stage and late Aptian evaporites (specific)

During the sag basin development, the effective elastic thickness of the crust reached minimum values of 6-8 km. Extensional faulting ceased, uplift and erosion of foot-wall blocks attenuated, and in consequence the sediment flux diminished by about 30%. By Middle-Late Aptian times, both the Campos and Santos shelf segments had experienced a decrease in thermo-tectonic subsidence by approximately 35% (trend ST2). However, along the continental slope subsidence values remained nearly constant (85-120 m/m.y.); this basin area was controlled by thermal-sag subsidence and the flexural response of the crust to widespread transitional clastic deposits. Due to reduction in the flexural rigidity, the flexural subsidence component enhanced up to 30% of total subsidence (Fig. 5.6). Prograding fluvial-deltaic systems on the inner-middle shelf laterally graded to fine-grained lacustrine sediments and carbonates toward the central basin (present-day upper-middle slope). During a second order eustatic sea-level fall in the Middle Aptian (117 Ma) approximately 220-250 m of the lower Aptian unit was removed from both the Campos and Santos shelves and redeposited basinward. As the eustatic sea-level rose in the Late Aptian (116-115 Ma), the erosional hiatus was covered by retrogradational-aggradational fining-upward fluvial-lacustrine deposits and intercalated limestones. In the central basin part, reworked sandstones grading upward to siltstones and hemipelagic carbonates were deposited in bathyal environments with 900-950 m of water depth. Although the sag basin development was fairly similar in both basins, the Santos continental shelf was broader and tectonically more stable than the Campos shelf segment. This distinct development appears to be associated to the larger extension of the São Paulo Plateau in the Santos Basin and the occurrence of thermal anomalies due to an aborted rift segment (see Mohriak et al., 2010; Scotchman et al., 2010).

By Late Aptian times, sag depocenters had expanded to around 160 km wide (to the modern lower slope) and were characterized by smooth topography. This setting coincided with semi-arid and dry climate conditions during the Aptian (Moore et al., 1995; Skelton, 2003), enabling the precipitation of evaporites in the latest Aptian (112-115 Ma; Karner and Gambôa 2007; Contreras et al., 2010). Based on the quantitative results described above, a simplified model for the salt basin formation was erected based on four key parameters: (1) pre-salt sag depocenters with subsidence rates of 85-120 m/m.y.; (2) pre-salt paleowater depths between 100-250 m on the shelf and 900-950 m in the central basin part; (3) siliciclastic supply below 200 m²/m.y, which may be taken as an indication of minor water flux from rivers due to dry climate; (4) marine water influx triggering an appropriate water-level and high salinities. Based on these model conditions (later discussed in Section 5.6.2), rates of salt precipitation reached 560 mm/yr in the Santos Basin and 610 mm/yr in the Campos Basin. The resultant salt thicknesses were 520-1,200 m along the modern continental shelf and 1,900-2,200 m towards the central basin part (Figs. 5.8 and 5.9).

5.5.2 Middle Aptian to Late Albian post-rift stage

Brazilian margin (general)

With the onset of post-rift thermal cooling and contraction of the lithosphere, the flexural rigidity of the crust started to increase. By the Late Albian, T_e values had reached 21 km in the Pelotas margin segment and 12-13 km in the Santos-Campos segment. Despite these differences in the flexural strength of the crust, the three basins analyzed followed a comparable post-rift subsidence pattern: Albian to Maastrichtian subsidence rates gradually decreased (trend ST3) following the thermal curve of McKenzie's model (1978). This subsidence development, combined with the rising eustatic sea-level signal created appropriate basin conditions for the development of wide carbonate platforms in the Albian. Geodynamic reconfigurations indicate that this development coincided with the connection of the Central and South Atlantic Ocean (Torsvik et al., 2009; Moulin et al., 2010) and a change to humid-tropical climate conditions (Skelton et al., 2003; Ford and Golonka, 2003), facilitating marginal organism associations and carbonate build-up.

Pelotas Basin (specific)

The post-rift stage in the Pelotas Basin is indicated by increased subsidence values along the entire shelf-to-basin transition (60-75 m/m.y.; trend ST2). Coastal retrogradation with an important component of aggradation controlled the Late Aptian-Early Albian shelf development. Due to the low basin relief, coarse-grained alluvial to deltaic deposits were deposited on the shelf realm (Cassino Fm.), while siltstones and hemipelagic shales dominated the central and distal basin parts. As the bathymetry increased in the Middle Albian, lacustrine to shallow-marine mixed siliciclastic-carbonate deposits occurred (Tramandaí and Portobelo Fms.). On the outer shelf, massive bioclastic limestones reached average production rates of 130-140 m/m.y. By the Middle Albian,

a rimmed carbonate ramp had prograded over 120 km, to the location of the recent upper slope. During this development, paleowater depths near the shelf margin gradually rose from 90-100 m in the Early Albian to 300 m in the Late Albian. Basinward, a gentle slope with depositional gradients of 3°-4° was formed and paleowater depths increased to 1,500 m. In this area (120-340 km on the section), marine shales and calcilutites were intercalated with sporadic gravitational debris flows (Atlântida Fm.).

Santos and Campos basins (specific)

Based on the best-fit subsidence and paleowater depths model, the transition from syn-rift lithospheric stretching to seafloor spreading appears a gradual process during the Early Albian (112-108 Ma). After Late Aptian salt precipitation, paleobathymetry ranged from 30-40 m on the inner shelf to 180-200 m toward the central basin part. On the continental shelf, an abrupt decrease in subsidence values during the Early to Middle Albian (trend ST2) is compatible with the development of a stable carbonate platform. With the retrogradation of the coastline and the shift to humid climatic conditions in the Albian, coastal sediment reworking and erosion intensified; as a result, in both the Santos and Campos basins the sediment flux increased by about 10-15%. Fluvial-deltaic coarse-grained deposits on the inner shelf (Florianópolis and Goitacás Fms. respectively) laterally graded to shallow-marine fine-grained siliciclastics and high-energy carbonate banks. Average carbonate production rates varied between 105-115 m/m.y. in the middle-outer shelf and 190-225 m/m.y. on the rimmed shelf edge (Guarujá Fm. in the Santos Basin; Quissamã, Outeiro Fms. in the Campos Basin). By the Middle Albian, a carbonate ramp with depositional gradients below 1° had prograded over 90-110 km in both the Campos and Santos basins. On the Campos shelf segment, bathymetries stayed between 260-280 m and enabled carbonate build-up until the Late Albian-Cenomanian (98-99 Ma). In contrast, Middle-Late Albian (~104 Ma) bathymetries on the Santos shelf area increased up to 300-330 m, and carbonate ramps were drowned. Forward modeling suggests that these distinctive basin conditions resulted from the smoother and wider Santos shelf segment, combined with slightly lower rates of carbonate production.

Along the central basin part, differential thermal contraction with the distance from the spreading center caused laterally variable subsidence values, 45-50 m/m.y. in the deep basin increasing to 95-115 m/m.y. on the upper slope. Sporadic turbidite flows were associated to falls in the relative sea-level (112 and 106 Ma) cutting into Early-Middle Albian shallow-water deposits. The basin topography and distribution of the sediment loading was a crucial factor on the onset of salt remobilization. A 120 km-wide Santos shelf segment laterally changing to slope gradients of 1°-2° resulted in a fairly homogeneous distribution of the basin fill and minor salt remobilization before the Late Albian (102-100 Ma). In the Campos Basin, a narrower shelf segment (80 km-wide) and recurrent events of gravitational sediment transport (debris flows and occasional turbidites) generated

differential sediment loading and slope depositional gradients of 3° - 4° , which resulted in gravity-gliding salt remobilization since the Middle Albian (108-106 Ma). In both the Campos and Santos basins, the continental to oceanic crust transition (COT) was characterized by thermally-induced uplift over a 50-km wide zone on the lower slope (see Fig. 4.4). This area coincides with a bathymetric scarp located at around 340 km from the modern coastline (Fig. 5.1). This feature appears to represent the signature of the distal continental edge, where mantle/lower crust exhumation occur during the syn-rift sag stage (Aslanian et al., 2009).

5.5.3 Late Cretaceous early drift stage

Brazilian Margin (general)

The decrease in thermo-tectonic subsidence during the Cenomanian-Maastrichtian early drift stage (99.6-65.5 Ma; trend ST3) was controlled by lithospheric thermal contraction. Nonetheless, a Late Cretaceous eustatic sea-level rise caused an increase in accommodation space and paleobathymetry. This trend of water deepening and transgression generated Turonian to Coniacian (92-90 Ma) disconformities in the three basins. As the continental margin depocenters expanded, the thermal contraction of the lithosphere and the concomitant increase in the flexural rigidity resulted in basin tilting, coupled with flexural rebound and erosion of the shelf areas. Episodic exhumation of continental source areas triggered significant changes in the sediment supply and deep-water sand volumes, especially in the Santos Basin.

Pelotas Basin (specific)

The Cenomanian to Campanian (99.6-82 Ma) retrogradational pattern was interrupted since the Late Turonian (88-82 Ma) by short-term aggradational to progradational trends (1-2 m.y. duration). These shifts occurred during a period of slight but persistent flexural rebound of the shelf, which is manifested in the temporally decreasing subsidence rates, from 40 m/m.y. in the Turonian to 25 m/m.y. in the Santonian (Fig. 5.6). As a result, the bathymetry of the shelf margin reduced to 50-70 m, and so sedimentation patterns became more sensitive to fluctuations in the eustatic sea-level and sediment supply. Two of the most noticeable aggradational-progradational pulses occurred during eustatic sea-level falls in the Late Turonian (89-88 Ma) and Santonian (85-84 Ma). From the Campanian to the Maastrichtian (84-65.5 Ma), shelfal subsidence renewed (35 m/m.y.), sediment supply diminished, and coastal retrogradation was re-established. The shallow-water basin fill is therefore characterized by retrogradational fine-grained sandstones, siltstones and shales (Cidreira Fm.) affected by intermittent periods of sediment reworking and bypass. The continental slope and deep basin margin were characterized by a continuous decrease in subsidence rates from the Cenomanian (55-60 m/m.y.) to the Maastrichtian (20-28 m/m.y.). Due to the relative low density of the deep-marine shales-dominated succession, the flexural component accounted

for only 18-22% of total subsidence and the slope gradient did not exceed 5°-7°. Recurrent debris flows and occasional sand-poor turbidites were connected to the eustatic-driven progradational trends. By Maastrichtian-Paleocene times, the shelf margin featured water depths of 300-400 m, whereas the oceanic domain reached 2,500-2,600 m.

Santos Basin (specific)

After Cenomanian-Middle Turonian coastal retrogradation, the Coniacian-Maastrichtian shelf development was controlled by a trend of high siliciclastic supply, with a total sand content of 60-65%. Amalgamated coarse-grained fluvial-deltaic deposits (Santos Fm.) laterally graded to siltstones of prodelta facies near the shelf edge (Juréia Fm.). This progradational trend occurred during a period of tectonic uplift of the Serra do Mar in the Santos hinterland, which have been constrained by apatite fission track analysis in previous studies (later described in Section 5.6.3). With the rapid increase in the sediment loading and compaction of the underlying Cenomanian-Coniacian shales-dominated succession, the shelf experienced a subsidence increase of 18-20% during the Campanian to Maastrichtian. Nevertheless, accommodation drastically reduced and the progradational front repeatedly collapsed, generating sand-rich turbidites flows (Ilhabela Mb.). Eustatic sea-level falls generated occasional debris flows, particularly important in the Early Campanian (82-80 Ma) and Early Maastrichtian (70-68 Ma). Forward modeling suggests that laterally constant and increased Santonian-Maastrichtian stratigraphic thicknesses (1,200 m) along the shelf-upper slope realm generated a uniform lithostratigraphic pressure field with minor differential sedimentary loading (vertical subsidence) which precluded upslope salt extension. However, toward the middle-lower slope, the basin topography reached 9°-10° of inclination, triggering downdip salt compression with the formation of diapirs, thrust faults and inverse faults. In the deep basin margin, hemipelagic shales intercalated with reworked debris flows were deposited in water depths of between 1,900-2,100 m, similar to the Campos deep basin setting.

Campos Basin (specific)

The Cenomanian to Maastrichtian overall retrogradational pattern was controlled by a long-lasting rise in eustatic sea-level, which counteracted the reduction in accommodation space due to the Late Cretaceous decrease in subsidence values. The sediment supply was relatively constant, with an average sand content of 45-50%. Fluvial-deltaic sandstones and siltstones on the inner-middle shelf laterally graded to reworked fine-grained prodelta and shallow-marine deposits on the shelf edge. In order to reproduce the deep-water stratigraphic thicknesses observed in the seismic and well data, Maastrichtian-Paleocene sediment supply rates required an increase of 110% in comparison with the input rates derived from inverse-basin modeling (Fig. 5.5). This trend suggests an extrabasinal tectonic factor affecting the basin development, probably associated

to the uplift of the Serra do Mar and the thermal effect of the Trindade mantle plume (Zalán and Oliveira, 2005). Gravitational sediment flows, principally turbidites, were associated to collapse events of the progradational front during falls in eustatic sea-level, for instance in the Late Turoonian (89-88 Ma), Santonian-Campanian (84-83 Ma) and Late Campanian (76-75 Ma). Although the duration of these events was below the temporal resolution of the seismo-stratigraphic framework, forward stratigraphic simulations allowed to evaluate their effects on the basin development. Assuming that large sand volumes (6,000-6,500 m²/m.y.) were exported to the deep-marine setting, a rapid increase in the flexural loading from Santonian to Maastrichtian times produced the best match with the basin configuration and sand thicknesses penetrated by the calibration wells (Fig. 5.2). This tectonically-induced sediment supply peak had two main effects on the final model: (i) subsidence rates were 30-35% higher than the input data derived from inverse-basin modeling; (ii) downslope salt remobilization intensified, providing a plausible model for halokinesis-driven sediment redistribution and deformation of the basin floor topography.

5.5.4 Paleogene mature drift stage

Brazilian Margin (general)

The Maastrichtian-Paleocene boundary is marked by a eustatic-driven erosive unconformity (58-56 Ma), which can be used as a regional correlation marker (Table 5.1). During this event, approximately 320-340 m of Upper Maastrichtian-Lower Paleocene (68-58 Ma) sediment were removed from the Pelotas and Santos shelf segments and re-deposited basinwards; in the Campos Basin the average eroded thicknesses were about 260-280 m. The correlative forced regressive packages include turbidites, debris flows, and in the Pelotas Basin block slides.

During the Paleogene to Neogene mature drift stage (trends ST4 to ST6), tectonic reactivation of basement blocks continued to cause major variations in the rates of clastic supply and sand volumes exported to the deep-marine setting. With the increase in the sediment and water loads, the flexural subsidence component became the dominant control on total subsidence since the Middle Eocene, while the thermo-tectonic component became secondary (see percentages in Fig. 5.6). Forward stratigraphic simulations allowed to determine the most significant deformation and stratigraphic controls on the Paleogene-Neogene sedimentation/erosion patterns, which in order of importance include: (i) exhumation of sediment source areas affecting the sediment supply and distribution of the sediment loading offshore; (ii) eustatic sea-level fluctuations with changes in the rates of accommodation and coastal erosion; (iii) instability conditions of the shelf margin and eventual catastrophic sediment-failure; (iv) salt remobilization affecting the basin topography and distribution of deep-water depocenters.

Pelotas Basin (specific)

The flexural response of the crust to the imposed sediment and water loads exerted the main control on the basinwide subsidence increase from the Paleocene (25-50 m/m.y.) to the Late Eocene (55-88 m/m.y.). Incision channels and Maastrichtian-Paleocene coarse-grained regressive sandstones were covered by fining-upward deltaic to shallow-marine fine-grained sandstones intercalated with siltstones and shales (Cidreira Fm.). This retrogradational trend, controlled by a rise in the relative sea-level and low sedimentation rates, led to a lack in sediment cohesion and little compaction. Recurrent sediment bypass and collapse events of the shelf-edge during the Early Eocene resulted in a steep depositional front with approximately 15° declivity. In the Middle-Late Eocene the sediment supply increased by about 80% (with a sand fraction of 40-45%), which led to wide fluvial-deltaic progradation and to rebuild of the shelf. This trend has been associated to a volcanic event in the Eastern Paraguay Province indicated by Peyve (2010). A 2nd order eustatic sea-level fall in the Middle Eocene (48 Ma) and another in the Late Eocene (37-34 Ma) represent two events of major shelfal erosion linked to debris flows downslope. During the Oligocene, alternating periods of retrogradation (34-30 Ma; 26-24 Ma) and progradation (30-26 Ma) induced sediment bypass and instability conditions of the shelf edge-upper slope realm. Intercalated transgressive shales décollements (condensed surfaces toward the outer shelf), depo-sited during transgressive pulses, enabled recurrent events of shelf-edge failure. Due to the large gravity-driven sediment volumes in basinward direction (5,000-6,000 m²/m.y.), the highest sedimentation rates and flexural loading occurred on the middle-lower slope. Seismic facies show packages of contorted reflectors with basal scours, which reflect landslides and erosive debris flows. Intercalated high-amplitude, sub-horizontal and less deformed layers have been interpreted as occasional turbidite flows (Fig. 5.12g).

Santos Basin (specific)

During the Paleogene, the Santos shelf segment underwent intermittent flexural-induced uplift, erosion and unloading. This pattern is indicated by Paleocene to Oligocene decreasing subsidence values (trend ST4) and sediment reworking along the shelf. During the Late Paleocene and Early Eocene, the sediment supply reduced by 50% and the sand fraction varied around 45-50%. As a result of this change, and the rising eustatic sea-level, the preceding progradational pattern shifted to retrogradation with a minor component of aggradation. In the Middle Eocene, the sediment supply increased and fluvial-deltaic to shallow-marine progradational to aggradational deposits reached the upper slope. This succession was partly removed during eustatic sea-level falls in the Middle Eocene (50-48 Ma) and the Middle-Late Eocene (42-40 Ma). This latter eustatic event was particularly important since it was associated to collapse of the progradational front. Large sediment volumes were transported basinward by turbidite and debris flows during the whole Eocene, generating a rapid increase in the sediment loading. Average subsidence values reached

35-55 m/m.y., and the slope gradient increased up to 13°-14°. Toward the lower slope, salt diapirs intruded the Paleogene succession, generating local-scale depressions trapping occasional turbidite flows and salt-induced sediment slumps (Fig. 5.11f). Forward modeling results indicate that a relative constant sediment flux during the Paleocene and Eocene was coeval with a gradual increase in slope gradients facilitating upslope salt extension. On the other hand, maximum peaks in sedimentation (e.g. in the Coniacian-Maastrichtian) tend to restrict salt extension, although it may reinforce downslope salt compression and vertical flow. In the Early Oligocene, sediment supply dropped again and retrogradation to aggradation occurred. Deltaic sandstones and siltstones (Ponta Aguda Fm.) back-stepped until the Late Oligocene, when a trend of high sediment supply (28-23 Ma) led to the restoration of a wide and flat progradational front. The shallow-water succession consists of fine-grained fluvial-deltaics laterally grading to mixed siliciclastic-carbonate facies (Iguape Fm.) with carbonate production rates of 50-55 m/m.y. Basinward, sediment bypass and shelf-edge failure generated clastic-carbonate turbidites and sporadic debris flows.

Campos Basin (specific)

Between the Paleocene to Late Eocene, the Campos Basin experienced an increase in subsidence along the entire shelf-to-basin transition, from 15-30 m/m.y. to 30-70 m/m.y. (trend ST4). This trend was thermally-controlled by lithospheric contraction of the crust coupled with the flexural sediment loading and major salt remobilization along the slope to deep basin margin. After intense sediment erosion and reworking of Maastrichtian-Early Paleocene fluvial-deltaic deposits, a retrogradational-aggradational succession, with an average sand content of 35%, was deposited during the Early Eocene (Emborê Fm., São Tomé Mb.). As the coastline back-stepped, traction-driven siliciclastics diminished toward the outer shelf, allowing carbonate build-up with average production rates of 60-70 m/m.y. (Grussaí Mb.). Basinward, sand- to silt-rich turbidites were trapped in salt-induced topographic barriers, encased by marine shales and occasional debris flows (Ubatuba Fm.). In the Early Oligocene, the sediment supply increased by approximately 60%, causing progradation of sand-dominated (45-50%) fluvial-deltaic deposits (São Tomé Mb.). This trend of rapid sedimentation and shelf widening led to insufficient sediment cohesion and bypass, producing recurrent events of shelf-edge collapse during the Early Oligocene (32-29 Ma). In the Late Oligocene, the shelf segment became fairly stable, flat and featured bathymetric conditions of 150-180 m. This setting allowed carbonate build-up toward the outer shelf (Siri Mb.) with average production rates of 80-85 m/m.y. during a retrogradational-aggradational trend. These variations in the depositional patterns, coupled with sediment collapse events of the shelf-edge and abrupt changes in the sediment loading along the slope, generated laterally and temporally variable subsidence rates during the Oligocene (from 15 m/m.y. to 65 m/m.y.). Similar to the Santos Basin, hemipelagic shales and mud-dominated debris flows overstepped the diapiric province and cut into the oceanic basin fill (Fig. 5.12).

5.5.5 Neogene mature drift stage

Brazilian margin (general)

The Neogene represents a stage of sediment infill and reduction in bathymetry. The subsidence distribution along the three modeled seismic sections reflects uplift of the southeastern Brazilian continental shelf and progressive tilting basinward, with the highest rates of sedimentation and subsidence on the lower continental slope. Depositional trends were mainly controlled by changes in sediment supply, occasionally overprinted by eustatic sea-level fluctuations triggering sediment bypass and unloading. Gravitational sediment flows, and their interactions with slope-parallel marine currents were the main factors influencing deep-marine sedimentary systems, and also affected the distribution of the sediment loading.

Pelotas Basin (specific)

The subsidence values along the Pelotas shelf segment diminished from 55 m/m.y. in the Early Miocene to 35 m/m.y. in the recent times. In contrast, flexurally-driven increasing subsidence rates in the slope to deep basin margin varied between 75-90 m/m.y. In order to reproduce the shelf-to-slope configuration in the model, recurrent episodes of catastrophic shelf-edge failure had to occur during the Early Miocene (24-16 Ma). During this time, low bathymetric conditions (water depths below 150 m) and high clastic supply with a total sand fraction of 20-25% existed. A eustatic sea-level fall in the Early Miocene (23-22 Ma) removed about 180-200 m of fluvial-deltaic sand-dominated deposits, transported as shelf-block slides and debris flows to the upper-middle slope (Fig. 5.12g). In the following, a short-term eustatic sea-level rise in the Middle Miocene enhanced the available accommodation space, and consequently the shelf sediment failure ceased. The Middle-Late Miocene unit (14-10 Ma) reflects a trend of retrogradation to aggradation of fine-grained sandstones and siltstones. From the Pliocene to the Holocene, the sediment supply has gradually increased by about 25% triggering progradation. Due to the continuous reduction in the shelfal accommodation space, large sediment volumes were directly exported to the deep-marine setting, probably associated to episodic shelf-edge failures. The upper slope realm progressively became sharp and steep (approx. 20°). The deep-water sedimentary systems were controlled by suspension-driven pelagic shales intercalated with shelf-fed debris flows. These gravitational flows were associated to repeated eustatic sea-level falls, particularly important in the Late Pliocene (3-2 Ma). With the increase in the sediment loading and rapid overburden downslope, Paleogene-Neogene gas hydrate accumulations, probably associated to contourites and pelagic shales, generated cross-stratal fluid migration features (chimneys and pockmarks), mud diapirs and sediment failure on the lower slope (Fig. 5.12h).

Santos and Campos basins (specific)

Although the Campos and Santos basins exhibit distinctive architectures, the controlling factors on accommodation space and sediment distribution were comparable during the Neogene. Similar to the Pelotas Basin, flexure-induced uplift and sediment bypass were dominant processes on the Miocene to Holocene shelf development. During the eustatic sea-level fall in the Early Miocene, average thicknesses of 120-140 m (Campos Basin) and 150-170 m (Santos Basin) of deltaic to shallow-marine sand-dominated successions were removed and re-deposited as turbidites and minor debris flows along the slope. The uppermost Early Miocene unit reflects a short-term period of retrogradation. In the Middle Miocene, the sediment supply increased by 15-30%, with an average sand fraction of 50-60% in both basins. During this trend, progradation to aggradation occurred, and the exceeding sediment volumes were redeposited as turbidites down slope. Increasing flexural loading and syn-sedimentary salt remobilization triggered major lateral changes in subsidence along the slope, between 48 m/m.y. and 80 m/m.y. A eustatic sea-level fall in the Late Miocene (11-8 Ma) caused strong erosion of deltaic to shallow-marine sand-rich deposits, generating a shelf-wide unconformity. Salt-bounded mini-basins show complex lithofacies associations affected by the interplay of turbidites, debris flows, halokinesis-related slumps and contourite channel-drift systems (Fig. 5.11). Basinward, low-density debris flows overstepped the continental slope and cut into hemipelagic oceanic deposits, forming amalgamated basin-floor fans intercalated with pelagic shales at about 4,000 m of water depth (Fig. 5.12j, 5.12k).

5.6 Discussion

Forward stratigraphic modeling provides insights in to the individual contribution of subsidence, eustasy and sediment supply on the basin development beyond the available temporal seismostratigraphic resolution. A wide range of possible controls on stratal patterns was quantified, including both sediment-related and deformation parameters, such as the flexural rigidity of the crust, salt precipitation rates, shelf width and stability conditions, causal mechanisms and types of gravitational sediment flows, sand volumes exported to the deep-marine setting, sediment-transport efficiency and salt remobilization effects. Sensitivity analysis provides feasible geological scenarios and basin conditions, which can be evaluated until the numerical modeling data match the features observed in nature. Although many interpretations and predictions can be made upon the modeling data, the following discussion involves the most relevant subjects on the evolution of rifted continental margins and the key factors controlling the great hydrocarbon potential of southeastern offshore Brazil.

5.6.1 Syn-rift crust deformation (Barremian-Middle Aptian, 130-115 Ma)

Although the Pelotas, Santos and Campos basins shared a comparable rift origin during the Early Cretaceous break-up of Gondwana, distinctive mechanisms of continental extension along the Brazilian margins caused significant differences in the flexural rigidity of the crust, fault geometry and configuration of syn-rift depocenters between basins. Sensitivity analysis of the effective elastic thickness (T_e) and subsidence rates have been applied to reconstruct the Barremian-Aptian tectono-stratigraphic evolution of the Pelotas and the Santos-Campos margin segments (Fig. 5.10). In the absence of heat flow data, changes in the thermal stage of the lithosphere and their implications for the mechanical behaviour of fault blocks can be only considered in terms of the best-fit of the subsidence values determined during modeling. Although the interpretations on the occurrence of an intra-crustal detachment (Karner et al., 2003) and lower crustal deformation reconcile the subsidence patterns and stratigraphy data, they are not conclusive and need to be adjusted by deep refraction, gravity or magnetic data.

Recent studies on magma-rich continental margins indicate that voluminous volcanism accompanied by intrusions increase the crustal density and preclude low-angle detachment faults and decoupling (Rosenbaum et al., 2008). Accordingly, sensitivity tests of the effective elastic thickness in the Pelotas volcanic segment indicate an increase in the crustal thickness and the flexural rigidity, which preclude fault displacement and block rotation. The section analyzed in this study as well as wide-angle profiles from the Namibian conjugate margin (Gladczenko et al., 1998; Bauer et al., 2000) display foot-wall and hanging-wall blocks with minor displacement along high-angle extensional faults, which die out in the Barremian volcanic wedges (Fig. 5.10a, b). Based on refraction, reflection and gravity data, Gladczenko et al. (1998), Hinz et al. (1999) and Bauer et al. (2000) recognized a high-density lower crust intruded by abundant basaltic dikes. These magmatic intrusions seem to reduce the extensional stress and contribute to accommodate the amounts of lithosphere extension without ductile deformation of the lower crust layer. These interpretations are compatible with recent deep-crust geophysical studies on the magma-assisted active continental rift of the Gulf of Aden in Somalia (Kendall et al., 2005; Corti, 2009). In these models, abundant basaltic flows emanated from fissures in the lower crust, generating an upper crustal layer affected by low far-field plate stresses, and underlain by a heavily intruded and thinned lower crust-mantle interface.

Based on the best-fit configuration to the Barremian basin architecture, and the predicted flexural crustal evolution, continental extension along the Pelotas Basin appears to have been mainly controlled by mantle upwelling and extrusion of basaltic flows. The continental-transitional lithosphere reached around 17-19 km of thickness and was affected by high-angle extensional faults during the Barremian. Cooling and stabilization of the volcanic wedges in the landward direction exerted the main control on syn-rift subsidence. Nonetheless, submarine volcanic extrusions

and crustal extension continued to the Middle Aptian continental break-up (~120-118 Ma). With the onset of seafloor spreading, thermal contraction triggered a gradual increase in the flexural rigidity (T_e values of 19-21 km). Middle-Late Aptian open-marine water circulation and clastic transitional to carbonate deposits prograded and capped syn-rift fault-bounded depocenters (Fig. 5.10c, d). This tectono-stratigraphic setting appears to have precluded the formation of Barremian-Aptian restricted marine depocenters with accumulation of organic-rich shales.

Investigations on the Campos-Santos basins (Karner et al., 2003; Aslanian et al., 2009; Unternehr et al., 2010), the analogous divergent margins of Norway, northwest Australia and Iberian-Newfoundland (Kusznir et al., 2005; Kusznir and Karner, 2007; Reston et al., 2007) as well as on the active rift of the Red Sea (Cochran and Karner, 2007) suggest that depth-dependent lithospheric stretching and mantle exhumation are the dominant processes on lithosphere extension on magma-poor rifted margins. During the Late Barremian-Late Aptian decrease of the effective elastic thickness, the flexural response to the sediment loading amplified. As a result, Aptian subsidence values increased by 20-24% with respect to previous inverse-basin modeling data, which considered a constant T_e value (compare Tables 4.5 and 5.2). Therefore, temporal variations in the flexural rigidity of the crust must be considered on the restoration of the rifted margin depocenters and paleowater depths.

In the Early Barremian, hanging-wall subsidence and foot-wall uplift was controlled by high-angle normal faults (Figs. 5.10a and 5.10e). This stage of brittle deformation was accompanied by erosion of the uplifted blocks and sediment transport to the adjacent subsiding blocks. As margin extension continued, the flexural rigidity of the crust was attenuated (8-10 km), and the rheological properties changed. The angle of the normal faults progressively decreased and evolved to listric faults that sole into a flat intra-crustal detachment separating the brittle upper crust from the plastic lower crust layer (Figs. 5.10f-g). This setting facilitated episodic tectonic reactivations with rotational displacement of hanging-wall blocks and continued uplift and erosion of the foot-wall blocks. The eroded material formed clastic wedges ("triangle zones") on the hanging-wall blocks, enhancing the flexural loading to approximately 30% of total subsidence (Table 5.2). Fault-offset and tilting of the depressed blocks were coupled to a flexural-driven push-upward effect and further uplift of foot-wall blocks. Modeling results calibrated with the stratigraphic data, suggest that brittle extension occurred until the Late Barremian in the Santos Basin and the Early Aptian in the Campos Basin. Subsequently, high rates of thermo-tectonic subsidence and the continued decrease in the flexural rigidity until the end of the Aptian reflect the stage of basin sagging. The interplay between lithospheric stretching (generating subsidence) and heat advection (generating uplift) triggered relatively constant subsidence rates along a 120 km-wide part of the transect, which extend from the outer shelf to the modern lower slope (cf. Continental Slope Domain by Aslanian et al., 2009). The resultant smooth basin topography and relatively uniform paleobathymetries coincided with

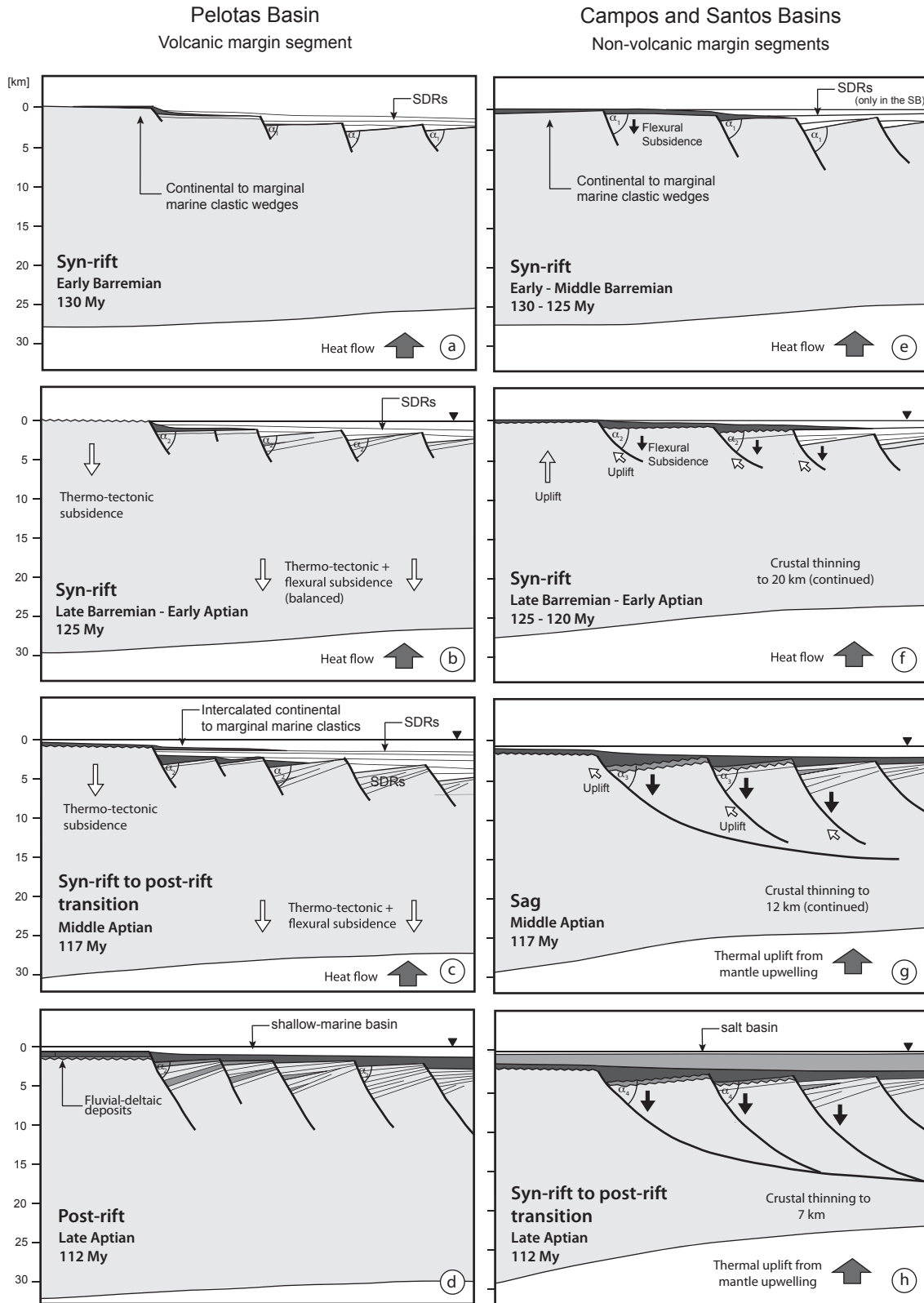


Fig. 5.10 Model of syn-rift lithosphere deformation based on numerical modeling results. Crustal thickening and high flexural rigidity due to transient magmatism (SDRs), probably associated to intrusions in the lower crust, enabled high-angle extensional faults ($\alpha_1 > \alpha_2$) in the Pelotas volcanic-type margin segment (a, b). The following thermal contraction of volcanic deposits and remnant extensional faulting led to continental break-up in the Middle Aptian (c, d). Extensional faulting and minor volcanism characterized the initial Barremian syn-rift phase in the Santos-Campos margin segment (e); Late Barremian-Aptian depth-dependent stretching triggered significant continental thinning and a reduction in the flexural strength of the crust (f, g). Flexure-induced subsidence (black arrows) was a key factor on the progressive block rotation and formation of low-angle listric faults ($\alpha_2 > \alpha_3 > \alpha_4$); subsiding hanging-wall blocks caused further uplift of the contiguous foot-wall blocks (white arrows). Widespread thermal type sag subsidence due to major continental thinning, combined with adequate arid climate condition caused precipitation of evaporites in the Late Aptian (h).

dry climate conditions and high evaporation rates, allowing widespread precipitation of salt during the latest Aptian (115-112 Ma), just prior to the continental break-up (Fig. 5.10h).

5.6.2 Salt deposition in the Campos and Santos basins (Late Aptian, 115-112 Ma)

One of the main issues of the Southern Atlantic development includes the sag basin formation and deposition of evaporites. Different geodynamic and tectonic models (e.g. Marton et al., 2000; Karner et al., 2003; Davison, 2007; Karner and Gambôa, 2007) have been proposed to reconstruct the tectonic regime and basin conditions controlling the precipitation of very thick deposits of evaporites across the Brazilian and West African conjugate margins. In this study, forward modeling allowed to quantitatively analyze key controls on accommodation space and simulate the salt basin conditions based on four major parameters: 1) subsidence; 2) pre-salt water depths; 3) siliciclastic influx; 4) marine water inflow. The resultant salt thicknesses reach 1,900-2,200 m in the central basin part (Figs. 5.8 and 5.9). The predicted precipitation rates varied between 56×10^4 m/m.y. (560 mm/yr) in the Santos Basin and 61×10^4 m/m.y. (610 mm/yr) in the Campos Basin. These values are comparable with estimates of 400-700 mm/yr by Nunn and Harris (2007), based on stratigraphic and geochemical modeling of the South Atlantic salt basins.

1) The salt succession has been considered the upper part of the sag basin fill, deposited shortly prior to continental break-up (Karner and Gambôa, 2007; Mohriak et al., 2008; Torsvik et al., 2009; Contreras et al., 2010). In agreement with current models of lithospheric thinning and continental break-up (Karner and Gambôa, 2007; Kusznir and Karner, 2007; Huisman and Beaumont, 2008), depth-dependent stretching in our model spans 13 m.y. (125-112 Ma). This stage was controlled by low T_e values (6-10 km) and thermal sag subsidence, with rates between 85 m/m.y. on the shelf and 120 m/m.y. along the slope, the area where major continental stretching occurred.

2) The sag pre-salt basin contained lacustrine to bathyal environments. Paleowater depths of 100-250 m on the continental shelf gradually increased to 600 m on the modern upper slope, and 950 m near the transition to oceanic crust. This paleobathymetric profile is compatible with water depths of 500-650 m near the Atlantic hinge by Karner et al. (2003). Therefore, salt precipitation along the Brazilian margin started in a shallow- to deep-water setting in a deep basin, which featured a gradual decrease in paleowater depths as the accommodation space was consumed during the precipitation of salt.

3) The predicted sediment lithofacies calibrated by the available wells on the continental shelf-middle slope indicate extensive pre-salt carbonate deposits with a very low siliciclastic input during the Early-Middle Aptian (Davison, 2007; Contreras et al., 2010). The best-fit model was achieved using siliciclastic input rates of $150 \text{ m}^2/\text{m.y.}$, largely consistent with a minor river delivery due to the

arid climate conditions in the Aptian (Skelton, 2003; Karner and Gambôa, 2007).

4) Because depositional salt thicknesses (approximately up to 2.5 km) greatly exceed the pre-salt accommodation space available (max. 0.95 km), and thermo-tectonic subsidence alone can not compensate the consumption of the accommodation space during the precipitation of salt, a marine water inflow was required to reproduce the very thick salt deposits. Considering the pre-salt basin dimensions (230-240 km large and 100 to 950 deep) and the assumed time span for salt precipitation (115-112 Ma), the water inflow was set to $80 \times 10^6 \text{ m}^3/\text{m.y.}$ It represents a source of marine-type brine necessary to keep up adequate water depths of 100-150 m and saturation conditions. Forward modeling in this study does not provide conclusive data on marine water sources. However, considering the basin dimensions, it is very unlikely that seepage of seawater through the Rio Grande barrier alone (Nunn and Harris, 2007) provided sufficient water volumes to maintain the rates of salt precipitation, although it could represent a brine source. On the other hand, seismic facies and biostratigraphic content in this study do not provide any indication for marine incursions over the Rio Grande barrier during the Aptian. Based on the forward modeling results and published crustal reconfigurations of the syn-rift Southern Atlantic system (e.g. Gladczenko et al., 1997; Fairhead and Wilson, 2005; Mohriak et al., 2010), an alternative water source for the salt basin may have been associated to structurally-controlled seaways across the Walvis Ridge-Rio Grande Rise. Fairhead and Wilson (2005), based on free air gravity and GPS data, suggested that these wrench zones were genetically associated to periods of stress release of the Southern Atlantic plate, which in the Santos-Campos margin segment initiated in Early Aptian times. These local-scale seaways would have kept restricted marine water circulation and marine-type brines for the salt basin, allowing open-marine faunal associations later in the Albian, when total breaching of the Walvis-Rio Grande Ridge system appear to have occurred (Torsvik, et al., 2009).

5.6.3 Post-rift to drift sedimentary evolution (Albian to recent times, 112-0 Ma)

After widespread salt precipitation, the maximum bathymetries in both the Campos and Santos basins did not exceed 200 m. Despite the transition to the post-rift development generated a decrease in subsidence, paleowater depths and accommodation space rapidly increased due to the connection of the Southern and Central Atlantic in the Albian (Moulin et al., 2010). During the post-breakup margin evolution, shifting proportions of thermo-tectonic, flexural and compaction-induced subsidence were crucial for the basin development. After the long-term decrease in thermo-tectonic subsidence during the 'passive margin stage' in the Late Cretaceous, the subsidence development was primarily controlled by changes in the flexural sediment loading since the Early Eocene (48.6 Ma).

As shown in Fig. 5.5, sediment supply was highly variable in time and between basins. Positive changes of up to 70% may occur over time intervals of 4-6 m.y., generating abrupt rises in the

flexural loading by 15-20% after lag times of 6-12 m.y. (e.g. the Eocene in the Pelotas Basin, the Coniacian-Paleocene in the Santos Basin, and the Oligocene-Early Miocene in the Campos Basin). The comparison of the sedimentation history offshore with onshore structural reconfigurations and fission-track geochronology reveal that positive changes in sediment supply coincide with tectonic reactivations of the sediment source areas in the hinterland (Gallagher et al., 1994, 1995; Almeida and Carneiro, 1998; Cobbold et al., 2001; Tello Saenz et al., 2003, 2005; Ribeiro et al., 2005; Strugale et al., 2007; Franco-Magalhaes et al., 2010). These events were related to the effects of the Trindade mantle plume and the Andean orogeny during the Late Cretaceous to Neogene geodynamic evolution of South America. Fission-track data analyses indicate varying timing and rates of denudation between the orogenic belts and basement blocks in the southwest (Don Feliciano Belt, Rio Grande Shield) and the northeast area of the Brazilian continental margin (Serra do Mar, Serra da Mantiqueira, Ponta Grossa Arch).

Existing fission-track data analysis on the Dom Feliciano Belt (Borba et al., 2002) and tectono-magmatic reconfigurations of the southernmost Brazilian continental margin (Peyve, 2010) indicate overall tectonic quiescence after the Jurassic/Cretaceous Serra Geral volcanic event. These interpretations are compatible with relative constant Late Cretaceous sediment supply in the Pelotas Basin. Conversely, a peak in sediment supply in the Santos Basin illustrates well the 2.5 km-uplift of the Serra do Mar in the Coniacian (86 ± 4 Ma; Vignol-Lelarge, et al., 1994). Thermochronological data of Franco-Magalhaes et al. (2010) indicate that exhumation of the Serra do Mar and emplacement of alkaline bodies during the Maastrichtian to Paleocene (e.g. Poços de Caldas-Cabo Frio Lineament) were related to the Trindade mantle plume. Furthermore, tectonic reconfigurations of Cobbold et al. (2007) indicate that periods of tectonic uplift may have been linked to intra-plate compression of the South American plate during the Peruvian phase of Andean orogeny (90-75 Ma). Although this event was less noticeable in shelfal depositional patterns in the Campos Basin, the calculated sediment supply rates and sand volumes exported to deep-marine setting reflect an extrabasinal tectonic factor controlling the Late Cretaceous-Paleocene high sedimentation rates (compare with Fetter et al., 2009). However, this trend was masked by a post-depositional gravity-gliding salt flow and major sediment remobilization basinward.

The thicknesses of the Paleogene-Neogene succession in the Pelotas Basin could not be reproduced by the decompacted sediment input rates derived from inverse-basin modeling. Sediment volumes by about 10% larger than the input rates (Fig. 5.5) were necessary to match the stratigraphic thicknesses of the Middle-Late Eocene and the Middle-Late Miocene successions. By comparison with existing tectono-stratigraphic reconfigurations, these pulses may be connected to the transpressional regime during the Quechuan and Incaic phase of the Andean orogeny (Cobbold et al., 2007) and alkaline intrusions in the province of eastern Uruguay indicated by Peyve (2010). However, the predominant fine-grained siliciclastic input suggest large transportation distances from the source terrains, in contrast to the Santos and Campos basins.

After the Coniacian-Paleocene dynamic continental uplift, the Santos Basin was barely affected by tectonic reactivations in the hinterland. The Eocene and Oligocene, represent a stage of levelling and reorganization of the drainage pathways (Almeida and Carneiro, 1998; Modica and Brush, 2004), indicated by a steady supply of medium- to fine-grained siliciclastics and gradual shelfal progradation. In the Campos Basin, Oligocene sedimentation rates amplified by about 50% and the sand input volumes reached 60-65%. This trend is largely consistent with the capture and deviation of the Paraíba do Sul drainage system from the Santos to the Campos Basin in the Early Oligocene (Modica and Brush, 2004). During the Miocene, intra-plate compression linked to the Quechuan phase of Andean orogeny (25-0 Ma) produced a relative high influx of medium- to coarse-grained sand (40-60%) for both the Campos and Santos basins.

5.6.4 Deep-water depositional systems and implications for hydrocarbon prospectivity

The Santos and Campos basins represent two of the most prolific sedimentary basins of the Southern Atlantic conjugate margins. Producing reservoirs are present from the continental shelf to the lower slope (water depths of 2,500-3,000 m) and involve a variety of lithologies and ages: (i) Barremian-Aptian mixed siliciclastic and carbonates, (ii) Albian carbonates, and (iii) Late Cretaceous to Neogene sand-rich turbidites, the most important petroleum reservoirs offshore Brazil (Bruhn, et al., 2003). Several publications based on 2D as well as 3D seismics and well data provide depositional settings and lithofacies analyses of deep-marine reservoirs (Peres, 1993; Bruhn and Walker, 1995; Machado Jr. et al., 2004; Fontanelli et al., 2009). Most of these studies center on sand-rich turbidite levee-channel systems and basin-floor fans fed by a main canyon on the shelf edge-upper slope realm. Only few published investigations (e.g. Machado et al., 2004; Duarte and Viana, 2007; Fetter et al., 2009) involve a comprehensive examination of the broad depositional scenario and elements controlling the deep-marine sedimentary systems of the Campos and Santos basins. Moreover, the implications of mass transport complexes and contourites for the distribution of lithofacies and hydrocarbon prospectivity remain unclear (Viana et al., 2007), mainly in the Pelotas Basin due to the lack of proven hydrocarbon accumulations. Although 2D forward stratigraphic modeling in this study can not resolve the large variety of depositional elements controlling the Albian to Holocene deep-water sedimentary systems, its combination with seismo-stratigraphy allowed to estimate the location and extension of the deep-marine deposits identified in seismic and well data, including turbidite channel-levee systems and lobes, contourite channel-drift systems, debris flows, slumps and block slides (Figs. 5.11 and 5.12).

Table 5.4 summarizes the most important periods of downslope sedimentation, types of flow and genetic controls during the divergent margin phase. Tectonic reactivations in the hinterland are typically manifested by an increase in the sand volumes and turbidites, which occasionally ex-

tend for 200-250 km basinward, while the proportion of debris flows tend to decrease (e.g. Late Cretaceous in the Santos Basin, Oligocene in the Campos Basin, Eocene in the Pelotas Basin). In contrast, periods of structural inactivity are related to minor turbidite deposition restricted to the upper slope (e.g. Eocene in the Campos Basin and Oligocene in the Santos and Pelotas basins). Mass transport complexes, including debris flows and landslides are genetically related to stratigraphic controls (i.e. relative sea-level, coastal plain and shoreface gradient), called 'downstream factors' in the sequence stratigraphic model of Catuneanu (2006). However, the process/response relationship in the model indicates that downstream controls typically modify the sediment cohesion and instability conditions of the shelf realm, triggering intrabasinal structural deformation, such as shelf-to-slope sediment failure, abrupt changes in slope gradients and sediment-driven salt withdrawal. In addition, modeling results and seismic facies indicate that bottom-currents and the formation of contourites were particularly important in the distribution of deep-marine lithofacies since the Paleogene, triggering significant departures from the stratigraphic thicknesses and sedimentation rates calculated in the model.

Campos Basin

During the Albian and Cenomanian, turbidites mainly composed of fine- to medium-grained sandstones (25-30%) and a fraction of bioclastic fragments (15-20%) were deposited along the outer shelf to the modern middle slope (Namorado Fm.). They form basinward-dipping rafts limited by salt-related listric faults below the shelf edge-upper slope. Intra-slope salt troughs contain low-amplitude to transparent packages of pelagic shales up to 200-300 m thick, embedding high-amplitude lenticular turbidite wedges with maximum thicknesses of 100 m. The predicted porosities range between 20-25% on the outer shelf and 15-18% on the slope, suggesting that good reservoirs conditions extend from the in situ shallow-water Albian carbonates to the middle slope. Santonian-Maastrichtian turbidites are distributed to the lower slope (Carapebus Fm.). The predicted average sand content of 50% and porosities of 10-20% increase into the Maastrichtian interval to 60% and 15-25% respectively. Intercalated debris flows caused partial erosion and redistribution of the turbidite tops, generating local-scale decreases in porosities to 5-10%. Low-amplitude reflectors with long-lateral continuity correspond to suspension-driven pelagic shales, which represent good quality seals between 100-200 m of thickness.

During the Paleogene forced-regression system, deltaic-fed sand-dominated turbidites with porosities of 15-20% were confined to the upper-middle slope due to salt-induced topographic obstacles. They form stratigraphic lenses with maximum thicknesses of 80-100 m encased by pelagic shales and occasional debris flows at the top. Toward the lower slope, bottom-currents caused intense sediment redistribution and lithofacies heterogeneities. The predicted deep-marine facies indicate up to 200 m-thick and 2 km-wide sand-rich intervals with uncertain porosities,

which correspond to contourite drifts identified in the seismic profile (Fig. 5.11a). The Eocene-Oligocene basin fill contains the most complex deep-marine facies assemblage in the Campos Basin, controlled by the interaction of debris flows, turbidites and contourites. Eocene turbidite channel-levee systems (Fig. 5.11b) show thickness of 80-120 m and porosities of 10-15%. These intervals are encased in silt- to mud-rich debris flows or hemipelagic shales with highly variable seal quality. Toward the lower slope, turbidites are fairly absent, while the proportion of debris flows and contourites increases. In the Oligocene, deep-marine sand volumes transported by turbidite currents increased by around 40%. Predicted sediment lithofacies (calibrated by two of the available wells) show Lower Oligocene siliciclastic-carbonate turbidites with porosities of 15-18% on the upper-middle slope, grading into mud-rich debris flows and contourite channel-drifts on the lower slope. In turn, Upper Oligocene sand-rich turbidites were widely distributed on the lower slope and display enhanced reservoir quality (average porosities of 25-30%) in comparison with the Eocene counterparts. Although individual thicknesses of the Oligocene turbidites usually did not exceed 100 m, salt deformation generated amalgamated wedges with total thicknesses of up to 300 m and pinch-outs against intra-diapir salt troughs. Halokinesis-related slumps and debris flows caused local-scale facies heterogeneities and porosities of 5-10% in Oligocene turbidites.

A major strike-oriented channel located at the shelf break cut into the upper Oligocene-Holocene succession (see Fig. 5.1). On the upper slope, the Miocene-Holocene basin fill is mainly composed of amalgamated mass transport complexes of 1,000 m of total thickness, which gradually thin out on the lower slope over 150 km. Medium- to low-amplitude wavy reflectors and intercalated erosional surfaces reflect internal debris flows systems with basal scours (Fig. 5.11c). Sand-rich Early Miocene intervals were deeply eroded from the upper-middle slope and redeposited basinward. However, stratigraphic simulations and well data indicate that remnant thin turbidite lobes and reworked sandstones deposited in erosive scours represent high-quality reservoirs with porosities of 18-20% and maximum thickness of 60-70 m.

Santos Basin

During the Albian to Turonian, deep-water sedimentation was controlled by widespread deposition of marine shales and hemipelagic carbonates with intercalated debris flows. The predicted Albian turbidite flows are composed of bioclastics and medium- to coarse-grained sandstones forming stratigraphic lenses with maximum thickness of 10-15 m along the modern upper-middle slope. Up-section, the Santonian-Maastrichtian basin fill includes the largest sand-rich turbidite volumes in the Santos Basin. Seismic facies indicate channel-levee turbidite systems confined to salt- and fault-bounded depocenters and intercalated with debris flows (Fig. 5.11d). The turbidites are characterized by high-amplitude parallel reflectors forming packages of 180-220 m with porosities between 12% and 35%. The lower porosity values generally occur adjacent to the diapirs flanks mainly due to halokinesis-related slumps. During the Paleocene to Early Eocene, the sand

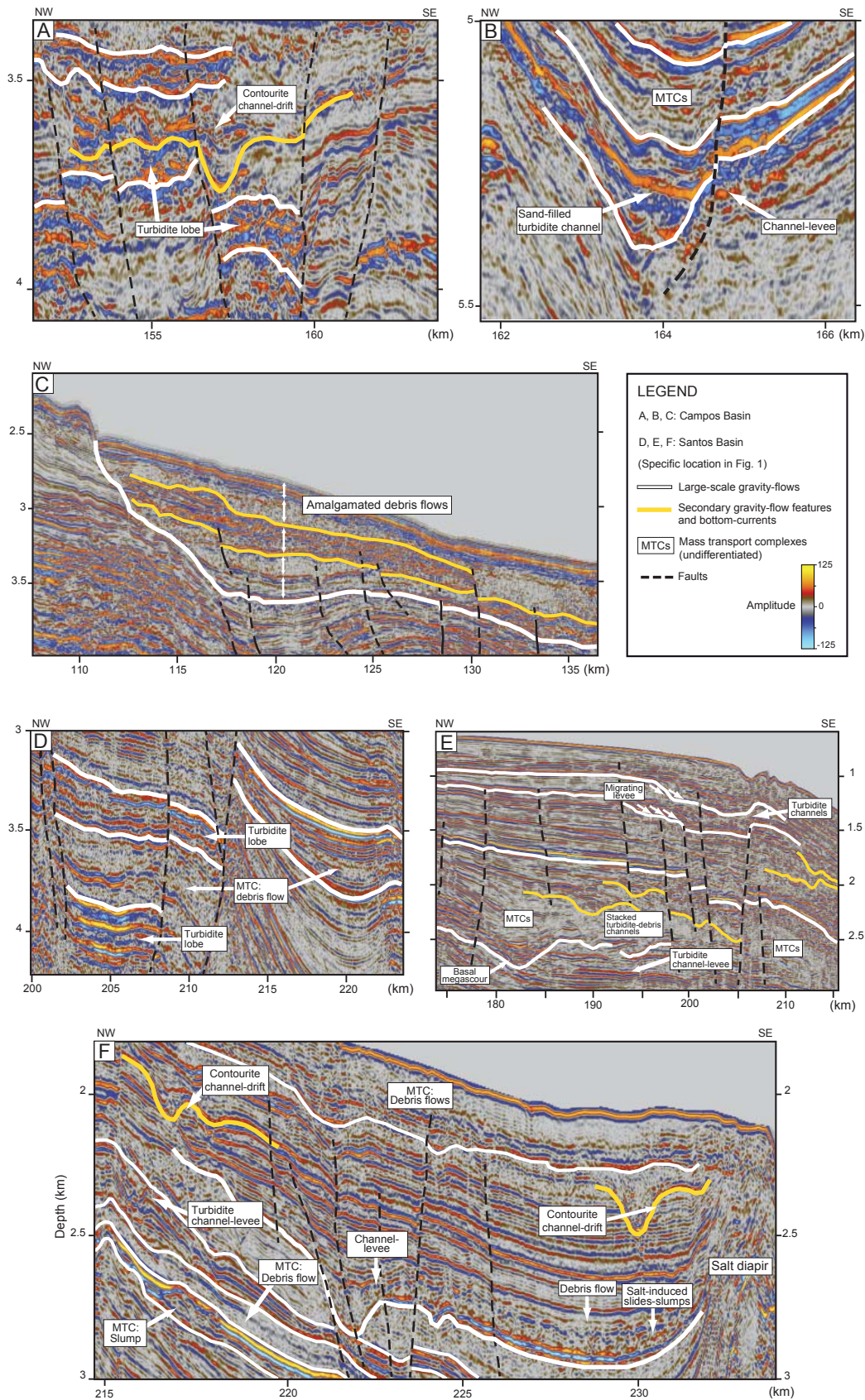


Fig. 5.11 Deep-water seismic features and depositional systems in the Campos and Santos basins. Location given in Fig. 1, insets A-F. (A) Campos Basin, lower slope: Eocene turbidite channel; (B) Campos Basin, lower slope to basin margin: Oligocene turbidite fans cut by salt-induced faults and contourite channels-drift systems; (C) Campos Basin, middle to lower slope: Late Miocene-Holocene mass transport complexes (debris flows and slumps) eroding the Early-Middle Miocene basin fill; (D) Santos Basin, middle-lower slope: Late Cretaceous turbidites intercalated with debris flows; (E) Santos Basin, upper-middle slope: Eocene to Miocene stacked mass transport complexes, bottom-current channels and turbidite levee-channel deposits; (F) Santos Basin, lower slope: stacked turbidites and debris flows cross-cut by contourites.

5. Forward stratigraphic modeling

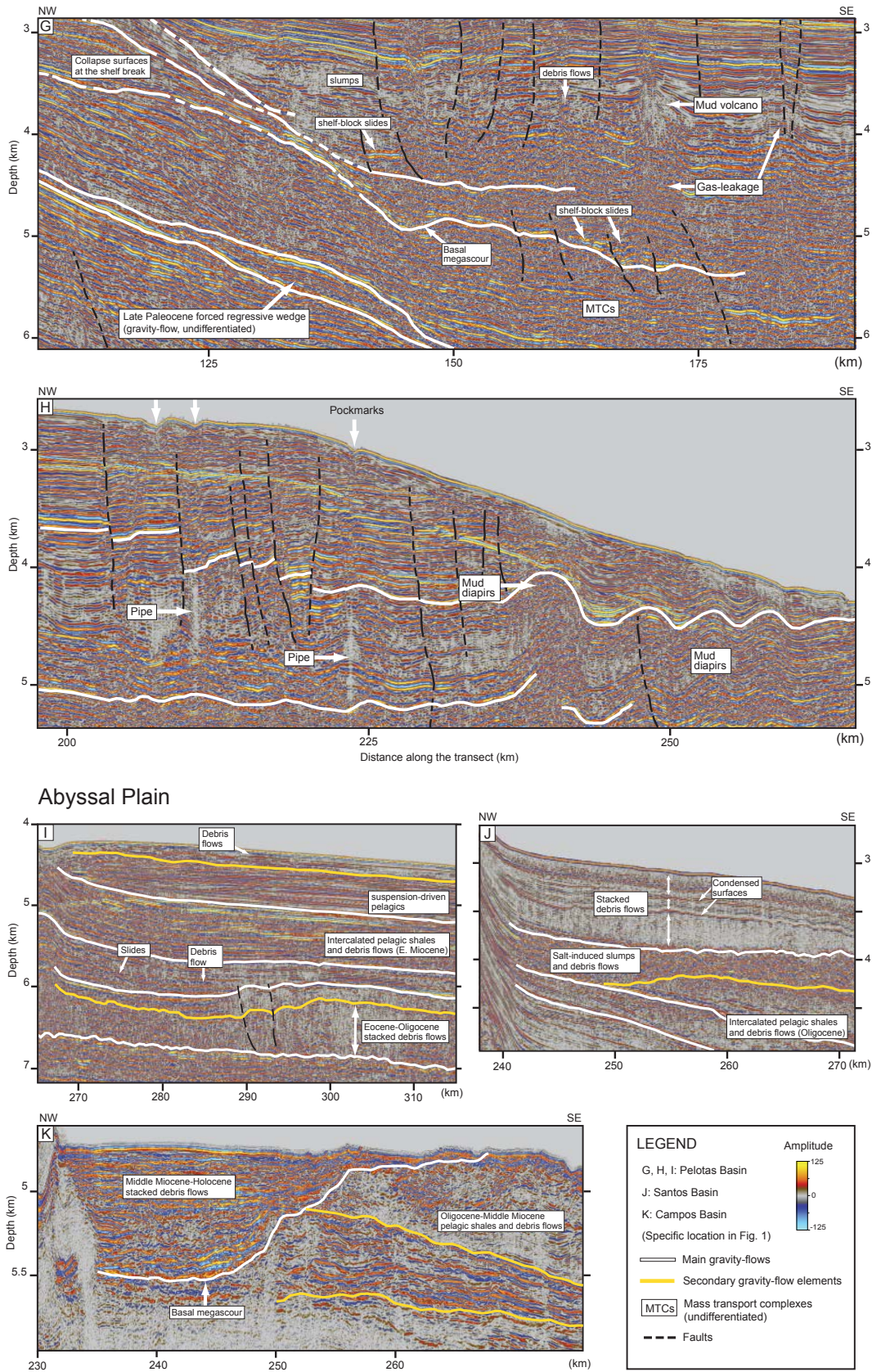


Fig. 5.12 Deep-water seismic features and depositional systems in the Pelotas, Santos and Campos basins. Location given in Fig. 1 insets G-K. (G) Pelotas Basin, middle slope: Paleocene to Late Miocene amalgamated mass transport complexes from shelf margin and slope collapse, with mud volcanoes and gas chimneys; (H) Pelotas Basin, lower slope to basin margin: gas-leakage features, including chimneys and pockmarks associated to mud diapirs; (I) Campos Basin, basin margin, (J) Santos Basin lower slope to basin margin, and (K) Pelotas Basin, basin margin: erosive mass transport complexes and pelagic deposits.

volumes exported to deep-marine setting reduced considerably. Gravitational sedimentation was largely controlled by recurrent debris flows and contourites on the upper slope. Turbidites were rare, showing maximum thicknesses of 20-30 m and uncertain porosity values. The best quality intervals correspond to the Paleocene forced regression wedges on the outer shelf-upper slope, which show poorly-sorted sandstones with maximum thickness of 80-90 m and porosities between 15-18%. Up-section, the Middle-Late Eocene deep-marine sand-dominated intervals penetrated by the calibration wells show well-sorted turbidites with average porosities of 24-26%. They are characterized by high-amplitude, sub-parallel to parallel reflectors cut by debris flows with erosional bases (Fig. 5.11e). Toward the lower slope, low-amplitude to transparent reflector packages indicate high proportions of marine shales and debris flows. Contourite deposits were difficult to distinguish due to the reduced sand content. During the Oligocene, eustatic-driven debris flows and hemipelagic shales dominated the deep-marine basin fill of the Santos Basin (Fig. 5.11f). Occasional turbidite flows formed stratigraphic lenses with maximum thicknesses of 100-120 m, which are mainly present into the Late Oligocene and Early Miocene units. The predicted porosity values range between 10% and 35%. The lower values are associated to contourite drifts and halokinesis-driven slumps cutting into the sand-dominated turbidites.

Pelotas Basin

The Middle-Late Aptian post-rift succession is mainly composed of fining-upward siliciclastic deposits with porosities of 3-8% on the shelf and 3-10% along the slope. The Albian carbonate unit includes mixed siliciclastic-carbonate deposits with average porosities of 5-12% on the inner shelf increasing to 10-15% toward the shelf edge-upper slope. Basinward, the predominant lithotypes include mud-rich carbonates with maximum porosities of 5%. The deep-water Late Cretaceous to Eocene basin fill is mainly composed of hemipelagic shales and mud-rich debris flows. Turbidites occurred principally in the Campanian and the Late Paleocene successions, which display maximum thicknesses of 70-90 m, a relative low sand content (25-30%) and porosities ranging from 5% to 20% in the available wells (Fig. 5.2). Intercalated progradational and retrogradational trends during the Oligocene generated instability conditions, for instance shelf-edge sediment failure and block slides on the upper-middle slope. The predicted porosities reach maximum values of 15%, but due to the lack of calibration wells their reservoir potential could not be assessed. Toward the lower slope, gas chimneys and pockmarks appear to be associated to the release of gas hydrates (Rosa et al., 2006) during the rapid overburden of Eocene-Early Miocene marine shales and contourites. These features triggered instability conditions of the lower slope and deep-marine sediment remobilization with deposition of debris flows in the oceanic basin during the Neogene.

Age	Campos		Santos		Pelotas	
	Control	Type of flow and extension	Control	Type of flow and extension	Control	Type of flow and extension
Late-Middle Miocene	E Bc, Sc Bc, St	Debris; ls Contourites, ls Debris, contourites; dbm	E Bc St	Debris; ls Contourites, ls Debris; dbm	E	Debris; ls
Early Miocene	E Bc, Sc	Debris, ls Contourites, ls Turbidites, ms	E Bc St	Debris; ls Contourites, ls Debris; dbm	T, Sc E	Block slides; ms Debris; ls
Late Oligoc.	E	Turbidites; ls Debris, ms Contourites, ls	E Bc	Debris; ls Contourites, ls	T, Sc	Block slides; ms Debris; ls
Early Oligoc.	E Sc	Debris; ls Turbidites; ms Contourites; ls	E Bc	Debris; ls Contourites, ls	E	Debris, ls
Late Eocene	E T Bc	Debris; ms Turbidites; ls Contourites; ls	E T	Debris; ls Turbidites; ls	E	Debris; ls
Middle Eocene	T	Turbidites; ls Debris; ls Contourites; ls	E T	Debris; ls Turbidites; ls	E	Debris; ls
Early Eocene	Bc T	Turbidites; ls	E T	Debris; ls Turbidites; ls		
Paleocene	T E	Turbidites; ls	T E	Turbidites; ls Debris; ms	E	Debris; ms
Maastrichtian-Coniacian	T	Turbidites; ls Debris; ms	T, Sc E	Turbidites; ls Debris; ls	E	Debris; ls
Turonian-Cenomanian	E	Debris; ms	E	Debris; ls	E	Debris; ls
Albian	E	Debris; ms Turbidites; ms	E	Debris; ms Turbidites; ms	E	Debris, ms

Table 5.4 Summary of deep-marine sediment flows indicating the stratigraphic and structural controls predicted by forward stratigraphic modeling (T: tectonism; E: eustasy; Bc: bottom-currents; Sc: sediment collapse) and the extension into the basin calibrated with the seismic and well data (us: upper slope; ms: middle slope, ls: lower slope; dbm: deep basin margin).

6. Final conclusions

The integrated basin analysis, including sequence-stratigraphy, inverse-basin and forward stratigraphic modeling provided tectono-stratigraphic plausible models and quantitative chronological information for the Barremian syn-rift to Holocene mature drift evolution of the Pelotas, Santos and Campos basins. The predicted depositional trends, distribution of lithofacies and paleowater depths were calibrated with the seismic geometries, sedimentologic and biostratigraphic data from wells. This approach allowed to determine the main deformation and sedimentary processes on the rifted margin development of southeastern Brazil, and to recognize the key factors on the model deviations.

The mechanisms of lithosphere deformation during the south-to-north break-up of Gondwana in the Early Cretaceous had major implications in the long-term flexural evolution and architecture of the marginal sediment depocenters. In the Pelotas Basin, Barremian syn-rift extensive volcanism caused an increase of the flexural rigidity of the crust, restricted fault-displacement and precluded the formation of deep syn-rift depocenters. Along the Santos-Campos basins, minor volcanism and depth-dependent stretching led to a significant decrease in the flexural rigidity of the crust. This tectonic regime was crucial for the formation of listric faults and deep lacustrine depocenters: periods of fault reactivation were characterized by deposition of transgressive mud-rich carbonates and shales; periods of tectonic quiescence were characterized by erosion of the uplifted blocks and deposition of sand-dominated progradational successions. Fault-bounded structural highs featured appropriate bathymetric conditions for massive bioclastic limestones, which include major syn-rift reservoirs in both the Santos and Campos basins. During the Aptian sag stage, wide and smooth-relief depocenters, underlain by extremely stretched continental crust, were characterized by laterally constant subsidence rates (85-120 m/m.y) and bathymetries between 100 m and 950 m. The proposed model for salt basin formation considers that sag basins were connected to a brine-source of marine-type. Increasing salinities and arid climate conditions during the Aptian allowed the deposition of up to 2,200 m of evaporites in a time span of 3 m.y. (115-112 Ma).

The post-breakup development in each the Pelotas, Santos and Campos basins was largely controlled by differential thermal contraction of the crust and tectono-magmatic events in the hinterland, which strongly affected the deposition patterns offshore. Periods of exhumation and erosion of the sediment source areas are directly related to high rates of sediment supply, trends of shelf progradation and sand-rich turbidites. Maximum peaks in the sediment supply and increases in the sediment loading restricted upslope salt extension. However, gravitational sediment flows, and larger deep-marine sand volumes, enhanced downslope salt compression and formation of diapirs. These variations in the deformation patterns resulted in a temporal disconnection between

the upslope and downslope salt remobilization. In the Santos Basin, downslope salt compression and diapirism during the Campanian-Maastrichtian and Late Oligocene-Middle Miocene was coeval with minor salt remobilization upslope; in the Campos Basin this mechanical detachment of the salt layer occurred during the Paleocene, Middle Eocene and Early Miocene. Syn-sedimentary salt deformation may enhance the reservoir potential by the amalgamation of sand-rich wedges in salt troughs and the creation of stratigraphic traps by pinch-outs against salt diapirs. On the other hand, the reservoir architecture and traps may be degraded by halokinesis-induced slumps and redistribution of sand-rich slope and basin-floor fans deposited above salt structures.

Gravitational sediment flows and the occurrence of either turbidites or mass transport complexes primarily depend on the sediment input, the lithotypes delivered from the shelf and the causal mechanisms (i.e. tectonism, sea-level, catastrophic sediment collapse). Forward modeling indicate that turbidite flows are associated to periods of tectonic uplift of the sediment source areas and periods of strong continental and coastal erosion. Eustatic-sea-level fluctuations are not a typical causal mechanism of turbidites; however, depending on the shelf stability conditions, depositional gradient and lithotypes, a rapid sea-level fall may induce the collapse of the sand-rich progradational front triggering block slides and/or turbidite flows. Modeling results and the interpretations in this study are largely consistent with the classification of mass transport complexes by Moscardelli and Wood (2008). Debris flows are mainly associated to relative sea-level falls and periods of mud-rich clastic sedimentation (attached MTCs). Transgressive decollement surfaces and updip salt extension may cause instability of the shelf edge-upper slope realm, resulting in catastrophic debris flows or block slides usually restricted to the upper-middle slope (detached MTCs). In addition, gas hydrates release and bottom-currents appears to induce debris flows along the lower slope to basin margin. Slumps are usually associated to salt diapirs and sediment remobilization toward their flanks. The hydrocarbon prospectivity of mass transport complexes is generally reduced by lateral discontinuous sand bodies, which in most cases show low porosities and permeabilities.

Hydrocarbon potential and salt deformation effects

The predicted tectono-stratigraphic development reveals significant differences in the conditions for hydrocarbon generation and trapping between the Pelotas, Santos and Campos basins. The syn-rift succession along the southern Brazilian margin thins in southward direction, which resulted in the absence of late Barremian-Aptian lacustrine source rocks in the Pelotas Basin. Nonetheless, Cenomanian-Turonian marine shales appear to have reached adequate conditions for hydrocarbon generation since the Late Eocene (Fig. 6.1a.) However, the increased stratigraphic thickness of the Miocene succession toward the slope led to gas-window conditions and probably overmaturation (Fig. 6.1b). This assumption is consistent with the interpreted concentrations of gas

hydrates and gas release features identified in the seismic data and in previous studies on the Pelotas Basin (e.g. Rosa et al., 2006; Santa Ana et al., 2008). The development of gas hydrates accumulations as alternative energy resources is limited by insufficient information about in situ conditions and eventual recovery rates (no drilling in deep and ultra-deep waters). Toward the continental shelf, smaller stratigraphic thicknesses may allow suitable overburden depths for oil generation. However, the intense erosional events of the shallow-marine sand-dominated successions during the Paleogene and Neogene represents a limiting factor on the presence of reservoirs and good-quality traps, which appear only to occur in Paleogene lenticular-shaped bodies of sandstones along the upper-middle slope. The thick Neogene basin fill, mainly composed of siltstones and shales, provides potential seals for deeper reservoirs. In the Santos and Campos basins, it is possible to visualize the strong influence of salt remobilization on the lithostatic pressure and maturation of both late Barremian-Aptian and Cenomanian-Turonian source rocks intervals.

Salt-induced deformation started in the Albian post-rift stage with horizontal extension on the shelf margin and compression downslope. As previously mentioned, the deformation styles and rates of salt remobilization depend on the interactions between sediment loading and gravity-induced gliding of the salt layer. Salt structures in the Santos and Campos basins (i.e., diapirs, listric and growth faults, up-dip pinch-outs, salt welds) played a decisive role on the distribution of reservoir facies and depocenters as well as on the fluid migration pathways and heat flow.

In the Santos Basin, Upper Cretaceous to Neogene producing reservoirs confirm hydrocarbon generation from Early Cretaceous and Late Cretaceous source rocks (see Katz and Mello, 2000; Carminatti et al., 2008). On the one hand, the high thermal conductivity of the salt dissipates the heat flow efficiently, causing therefore a delay in the maturation of both Late Barremian-Middle Aptian and Cenomanian-Turonian source rocks (compare with Mello et al., 1995). On the other hand, salt flow redistributed sedimentary loads and modified lithostratigraphic pressure fields of the sub-salt succession; thicknesses and related thermal anomalies are much more complicated in areas affected by salt tectonics than in areas where the salt is still in place. Due to the high degree of pressure dissipated during the deformation of the salt layer, mechanical compaction and textural porosity decrease in potential syn-rift reservoirs were also delayed. As shown in Fig. 6.1d, areas of salt withdrawal with formation of diapirs allow the sub-salt successions to remain within the oil-window for a longer time. In contrast, in areas of salt escape (inter-diapir troughs) the overburden thicknesses and lithostatic pressure increase, which can eventually led the underlying source rocks intervals into the gas-window or overmature conditions (Fig. 6.1c). Apart from the effect on hydrocarbon generation in sub- and post-salt source rocks, salt deformation plays a key role in the formation of traps and hydrocarbon migration ways. Although oil generation was possible since the Eocene and from comparable source rocks intervals in both the Santos and Campos

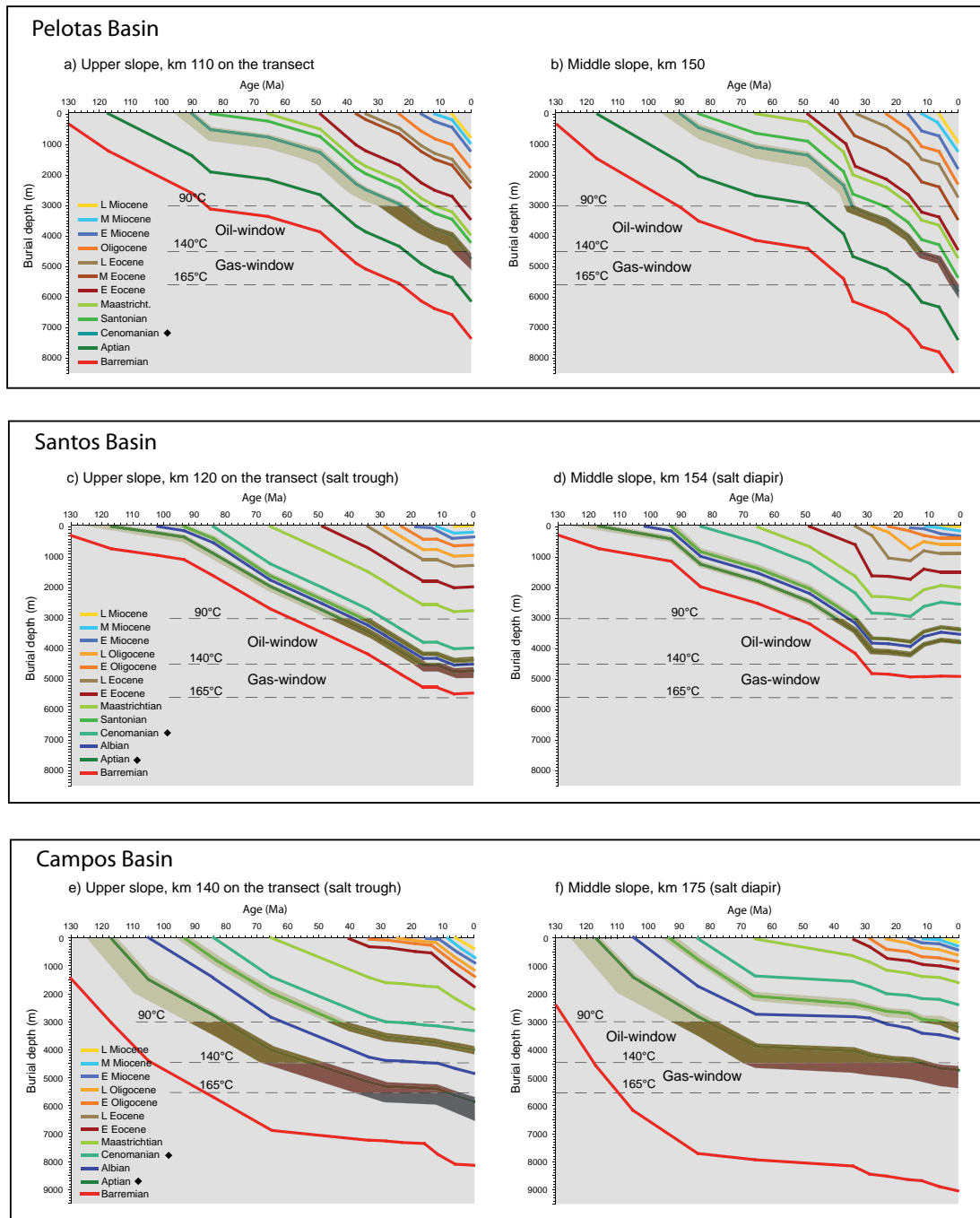


Fig. 6.1 Burial depth history for the Barremian-Holocene stratigraphic succession in each the Pelotas, Santos and Campos basins. Two locations on the middle slope have been chosen to compare the basin-specific overburden evolution and the implications for the maturation of both potential source rocks intervals (♦), late Barremian-Middle Aptian syn-rift lacustrine and Cenomanian-Turonian marine shales.

basins, hydrocarbon reserves in the post-salt succession of the Santos Basin are considerably smaller than in the Campos Basin (see Coward et al., 1999). It is proposed that a predominant compressional salt deformation style in the Santos Basin restricted the creation of pathways from syn-rift shales to the Late Cretaceous-Neogene succession. Thus, the salt succession appears to represent a good-quality regional top-seal for sub-salt reservoirs, which are highly prolific as confirmed by recent discoveries (Tupi, Jupiter and Carioca/Sugar Loaf; Carminatti et al., 2008).

The predicted Barremian-Holocene burial history for the Campos Basin indicates that potential source rocks intervals in the distal part of syn-rift sag depocenters (modern continental slope) may be overmatured (Fig. 6.1e). Despite this unfavorable scenario, the possibility of hydrocarbon generation and migration during adequate overburden conditions in the Late Cretaceous (or secondary hydrocarbon generation in the Paleogene) has not been confirmed so far. However, the time-equivalent organic-rich intervals deposited in syn-rift depressions below the continental shelf have proven to contain excellent generating source rocks (Berman, 2008). Different than in the Santos Basin, Cenomanian-Turonian marine shales in the Campos Basin do not represent proven source rock intervals despite the favorable TOC levels (1-4%: Davison, 1999). Widespread salt-induced deformation has altered their original distribution and affected the potential maturation, also due to local differences in overburden. The restored basin architecture and stratigraphic thickness show that burial depths for oil generation from Cenomanian-Turonian marine shales have been sufficient only in salt-related depocenters and since the Middle Miocene (Fig. 6.1f). Due to the presence of sand-rich turbidite deposits, these areas are prospective for exploration, although insufficient time for hydrocarbon generation represents an important constraint.

The combination of qualitative and quantitative analytical methods, based on the integration of seismic and well data, has demonstrated to be a consistent approach to interpret the signature of processes of lithospheric deformation leading to formation of continental margins, the implications of these processes on the long-term flexural behaviour of the crust and the evolution of accommodation space for sedimentation. Numerical basin modeling allows to investigate geological hypotheses by adjusting the parameters and observing the model response. The reliability of multiple possible geological scenarios can be tested, and the best-fit reasonable geological frameworks matching the data can be analyzed. This information is valuable for the prediction of the ancient tectonic and sedimentary systems controlling the continental margin topography, basin formation, paleo-environments, onshore-offshore sediment pathways, sediment volumes input the marine setting, mechanism of transport and deep-marine sediment redistribution, all of them key aspects on the preservation of the natural geological cycles as well as on the impact of exploration and production of natural resources.

References

- Almeida, F.F.M. and Carneiro, C.D.R., 1998. Origem e evolução da Serra do Mar. *Revista Brasileira de Geociências*, 28, 135-150.
- Anderson, N.L. and Fressen, E.K., 1991. Differential compaction of Winnipegosis reef - a seismic perspective. *Geophysics*, 56 (1), 142-147.
- Anjos-Zerfass, G.S., Souza, P. A. and Chemale, F., 2008. Biocronoestratigrafia da Bacia de Pelotas: estado atual e implicação na geologia do petróleo. *Revista Brasileira de Geociências*, 38 (2), 47-62.
- Anka, Z., Sérrane, M., Lopez, M., Scheck-Wenderoth, M. and Savoye, B., 2009. The long-term evolution of the Congo deep-sea fan: A basin-wide view of the interaction between a giant submarine fan and a mature passive margin (ZaiAngo project). *Tectonophysics*, 470, 42-56.
- Aslanian, D., Moulin, M., Olivet, J.L., Unternehr, P., Matias, L., Bache, F., Rabineau, M., Nouzé, H., Klingelhoefer, F., Contrucci, I. and Labails, C., 2009. Brazilian and African passive margins of the central segment of the South Atlantic Ocean: kinematic constraints. *Tectonophysics*, 468, 1-4, 98-112.
- Barboza, E.G., Rosa, M.L.C.C. and Ayup-Zouain, R.N., 2008. Cronostratigrafia da Bacia de Pelotas: uma revisão das seqüências deposicionais. *Porto Alegre, GRAVEL*, 6 (1), 125-138.
- Bassetto, M., Alkmim, F., Szatmari, P. and Mohriak, W.U., 2000. The oceanic segment of the southern Brazilian margin: morpho-structural domains and their tectonic significance, in: Mohriak, W.U. and Talwani, M. (Eds.), *Atlantic Rifts and Continental Margins*. American Geophysical Union, Monograph 115, 235-259.
- Bate, R., 1999. Non-marine ostracod assemblages of the Pre-Salt rift basins of West Africa and their role in sequence stratigraphy. in: Cameron, N.R., Bate, R.H. and Clure, V.S. (Eds.), *The Oil and Gas Habitats of the South Atlantic*. Geological Society of London, Special Publications 153, 283-292.
- Bauer, K., Neben, S., Schreckenberger, B., Emmermann, R., Hinz, K., Fechner, N., Gohl, K., Schulze, A., Trumbull, R.B. and Weber, K., 2000. Deep structure of the Namibia continental margin as derived from integrated geophysical studies. *Journal of Geophysical Research*, 105, B11, 25829-25853.
- Berman, A., 2008. Three super-giant fields discovered in Brazil's Santos Basin. What's new in exploration? *World Oil*, 229 (2), 23-24.

Blaich, O.A., Faleide, J.I., Tsikalas, F., Franke, D. and León, E., 2009. Crustal-scale architecture and segmentation of the Argentine margin and its conjugate off South Africa. *Geophysical Journal International*, 1-21.

Boillot, G., Recq, M., Winterer, E.L., Meyer, A.W., Applegate, J., Baltuck, M., Bergen, J.A., Comas, M.C., Davies, T.A., Dunham, K., Evans, C.A., Girardeau, J., Goldberg, G., Haggerty, J., Jansa, L.F., Johnson, J.A., Kasahara, J., Loreau, J.P., Luna-Sierra, E., Moullade, M., Ogg, J., Sarti, M., Thurow, J. and Williamson, M., 1987. Tectonic denudation of the upper mantle along passive margins: a model based on drilling results (ODP leg 103, Western Galicia Margin, Spain). *Tectonophysics*, 132, 335-342.

Borba, A.W., Vignol-Lelarge, M.L.M. and Misuzaki, A.M.P. 2002. Uplift and denudation of the Caçapava do Sul granitoids (Southern Brazil) during late Paleozoic and Mesozoic constraints from apatite fission track data. *Journal South American Earth Sciences*, 15, 683-692.

Bowman, S.A. and Vail, P.R., 1999. Interpreting the stratigraphy of the Baltimore Canyon section offshore New Jersey with PHIL, a stratigraphic simulator, in: Harbaugh, J.W., Watney, W.L., Rankey, E.C., Singlerland, R., Goldstein, R.H. and Franseen, E.K. (Eds.), *Numerical Experiments in Stratigraphy: Recent Advances in Stratigraphic and Sedimentologic Computer Simulations*. SEPM Special Publication, 62, 117-138.

Bruhn, C.H.L. and Walker, R.G., 1995. High-resolution stratigraphy and sedimentary evolution of coarse-grained canyon-filling turbidites from the Upper Cretaceous transgressive megasequence, Campos Basin, offshore Brazil. *Journal of Sedimentary Research*, B65 (4), 426-442.

Bruhn, C.H.L., Gomes, J.A., Lucchese Jr., C., Johann, P.R.S., 2003. Campos Basin: reservoir characterization and management – Historical overview and future challenges. OTC 15220, Offshore Technology Conference, Houston, Texas, 2003.

Bueno, G.V., Zacharias, A.A., Oreiro, S.G., Cupertino, J.A., Falkenheim, F.U.H. and Martins, M.A., 2007. Bacia de Pelotas. *Boletim de Geociências da Petrobras*, Rio de Janeiro, 15 (2), 551-559.

Burgess, P.M., Lammers, H., Van Oosterhout, C. and Granjeon, D., 2006. Multivariate sequence stratigraphy: Tackling complexity and uncertainty with stratigraphic forward modeling, multiple scenarios, and conditional frequency maps. *AAPG Bulletin*, 90 (12), 1883-1901.

Burgess, P.M., Steel, R.J., and Granjeon, D., 2008, Stratigraphic forward modeling of basin-margin clinoform systems: implications for controls on topset and shelf width and timing of formations of shelf-edge deltas, in: Hampson, G.J., Steel, R.J., Burgess, P.M., and Dalrymple, R.W. (Eds.), *Recent Advances in Models of Siliciclastic Shallow-Marine Stratigraphy*. SEPM, Special Publication 90, 3-12.

- Cainelli, C. and Mohriak, W.U., 1999. Some remarks on the evolution of sedimentary basins along the eastern Brazilian continental margin. *Episodes*, 22 (3), 206-216.
- Cande, S.C., LaBrecque, J.L., and Haxby, W.B., 1988. Plate kinematics of the South Atlantic: Chron 34 to present. *Journal Geophysical Research*, 93 (B11), 13479-13492.
- Carminatti, M., Wolff, B. and Gamboa, L., 2008. New exploratory frontiers in Brazil. 19th World Petroleum Congress, Spain 2008.
- Castillo, L.L.A., Kazmierczak, T.S. and Chemale, Jr. F., 2009. Rio Grande Cone tectono-stratigraphic model Brazil: seismic sequences. *Earth Sciences Research Journal*, 13 (1) 40-53.
- Catuneanu, O., 2006. *Principles of Sequence Stratigraphy*. Elsevier Science Ltd., Amsterdam, pp. 375.
- Catuneanu, O., Abreu, V., Bhattacharya, J.P., Blum, M.D., Dalrymple, R.W., Eriksson, P.G., Fielding, C.R., Fisher, W.L., Galloway, W.E., Gibling M.R., Giles, K.A., Holbrook, J.M., Jordan, R., Kendall, C.G.St.C., Macurda, B., Martinsen, O.J., Miall, A.D., Neal, J.E., Nummendal, D., Pomar, L., Posamentier, H.W., Pratt, B.R., Sarg, J.F., Shanley, K.W., Steel, R.J., Strasser, A., Tucker, M.E. and Winker, C., 2009. Towards the standardization of sequence stratigraphy. *Earth-Sciences Reviews*, 92 (1-2), 1-33.
- Chang, H.K., Kowsmann, R.O., Figueiredo, A.M.F. and Bender, A.A., 1992. Tectonics and stratigraphy of the East Brazil rift system: an overview, in: Ziegler, P.A. (Ed.), *Geodynamics of Rifting, Volume II. Case History Studies on Rifts: North and South America and Africa*. *Tectonophysics*, 213, 97-138.
- Clemson, J., Cartwright, J. and Booth, J., 1997. Structural segmentation and the influence of basement structure on the Namibian passive margin. *Journal of the Geological Society*, 154 (3), 477-482.
- Clennell, M.B., 2000. Hidrato de gás submarino: natureza, ocorrência e perspectivas para exploração na margem continental brasileira. *Brazilian Journal of Geophysics*, 18 (3), 397-409.
- Cobbold, P.R., Szatmari, P., Demercian, L.S., Coelho, D. and Rosello, E.A., 1995. Seismic and experimental evidence for thin-skinned horizontal shortening by convergent radial gliding on evaporites, deep-water Santos Basin, Brazil, in: Jackson, M.P.A., Roberts, D.G. and Snelson, S. (Eds.), *Salt Tectonics: A Global Perspective*. AAPG Memoir, 65, 305-321.
- Cobbold, P.R., Meisling, K.E. and Mount, V.S., 2001. Reactivation of an obliquely rifted margin, Campos and Santos basins, southeastern Brazil. *AAPG Bulletin*, 85 (11), 1925-1944.

Cobbold, P.R., Rosello, E.A., Roprech, P., Arriagada, C., Gómez, L.A. and Cláudio, L., 2007. Distribution, timing, and causes of Andean deformation across South America, in: Ries, A.C., Butler, R.W.H. and Graham, R.H. (Eds.), *Deformation of the Continental Crust: The Legacy of Mike Coward*. Geological Society of London, Special Publications, 272, 321-343.

Cochran, J.R and Karner, G.D., 2007. Constraints on the deformation and rupturing of continental lithosphere of the Red Sea: the transition from rifting to drifting, in: Karner, G.D., Manatschal, G. and Pinheiro, L.M. (Eds.), *Imaging, Mapping and Modelling Continental Lithosphere Extension and Breakup*. Geological Society of London, Special Publications, 282, 265-289.

Coimbra, J.C., Carreño, A.L. and Anjos, G.S., 2009. Biostratigraphy and paleoceanographical significance of the Neogene planktonic foraminifera from the Pelotas Basin, southernmost Brazil. *Revue de Micropaléontologie*, 52, 1-14.

Contreras, J., Zühlke, R., Bowman, S. and Bechstädt, T., 2010. Seismic stratigraphy and subsidence analysis of the southern Brazilian margin (Campos, Santos and Pelotas basins). *Marine and Petroleum Geology*, 27, 1952-1980.

Contrucci, I., Matias, L., Moulin, M., Géli, L., Klingelhofer, F., Nouzé, H., Aslanian, D., Olivet, J.L., Réhault, J.P. and Sibuet J.C., 2004. Deep structure of the West African continental margin (Congo, Zaïre, Angola), between 5°S and 8°S, from reflection/refraction seismics and gravity data. *Geophysical Journal International*, 158, 529-553.

Corti, G., 2009. Continental rift evolution: from rift initiation to incipient break-up in the Main Ethiopian Rift, East Africa. *Earth Science Reviews*, 96, 1-53

Costa, L. and Silva, M.B., 2010. Investigação de ocorrência de hidrato de gás na Bacia de Pelotas Brasil. Resumos XIX Congresso de Iniciação Científica – XII Eocontro de Pós-Graduação, Universidade Federal de Pelotas.

Coward, M.P., Purdy, E.G., Ries, A., Smith, D.G., 1999. The distribution of petroleum reserves in basins of the South Atlantic margin, in: Cameron, N.R., Bate, R.H. and Clure, V.S. (Eds.), *The Oil and Gas Habitats of the South Atlantic*. Geological Society of London, Special Publications 153, 101-131.

Crosby, A., White, N., Edwards, G. and Shillington, D., 2008. Evolution of the Newfoundland-Iberia conjugated rifted margins. *Earth and Planetary Science Letters*, 273, 214-226.

- Davison, I., 1999. Tectonics and hydrocarbon distribution along the Brazilian South Atlantic margin, in: Cameron, N.R., Bate, R.H. and Clure, V.S. (Eds.), *The Oil and Gas Habitats of the South Atlantic*. Geological Society of London, Special Publications, 153, 133-151.
- Davison, I., 2007. Geology and tectonics of the South Atlantic Brazilian salt basins, in: Ries, A.C., Butler, R.W.H. and Graham, R.H. (Eds.), *Deformation of the Continental Crust: The Legacy of Mike Coward*. Geological Society of London, Special Publications, 272, 345-356.
- Deckelman, J.A., Lou, S., D'onfro, P.S. and Lahann, R.W., 2006. Quantitative assessment of regional siliciclastic top-seal potential: a new application of proven technology in the Pelotas Basin, offshore Brazil. *Journal of Petroleum Geology*, 29 (1), 83-96.
- Demercian, S., Szatmari, P. and Cobbold P.R., 1993. Style and pattern of salt diapirs due to thin-skinned gravitational gliding, Campos and Santos basins, offshore Brazil. *Tectonophysics*, 228, 393-433.
- Dias, J.L., 2005. Tectônica, estratigrafia e sedimentação no Andar Aptiano da margem leste brasileira. *Boletim de Geociências da Petrobras*, Rio de Janeiro, 13 (1), 7-25.
- Dias, J.L., Sad, A.R.E., Fontana, R.L. and Feijó, F.J., 1994. Bacia de Pelotas. *Boletim de Geociências da Petrobras*, 8, 235-245.
- Dias-Brito, D., 1987. A Bacia de Campos no Mesocretáceo- uma contribuição a paleoceanografia do Atlântico Sul Primitivo. *Revista Brasileira de Geociências*, 17, 162-167.
- Dias-Brito, D. and Azevedo, R.L.M., 1986. As sequências deposicionais marinhas da Bacia de Campos sob a ótica paleoecológica. *XXXIV Congresso Brasileiro de Geologia*, Goiânia, 38-49.
- Duarte, C.S.L. and Viana, A.R., 2007. Santos drift system: stratigraphic organization and implications for late Cenozoic palaeocirculation in the Santos Basin, SW Atlantic Ocean, in: Viana, A.R. and Rebesco, M. (Eds.), *Economic and Palaeoceanographic Significance of Contourite Deposits*. Geological Society of London, Special Publications, 276, 171-198.
- Eagles, G. and König, M., 2008. A model of plate kinematics in Gondwana breakup. *Geophysical Journal International* 173, 703-717.

Eitel, B., Kadereit, A., Blümel, W. D., Hüser, K., Lomax, J. and Hilgers, A., 2006. Fluvial deposits in the Upper Hoanib river catchment, northwestern Namibia: new evidence of environmental changes before and after the Last Glacial Maximum at the eastern Namibia Desert Margin. *Palaeogeography, Palaeoclimatology, Palaeoecology*, 234, 201-222.

Emmerich, A., Tscherny, R., Bechstädt, T., Büker, C., Glasmacher, U.A., Littke, R. and Zühlke, R., 2008. Numerical simulation of the syn- to post-depositional history of a prograding carbonate platform: the Rosengarten, Middle Triassic, Dolomites, Italy, in: Boer, P., Postma, G., Van der Zwan, K., Burgess, P. and Kukla, P. (Eds.), *Analogue and Numerical Modelling of Sedimentary Systems: From Understanding to Prediction*. Special Publication, International Association Sedimentology, 40, 1-36.

Fairhead, J.D. and Wilson, M., 2005. Plate tectonic processes in the South Atlantic Ocean: Do we need deep mantle plumes?. *GSA Special Papers*, 388, 537-553.

Fetter, M., De Ros, L.F. and Bruhn, C.H.L., 2009. Petrographic and seismic evidence for the depositional setting of giant turbidite reservoirs and the paleogeographic evolution of the Campos Basin, offshore Brazil. *Marine and Petroleum Geology*, 26, 824-853.

Fontana, R.L., 1989. Evidências Geofísicas da presença de hidratos de gás na Bacia de Pelotas-Brasil. *Primer Congresso Sociedade Brasileira de Geofísica*, 7 (1), 93.

Fontana, R.L., 1996. Geotectônica e sismoestratigrafia da Bacia de Pelotas plataforma de Florianópolis. *Tese de Doutorado, Universidade Federal do Rio Grande do Sul, Porto Alegre/RS*, pp. 214.

Fontana, R.L. and Massumeci, A., 1994. Hydrates offshore Brazil, in: *International Conference of Natural Gas Hydrates. Annals of the New York Academy of Sciences*, 175, 106-113.

Ford, D. and Golonka J., 2003. Phanerozoic paleogeography, paleoenvironment and lithofacies of the circum-Atlantic margins. *Marine and Petroleum Geology*, 20, 248-285.

Franco-Magalhaes, A. O. B., Hackspacher, P. C., Glasmacher, U.A. and Saad, A. R., 2010. Rift to post-rift evolution of a "passive" continental margin: the Ponta Grossa Arch, SE Brazil. *International Journal Earth Sciences*, doi: 10.1007/s00531-010-0556-8.

Gallagher, K., Hawkesworth, C.J. and Mantovani, M.S.M., 1994. Rifting, magmatism and topography on the continental margin of southern Brazil. *Journal of Geophysical Research*, 99 (B9), 18, 117-18-145.

- Gallagher, K., Hawkesworth, C.J. and Mantovani, M.S.M., 1995. Denudation, fission track analysis and the long-term evolution of passive margin topography: application to the southeast Brazilian margin. *Journal of South America Earth Sciences*, 8 (1), 65-77.
- Galloway, W.E., 2004. Accommodation and the sequence stratigraphic paradigm. *Reservoir*, Canadian Society of Petroleum Geologists, 31 (5), 9-10.
- Gibbons, M.J., Williams, A.K., Piggot, N. & Williams, G.M., 1983. Petroleum geochemistry of the Southern Santos Basin, offshore Brazil. *Journal Geological Society, London*, 140, 423-430.
- Gladchenko, T.P., Hinz, K., Eldholm, O., Meyer, H., Neben, S. and Skogseid, J., 1997. South Atlantic volcanic margins. *Journal of the Geological Society, London*, 154, 465-470.
- Gladchenko, T.P., Skogseid, J., and Eldholm, O., 1998. Namibia volcanic margin. *Marine Geophysical Researches*, 20, 313-341.
- Goldhammer, R.K., 1997. Compaction and decompaction algorithms for sedimentary carbonates. *Journal of Sedimentary Research*, 67 (1), 26-35.
- Gomide, J., 1989. Bacia de Pelotas – Biocronoestratigrafia baseada em nanofósseis calcários, in: SBP, Congresso Brasileiro de Paleontologia, 11, Anais, 338-351.
- Gradstein, F., Ogg, J. and Smith, A., 2004. *A Geologic Time Scale*. Cambridge University Press, pp. 589.
- Guardado, L.R., Gamboa, L.A.P. and Luchessi, C.F., 1989. Petroleum geology of the Campos Basin, Brazil, a model for producing Atlantic type basin, in: Edwards, J.D. and Santogrossi, P.A. (Eds.), *Divergent/Passive Margin Basins*. AAPG Memoir, 48, 3-79.
- Guardado, L.R., Spadini, A.R., Brãndao, J.S.L. and Mello, M.R., 2000. Petroleum system of the Campos Basin, Brazil, in: Mello, M.R. and Katz, B. (Eds.), *Petroleum Systems of South Atlantic Margins*. AAPG Memoir, 73, 317-324.
- Hardenbol, J., Thierry, J., Farley, M.B., Jacquin, T., Graciansky P.C. and Vail, P., 1998. Mesozoic and Cenozoic sequence chronostratigraphic framework of European basins, in: Graciansky, P.-C., Hardenbol, J., Jacquin, T. and Vail, P.R. (Eds.), *Mesozoic-Cenozoic Sequence Stratigraphy of European Basins*. SEPM Special Publication, 60, and chart supplements.

Hasler, C.-A., Adams, E.W., Wood, R. and Dickson, J.A.D., 2008. Fine-scale forward modelling of a Devonian patch reef, Canning Basin, Western Australia, in: de Boer, P.L., Postma, G., van der Zwan, C.J., Burgess, P.M. and Kukla, P. (Eds.), *Analogue and Numerical Forward Modelling of Sedimentary Systems; from Understanding to Prediction*. IAS Special Publications, 40, 37-64.

Hirsch, K.K., Scheck-Wenderoth, M., van Wees, J.-D., Kuhlmann, G. and Paton, D.A., 2010. Tectonic subsidence history and thermal evolution of the Orange Basin. *Marine and Petroleum Geology*, 27, 565-584.

Huisman, R.S. and Beaumont, C., 2008. Complex rifted continental margins explained by dynamical models of depth-dependant lithospheric extension. *The Geological Society of America. Geology*, 36 (2), 163-166.

Hunt, D. and Tucker, M.E., 1992. Stranded parasequences and the forced regressive wedge systems tract: deposition during base-level fall. *Sedimentary Geology* 81, 1-9.

Iaffaldano, G. and Bunge, H.-P., 2009. Relating rapid plate-motion variations to plate-boundary forces in global coupled models of the mantle/lithosphere system: Effects of topography and friction, *Tectonophysics*, 474 (106), 393-404.

Jackson, M.P.A., Cramez, C. and Fonck, J.M., 2000. Role of subaerial volcanic rocks and mantle plumes in creation of South Atlantic volcanic margins: implications for salt tectonics and source rocks. *Marine and Petroleum Geology*, 17, 477-498.

Karner, G., 2000. Rifts of the Campos and Santos basins, southeastern Brazil: distribution and timing, in: Mello, M.R. and Katz, B. (Eds.), *Petroleum Systems of South Atlantic Margins*. AAPG Memoir, 73, 301-315.

Karner, G.D. and Driscoll, N.W., 1999a. Style, timing and distribution of tectonic deformation across the Exmouth Plateau, northwest Australia, determined from stratal architecture and quantitative basin modeling, in: Mac Niocaill C. and Ryan P.D. (Eds.), *Continental Tectonics*. Geological Society of London, Special Publications, 164, 271-311.

Karner, G.D. and Driscoll, N.W., 1999b. Tectonic and stratigraphic development of the West African and eastern Brazilian margins: insights from quantitative basin modeling, in: Cameron, N.R., Bate, R.H. and Clure, V.S. (Eds.), *The Oil and Gas Habitats of the South Atlantic*. Geological Society of London, Special Publications, 153, 11-40.

Karner, G.D., Driscoll, N.W., McGinnis, J.P., Brumbaugh, W.D. and Cameron, N.R., 1997. Tectonic significance of syn-rift sediment packages across the Gabon-Cabinda continental margin. *Marine and Petroleum Geology*, 14, 973-1000.

Karner, G.D., Driscoll, N.W and, Barker D.H.N., 2003. Syn-rift regional subsidence across the West African continental margin: the role of lower plate ductile extension, in: Arthur, T.J., MacGregor, D.S. and Cameron, N.R. (Eds.), *Petroleum Geology of Africa: New Themes and Developing Technologies*. Geological Society of London, Special Publications, 207, 105-129.

Karner, G.D., Manatschal, G. and Pinheiro, L.M., 2007. Imaging, mapping and modelling continental lithosphere extension and breakup: an introduction, in: Karner, G.D., Manatschal, G. and Pinheiro, L.M. (Eds.), *Imaging, Mapping and Modelling Continental Lithosphere Extension and Breakup*. Geological Society of London, Special Publications, 282, 1-8.

Karner, G.D. and Gambôa, L.A.P., 2007. Timing and origin of the South Atlantic pre-salt sag basins and their capping evaporites, in: Schreiber, B.C., Lugli, S. and Babel, M. (Eds.), *Evaporites through Space and Time*. Geological Society of London, Special Publications, 285, 15-35.

Katz, B.J. and Mello, M.R., 2000. Petroleum systems of South Atlantic marginal basins – an overview, in: Mello, M.R. and Katz, B. (Eds.), *Petroleum Systems of South Atlantic Margins*. AAPG Memoir, 73, 1-13.

Kendall, J.-M., Stuart, G.W., Ebinger, C.J. Bastow, I.D. and Keir, D., 2005. Magma-assisted rifting in Ethiopia. *Nature*, 433, 146-148.

Koutsoukos, E.A.M., 1982. Geohistória e paleoecologia das bacias marginais de Florianópolis e Santos, in: SBG, *Congresso Brasileiro de Geologia*, 32, Anais, 2369-2382.

Koutsoukos E.A.M., 1984. Evolução paleoecológica do Albiano ao Maastrichtiano na área noroeste da bacia de Campos, Brasil, com base em foraminíferos: *Anais do XXXIII Congresso Brasileiro de Geologia*, 2, 685-698.

Koutsoukos E.A.M., 1987. A área noroeste da Bacia de Campos, Brasil, do Mesocretáceo ao Neocretáceo: evolução paleoambiental e paleogeográfica pelo estudo de foraminíferos. *Revista Brasileira de Geociências*, 17 (2), 168-172.

Kumar, N., Gamboa, L.A.P., Schreiber, B.C. and Macle, J., 1977 *Geologic History and Origin of the Sao Paulo Plateau (Southeastern Brazilian Margin), comparison with the Angolan Margin and early evolution of the Northern South Atlantic*. Initial Reports of the Deep Sea Drilling Project. Washington D.C., 39, 927-945.

Kuszniir, N.J., Roberts, A.M. and Morley, C.K., 1995. Forward and reverse modelling of rift basin formation, in: Lambiase, J.J. (Ed.), *Hydrocarbon Habitat in Rift Basins*. Geological Society of London, Special Publications, 80, 33-56.

Kusznir, N.J., Hunsdale, R., Roberts, A.M. and iSIMM Team. 2005. Timing and Magnitude of depth-dependent lithosphere stretching on the S. Lofoten and N. Vøring continental margins offshore Mid-Norway: implications for subsidence and hydrocarbon maturation at volcanic rifted margins, in: Dore, A.G. and Vining, B.A. (Eds.) *Petroleum Geology: North-West Europe and Global Perspectives – Proceedings of the 6th Petroleum Geology Conference*. Geological Society, London, 767-783.

Kusznir, N.J. and Karner, G.D., 2007. Continental lithospheric thinning and breakup in response to upwelling divergent mantle flow: application to the Woodlark, Newfoundland and Iberia margins, in: Karner, G.D., Manatschal, G. and Pinheiro, L.M. (Eds.), *Imaging, Mapping and Modelling Continental Lithosphere Extension and Breakup*. Geological Society of London, Special Publications, 282, 389-419.

Lavier, L. and Manatschal, G., 2006. A mechanism to thin the continental lithosphere at magma-poor margins. *Nature*, 440, 324-328.

Lentini, M.R., Fraser, S.I., Sumner, H.S. and Davies, R.J., 2010. Geodynamics of the central South Atlantic conjugate margins: implications for hydrocarbon potential. *Petroleum Geoscience*, 16 (3), 217-229.

Leroy, M., Gueydan, F. and Dauteuil, O., 2008. Uplift and strength evolution of passive margins inferred from 2-D conductive modelling. *Geophysical Journal International*, 172, 464-476.

Macdonald D., Gomez-Perez, I., Franzese, J., Spalletti, L., Laever, L., Gahagan, L., Dalziel, I., Thomas, C., Trewin, N., Hole, M. and Paton, D., 2003. Mesozoic break-up of SW Gondwana: implications for regional hydrocarbon potential of the southern South Atlantic. *Marine Petroleum Geology*, 20, 287-308.

Macdonald D., Gomez-Perez, I., Franzese, J., Spalletti, L., Laever, L., Gahagan, L., Dalziel, I., Thomas, C., Trewin, N., Hole, M. and Paton, D., 2003. Mesozoic break-up of SW Gondwana: implications for regional hydrocarbon potential of the southern South Atlantic. *Marine Petroleum Geology*, 20, 287-308.

Machado Jr. D.L., da Silva, D.F., Selbach, H.S. and da Silva, C.E., 2004. Restauração estrutural de seções e previsibilidade de petróleo em Roncador, Bacia de Campos. *Boletim de Geociências da Petrobras*, Rio de Janeiro, 12 (1), 89-101.

Machado, L.C., Kowsmann, R.O., de Almeida Jr., W., Murakami, C.Y., Schreiner S., Miller, D.J. and Vasconcelos, P.O., 2004. Geometria da porção proximal do sistema deposicional turbidítico moderno da Formação Carapebus, Bacia de Campos; modelo para heterogeneidades de reservatório. *Boletim de Geociências da Petrobras*, Rio de Janeiro, 12 (2), 287-315.

- McKenzie, D., 1978. Some remarks on the development of sedimentary basins. *Earth and Planetary Science Letters*, 40, 25-32.
- Marton, L.G., Tari, G.C. and Lehmann, C.T., 2000. Evolution of the Angolan passive margin, West Africa, with emphasis on post-salt structural styles, in: Mohriak, W.U. and Talwani, M. (Eds.), *Atlantic Rifts and Continental Margins*. American Geophysical Union, Monograph 115, 129-149.
- Matos, R.D., 2000. Tectonic evolution of the equatorial South Atlantic, in: Mohriak, W.U. and Talwani, M. (Eds.), *Atlantic Rifts and Continental Margins*. American Geophysical Union, Monograph 115, 331-354.
- Meisling, K., Cobbold, P.R. and Mount, V.S., 2001. Segmentation of an obliquely rifted margin, Campos and Santos basins, southern Brazil. *AAPG Bulletin*, 85 (11), 1903-1924.
- Mello, M.R., Karner, G. and Anderson R., 1995. Role of salt in restraining the maturation of subsalt source rocks. *Marine and Petroleum Geology*, 12 (7), 697-716.
- Mello, M.R. and Maxwell, J.R., 1990. Organic geochemical and biological marker characterization of source rocks and oils from lacustrine environments in the Brazilian continental margin, in: Katz, B.J. (Ed.), *Lacustrine Basin Exploration*. AAPG Memoir, 50, 77-97.
- Meyers, J.B., Rosendahl, B.R., H. Groschel-Becker, Austin, J.A. and Rona P.A., 1996. Deep penetrating MCS imaging of the rift-to-drift transition, offshore Douala and North Gabon basins, West Africa. *Marine and Petroleum Geology*, 13, 791-835.
- Mitchum Jr., R.M., 1977. Seismic stratigraphy and global changes of sea level, part 11: glossary of terms used in seismic stratigraphy, in: Payton, C.E. (Ed.), *Seismic Stratigraphy – Applications to Hydrocarbon Exploration*. AAPG Memoir, 26 205-212.
- Modica, C. and Brush, E., 2004. Post-rift sequence stratigraphy, paleogeography, and fill history of the deep-water Santos Basin, offshore southeast Brazil. *AAPG Bulletin*, 88 (7), 923-945.
- Mohriak, W.U., Mello, M.R., Karner, G.D., Dewey, J.F. and Maxwell, J.R., 1990. Structural and stratigraphic evolution of the Campos Basin, offshore Brazil, in: Tankard, A.J. and Balkwill, H.R. (Eds.), *Extensional Tectonics and Stratigraphy of the North Atlantic Margins*. AAPG Memoir, 46, 577-598.

Mohriak, W.U., Macedo, J.M., Castellani, R.T., Rangel, H.D., Barros, A.Z.N., Latgé, M.A.L., Ricci, J.A., Mizusaki, A.M.P., Szatmari, P., Demercian, L.S., Rizzo, J.G. and Aires, J.R., 1995. Salt tectonics and structural styles in the deep water province of the Cabo Frio region, Rio de Janeiro, Brazil, in: Jackson, M.P.A., Roberts, D.G. and Snelson, S. (Eds.), *Salt Tectonics: A Global Perspective*. AAPG Memoir, 65, 273-304.

Mohriak, W.U., Rosendahl, B.R., Turner, J.P. and Valente, S.C., 2002. Crustal architecture of South Atlantic volcanic margins, in: Menzies, M.A., Klemperer, S.L., Ebinger, C.J. and Baker, J. (Eds.), *Volcanic Rifted Margins*. Special Paper Geological Society of America, 362, 159-202.

Mohriak, W.U., Nemčok, M. and Enciso, G., 2008. South Atlantic divergent margin evolution: rift border uplift and salt tectonics in the basins of SE Brazil, in: Pankhurst, R.T., Trouw, R.A.J., Brito Neves, B.B. and Wit, M.J. (Eds.), *West Gondwana: Pre-Cenozoic Correlations across the South Atlantic Region*. Geological Society of London, Special Publications, 294, 365-398.

Mohriak, W.U., Nóbrega, M., Odegard, M.E., Gomes, B.S. and Dickson W.G., 2010. Geological and geophysical interpretation of the Rio Grande Rise, south-eastern Brazilian margin: extensional tectonics and rifting of continental and oceanic crusts. *Geological Society of London, Petroleum Geoscience*, 16, 231-245.

Moore, G.T., Barron, E.J., Bice, K.L., and Hayashida, D., 1995. Paleoclimatic controls on Neocomian-Barremian (Early Cretaceous) lithostratigraphy in northern Gondwana's rift lakes interpreted from a general circulation model simulation, in: Huc, A.-Y. (Ed.), *Paleogeography, Paleoclimate, and Source Rocks: AAPG Studies in Geology*, 40, 173-189.

Moreira, J.L.P., Madeira, C.V., Gil, J.A. and Machado, A.P.M., 2007. Bacia de Santos. *Boletim de Geociências da Petrobras, Rio de Janeiro*, 15 (2), 531-549.

Moscardelli, L. and Wood, L., 2008. New classification system for mass transport complexes in offshore Trinidad. *Basin Research*, 20, 73-98.

Moulin, M., Aslanian, D., Olivet, J-L., Contrucci, I., Matias, L., Géli, L., Klingelhoefer, F., Nouzé, H., Réhault, J-P. and Unternehr, P., 2005. Geological constraints on the evolution of the Angolan margin based on reflection and refraction seismic data (ZaiAngo project). *Geophysical Journal International*, 162, 793-810.

Moulin, M., Aslanian, D. and Unternehr, P. 2010. A new starting point of the south and equatorial Atlantic Ocean. *Earth Sciences Reviews*, 98, 1-37.

Nadin, P.A. and Kusznir N.J., 1995. Paleocene uplift and Eocene subsidence in the northern North Sea Basin from 2D forward and reverse stratigraphic modeling. *Journal of Geological Society, London*, 152, 833-848.

- Nadin, P.A. and Kusznir N.J., 1996. Forward and reverse stratigraphic modeling of Cretaceous-Tertiary post-rift subsidence and Paleogene uplift in the Outer Moray Firth Basin, central North Sea, in: Knox, R.W.O'B., Corfield, R.M. and Dunay, R.E. (Eds.), Correlation of the Early Paleogene in Northwest Europe. Geological Society of London, Special Publications, 101, 43-62.
- Neal, J. and Abreu, V., 2009. Sequence stratigraphy hierarchy and the accommodation succession method. Geological Society of America. *Geology*, 37 (9), 779-782.
- Nunn, J.A. and Harris, N.B., 2007. Subsurface seepage of seawater across a barrier: a source of water and salt to peripheral salt basins. *GSA Bulletin*, 119 (9-10), 1201-1217.
- Nürnberg, D. and Müller, R.D., 1991. The tectonic evolution of the South Atlantic from the Jurassic to present. *Tectonophysics* 191, 27-53.
- Ojeda, H.A., 1982. Structural framework, stratigraphy, and evolution of Brazilian marginal basins. *AAPG Bulletin*, 66, 732-749.
- Oreiro, S. G., 2006. Magmatism e sedimentação em uma area na plataforma continental de Cabo Frio, Rio de Janeiro, Brasil, no intervalo Cretáceo Superior-Terciário. *Boletim de Geociências da Petrobras, Rio de Janeiro*, 14 (1), 95-112.
- Payton, C.E., 1977. *Seismic Stratigraphy – Applications to hydrocarbon exploration*. AAPG Memoir 26, pp. 516.
- Pereira, M.J., Barbosa, C., Agra, J., Gomes, J.B, Aranha, L.G.F., Saito, M., Ramos, M., De Carvahlo, M.D., Stamato, M. and Bagni, O., 1986. Estratigrafia da Bacia de Santos: Análise das Sequências, Sistemas Depositionais e Revisão Litoestratigráfica. XXXIV Congresso Brasileiro de Geologia, Goiânia, Goiás, 1, 65-79.
- Pereira, M.J., Trindade, L.A.F. and Gaglianone, P.C., 1984. Origem e evolução das acumulações de hidrocarburos na Bacia de Campos: Anais do XXXIII Congresso Brasileiro de Geologia, 10, 4763-4777.
- Pereira, M.J., 1992. Considerações sobre a estratigrafia do Cenomaniano-Santoniano em algumas bacias marginais brasileiras e suas implicações na história tectônica e sedimentar da margem continental. *Boletim de Geociências da Petrobras, Rio de Janeiro*, 6, 171-176.
- Pereira, M.J. and Feijó, F., 1994. Bacia de Santos. *Boletim de Geociências da Petrobras, Rio de Janeiro*, 8 (1), 219-234.

Peres, W.E., 1993. Shelf-fed turbidite system model and its application to the Oligocene deposits of the Campos Basin, Brazil. *AAPG Bulletin*, 77 (1), 81-101.

Peyve, A.A. 2010. Tectonics and magmatism in eastern South America and the Brazil Basin of the Atlantic in the Phanerozoic. *Geotectonics*, 44 (1), 65-70.

Posamentier, H.W., Jervey, M.T. and Vail, P.R., 1988. Eustatic controls on clastic deposition I – conceptual framework. in: Wilgus, C.K., Hastings, B.S., Kendall, C.G.St.C., Posamentier, H.W., Ross, C.A., Van Wagoner, J.C. (Eds.), *Sea Level Changes – An Integrated Approach*. SEPM Special Publication, 42, 110-124.

Posamentier, H.W. and Vail, P.R., 1988. Eustatic controls on clastic deposition II – sequence and systems tract models, in: Wilgus, C.K., Hastings, B.S., Kendall, C.G.St.C., Posamentier, H.W., Ross, C.A., Van Wagoner, J.C. (Eds.), *Sea Level Changes – An Integrated Approach*. SEPM Special Publication, 42, 125-154.

Rabinowitz, P.D. and LaBrecque, J.L., 1979. The Mesozoic South Atlantic Ocean and evolution of its continental margins. *Journal of Geophysical Research*, 84 (B11), 5973-6002.

Rangel, H., Martins, F.A.L., Esteves, F. and Feijó, F., 1994. Bacia de Campos. *Boletim de Geociências da Petrobras*, Rio de Janeiro, 8 (1), 203-217.

Reston, T.J., 2007. The formation of non-volcanic rifted margins by the progressive extension of the lithosphere: the example of the West Iberian margin, in: Karner, G.D., Manatschal, G. and Pinheiro, L.M. (Eds.), *Imaging, Mapping and Modelling Continental Lithosphere Extension and Breakup*. Geological Society of London, Special Publications, 282, 77-110.

Ribeiro, L.F.B., Hackspacher, P.C., Ribeiro, M.C.S., Hadler Neto, J.C., Tello, S.C.A., Iunes, P.J., Franco, A.O.B. and Godoy, D.F., 2005. Thermotectonic and fault dynamic analysis of Precambrian basement and tectonic constraints with the Parana Basin. *Radiation Measurements*, 39 (6), 669-673.

Roberts, A.M., Yielding G., Kusznir, N.J., Walker, I.M. and Dorn-Lopez, D., 1995. Quantitative analysis of Triassic extension in the northern Viking Graben. *Journal of the Geological Society, London*, 152, 15-26.

Roberts, A.M., Lundin, E.R. and Kusznir, N.J., 1997. Subsidence of the Vøring Basin and the influence of the Atlantic continental margin, in: Roberts, A.M. and Kusznir, N.J. (Eds.), *Tectonic, Magmatic and Depositional Processes at Passive Continental Margins*. Geological Society of London, Special Publications, 154, 551-557.

- Roberts, A.M., Kuszniir, N.J., Yielding, G. and Styles, P. 1998. 2D flexural backstripping of extensional basins: the need for a sideways glance. *Petroleum Geoscience*, 4, 327-338.
- Rosa, M.L.C.C., Ayup-Zouain, R.N. and Barboza, E.G., 2006. Utilização de seções sísmicas 2D na identificação de zonas de escapes de fluidos. *GRAVEL*, 4, 109-118.
- Rosenbaum, G., Weinberg, R.F. and Regenauer-Lieb, K., 2008. The geodynamics of lithospheric extension. *Tectonophysics*, 458, 1-8.
- Santa Ana, H., Latrónica, L., Tomasini, J., Morales, E., Ferro, S., Gristo, P. and Machado, L., 2008. Economic and exploratory review of gas hydrates and other gas manifestations of the Uruguayan continental shelf. *Proceedings of the 6th International Conference of Gas Hydrates (ICGH 2008)*, Vancouver, British Columbia, Canada.
- Scheck-Wenderoth, M., Maystrenko Y., Cacace, M. and Hirsch, K., 2010. What can we learn from 3D lithosphere-scale models of sedimentary basins? *Geophysical Research Abstracts*, 12, EGU 2010-4666.
- Scheibner, C., Kuss, J. and Speijer, R.P., 2003. Stratigraphic modeling of carbonate platform-to-basin sediments (Maastrichtian to Paleocene) in the Eastern Desert, Egypt. *Paleogeography, Paleoclimatology, Paleocology*, 200, 163-185.
- Scholle, P.A. and Halley, R.B., 1985. Burial diagenesis: out of sight, out of mind, in: Schneidermann, N. and Harris, P.M. (Eds.), *Carbonate Cements*. SEPM, Special Publication 36, 303-328.
- Scotchman, I.C. Gilchrist, G., Kuszniir, N.J., Roberts, A.M. and Fletcher, R. 2010. The breakup of the South Atlantic Ocean: formation of failed spreading axes and blocks of thinned continental crust in the Santos Basin, Brazil and its consequences for petroleum system development, in: Vining, B.A. and Pickering, S.C. (Eds.), *From Mature Basins to New Frontiers – Proceedings of the 7th Petroleum Geology Conference*. Geological Society of London, *Petroleum Geology Conference Series*, 7, 855-866.
- Siqueira, M.C., 2007. Termocronologia e história tectônica da Serra do Mar e implicações no controle deposicional da Bacia de Santos. Tese de Doutorado, Universidade Estadual Paulista, Rio Claro, Brazil, pp. 227.
- Skelton, P., Spicer, R., Kelley, S. and Gilmour, I. 2003. *The Cretaceous World*. Skelton P. (Ed.) Cambridge University Press. pp. 360.

Sloss, L.L., 1963. Sequences in the cratonic interior of North America. *Geological Society of America Bulletin* 74, 93-114.

Steckler, M.S. and Watts, A.B., 1978. Subsidence of the Atlantic-type continental margin of New York, *Earth Planetary Science Letters*, 41, 1-13.

Stollhofen, H., Gerschütz, S., Stanistreet, I.G. and Lorenz, V., 1998. Tectonic and volcanic controls on Early Jurassic rift-valley lake deposits interleaved with Karoo flood basalts, southern Namibia. *Paleogeography, Paleoclimatology, Paleocology*, 140, 185-215.

Stollhofen, H., Werner, M., Stanistreet, I.G. & Armstrong, R.A., 2008. Single zircon U/Pb dating of Carboniferous-Permian tuffs, Namibia, and the intercontinental deglaciation cycle framework, in: Fielding, Chr.R., Frank, T.D. & Isbell, J.L. (Eds.) *Resolving the Late Paleozoic Ice Age in time and space*, *Geol. Soc. Amer. Spec. Paper* 441, 83-96.

Stow, D.A.V., Faugères J.-C, Howe, J.A. Pudsey C.J. and Viana A.R., 2002. Bottom currents, contourites and deep-sea sediment drifts: current state-of-the-art, in: Stow, D.A.V., Pudsey, C.J., Howe, J.A., Faugères, J.-C. Viana, A.R. (Eds.), *Deep-Water Contourite Systems: Modern Drifts and Ancient Series, Seismic and Sedimentary Characteristics*. Geological Society of London, *Memoirs*, 22, 7-20.

Strugale, M., Rostirolla, S.P., Mancini, F., Portela, C.V., Fonseca, F.J. and de Freitas R.C., 2007. Structural framework and Mesozoic-Cenozoic evolution of Ponta Grossa Arch, Paraná Basin, southern Brazil. *Journal of South American Earth Sciences*, 24, 203-227.

Talwani, M. and Abreu, V., 2000. Inferences regarding initiation of oceanic crust formation the U.S. East Coast margin and conjugate South Atlantic margins, in: Mohriak, W.U. and Talwani, M. (Eds.), *Atlantic Rifts and Continental Margins*. American Geophysical Union, *Monograph* 115, 211-233.

Tello Saenz, C.A., Hackspacher, P.C., Hadler Neto, J.C., Iunes, P.J., Guedes, S., Ribeiro L.F.B. and Paulo, S.R., 2003. Recognition of Cretaceous, Paleocene, and Neogene tectonic reactivation through apatite fission-track analysis in Precambrian areas of southeast Brazil: association with the opening of the South Atlantic Ocean. *Journal of South American Earth Sciences*, 15, 765-774.

Tello Saenz, C.A., Hadler Neto, J.C., Iunes, P.J., Guedes, Hackspacher, P.C., S., Ribeiro L.F.B., Paulo, S.R. and Osorio, A.M., 2005. Thermochronology of the South American platform in the state of São Paulo, Brazil, through apatite fission tracks. *Radiation Measurements*, 39, 635-640.

- Torsvik, T.H., Rouse, S., Labails, C. and Smethurst, M.A., 2009. A new scheme for the opening of the South Atlantic Ocean and the dissection of an Aptian salt basin. *Geophysical Journal International*, 177, 1315-1333.
- Unternehm, P., Péron-Pinvidic, G., Manatschal, G., and Sutra, E., 2010. Hyper-extended crust in the South Atlantic: in search of a model. *Petroleum Geoscience*, 16, 207-215.
- Vail, P.R., Mitchum Jr., R.M. and Thompson III, S., 1977. Seismic stratigraphy and global changes of sea level, part 3: relative changes of sea level from coastal onlap, in: Payton, C.E. (Ed.), *Seismic Stratigraphy – Applications to Hydrocarbon Exploration*. AAPG Memoir, 26, 63-81.
- Vail, P.R., Hardenbol, J., and Todd, R.G., 1984. Jurassic unconformities, chronostratigraphy and sea-level changes from seismic stratigraphy and biostratigraphy, in: Schlee, J.S. (Ed.), *Interregional Unconformities and Hydrocarbon Accumulation*. AAPG Memoir 36, 129-144.
- Van Wagoner, J.C., Mitchum Jr., R.M., Campion, K.M. and Rahmanian, V.D., 1990. Siliciclastic sequence stratigraphy in well logs, core, and outcrops: concepts for high-resolution correlation of time and facies. *AAPG Methods in Exploration Series*, 7, pp. 55.
- Veselovsky, Z., Bechstädt, T. and Zühlke, R., 2008. Structural, reverse-basin and forward stratigraphic modelling of the Southern Cantabrian Basin, NW Spain, in: Boer, P., Postma, G., Van der Zwan, K., Burgess, P. and Kukla, P. (Eds.), *Analogue and Numerical Modelling of Sedimentary Systems: From Understanding to Prediction*. Special Publication, International Association Sedimentology, 40, 65-96.
- Viana, A., 2002. Seismic expression of shallow- to deep-water contourites along the south-eastern Brazilian margin. *Marine Geophysical Researches*, 22, 509-521.
- Viana, A.R., Almeida Jr., W., Nunes, M.C.V. and Bulhões, 2007. The economic importance of contourites, in: Viana, A.R. and Rebesco, M. (Eds.), *Economic and Palaeoceanographic Significance of Contourite Deposits*. Geological Society of London, Special Publications, 276, 1-23.
- Vignol-Lelarge, M.L.M., Soliani Jr.E., and Poupeau, G., 1994. Datação pelos traços de fissão do domínio meridional da Serra do Mar (Arco de Ponta Grossa - Brasil), in: *Congresso Brasileiro de Geologia*, 38, Baln. Camboriú, 1994. *Boletim de Resumos Expandidos, SBG. 2*, 379-380.
- Watts, A.B., Karner, G.D. and Steckler, M.S., 1982. Lithospheric flexure and evolution of sedimentary basins, in: *The Evolution of Sedimentary Basins*. Philosophical Transactions of the Royal Society, London, Series A, Mathematical and Physical Sciences, 305 (1489), 249-281.

Watts, A.B., 1988. Gravity anomalies, crustal structure and flexure of the lithosphere at the Baltimore Canyon Trough, *Earth Planetary Science Letters*, 89, 221-238.

Watts, A.B., 2001. *Isostasy and flexure of the lithosphere*. Cambridge University Press. pp. 458.

Welte, D.H., Horsfield, B. and Baker, D.R., 1997. *Petroleum and Basin Evolution*. Springer-Verlag, pp. 535.

Winter, W.R. Jahnert R.J. and França, A.B., 2007. Bacia de Campos. *Boletim de Geociências da Petrobras*, Rio de Janeiro, 15 (2), 511-529.

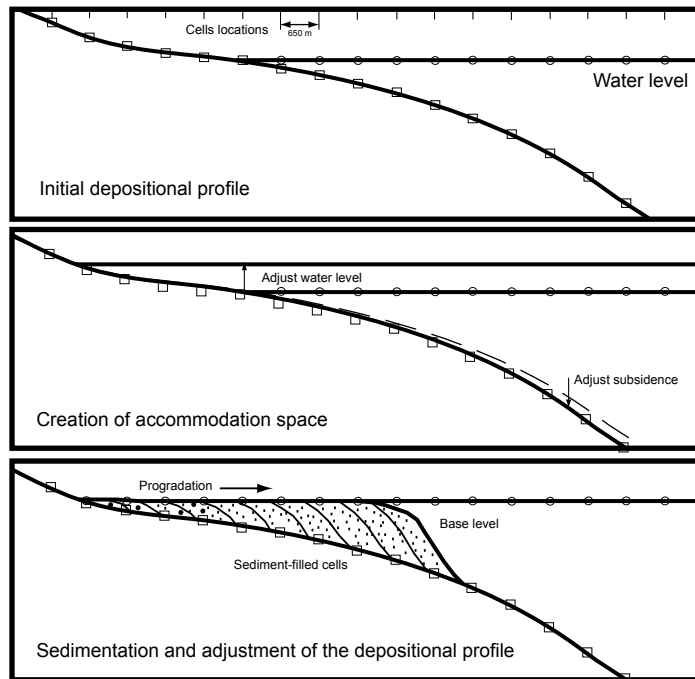
Zalán, P.V. and Oliveira, J.A.B., 2005. Origem e evolução estrutural do sistema de riftes Cenozóicos do Sudeste do Brasil. *Boletim de Geociências da Petrobras*, Rio de Janeiro, 13 (2), 269-300.

Zanotto, O.A. 1993. Erosão pós-Cretáceo na Bacia do Paraná, com base em dados de reflectância vitrinita, in: *Resumos Simpósio Sul-Brasileiro de Geología*, 5, SBG, Curitiba, 58.

Ziegler, P.A. and Cloetingh, S., 2004. Dynamic processes controlling evolution of rifted basins. *Earth-Science Reviews*, 64, 1-50.

Zühlke, R., Bouaouda, M.S., Ouajhain, B., Bechstädt, T. and Leinfelder, R., 2004. Quantitative Mesozoic development of the eastern Central Atlantic continental shelf, western High Atlas, Morocco. *Marine and Petroleum Geology*, 21, 225-276.

Appendix A



The computational workflow for each time-step and cell in forward modeling includes the following steps:

- (1) The initial profile is adjusted for tectonic and water level specifications, and the intersection with sea-level is located.
- (2) As the forward simulation starts, a first package of sediment is deposited and the flexural response of the crust to the initial water and sediment load is calculated.
- (3) The compaction-induced depth change of the first stratigraphic layer is adjusted as a function of depth and sediment type.
- (4) The profile is modified by erosion where it lies above the base level.
- (5) The depositional profile progrades in basinward direction until the traction load portion of sediment supply is exhausted.
- (6) The carbonate factory produces sediment as a function of the bathymetry, position on the margin and distribution of siliciclastic input. The excess productivity is redistributed and subsequently added to the pelagic fraction.
- (7) Newly deposited sediment is removed from slopes steeper than the stability level.
- (8) The removed sediment portion is transported basinward by sliding, slumping or turbidite currents and deposited.

Flexural loading algorithm

$$h = \frac{\sqrt[3]{12D(1-n^2)}}{E}$$

h: flexural loading

D: flexural rigidity

n: Poisson's ratio

E: Young's modulus (constant 0.25)

The flexural loading of the margin is projected to the limit of the flexural wavelength (Table 4.3). The flexural rigidity of the crust (D) is separately calculated as a function of the water, sediment and mantle density (see Bowman and Vail, 1999).

Compaction algorithm

$$\varphi(Z) = \frac{\varphi_0}{1 + (Z \times r_c)}$$

φ : porosity

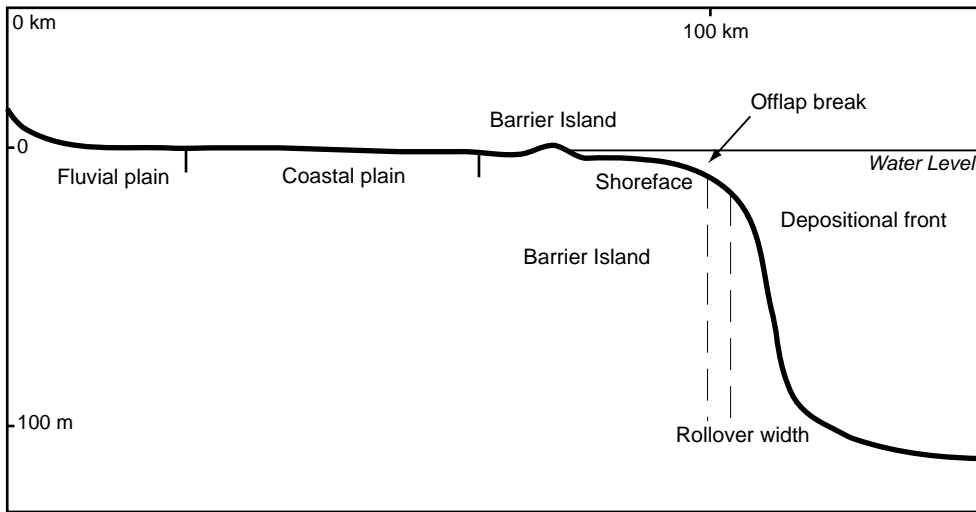
Z: depth in meters

φ_0 : Initial porosity

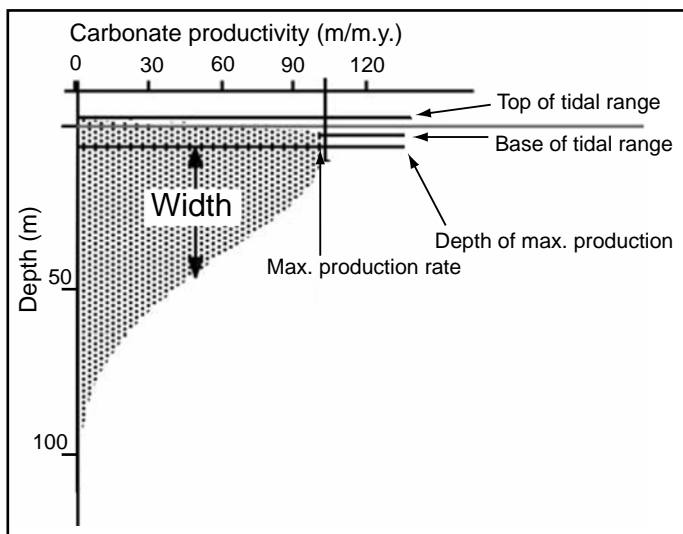
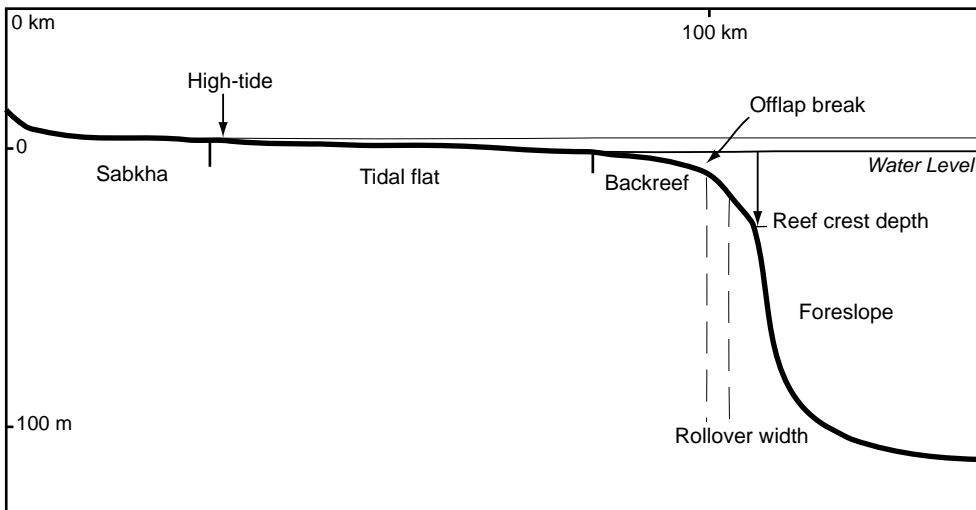
r_c : compaction coefficient (see Table 4.2)

Before deposition of a new layer, PHIL calculates the mean depth for the underlying intervals and determines the porosity. As the next stratigraphic unit is deposited, the thicknesses decrease as required for the loss of porosity due to the imposed loads (see Bowman and Vail, 1999).

Depositional siliciclastic profile established by traction processes



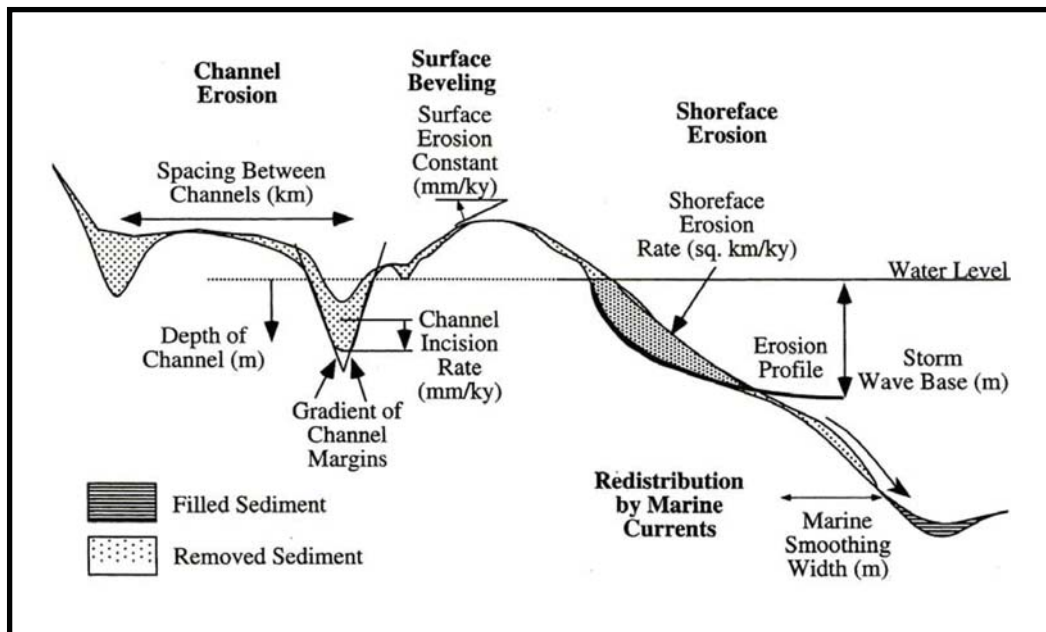
Geometry of carbonate platform established by traction processes



The carbonate productivity function is controlled by the width of production, depth of maximum production and maximum production rate.

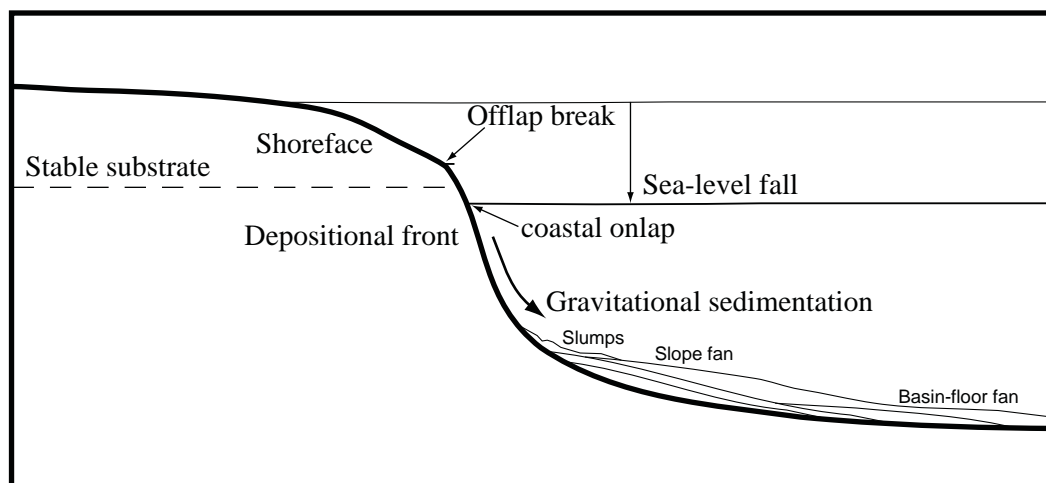
The top of the tidal range marks the upper boundary of carbonate production (Bowman and Vail, 1999).

These parameter values are shown in Table 5.3.



Erosional profile and controlling variables (Bowman and Vail, 1999).

Shoreface erosion and marine currents were particularly important in modeling of the Brazilian rifted margin.



Conditions to produce gravity-flow sedimentation (Modified from Bowman and Vail, 1999).

- (i) relative sea-level fall below the offlap break to generate slope and basin-floor fans.
- (ii) no accommodation space available on stable substrate triggers sediment slumps.

Appendix B

Sensitivity analysis provided the best-fit parameter values to achieve the stratal architectures and distribution of lithofacies. The following Tables display the temporal adjustments consecutively implemented at specific time intervals during the modeling procedure. Original input values and ranges can be visualized in Table 5.3.

B1. Pelotas Basin

Chronostratigraphic layer [Ma]	Parameters	Best-fit values
122	Sand (%)	45
	Pelagic max. production rate (m/m.y.)	30
116	Carbonate sedimentation	On
	Traction transport (%)	30
	Pelagic max. production rate (m/m.y.)	10
110	Sand (%)	10
	Pelagic max. production rate (m/m.y.)	30
104	Carbonate sedimentation	Off
	Pelagic max. production rate (m/m.y.)	10
	Sand (%)	35
	Traction transport (%)	20
100	Pelagic max. production rate (m/m.y.)	6
84	Traction transport (%)	25
	Pelagic max. production rate (m/m.y.)	12
	Sand (%)	15
	Marine currents	6000
68	Traction transport (%)	50
	Marine currents	10000
48	Pelagic max. production rate (m/m.y.)	30
32	Pelagic max. production rate (m/m.y.)	15
	Depositional front gradient siliciclastics	0.08
24	Carbonate sedimentation	On
	Sand (%)	45
	Depositional front gradient siliciclastics	0.09
16	Traction transport (%)	15

Based on the essential input parameters, i.e. subsidence rates, eustatic sea-level, effective elastic thickness (Fig. 5.4) and sediment supply rates (Fig. 5.5), the tectono-stratigraphic configuration of the Pelotas Basin was achieved by adjusting three main sediment-related parameters, the shelf front and marine currents. Variations in the percentage of sandstones are related to tectonic events with uplift and exposure of source terrains delivering higher sand volumes into the basin; on the other hand, reductions in the sand volumes can be interpreted as periods of tectonic quiescence, changes in the drainage pathways or lower erosion rates (associated to climate conditions). Changes in depositional gradients were needed in order to counteract catastrophic events of shelf-edge failure and maintain realistic adequate basin conditions for logical modeling outputs.

B2. Santos Basin

Chronostratigraphic layer [Ma]	Parameters	Best-fit values
122	Sand (%)	45
	Pelagic max. production rate (m/m.y.)	40
	Traction transport (%)	Off
	Carbonate sedimentation	On
116	Evaporites	On
	Sand (%)	5
	Pelagic max. production rate (m/m.y.)	10
110	Evaporites	Off
	Pelagic max. production rate (m/m.y.)	30
	Depositional front gradient siliciclastics	0.09
	Depositional front gradient carbonates	0.045
106	Carbonate sedimentation	Off
	Pelagic max. production rate (m/m.y.)	20
	Sand (%)	25
98	Sand (%)	15
84	Sand (%)	55
	Pelagic max. production rate (m/m.y.)	45
66	Sand (%)	30
	Depositional front gradient siliciclastics	0.05
	Pelagic max. production rate (m/m.y.)	10
34	Carbonate sedimentation	On
	Sand (%)	15
	Pelagic max. production rate (m/m.y.)	10
	Marine currents	10000
22	Pelagic max. production rate (m/m.y.)	45
16	Pelagic max. production rate (m/m.y.)	10

The tectono-stratigraphic configuration of the Santos Basin was achieved by adjusting four main sediment-related parameters, the declivity of the shelf front in both siliciclastics and carbonate systems, and the effect of marine currents. Comparable to the Pelotas Basin, variations in the percentage of sandstones are related to tectonic events, whereas reductions may imply tectonic quiescence, changes in the drainage pathways or lower erosion rates (associated to climate conditions). Frequent changes in maximum rates of pelagic sedimentation reflect the strong impact of deep-marine currents on sediment bypass and redistribution, simulated as a function of pelagic accumulation and marine currents. Changes in depositional gradients were needed in order to counteract catastrophic events of shelf-edge failure and maintain realistic adequate basin conditions.

B3. Campos Basin

Chronostratigraphic layer [Ma]	Parameters	Best-fit values
122	Sand (%)	45
	Traction transport (%)	40
	Depositional front gradient siliciclastics	0.08
	Carbonate sedimentation	On
116	Evaporites	On
	Pelagic max. production rate (m/m.y.)	10
110	Evaporites	Off
	Pelagic max. production rate (m/m.y.)	30
102	Carbonate sedimentation	Off
	Sand (%)	15
	Pelagic max. production rate (m/m.y.)	20
	Depositional front gradient siliciclastics	0.03
84	Depositional front gradient siliciclastics	0.06
	Pelagic max. production rate (m/m.y.)	40
66	Sand (%)	30
	Pelagic max. production rate (m/m.y.)	10
48	Sand (%)	25
	Carbonate sedimentation	On
34	Sand (%)	45
	Traction transport (%)	20
	Pelagic max. production rate (m/m.y.)	30
22	Pelagic max. production rate (m/m.y.)	45
	Depositional front gradient siliciclastics	0.07
14	Pelagic max. production rate (m/m.y.)	30

The tectono-stratigraphic configuration of the Campos Basin was achieved by adjusting four main sediment-related parameters, the declivity of the shelf front and the effect of marine currents. Variations in the percentage of sandstones are related to tectonic events with uplift and exposure of source terrains delivering higher sand volumes into the basin; on the other hand, reductions in the sand volumes can be interpreted as periods of tectonic quiescence, changes in the drainage pathways or lower erosion rates (associated to climate conditions). Changes in depositional gradients were needed in order to counteract catastrophic events of shelf-edge failure and maintain realistic adequate basin conditions.

Papers in peer-review journals

Jorham Contreras, Rainer Zühlke, Scott Bowman & Thilo Bechstädt, 2010. Seismic stratigraphy and subsidence analysis of the southern Brazilian margin (Campos, Santos, and Pelotas basins). *Marine and Petroleum Geology*, 27, 1952-1980.

Papers in preparation

Jorham Contreras, Rainer Zühlke, Scott Bowman & Thilo Bechstädt. Inverse basin modeling of key segments of the southern Brazilian rifted margin (Campos, Santos, and Pelotas basins). Corrections after first revision in *Basin Research*.

Jorham Contreras, Rainer Zühlke, Scott Bowman & Thilo Bechstädt. Forward stratigraphic modeling of the southern Brazilian continental margin (Campos, Santos, and Pelotas basins). To be submitted to *American Association of Petroleum Geologists Bulletin* (AAPG)

Abstracts in international meetings

II Central & North Atlantic Conjugate Margins Conference, Lisbon 2010. "Seismic stratigraphy and numerical basin modeling of the southern Brazilian margin (Campos, Santos, and Pelotas basins)".

72nd EAGE Conference & Exhibition incorporating SPE EUROPEC Barcelona, 14-17 June 2010. "Seismic stratigraphy and numerical basin analysis of the southern Brazilian margin".

GSL International Conference: Modelling of Sedimentary Basins and their Petroleum Systems. London. June, 2010. "Seismic stratigraphy and numerical basin modelling of the southern Brazilian margin".

SEPM-CES, Sediment 2009, Kraków, Poland. "Seismo-stratigraphy and basin analysis of the Campos, Santos and Pelotas basins, southern Brazilian continental margin".

71st EAGE Conference & Exhibition, SPE EUROPEC, Amsterdam 2009. "Seismo-stratigraphy and basin modelling for key segments of the southern Brazilian passive continental margin".

IAS-SEPM Central European Union 2008. Bochum-Germany. "Basin Analysis and Numerical Modelling of Brazilian and Uruguayan passive continental margins".

Sediment 2007. Brixen/Bressanone-Italy. "Basin Analysis and Numerical Modelling of South Atlantic conjugate passive continental margins".

4th Meeting of SEPM Central European Union 2006. Göttingen-Germany. "Basin Analysis and Numerical Modelling of the South American and West African continental margins: First Results".

Acknowledgments

First of all I would like to express my sincere gratitude to my supervisor Dr. Rainer Zühlke for allocating the data and technical facilities to develop the project as well as for his revisions, suggestions and knowledge of modeling that made possible the international contributions, publications and writing of this thesis.

To my second supervisor, Prof. emer. Dr. Thilo Bechstädt, for offering me the opportunity to develop this project and his suggestions during the writing of the thesis.

I am grateful to Scott Bowman and his associates for supply the data as well as for his valuable comments and explanations on numerical basin modeling.

Very special thanks to Francisco Cueto for his unconditional help, last-second practical solutions, talks and critics.

This project was funded by Steinbeis-Transfer Centre at the University of Heidelberg, IPP program, Fundayacucho (Venezuela) and the Deutscher Akademischer Austausch Dienst (DAAD).

Many thanks to my colleague, office-, conference-mate and friend Ewa for her advices and discussions... thanks a lot!

To all my colleagues specially Christian, Axel, Torben, Natalia, Enric and Fabio for their help as well as the members of the Mensa-team, Carsten, Iris, Thomas, Sonja, Dominik, Rodriguillo, Bladimiro, Hans Eited, Tom, Judith, El Che, and many others for the entertaining discussions.

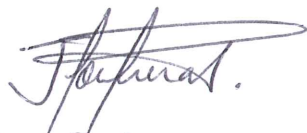
To everyone in the Institut für Geowissenschaften for their assistance in all admin tasks.

Thanks go to all that helped me to improve and complete this research project.

Eidesstattliche Erklärung

Hiermit erkläre ich, Jorham Contreras (geb. 31.12.1979 in Caracas, Venezuela), an Eides statt, dass ich die vorgelegte Dissertation selbst verfasst und mich dabei keiner anderen als der von mir ausdrücklich bezeichneten Quellen und Hilfen bedient habe.

Ich, Jorham Contreras (geb. 31.12.1979 in Caracas, Venezuela), erkläre zudem an Eides statt, dass ich an keiner anderen Stelle ein Prüfungsverfahren beantragt habe, dass ich die Dissertation nicht in dieser oder anderer Form bereits anderweitig als Prüfungsarbeit verwendet habe und dass ich sie an keiner anderen Fakultät als Dissertation vorgelegt habe.



Jorham Contreras

Heidelberg, 31.05.2011.